The role of pre-existing inflammation in the skin in modulating the outcome of arbovirus infection

Ailish McCafferty

Submitted in accordance with the requirements for the degree of Doctor of Philosophy

University of Leeds
Faculty of Medicine and Health
School of Medicine

Leeds Institute of Medical Research

June 2024

I confirm that the work submitted is my own and that appropriate credit has been given where reference has been made to the work of others.

Acknowledgements

Firstly, I would like to thank my supervisor Dr Clive McKimmie for the opportunity to undertake this PhD project and for his support throughout. As well as invaluable scientific advice, he has also consistently provided a positive outlook (no matter the results of the experiment…) and many inspirational pep talks. I also want to thank Dr Marieke Pingen, my first mentor in science, who not only inspired me to embark on this path researching our *Aedes* friends but also nurtured my ambitious spirit. I likely would not have even thought about applying for this PhD if it was not for you. Thank you also goes to my co-supervisors Dr Kave Shams and Dr Mihaela Lorger for their guidance and support.

A massive thank you goes to two of my best friends, Amy and Samantha. I would not be submitting this thesis without your friendship. Thank you for all the coffee/lunch/donut/snack breaks which kept me sane during long days in the lab and for all the delicious dinners (a.k.a therapy sessions) and pink bubbles we shared outside of work. Liam too, thank you for all the laughs, calzones and enthusiastic encouragement to never take life too seriously.

I was lucky enough to begin this journey with the best group of people who were some of my first friends in Leeds, the 5th DiMeN DTP Leeds cohort: Abi, Andreas, Sam, Katy and George. From sitting outside the pub in the freezing cold the first time we all met in COVID times, to the many trips around the North for training events – it's been a joy. I can't wait to see what you all go on to do next and I'm grateful to have had the privilege to have shared this experience with you all.

This project would not have been possible without the guidance and help provided by the technical staff at the university, particularly in the SBS animal house and the flow cytometry facility. I would also like to thank Dr Ian Carr in the Next Generation Sequencing Facility for his assistance with some of the data analysis in this project. I also want to express my appreciation to all the wonderful members of VHIT, Yonca, Amani and Zahra, and to all the fabulous people on Level 5 in Wellcome Trust Brenner Building for their friendship and especially for pub Fridays – the real backbone of my PhD!

Next, I want to thank all of the wonderful people outside of the lab who have filled my downtime with laughs and fantastic memories. I owe so much to two of the most important people in my life: Siân and Elley. Thank you for our wonderfully fun weekends in Leeds/Birmingham/Manchester/Cardiff/Glasgow and always being there for me. I could not have hoped to meet two better friends when we set out on our little adventure in Adelaide back in the day. Since then, you have been a constant source of inspiration to me with the amazing things you achieve in your lives. If I can accomplish a fraction of what you both have then I will be a very happy bunny indeed.

Thank you to my fabulous friends Aimee and Fraser who have always made so much effort to make our long-distance friendship work! I'll be forever grateful for all the trips you have made to Leeds to see us. Some of the best memories I have of this city are shared with you guys. Thank you also to my oldest friend, Emma, for always being by my side and providing me with endless laughs along the way. To the Browns/Maguires, thank you for making our trips home a joy!

I also owe so much to my family: Mum, Dad, Niamh and Gran Prow. Thank you for your unconditional support, not only through my PhD, but since as long as I can remember. Thanks for encouraging me to be the best version of myself and to pursue my interests. Everything I do is to make you proud. A special shout out goes to Gran Prow, for inspiring me to accept every opportunity offered to me: knowing my wonderful Gran moved to Malaysia back when there was no such thing as Facetime made it a whole lot easier to move 4 hours down the A1.

Finally, and most importantly, thank you to my fiancé Danny for your continual support in everything I do. I really could not have got through this PhD without your constant encouragement and love. You are a human ray of sunshine which means that no matter how my work day goes, I get to come home to you at the end of it and then I'm instantly cheerful! Thank you for moving to Leeds without having visited beforehand – a fact that sums up your amazing 'Why not!' attitude when faced with any opportunity, which makes our life together a joy. Thank you for exploring this delightful city with me and making it our home; from all the trips to breweries and new restaurants to our little daytrips around Yorkshire. I've loved every second of this adventure we have had together.

Abstract

As climate change expands mosquito habitats, the incidence of mosquito-borne virus infections is rising. Understanding of factors which underlie variability in susceptibility to arbovirus infections between individuals is limited. Identifying such factors would provide a better understanding of arbovirus pathogenesis to aid development of more effective vaccines and antivirals. This thesis identifies two factors which modulate host susceptibility to arbovirus infection in the skin: 1) UV exposure 2) the presence of pre-existing inflammation due to inflammatory disease. A unique *in vivo* model of natural arbovirus transmission, combining UV exposure, mosquito biting and virus infection at the same site, was used to investigate susceptibility to a model arbovirus, Semliki Forest virus (SFV), in UV-exposed skin. Prior erythemal UV exposure of skin, equivalent to sunburn, or repeated, sub-erythemal UV exposure of skin, mimicking daily tanning exposures, enhance subsequent arbovirus infection *in vivo*, causing an increase in virus replication at the inoculation site, the skin, and dissemination of virus. Susceptibility to infection is highest at 24h and 1-week post-UV exposure, although distinct mechanisms drive this at each timepoint. Virus-permissive leukocytes are recruited to UV-exposed skin by 24h post-UV exposure in response to elevated CCL2 expression. SFV utilises these infiltrating cells for replication. Contrastingly, by 1-week post-exposure, the damaged tissue is undergoing wound-healing, with an increase in actively proliferating cells, which SFV preferentially infects. Treatment of the UV burn with anti-inflammatory topical steroids offers partial protection against UV-mediated enhancement, by limiting viremia early post-infection but, crucially, does not prevent spread of virus to the brain, the main site of arbovirus pathology. Furthermore, we have found that PBMCs from patients with inflammatory skin conditions, either psoriasis or systemic sclerosis, are resistant to ZIKV infection *in vitro*. In psoriatic PBMCs, this is likely at least partly due to better induction of type I IFN responses compared to healthy PBMCs. This work identifies two novel factors which can alter host susceptibility to arbovirus infection.

Table of contents

List of tables

List of figures

Chapter 3

SFV infection is enhanced *in vivo* at an acute timepoint following an erythemal UV exposure, through recruitment of myeloid cells which are targeted by the virus

Chapter 5

Repeated sub-erythemal UV exposure *in vivo* is sufficient to increase host susceptibility to SFV infection

Chapter 6

Treatment of UV burn with anti-inflammatory steroid cream offers some protection from UV-mediated enhancement of infection *in vivo*

Abbreviations

3xIoUV	Sub-erythemal UV exposure given 3 times at 48h intervals
ADE	Antibody-dependent enhancement
AgBr1	Aedes aegypti bacteria-responsive protein 1
ARG1	Arginase 1
AWERB	Animal Welfare and Ethical Review Body
BHK-21	Baby hamster kidney cell
bp	Base pair
BSA	Bovine serum albumin
C6/36	Aedes albopictus clone C6/36
C	Capsid
CCL	CC-chemokine ligand
CCR	CC-chemokine receptor
CD	Cluster of differentiation
cDC	Classical dendritic cell
cDNA	Complimentary DNA
cGAS	Cyclic GMP-AMP synthase
CHIKV	Chikungunya virus
COVID-19	Coronavirus disease 2019
CTLA	Cytotoxic T-lymphocyte associated protein
CXCL	CXC-chemokine ligand
CXCR	CXC-chemokine receptor
DALY	Disability-adjusted life year
DAMP	Damage-associated molecular pattern
DC	Dendritic cell
DC-SIGN	Dendritic cell-specific intracellular adhesion molecule-3-grabbing nonintegrin
DEG	Differentially expressed gene
DENV	Dengue virus
DF	Dengue fever
DHF	Dengue haemorrhagic fever
DMEM	Dulbecco's modified eagle medium
ds	Double-stranded
DSS	Dengue shock syndrome
E	Envelope
ECM	Extracellular matrix
EDTA	Ethylenediaminetetraacetic acid

EdU	5-ethynyl-2'-deoxyuridine
ELISA	Enzyme-linked immunosorbent assay
EP-CAM	Epithelial cell adhesion molecule
ER	Endoplasmic reticulum
FBS	Fetal bovine serum
FcR	Fragment crystallisable receptor
FDA	Food and Drug Administration
GAG	Glycosaminoglycans
Gas6	Growth arrest-specific 6
H&E	Hematoxylin and eosin
HC	Healthy control
HCMV	Human cytomegalovirus
hiUV	Single, erythemal UV exposure
HO	Home Office
hpi	Hours post infection
HSV	Herpes simplex virus
i.p.	Intraperitoneal
ICAM	Intracellular adhesion molecule
IFIT	Interferon-induced protein with tetratricopeptide repeats
IFN	Interferon
IL	Interleukin
iNOS	Inducible nitric oxide synthase
IRF	Interferon-regulatory factor
ISG	Interferon-stimulated gene
JAK	Janus kinase
JEV	Japanese encephalitis virus
LIMR	Leeds Institute of Medical Research
M	Membrane
MACS	Magnetic activated cell sorting
MAYV	Mayaro virus
MDA	melanoma differentiation-associated protein
mDC	Myeloid dendritic cell
MED	Minimal erythema dose
MEM	Modified eagle medium
MerTK	Mer tyrosine kinase
MHC	Major histocompatibility complex
MOI	Multiplicity of infection
mRNA	Messenger RNA

Mxra8	Matrix remodelling-associated 8
NeSt1	Neutrophil-stimulating factor 1
NET	Neutrophil extracellular traps
NF-kB	Nuclear factor kappa-light-chain-enhancer of activated B cells
NGS	Next generation sequencing
NK	Natural killer
ns	Not significant
NS	Non-structural
ONNV	O'nyong-nyong virus
ORF	Open-reading frame
p.i.	Post infection
PAMP	Pathogen-associated molecular pattern
PASI	Psoriasis Area and Severity Index
PBMC	Peripheral blood mononuclear cell
PBS	Phosphate buffered saline
PCA	Principal component analysis
PCR	Polymerase chain reaction
pDC	Plasmacytoid dendritic cell
PDGF	Platelet-derived growth factor
PFA	Paraformaldehyde
PFU	Plaque forming unit
Poly(dA:dT)	poly(deoxyadenylic-deoxythymidylic) acid
prM	Premembrane
PRR	Pattern recognition receptor
Ps	Psoriasis
qPCR	Quantitative real-time PCR
RBC	Red blood cell
RIG-I	Retinoic acid-inducible gene-I
RPMI	Rosewell Park Memorial Institute
rRNA	Ribosomal RNA
RRV	Ross River virus
RSAD2	Radical S-adenosyl methionine domain-containing 2
RSV	Respiratory syncytial virus
RT	Room temperature
RT-PCR	Real time PCR
RVF	Rift Valley fever virus
s.c.	Subcutaneous
SARS-CoV-2	Severe-acute-respiratory-syndrome-related coronavirus-2

SBS	St James's Biomedical Services
SFV	Semliki Forest virus
SINV	Sindbis virus
ss	Single-stranded
SSc	Systemic sclerosis
STAT	Signal transducer and activator of transcription
STING	Stimulator of interferon genes
TAE	Tris-acetate-EDTA
TBEV	Tick-borne encephalitis virus
TGF	Transforming growth factor
Th	T helper
TLR	Toll-like receptor
Tm	Melting temperature
TNF	Tumour necrosis factor
TPB	Tryptose phosphate broth
UTR	Untranslated region
UV	Ultraviolet
UVI	Ultraviolet index
UVR	Ultraviolet radiation
VCAM	Vascular cell adhesion protein
VEEV	Venezuelan equine encephalitis virus
VEGF	Vascular endothelial growth factor
Vitamin D	25-hydroxy vitamin D_3
VLDLR	Very low-density lipoprotein receptor
VZV	Varicella zoster virus
WHO	World Health Organisation
WNV	West Nile virus
WT	Wild type
YFV	Yellow fever virus
ZIKV	Zika virus
χ^2	Chi-squared

Chapter 1: Introduction

1.1 Arboviruses

Arthropod-borne viruses (arboviruses) are transmitted through the bite of infected blood-feeding vectors, including mosquitos, ticks and flies[1]. As the arthropod takes a blood meal, saliva containing virus is injected into the host. This group of viruses consists of members of several virus taxa, notably the *Alphavirus*, *Orthoflavivirus* and *Orthobunyavirus* genera[2]. There are over 500 arboviruses and more than 100 of these can infect humans[3].

1.1.1 Mosquito-borne arboviruses: an emerging global health problem

Mosquitos are responsible for the spread of numerous arboviruses which cause significant disease in humans[4]. These include dengue virus (DENV), Zika virus (ZIKV) and chikungunya virus (CHIKV). The number of reported cases of mosquito-borne virus infections has risen dramatically over the last half century[5]. DENV has been a significant problem for humans for almost 60 years, but has seen a large uptick in the past few decades[6,7]. Other arboviruses, such as ZIKV and CHIKV, have emerged in populations more recently[8]. These emerging arboviruses have become more apparent in the public consciousness since the start of the 21st century due to the occurrence of several sporadic outbreaks in previously unaffected regions, which led to significant epidemics in the Americas in the 2010s.

1.1.1.1 Dengue virus

DENV is the most medically important mosquito-borne virus and has long been established in the human population[9]**.** However, case numbers have exploded in recent years, rising ten-fold between 2000 and 2019[10]. Last year, 2023, was the worst year on record in terms of DENV cases, with over 6 million confirmed infections taking place[11]. South America faced a large brunt of these cases, with Brazil being hit particularly hard[10]. Furthermore, this is likely a drastic underrepresentation of the actual number of cases, as the majority of cases cause mild or asymptomatic infections, which leads to underreporting or misdiagnosis[12]. Models have estimated that DENV is likely to be responsible for 390 million infections around the world each year[6]. The situation is only expected to get worse over the coming years; while it is estimated that over half

of the global population are currently at risk of DENV infection, this is expected to increase to 60% by 2080[7].

1.1.1.2 Chikungunya virus

In comparison to DENV, CHIKV was relatively unknown until recently. Outbreaks of CHIKV occurred sporadically until a major outbreak which started in 2004 in Kenya and subsequently spread to numerous other countries in Africa and Asia, before emerging for the first time in new regions, including Europe and the Americas in 2013[13]. In total, CHIKV spread to more than 100 countries during this outbreak, infecting over 10 million individuals globally. The number of cases did stabilise in the majority of areas for a few years after this. The exception to this was in South America, where cases continued to ebb and flow over time[14,15]. A serious resurgence took place on the continent in 2022-23[16,17]. Similar to the spike in DENV cases in 2023, the majority of these CHIKV cases also took place in Brazil and this wave remains ongoing. These recent outbreaks have solidified CHIKV's place as the second biggest arbovirus threat after DENV.

1.1.1.3 Zika virus

ZIKV is another emerging arbovirus infection. The virus was initially identified in Uganda in 1947, with the first case of human infection reported in Nigeria in 1954 century[18,19]. Following its discovery, there were very few (<20) reported ZIKV infections in the remainder of the century[20]. However, there have been multiple large-scale outbreaks in the last two decades, the most significant of which originated in French Polynesia in 2013/14[21]. From here, the virus spread to the Americas in 2015, starting in Brazil, causing the largest known outbreak of ZIKV thus far, with 440,000-1,300,000 suspected cases occurring in 2015 alone[22,23]. This outbreak led to the World Health Organisation (WHO) declaring ZIKV as a Public Health Emergency of International Concern[24]. The latest available figures from WHO state that, as of February 2022, ZIKV transmission had been identified in 89 countries worldwide[25].

1.1.2 The *Aedes* mosquito: a highly competent arbovirus vector

The *Aedes* genus of mosquito is a particularly important arbovirus vector[1]. Species within this large genus are the insects primarily responsible for the spread of a number of infections which cause significant disease in humans and animals, including DENV, CHIKV and ZIKV[26]. The *Ae. aegypti* species is the main vector for these infections, but they can also be transmitted by the *Ae. albopictus* and others[27]. The mosquito becomes infected after feeding on the blood of an infected individual[28]. The virus propagates in the midgut of the mosquito before spreading to other tissues, including the salivary glands, where it persists[29]. Following incubation, the vector can transmit virus through injection of its saliva when it bites a human.

Ae. aegypti mosquitoes are particularly efficient as vectors of virus due to several factors. Female mosquitoes feed on blood from mammals as they require a protein found in blood, isoleucine, for reproduction[30]. *Ae. aegypti* mosquitos have a preference for human blood[31]. As a result, they tend to live in urban environments near people. Overcrowding of populations in urban areas also maximises the number of people exposed to *Aedes* bites and increases probability that they can transmit virus between individuals. Furthermore, *Ae. aegypti* are day biters and so are highly active at the same time as humans, presenting plenty of transmission opportunities.

There are several methods used to try and control *Aedes* populations and limit spread of arbovirus infections[32]. However, traditional methods of mosquito control, such as the use of insecticide treated bed nets, have limited efficacy against *Aedes spp.*, due to their limited activity during the night[33]. More recently though, an alternative approach, involving the bacteria *Wolbachia*, has been rolled out in some endemic regions. Mosquito eggs are purposely infected with this bacterium and this provides adult mosquitos with resistance to arbovirus infection, resulting in reduced arbovirus transmission rates[34]. Although the mechanism behind this is not fully understand, it has been suggested that the bacteria may outcompete the virus for resources during infection. This method has been used against *Ae. aegypti* so far in several regions, including parts of China, the USA, and Brazil.

1.1.3 The changing burden of arbovirus infection

Arbovirus transmission zones are defined by the regions in which the *Aedes* vector is able to live[35]. *Ae. aegypti* is particularly vulnerable to cold climates as the optimal temperature for their egg development is between 25°C-30°C and so eggs will not survive through the winter season in areas where temperatures drop too low[36]. *Ae. albopictus* can better survive in colder temperatures and so can live in more temperate regions. However, it is a less competent vector[27]. The *Aedes spp.* lays eggs in stagnant water and so also prefers areas with high humidity or precipitation, rather than dry climates[37]. As a result of these confining factors, arboviruses are mostly transmitted in tropical and sub-tropical regions of the world (Figure 1.1). Because *Aedes* mosquitos are the vector for numerous arboviruses, the transmission zones of many of these overlap, leading to cocirculation of multiple arbovirus infections in populations[38]. This can result in regions being hit by outbreaks of multiple arboviruses at one time, as was the case in Brazil in 2023, with a surge in both CHIKV and DENV infections occurring simultaneously.

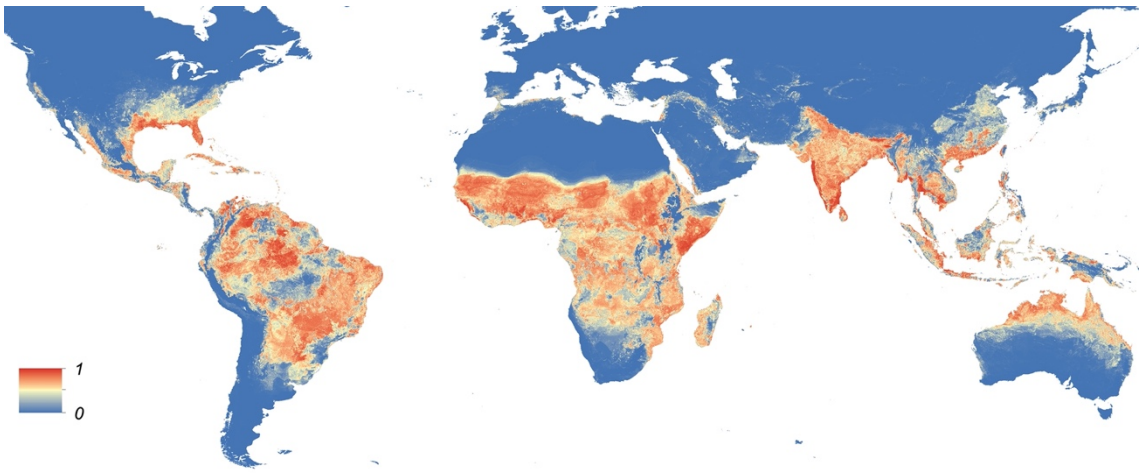

Figure 1.1 | Map showing global distribution of *Aedes aegypti*

Predicted distribution of the principal arbovirus vector *Ae. aegypti*. High occurrence (1) is represented in red, low occurrence is represented in blue (0). Figure taken from Kraemer et al. 2015[39].

The regions in which arboviruses are transmitted is expected to change over the coming decades[7,40,41]. This will expose new, immunologically naïve populations to these viruses which could have serious implications for infection outcomes. Already, there are arbovirus cases being reported in regions where

there was previously no transmission, including in Europe. There were 130 autochthonous, vector-transmitted cases of DENV in Europe in 2023, resulting from small outbreaks across France, Italy and Spain[42]. Furthermore, the first case of ZIKV in Europe was reported in 2019[43,44]. This is largely due to the *Aedes spp.* becoming established in new areas of the world[7,39,41]. Before 1970, Ae. aegypti was only found in 6 countries. Now, the vector is present in at least 136[45]. Importantly, *Ae. Aegypti* was classified as an established population in a European country, Cyprus, for the first time in 2022[46].

1.1.3.1 Climate change as a driver of arbovirus emergence

The rise in arbovirus outbreaks in recent years has led to the realisation of the threat posed by arboviruses to global health[8]. Unfortunately, this danger is only expected to increase in the future; both in terms of increasing frequency of outbreaks but also exposure of new populations to arboviruses. The emergence and re-emergence of arboviruses is driven by a number of factors, including climate change, urbanisation, migration, changing countryside management practices and globalisation[47].

Importantly, the expansion in vector habitat, briefly discussed in the previous section, is primarily driven by climate change. Global warming is expanding the regions in which insect vectors, such as *Ae. aegypti*, can reside. This means they are no longer restricted to the tropics and subtropics. This threatens to bring arboviral competent vectors into contact with different human populations and thereby exposing these individuals to risk of viral infection[48]. This issue is only expected to worsen over time as climate change continues to warm regions of the world where insect vectors previously couldn't inhabit. It is estimated that more than 3 billion individuals now inhabit regions in which *Aedes* mosquitoes are found[8]. In addition to this, there is evidence of ZIKV, CHIKV and DENV spread by another *Aedes* subtype, *Ae. albopictus,* which lives more readily in temperate climates[41,49–51]. However, transmission is also restricted by an upper temperature limit, as extreme temperatures negatively affect *Aedes spp.* survival[36,52]. Arbovirus transmission is already highly climate dependent, shown by variation in transmission rates year-on-year due to annual variations in temperature[7]. Therefore, it is predicted that some regions where

arboviruses currently circulate will eventually become too hot for transmission to occur as a result of climate change[53].

1.1.4 Arboviral disease

Those arboviruses which have experienced recent global re-emergence, such as ZIKV, CHIKV and DENV, are responsible for significant human disease burden. Typically, infection with one of these viruses presents with similar clinical signs, including an acute, febrile illness. These symptoms usually resolve without the need for hospitalisation. Indeed, most arbovirus infections are asymptomatic or mild. However, each of these viruses either can cause more serious complications or lead to chronic conditions. The severe forms of each of these diseases present differently from each other.

Although estimates vary, around 96 million of the total individuals infected with DENV annually experience symptomatic infections[6]. This most often presents as dengue fever (DF), with patients experiencing a fever, severe joint and muscle pain and sometimes a rash[54]. However, DENV infection can progress to more severe forms of the disease, dengue haemorrhagic fever (DHF) and dengue shock syndrome (DSS). This is characterised by leakage of plasma, which can lead to system-wide shock and organ failure. Although only ~1% of severe DENV cases are fatal, the large global burden of this virus means that the number of fatalities is significant[55]. There are 4 DENV serotypes, DENV-1, DENV-2, DENV-3 and DENV-4. Following an initial DENV infection, the individual develops immunity to that serotype. However, a subsequent infection with a different serotype results in an increased chance of developing severe disease[56].

Following ZIKV transmission, infected individuals often either display no symptoms or a mild illness, often characterised by a fever and a skin rash[57]. For a long time, it was thought that these were the only symptoms associated with ZIKV. It was only after the most recent explosive outbreak of the virus in South America that the clinical relevance of the disease was truly realised[58]. Observations from epidemiological studies made it clear that infection with ZIKV can cause severe neurological disease. Convincing evidence links ZIKV to the congenital condition microcephaly in babies infected in the womb, following

vertical transmission from an infected mother[59]. It is thought that this occurs as a result of ZIKV's tropism for the placenta and foetal brain, a feature which is unique to ZIKV amongst arboviruses but is also observed in human cytomegalovirus (HCMV) and herpes simplex virus (HSV) infection[60–62]. In addition to this, ZIKV has been associated with serious neurological sequelae in adults, most notably Guillain-Barré syndrome, but also myelitis and meningoencephalitis[63–68].

CHIKV is one of the exceptions to the rule that arboviral disease is predominately asymptomatic or mild, as the majority of CHIKV infections cause symptoms[69]. This presents primarily as rheumatic disease with individuals experiencing acute fever, rash and joint pain, or arthralgia, which can be intense. The acute symptoms generally resolve within weeks. However, joint pain can turn chronic. In 43% of symptomatic cases, symptoms last 3 months or longer and 21% of cases still suffer from the disease 12 months after infection[70]. This chronic aspect differentiates CHIKV from many other arboviruses. However, there are other arthritogenic arboviruses, including the genetically related Old World Alphaviruses: o'nyong-nyong (ONNV), Mayaro (MAYV) and Sindbis virus (SINV). The chronic nature of these diseases presents another dynamic to the burden presented by arbovirus infection, in terms of causing long-term disability and the associated care needs that come with this. Indeed, it has been estimated that 106,000 disability-adjusted life years (DALYs) are lost each year around the world due to CHIKV[71].

1.1.5 Diagnosis and treatment of arboviruses

The similarity in the symptoms caused by arboviral disease and cross-reactivity in diagnostic tests for some viruses, alongside the aforementioned overlapping transmission zones and shared vector, means it is often challenging for clinicians to accurately diagnose a patient with a specific arboviral infection[72]. Furthermore, infections often occur in regions with poor health provisions, meaning there is limited time and/or resources to make accurate laboratory diagnoses using ELISAs or RT-PCR. Therefore, it is recognised that arboviral infections, especially CHIKV and ZIKV, are likely underreported due to misdiagnosis[21].

There are currently no licensed antivirals or therapeutics available to treat arboviruses. Although mortality from severe DENV can be reduced with basic healthcare interventions, such as administration of intravenous fluids, when administered early during the onset of disease[73]. While there are vaccines available for some arbovirus infections, the efficacy of these is variable. Some are highly effective, such as the vaccine against Yellow Fever virus (YFV) which confers life-long immunity[74]. Others, including Japanese encephalitis virus (JEV), suffer from waning protection[75]. Unfortunately, there is also uncertainty surrounding the safety of some arboviral vaccines. The first DENV vaccine, Dengvaxia, became available in 2015[76]. However, since its rollout, there have been studies showing that it can increase the risk of severe DENV disease if given to individuals who had no pre-existing immunity to DENV at the time of vaccination[77]. Although the vaccine is still recommended for use in DENV immune recipients[78]. Nevertheless, the realisation of the threat posed by these infections has led to renewed efforts to develop safe, effective vaccines against them. Indeed, at the end of 2023 the first CHIKV vaccine was approved by the Food and Drug Administration (FDA)[79]. However, questions remain over its use also. A relatively large number of vaccine recipients report a CHIKV-like illness, with 2% of recipients experiencing ‘severe’ side effects[80]. Therefore, its value as an option for population-wide immunisation is limited. It is currently only recommended for individuals travelling to a region with an ongoing CHIKV outbreak. As well as these issues with existing arbovirus vaccines there are still no available vaccines for many major arboviruses, including ZIKV. Therefore, there is a clear unmet need for safe, effective vaccines to prevent arboviral disease.

However, the co-circulation of multiple arboviruses within one area presents challenges for vaccination. Prior exposure or vaccination against one arbovirus can generate cross-reactivity against other viruses within the same family, particularly flaviviruses[81,82]. Rather than providing broad-spectrum protection against multiple arboviruses with one vaccine, instead this can be detrimental to the host, as generation of sub-neutralising antibodies against flaviviruses can lead to antibody-dependent enhancement (ADE) of infection[83]. This, together

with the challenges in diagnosing these infections, highlights the need for pan-viral treatments or vaccines, which target multiple arboviruses.

1.1.6 Flaviviruses

The *Flavivirus* genus, in the *Flaviviridae* family, is of particular importance when considering arboviruses. The majority of flaviviruses are arboviruses and many cause significant human disease. Amongst these are DENV, ZIKV, YFV, and West Nile virus (WNV), all of which are mosquito-borne. There are also flaviviruses spread by other arthropods, including tick-borne encephalitis virus (TBEV). The following sections will focus on ZIKV, a flavivirus used in this thesis.

1.1.6.1 Structure and genome organisation

Elucidation of the ZIKV structure illustrated that Zika virions are structurally similar to other *Flavivirus* particles, particularly DENV, in that they are enveloped, spherical particles, with a diameter of ~70-100nm[84,85]. Each particle possesses a single stranded, positive-sense, RNA genome, 10,794 kb in length (Figure 1.2)[86]. All *Flavivirus* genomes possess a single open-reading frame (ORF) which codes for a polyprotein. This is flanked by 5' and 3' untranslated regions (UTRs). The viral polyprotein is processed into 3 structural proteins (capsid (C), premembrane/membrane (prM/M) and envelope (E)) and 7 non-structural proteins (NS1, NS2A, NS2B, NS3, NS4A, NS4B, NS5) by host and viral proteases during the viral replication cycle[60,87].

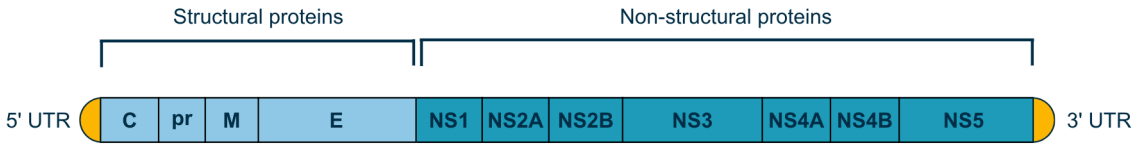

Figure 1.2 | ZIKV genome organisation

1.1.6.2 Mechanism of infection

There is limited understanding of the mechanism of ZIKV infection and its replication cycle due to its recent emergence. However, due to the structural similarities between ZIKV particles and other flaviviruses, especially DENV, the

replication cycle of other flaviviruses is often looked to as a guide for how ZIKV may act (Figure 1.3)[60]. Flaviviruses initially bind to the surface of host cells through attachment to surface receptors[88]. In the case of ZIKV, this likely occurs through binding of adhesion receptors. While several host receptors have been linked to ZIKV entry, including dendritic cell-specific intracellular adhesion molecule-3-grabbing nonintegrin (DC-SIGN) and Tyro3, there is significant evidence that ZIKV entry to cells is often dependent on binding to the tyrosine kinase receptor AXL[84]. ZIKV is able to bind the AXL ligand, growth arrest-specific 6 (Gas6), and it is thought that this enables the virus to interact with AXL on host cells[89]. This role is further supported by the presence of Gas6 in many of the tissues for which ZIKV has tropism for, including significant expression in the brain and male reproductive organs[90]. Following attachment, the virus gains access to the host cell through receptor-mediated endocytosis, a process which involves the ectodomain of the E viral glycoprotein[91].

The low pH environment within host cell endosomes triggers fusion of the virus with the endosomal membrane due to a conformational change of the E protein[92]. This allows the viral genome to be ejected into the cytosol to act as a messenger RNA (mRNA) template for the creation of the viral polyprotein at the endoplasmic reticulum (ER). Cleavage of this polyprotein leaves the 10 mature viral proteins. Following protein synthesis, production of new viral particles begins within pockets made from the ER membrane, known as spherules[93]. The replication process starts with the synthesis of negative-sense RNAs which are then used as a basis upon which new positive-sense RNAs are generated[94]. All of the NS viral proteins play a part in this process of RNA replication, with ZIKV NS5, which possesses RNA-dependent RNA polymerase activity, and NS3 playing particularly critical roles[95,96] From here, the new RNA associates with the viral C protein and together these bud into the lumen of the ER, incorporating both the ER membrane and the prM and E proteins as they go, to form new immature viral particles[88]. These non-infectious virions undergo further proteolytic processing in the Golgi network to cleave prM, leaving the mature M protein[90]. The newly-formed mature viral particles are released from the host cell by exocytosis at the cell surface[97].

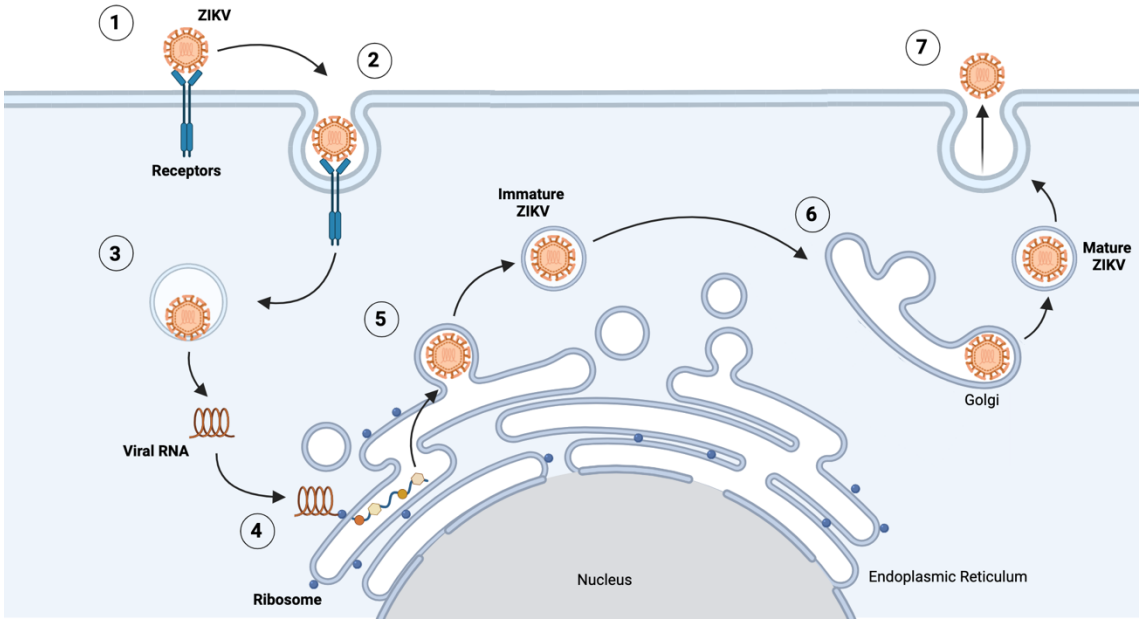

Figure 1.3 | Replication cycle of ZIKV

(1) Flavivirus binds to the cell surface via receptors, including DC-SIGN and Tyro3 in the case of ZIKV. **(2)** Receptor-mediated endocytosis facilitates entry of the virus to the host cell. **(3)** The virus fuses with the endosomal membrane and the virus RNA is ejected into the cytosol. **(4)** The viral polyprotein is synthesised at the ER, using the virus genome as a template, and is cleaved into the 10 virus proteins. **(5)** New virus particles are created within ER-derived spherules. **(6)** Further proteolytic processing of the virion in the Golgi network produces the mature, infectious virus particle. **(7)** Infectious virions leave the cell via exocytosis. Diagram made using BioRender.

1.1.7 Alphaviruses

The *Alphavirus* genus, belonging to the *Togaviridae* family, contains a number of medically important arboviruses, including CHIKV, ONNV, MAYV, Ross River (RRV) and Venezuelan equine encephalitis virus (VEEV)[98]. There are around 30 species of alphaviruses[99]. Interestingly, nearly all of the alphaviruses are mosquito-borne and are transmitted to vertebrate hosts, either human or animal, to cause disease[100]. Alphaviruses are broadly divided into Old World alphaviruses and New World alphaviruses, and can cause either arthralgia or encephalitis respectively. One of the exceptions to this rule are laboratory derived strains of Semliki Forest virus (SFV). Although this is classified as an Old World alphavirus, it is widely used as a model of neurotropic arbovirus infection, rather than arthritogenic infection[101]. Although mortality rates associated with alphaviruses are low, they cause significant morbidity due to the often chronic nature of symptoms associated infection[98]. The following sections

will largely focus on CHIKV, due to its medical relevance, and SFV, which is closely related to CHIKV and will be used as a model arbovirus throughout this thesis.

1.1.7.1 Structure and genome organisation

CHIKV forms spherical virions with a diameter of 60-70nm[102]. All alphaviruses possess single-stranded, positive-sense RNA genomes. The CHIKV genome is approximately 12kb long and consists of 2 ORFs split by a non-coding region, and flanked by a lengthy 3' untranslated region (UTR) and a 5' UTR which is shorter in length (Figure 1.4)[103]. There are 4 NS proteins (NSP1, NSP2, NSP3 & NSP4) which are translated from genomic RNA. The remaining 5 structural proteins (C, E3, E2, 6K, E1) are produced during RNA synthesis, from subgenomic RNA[104].

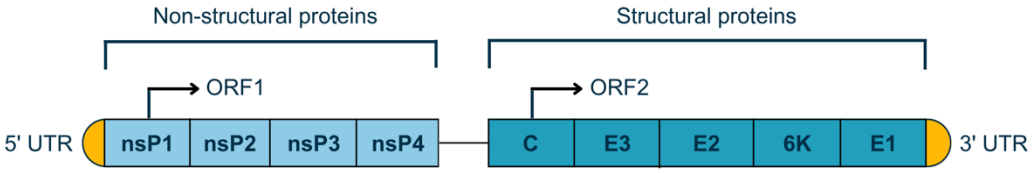

Figure 1.4 | CHIKV genome organisation

1.1.7.2 Mechanism of infection

As discussed, CHIKV is the most medically relevant alphavirus and so it is important to understand its replication cycle in host cells. Following transmission, CHIKV uses the host cell adhesion molecule matrix remodelling-associated 8 (Mxra8) to gain entry to a variety of cell types during infection[105]. Mxra8 is expressed by epithelial cells, myeloid and mesenchymal cells, including dermal and synovial fibroblasts. However, CHIKV infection was not entirely abated in mice lacking Mxra8, suggesting that there may be more than one host receptor used by CHIKV to enter cells. One such attachment factor which has been put forward are glycosaminoglycans (GAGs). It has been shown that strains of CHIKV, representing the 3 major CHIKV genotypes, bind sulphated GAGs and that these polysaccharides are expressed by CHIKV target cells, including epithelial and endothelial cells and macrophages, which may explain the wide-spread tropism of CHIKV[106]. Similar to ZIKV, CHIKV enters host cells through clathrin-mediated endocytosis. Once inside the cell,

the viral polyproteins P123 and P1234 are translated from the viral RNA template. The nsP2 region has protease activity which is used to cleave the polyproteins, leaving the four mature NS proteins which are necessary for RNA synthesis[107]. Following translation, the CHIKV genomic RNA is replicated to produce new infectious virions.

Many of the details of CHIKV replication in the host cell are yet to be elucidated, however, it is likely that the CHIKV cycle is similar to that of other more widely-studied alphaviruses, such as SFV and SINV, and so these can be used as an analogue. In a similar manner to flaviviruses, replication of alphaviruses take place in spherules, formed from folded plasma membrane structures induced by the virus[108]. The polyprotein P123 and nsP4, the RNA-dependent RNA polymerase protein, form a replicase complex to produce negative-sense RNA from the genomic RNA[104]. This RNA template is then used to synthesise more positive-sense, genomic RNA. Sub-genomic RNA is also produced during this process by way of a sub-genomic promoter present in the negative-sense RNA molecule[109]. This allows for the synthesis of the remaining viral structural proteins. To ensure only genomic RNA is packaged into newly produced virions, a packaging signal is included in the section of CHIKV genomic RNA which encodes nsP2[67]. The CHIKV capsid structural protein possesses signal sequences allowing for import to and export from the nucleus during the replication cycle[110].

Once new CHIKV particles have been assembled at the cell membrane, they bud from the infected cell. Despite attempts by the host factor Tetherin to keep CHIKV attached to the membrane to prevent its release, viral nsP1 acts to downregulate Tetherin to allow budding to take place[111]. Interestingly, in polarised cells, such as endothelial cells lining blood-tissue barriers, budding occurs from the apical side of the cell guided by N-linked glycoproteins present in the viral envelope proteins. It is unclear which host factors are involved in this process. However, it is thought that this adaption to polarised cells could contribute to more severe CHIKV symptoms by facilitating entry to vulnerable tissues e.g. viral encephalitis caused by viral dissemination across the blood-brain barrier[112].

1.1.7.3 Semliki Forest virus: a model arbovirus

SFV is one of the most closely genetically related alphaviruses to CHIKV, a virus of great medical importance[100]. Its name originates from the forest in Uganda in which it was discovered in 1942[113]. SFV is endemic in regions of Africa, mostly circulating in animals[114]. However, there was a notable human outbreak, affecting 22 people in 1987 in the Central African Republic[115]. The only reported lethal case was in a laboratory worker who died of encephalitis after handling the virus in the 70s[116].

Since its discovery, SFV has become a standard model for arbovirus infection in mice[101]. Its relevance to human infection coupled with its ability to replicate in immunocompetent mice, unlike many other human arboviruses like DENV and ZIKV, makes it highly useful in these types of studies. SFV can cause neurotropic infection and encephalitis as a result. There are several different strains of SFV, which vary in potential disease severity. SFV4 originates from the original infectious clone but only causes low titre viremia and is not able to reach the brain when injected alone[117]. SFV6 is a more virulent strain, based on SFV4, which can disseminate to the brain after being transmitted at a remote site and cross the blood-brain barrier, causing lethal encephalitis[118]. This characteristic makes SFV6 of particularly beneficial for studying arbovirus-related pathology in the central nervous system. However, when the avirulent strain SFV4 is inoculated alongside an *Aedes* sp. mosquito bite, or with *Aedes* mosquito saliva, it can more efficiently reach the brain and cause mortality[119,120]. Its use in this way can be of great value in defining those key factors that define host susceptibility to infection when inoculated at mosquito bites.

Notably, there are several genetically modified strains of SFV6 which can be used for experimental purposes. For example, SFV6-mCHERRY which encodes a fluorescent protein, meaning that infected cells that express this virus encoded protein can be identified using immunofluorescence or flow cytometry[119,121]. Genetic modification in this way comes with a fitness cost to the virus, however, because SFV6 is so virulent, modified strains can still replicate effectively in mice. Both SFV4 and SFV6 are used in this thesis, however, it is worth noting that there are other strains of SFV which can be used

experimentally as well, including the virulent L10 strain and avirulent A7(74) strain[122].

1.2 Immune response to arboviruses

Infections by arboviruses are generally brought under control rapidly following transmission, evidenced by the relatively short course of illness experienced by most who have symptomatic infections[9]. This early curbing of infection suggests the virus is limited mainly by innate antiviral mechanisms and the expression of anti-viral IgM antibodies. Additionally, it appears that while the adaptive immune response does strengthen the overall response to arboviral infections during the acute infection phase, it is likely that they also contribute to immunopathology, including DHF and chronic arthralgia caused by DENV and CHIKV, respectively[123,124].

Before discussing the immune response in detail, it is important to note that there are a variety of limitations to current experimental models used to investigate host immunity to arboviruses. Much of the work done to elucidate the immune response to arboviral infection has been completed in cell lines rather than undertaken *in vivo,* which may mean that conclusions are drawn without a full understanding of the influence of other cell types and soluble mediators as part of the whole animal immune network. Additionally, when *in vivo* models are used, virus is most often administered in the absence of mosquito bites, which are known to shift cell tropism at the inoculation site to include infection of infiltrating leukocytes, enhance virus replication and increase efficiency of virus dissemination to blood and remote tissues[125,126]. Furthermore, many studies for important arboviruses, including DENV and ZIKV, have to be carried out in immunodeficient mice lacking the type I interferon (IFN) receptor, as these viruses do not replicate in wild type (WT) mice[127,128]. However, this is the most critical aspect of antiviral immune responses. Therefore, there are challenges in defining the relevance of some data published that do not incorporate these features.

1.2.1 Innate immune response to arbovirus infection

Prompt recognition of viral infection by host cell pattern-recognition receptors (PRRs) is vital for rapid initiation of the immune response and facilitates the

early control of infection by the innate system. These receptors generally recognise viral genetic material, including ssRNA, dsRNA and unmethylated CpG DNA, present intracellularly as the virus carries out its replication cycle[129]. There are a number of PRRs involved in the recognition of arboviral infection, namely the Toll-like receptor (TLR) family and the RNA helicases, retinoic acid-inducible gene I (RIG-I) and melanoma differentiation-associated protein 5 (Mda5)[130,131]. More recently, a role for the cyclic GMP-AMP synthase (cGAS)-stimulator of interferon genes (STING) complex in arboviral recognition has also been elucidated[132]. Activation of the PRRs occurs as a result of pathogen derived ligand interactions, triggering signalling cascades that lead to the activation of the transcription factors nuclear factor kappa-light-chain-enhancer of activated B cells (NF-kB), interferon regulatory factor (IRF) 3 and IRF7. These transcription factors control the production of a number of pro-inflammatory mediators which coordinate the antiviral immune response. Additionally, NF-kB brings about the expression of a number of pro-inflammatory cytokines and chemokines, including interleukin (IL)-1β, tumour necrosis factor (TNF)-a and C-X-C motif ligand (CXCL) 10; IRF3 and IRF7 induce the type I IFN expression[133].

Neutrophils are the first responders to mosquito-transmitted viral infection, attracted to the site early in the course of infection by high concentrations of neutrophil chemoattractants, including CXCL2[120,134]. It has been postulated that these chemokines are produced by local mast cells in response to the mosquito bite *in vivo*[120,135]. At the site of infection, neutrophils are known to deploy a range of tactics to try and control the infection including the expulsion of the contents of their toxic granules, phagocytosis of pathogens and the deployment of neutrophil extracellular traps (NETs) to catch microbes[136]. In the case of arboviral infection, recent evidence shows the use of NETs to neutralise CHIKV infection of mice in response to TLR7 signalling and reactive oxygen species[136,137]. A similar role has been ascribed to NETs in the control of DENV infection both *in vivo* and *in vitro*[138].

However, neutrophils also promote an inflammatory environment at the site of infection. This is likely done indirectly by releasing soluble mediators which act

to increase vascular permeability, which promotes leukocyte entry to the infection site[126]. However, their expression of chemokines, including CCL2, acts to attract other myelomonocytic cells, which express the cognate chemokine receptor C-C chemokine receptor (CCR) 2. The source of CCL2 at this early stage is unclear, however, levels at the arbovirus infection site in mice following a mosquito bite were ablated following neutrophil depletion[120]. Nevertheless, rather than this being of benefit to the host in its response to the virus, it appears that instead the arrival of these myelomonocytic cells may instead present the virus with new infection targets[120].

Further evidence for the role of neutrophils in the promotion of inflammation, which is beneficial to the virus, comes from the identification of mosquito salivary protein functions. A number of mosquito salivary factors have been shown to promote neutrophil recruitment and activation, Aedes aegypti bacteria-responsive protein 1 (AgBr1) and neutrophil-stimulating factor 1 (NeSt1) respectively, during ZIKV infection. AgBr1 upregulates the production of chemokines which act as neutrophil-attractants during ZIKV infection, While NeSt1 induces the activation of neutrophils[139,140]. Additionally, blocking either of these salivary proteins leads to reduced viral load and improves the outcome of infection, suggesting that promoting neutrophil recruitment and activation is beneficial to virus infection.

Monocytes are permissive to infection by a range of arboviral infections and often form the most significant leukocyte population at the infection site[141,142]. Additionally, the aforementioned mosquito salivary protein, NeSt1, acts to attract monocytes[140]. It was recently shown that the T cell chemoattractant CXCL10 drives the pathology of CHIKV infection in mice by promoting an infiltrate of immune cells, with mice deficient in the chemokine experiencing reduced viral loads and diminished leukocyte infiltrate compared to WT mice[141]. In addition to this, high levels of monocyte chemoattractants have been associated with arboviral disease pathology. For example, there was found to be an association between high levels of CXCL10 and CXCL9, both involved in the recruitment of monocytes/macrophages, in human patient serum and severe CHIKV arthritis[143]. As well as providing infection targets, it is thought that monocytes may act in a detrimental way by contributing to viral dissemination,

due to their ability to migrate to and enter other tissues[142]. However, there is conflicting evidence about the role of the monocyte-attractant CCR2-CCL2 axis in CHIKV pathogenesis. During CHIKV infection in *Ccr2-/-* mice, monocyte and macrophage recruitment to the joints, the site of CHIKV pathogenesis, is ablated[144]. However, rather than aid the host, this leads instead to neutrophil migration to the tissue, which drives joint destruction.

The antiviral type I IFN system is critical to the control of arboviral infection. This system consists of IFN-α and IFN-β, produced by leukocytes/immune cells and fibroblasts, respectively[145]. Both IFN-α and IFN- β signal through the IFN-α/β receptor, known as the IFNAR receptor, in an autocrine or paracrine fashion. This triggers signal transduction through the JAK/STAT pathway, causing the expression of interferon stimulated genes (ISGs). ISG products facilitate the antiviral function of the type I IFN system by interfering with viral replication through a variety of mechanisms, to prevent further infection of cells.

The innate response to arboviruses is dependent on type I IFN, indicated by the high susceptibility to a number of mosquito-borne alphavirus and flavivirus infections observed in IFN receptor deficient mice (*Ifnar1*$^{-/-}$)[128,145–147]. As a result, *Ifnar1*$^{-/-}$ mice are regularly used as a mouse model to study arboviral infections, as most arboviruses struggle to replicate in mice with intact type I IFN signalling[148]. Also, many arboviral infections have type I IFN-targeted evasion strategies suggesting that avoiding this system is beneficial for supporting arbovirus infection[149,150]. Despite this, therapeutic induction of IFN pathways, in the skin, at an early time point following arboviral infection than occurs in the natural infection course significantly reduces viral dissemination, showing the power of the type I IFN system against a range of arboviruses[119].

There are two major subsets of dendritic cells (DCs) which contribute to the antiviral immune response in different ways. Plasmacytoid dendritic cells (pDCs) are the major producers of type I IFN in the blood and spleen, during arboviral infection and may be vital contributors to innate defence as a result[151]. A dampened pDC response has been associated with higher viral loads and more severe arboviral disease outcomes in infected human patients, suggesting that their induction of IFNs effectively limits viral replication to prevent spread[152].

Additionally, IFN production by pDCs appears to be triggered via interactions with infected cells rather than as a result of arboviral infection of pDCs themselves[153]. This means that they can avoid many of the mechanisms deployed by arboviruses to evade the type I IFN system, allowing them to carry out their function uninhibited.

Conversely, classical dendritic cells (cDCs) are primarily responsible for the priming, activation and differentiation of T cells in lymph nodes through antigen presentation on major histocompatibility complex (MHC) I or MHC II, provision of costimulatory signals and cytokines. Recent studies have shown that cDCs residing in the skin are early targets of DENV infection in mouse models and human skin samples[154,155]. Recognition of arboviral infection causes maturation of cDCs, evidenced by an increase in expression of MHC I and II and costimulatory molecules, including CD80, CD86 and CD40[156]. In addition to the direct antiviral effects of ISGs, their induction in DCs and macrophages also supports the induction of cellular and humoral immunity to arboviruses[157]. Following cDC activation and maturation, they migrate to the lymph node to carry out this function.

1.2.2 Adaptive immune response to arbovirus infection

While the innate immune response is critical for the control of acute arboviral infections, the adaptive immune system also contributes to clearance of cell-associated virus, and long-term protection, but can also play an important role in the immunopathology that underlies severe/chronic disease pathologies. During an antiviral immune response, naïve CD4+ and CD8+ T cells are primed and activated by mature DCs in the lymph nodes. Dependent on DC cytokine production and environmental cues, T cells differentiate towards one of several phenotypes. These subsets are characterised by their effector functions and production of specific cytokines. T cell-associated cytokines, including IL-10, IL-4 and IFN-γ, are produced during the immune response to arboviral infections and appear to be induced by mosquito bites and salivary factors[120,158,159].

CD8+ cytotoxic T cells are also a vital aspect of any antiviral immune response due to their ability to destroy virally infected cells, and thereby clear cell-associated virus. However, the importance of these T cell responses appears to

differ between arboviral infections. For example, CD8+ T cells are important in response to flaviviruses, with mice deficient in CD8+ T cells experiencing higher viral titres following ZIKV and DENV infections[160,161]. It appears likely that CD8+ T cells offer protection from flavivirus infection through production of IFN-γ, as high levels of this cytokine are associated with positive disease outcomes in patients[162]. Conversely, the T cell response to CHIKV in humans appears to be defined by the activation of the CD8+ response early during disease onset, with levels peaking at day 1 after symptom onset, suggesting that cytotoxic T cells act rapidly following the launch of the adaptive response to clear infected cells[123]. Despite this, cytotoxic T cells did not appear to be necessary for the control of infection with the alphavirus CHIKV in mice, as serum quantities of viral RNA in $CD8^{-/-}$ mice was not different from that of WT mice[163].

CD4+ T cells promote the antiviral response primarily by interacting with other immune cells through the production of soluble mediators, including providing vital support to B cells to induce antibody production. Interestingly, CD4+ T cells do not appear to be necessary to control flavivirus infection, as depletion of CD4+ T cells had no effect on DENV infection in mice, with viral titres, CD8+ T cell and B cell responses remaining the same[164]. However, during SFV infection they are required to provide help to B cells to class switch to enable IgG production[165]. This is crucial for host protection as IgM cannot enter the brain, the main site of SFV pathology.

However, T cells may also contribute to arboviral disease pathologies. High levels of activated T cells, both CD8+ and CD4+, have been linked to severe arthralgia following CHIKV infection[166]. In fact, a novel treatment for CHIKV infection was trialled in mice which included cytotoxic T-lymphocyte associated protein 4 (CTLA4)-Ig which blocks the activation of T cells. This successfully reduced swelling and ablated the monocyte and T cell infiltrate at joints[167]. Similarly, it has been shown in a mouse model of ZIKV infection, that in the case of insufficient control of the virus by the innate immune response, the recruitment of CD8+ T cells to the brain and their attempts to control infection in this sensitive organ contributes to severe neurological complications caused by ZIKV infection[168]. The association of DHF with secondary DENV infection alone provides evidence that the adaptive immune response is involved in disease

pathogenesis. However, this is further supported by the positive association between a large T cell response, characterised by high expression of the cytokines IFN-γ and TNF-α, and severe clinical symptoms in patients suffering from DHF[169]. Furthermore, CD8+ T cells are dispensable for controlling infectious virus during SFV infection in the central nervous system, however, they are required for inflammatory demyelination, which contributes to neurological pathology[165]. Therefore, it is likely that T cells contribute to immunity to arboviral infection during the acute response but that their long-term presence can contribute to severe arbovirus infection outcomes.

B cells play an important role in the response against arboviral infection, mainly through their production of viral epitope-specific antibodies which are able to neutralise pathogens. Following early control of arboviruses by IFN, the virus is cleared by antibody responses. These are mainly aimed at the E2 and E1 surface proteins of alphaviruses while they appear to be targeted at flavivirus E, prM and NS1 proteins[170,171]. CHIKV infection *in vitro*, antibodies block virion egress from host cells by causing the virus to aggregate at the cell surface[172]. Outside of antibody production, regulatory B cells, which act in an antibody-independent way to dampen the immune response via IL-10 production, may provide protection against severe arboviral disease outcomes. An association was found between low levels of regulatory B cells during the acute phase of DENV infection and severe DENV disease[173].

The human antibody response during arboviral infection is characterised by early production of IgM during the acute phase of infection which play a role in early neutralisation of virus[174–176]. This is followed by the production of IgG within a week of symptom onset and from this point, IgG antibodies take on the main role of virus neutralisation. Long term, IgM titers persist for 3-4 months before waning while IgG titers are stable for much longer, <1 year[175–177]. Additionally, early IgG production appears to be linked to protection from chronic CHIKV disease symptoms[178].

However, the antibody response also contributes to the pathogenesis of severe flavivirus infection. Primary infection with DENV confers an individual with lifelong immunity to the viral serotype that they were infected with. However,

secondary infection with heterotypic DENV is often much more severe and the antibody response contributes to this effect[179]. A certain number of antibodies must be attached to a viral particle in order for antibodies to neutralise flaviviruses. Therefore, the efficacy of antibody responses to flaviviruses is highly variable. A sub-neutralising antibody response can lead to ADE where DENV-antibody complexes are able to bind to FCγRs and use this interaction to entry cells, resulting in higher levels of viral replication which leads to increased viral loads and disease severity[157]. It has recently been shown that ADE can also occur during alphavirus infection in mice if the antibody response does not reach the neutralisation threshold[180].

Overall, the part played by the immune system in arboviral infection is nuanced and context specific. The type I IFN system induced by the innate immune response following viral recognition is necessary for infection control. However, some forms of inflammation appear to be beneficial for the virus, with neutrophil-driven recruitment of monocytes providing permissible targets of infection and perhaps a gateway to systemic spread. Likewise, it appears that the adaptive response acts as both friend and foe. T cell responses to arboviral infection appear in some contexts are required to e.g. aid clearance of virus, and provide lasting immune memory, but conversely can also contribute to immunopathology. In terms of the role of humoral immunity, while antibody responses are often key for neutralising virus and ‘mopping up’ any virus left over after initial clearance by the innate immune response, antibodies also have been shown to facilitate a number of arboviral infections, through ADE, by providing them with a docking point to gain entry to host cells.

1.2.3 Modulation of host susceptibility to infection by mosquito bite

In recent years, it has become widely accepted that the role played by the mosquito vector during arbovirus infection contributes more to infection outcomes than simply transmitting virus to the host; the mosquito bite itself enhances host susceptibility to infection. As discussed, an arbovirus is transmitted when an infected mosquito bites a host to take a blood-meal. However, as well as passing on virus, the mosquito also injects saliva and bacterial components into the skin during this process. Mosquito saliva is imbued with numerous bioactive molecules which facilitate the blood-feeding

process[181]. Some of these, such as sialokinin, have antihemostatic properties, which can prevent blood clotting and promote vasodilation, amongst other functions[126,182]. There are also proteins present in saliva, including the D7 protein family, which scavenge host proteins, including histamine, which promote itching following injury, to prolong the length of time the mosquito can feed for before the host notices[183].

However, as well as helping the mosquito find a blood meal, these salivary proteins can also modulate the host response to arboviruses. Indeed, when mice are infected with an arbovirus alongside a mosquito bite, mosquito saliva or salivary gland extract (SGE), there is an increase in virus replication in the skin and blood, resulting in dissemination to remote tissues and increased mortality as a result[120,134]. This is not the result of the trauma of the bite itself or the microbial components which are injected during transmission[126]. Indeed, it is the mosquito-encoded salivary gene products that causes this enhancement of arbovirus infection. Mosquito salivary proteins, such as sialokinin, increase vascular permeability, driving oedema at the bite site[126,182]. This facilitates entry of myeloid cells to the site of infection, some of which are susceptible to virus infection, such as monocytes[120,126]. Therefore, the mosquito bite appears to make the host more susceptible to arbovirus infection through interference with the host inflammatory response. Identifying factors which alter susceptibility to infection and which are common to all infections, such as the mosquito bite, could identify potential targets for developing pan-arboviral vaccines or therapeutics[119,184]. Such factors may also be of use in terms of stratifying patients at-risk of serious infection outcomes.

1.3 Skin biology

There are a number of complex interactions that occur during transmission of an arbovirus, involving input from the virus, the vector and the host. As arboviruses are transmitted via a mosquito bite at the skin, this intricate interplay during acute infection takes place at both the cellular and molecular level in this major organ. This makes it essential to understand skin biology when considering host susceptibility to arbovirus infection.

1.3.1 Skin structure

The skin is the main barrier site of the human body, protecting us from many external threats ranging from sterile injury to environmental agents, such as UV exposure, to skin-transmitted infections[185]. The two main layers of the skin are the epidermis and the dermis. The epidermis is the outermost layer of the skin and the dermis sits underneath this (Figure 1.5). Beneath the dermis, there is a subcutaneous fatty layer, the panniculus adiposus.

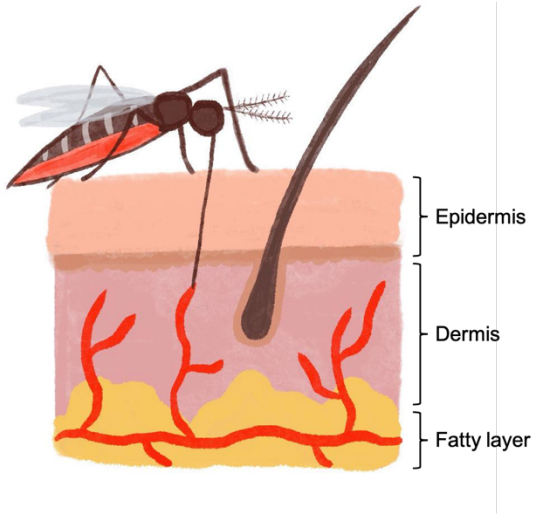

Figure 1.5 | Structure of the skin

The three main layers of the skin are the epidermis, dermis and the fatty layer, or panniculus adiposus. When a mosquito takes a blood meal, it probes the vascularised dermis looking for a blood vessel. As a result, arboviruses are transmitted in this layer.

The epidermis is a stratified epithelium which is split into five layers[186]. The stratum corneum is the outward facing layer. This is followed by the granular layer, the spinous layer and the basal layer, with the basement membrane separating the epidermis from the dermis. It is mainly keratinocytes that make up the epidermis and these are key for the self-renewal of the skin[187]. These proliferate in the basal layer and move up through the layers to replenish the tissue, differentiating as they progress. Other cell populations in the epidermis include melanocytes, which produce pigment, and some skin-resident immune cells, including the antigen-presenting Langerhans cells[185].

The dermis largely functions as a supportive structure in the skin. The extracellular matrix (ECM) components collagen and elastin are littered

throughout the dermis, facilitating the layer's function[188]. The cellular component of the dermis consists mainly of fibroblasts, which provide the ECM components, mast cells and resident monocytes/macrophages. The dermis has a network of blood vessels, which provide the blood supply for not only the dermis, but also the epidermis, which does not possess its own blood vasculature. For this reason, the dermis is the site where a mosquito probes when trying to source a blood meal (Figure 1.5)[189]. Consequently, arboviruses are transmitted at and mainly replicate in the dermis[154]. Dermal fibroblasts are permissive to infection with multiple arboviruses[145,190,191]. Although keratinocytes and Langerhans cells have also been shown to be susceptible to infection by several different arboviruses, including DENV and WNV *in vitro*, it is unlikely that they contribute significantly to the virus burden *in vivo*, due to their positioning in the epidermis[192–194].

As this thesis uses *in vivo* mouse models of arbovirus infection, it is worth highlighting some differences between human skin and mouse skin. Broadly, human and murine skin is similar. However, the epidermis and dermis in the skin of mice are both thinner than in human skin[195]. Furthermore, in murine skin there is a striated muscle layer, the panniculus carnosus, which sits beneath the fatty layer and separates the skin from the rest of the body[196]. Exceptions to this include the skin on mouse ears and the dorsal (upper) side of the feet, that lack underlying muscle. Furthermore, mice have a dense layer of hair, or fur, covering most of their bodies, whereas hair on human skin is much more sparsely distributed. However, experiments used within this thesis have been designed in such a way to minimise differences between the two. For example, infections are inoculated at the skin on the upper foot of mice, an area which is naturally hairless and so better mimics human skin.

1.3.2 Inflammation in the skin

Inflammation is triggered in the skin during infection or in response to other external stimuli, including UV exposure, as a means of protecting the host. Skin-resident immune cells kickstart inflammatory processes upon recognition of pathogen-associated molecular patterns (PAMPs) or damage-associated molecular patterns (DAMPs), which are present in the skin during infection and/or skin damage. In response, leukocytes, including Langerhans cells, and,

importantly, skin-specific keratinocytes and fibroblasts rapidly produce pro-inflammatory cytokines, including IL-1, TNF-α and IL-16[197]**.** Importantly, keratinocytes act as key regulators of inflammation in the skin, producing inflammatory mediators throughout the process. Consequently, they are implicated in the pathogenesis of many inflammatory skin conditions[198,199]. Cytokine expression can further amplify the inflammatory response, including by activating skin-resident immune cells, such as Langerhans cells and dermal cells such as resident macrophages and DCs. Recruitment of blood derived leukocytes and plasma components, such as complement is aided by permeabilisation of blood vasculature, presentation of chemokines and changes to adhesion molecule expression. Vascular permeability rapidly increases due to the actions of several molecules, including prostaglandins[200]. Together, this facilitates the entry of immune cells to the skin, requiring interactions with adhesion molecules expressed on endothelial cells, such as selectins and integrins[201]. Once in the skin, these cells can enact a number of mechanisms to modulate immunity to pathogens.

The first responders that are recruited to the skin during inflammation are circulating neutrophils and monocytes, which are attracted mainly in response to the chemokines CXCL2 and CCL2, respectively[185]. Monocytic cells differentiate into macrophages or DCs when they leave the circulation. Both macrophages and neutrophils can rapidly phagocytose pathogens or cell debris in the skin. These cells can also further drive inflammation by contributing to pro-inflammatory cytokine expression. Furthermore, neutrophils can release the antimicrobial contents of their intracellular granules, a process called degranulation, and trap infectious agents in NETS made of strings of DNA[202,203]. Macrophages, alongside dermal CD11b+ DCs, are professional antigen-presenting cells and so link the innate and adaptive response by presenting antigen-derived peptides to T and B cells on MHC class II[204,205]. Activated lymphocytes enact a more targeted response to ensure efficient clearance of any external threat.

Once pathogens have been cleared, it is vital that inflammation resolves to avoid further damage to the host tissue. However, this does not always occur[206]. Aberrant host inflammatory responses can be hugely damaging and can result

in a number of inflammatory skin conditions, such as psoriasis[207]. This is covered in more detail in Section 1.5.1.

1.3.3 Cutaneous wound healing

As introduced above, following an inflammatory response, the skin environment must switch from being highly pro-inflammatory, to anti-inflammatory in order to limit immunopathology[208]. In addition to protecting the skin from further damage, it is also vital to heal any cutaneous damage which occurred as a result of the inflammatory insult[209]. Of course, skin wounds can happen as a result of a number of events, from sterile injury to a bacterial infection. However, the process of cutaneous wound-healing has several key stages regardless of the causative agent.

There are 4 main phases which take place during wound healing: hemostasis, inflammation, proliferation and remodelling. The timing of these can overlap one another. If wound healing is successful, this process will return the skin back to the healthy, resting state with full barrier function. The first stage, hemostasis, occurs immediately after the skin barrier is broken when a wound is made. During this, blood vessels constrict and platelets form a clot to stem any bleeding as a result of clotting cascades[210]. Once this is under control, inflammation occurs in response to endogenous or exogenous insult. During this phase, any infectious agent present is cleared from the wound site. The inflammatory stage has been covered in detail in the previous section.

The final two stages are focussed on repairing the damaged cutaneous tissue[211]. Proliferation involves several processes. Fibroblasts cover the wound site to provide a scaffold on which cells can migrate over to rebuild the rest of the tissue[212]. This provisional structure is called the granulation tissue. Immune cells, particularly macrophages, orchestrate this process through production of cytokines and growth factors which drive fibroblast migration, including transforming growth factor beta (TGF-β)[213]. However, keratinocytes are also vital during this, both in terms of activating fibroblasts but also become highly proliferative to provide the building blocks for the rebuilding of the damaged epithelial layers, referred to as re-epithelialisation[210,214]. This occurs in response

to nitric oxide, produced my macrophages in the wound[215]. Angiogenesis takes place to revascularize the tissue, in response to growth factors vascular endothelial growth factor (VEGF) and platelet-derived growth factor (PDGF)[216]. Finally, the remodelling phase beings once the granulation tissue is in place. Fibroblasts differentiate into myofibroblasts in response to TGF-β. These cells produce ECM components, primarily collagen, which completes the process and forms scar tissue, a process that involves fibrosis[213].

Macrophages are critical throughout the wound healing process. During wound healing, macrophages undergo a switch in phenotype between the inflammation and proliferation phase; from highly pro-inflammatory M1 macrophages to anti-inflammatory M2 macrophages[217]. This change corresponds with altered receptor expression and cytokine production which reflects the different requirements in the tissue as the rebuilding process gets underway. M2 macrophages express a number of the key soluble mediators mentioned earlier, including pro-angiogenic growth factors including PDGF, VEGF and anti-inflammatory cytokines TGF-β and IL-10[218]. These cells therefore directly dampen the inflammatory environment in the skin and promote re-epithelialisation and blood vessel formation. When macrophages are depleted *in vivo* during the inflammation or proliferation phase, mice are unable to properly repair a cutaneous wound[219]. The effect of depletion at both of these stages has on tissue repair likely means that both the M1 macrophages, more prevalent during inflammation, and the M2 macrophages, the main macrophage type involved in proliferation, are critical for successful wound healing.

1.4 Ultraviolet radiation

The factors that modulate outcome to arbovirus infection remain to be understood. As discussed in Section 1.2.3, it is known that the mosquito bite required to transmit many arboviruses does itself drive inflammation, and that this inflammation worsens virus infection outcomes for the host[120,126]. Further evidence that suggests immune responses of the skin define outcome to infection are supported by those studies in which pre-priming IFN signalling, using a therapeutic agent, suppressed arbovirus infection[119]. Therefore, pre-existing inflammation at the site of infection, the skin, caused by other viral, host

or environmental factors have the potential to modulate host susceptibility to arbovirus infection.

Exposure to ultraviolet (UV) light is one of the main environmental factors which impacts human health[220]. UV exposure of the skin has numerous biological effects, which are discussed in more detail below. Furthermore, arboviruses are transmitted in regions where individuals are exposed to high levels of environmental UV light[35,221]. Therefore, it is important that any potential impact of UV exposure has on modulating host susceptibility to arbovirus is considered.

1.4.1 UV radiation as an environmental inducer of skin inflammation

UV light is one of three types of radiation emitted by the Sun, along with infrared and visible light[222]. However, UV is the only type to have damaging effects on the skin. There are three types of UV rays, categorised based on their wavelengths: UVA (long wavelength, 320-400nm), UVB (medium wavelength, 290-320nm) and UVC (short wavelength, 200-280nm)[223]. Only UVA and UVB reach the surface of the Earth and so are relevant to human health[224]. UV rays from the Sun consist of 95% UVA and 5% UVB[225].

There are differences between UVA and UVB in terms of their impact on the skin. UVB only penetrates the epidermis, whereas UVA goes deeper into the dermis[223]. UVB is unique in that it drives the skin's sunburn response[226]. Both contribute to skin aging and wrinkling as a result of chronic exposure[222]. UV radiation (UVR) directly damages DNA and proteins in the skin and triggers local ROS production, which is also harmful to DNA[227]. As a result, UV exposure is the main causative agent of skin cancer. UVB is the most harmful type and so is the most widely studied.

Exposure of the skin to UV does have some benefits. Sunlight drives vitamin D production, through the conversion of 7-dehydrocholesterol into pre-vitamin D_3, which eventually becomes vitamin D_3[228]. Humans need vitamin D to absorb calcium from food, to support bone development[229]. Individuals who live in regions of the world with lower levels of sunlight, such as the UK, often have to

take vitamin D supplements to boost natural levels[230]. Nevertheless, the risks of high levels of UV exposure are clear.

1.4.2 Effects of UVR exposure on the skin

The initial response to UV in the skin is inflammatory. UVR is absorbed by light-absorbing molecules, or chromophores, in the skin, including DNA, RNA and melanin[227]. Absorption by DNA, mainly in keratinocytes and Langerhans cells, drives inflammatory process due to the damage caused to DNA, with some cells undergoing apoptosis[231,232]. DAMPs produced during this are recognised by neighbouring keratinocytes via TLR3, 4 and 9[233–235]. Production of pro-inflammatory transcription factors, including NF-κB, is kickstarted in response to DAMPs produced during this[223]. This induces expression of a whole programme of inflammatory cytokines, including IL-10, IL-4 and TNF[236]. UV also causes blood vessels to dilate[237]. Together, this results in an influx of myeloid cells to the UV exposed skin[238]. This early inflammatory stage causes the skin to appear red, known as erythema, swell and feel hot to the touch[226]. These clinical signs define the condition sunburn.

Following this initial response, there is an increase in mitosis and DNA synthesis[239,240]. This results in proliferation of cells in the skin, particularly keratinocytes[241]. This hyperplasia causes a thickening of the epidermis[232,240]. It is thought that this occurs as a means of protecting from subsequent UV exposure. The melanin pigment produced by melanocytes in the epidermis also helps to protect against the negative consequences of UV exposure by absorbing much of the radiation[220,242]. It is produced in the basal layer and passed to keratinocytes for protection. Epidermal melanin expression and distribution increases following exposure to UV[243].

The immunomodulatory effects of UV exposure can be harnessed in terms of treating some inflammatory skin conditions, such as psoriasis, through phototherapy[207]. However, this feature also at least partially contributes to the generation of skin cancers, in addition to UV-mediated DNA damage[244]. It has also been shown to alter susceptibility to some infections, which is discussed further in Section 1.4.3.1.

1.4.2.1 Variable responses to UV exposure between individuals

UV exposure of the skin does not always result in sunburn. Skin can also darken, or tan, in response. Tanning occurs as a result of melanin production in response to UV[245]. Whether skin burns or tans is largely defined by the dose of UV the skin was exposed to and the skin phototype of an individual. The Fitzpatrick phototyping scale is widely used to characterise different skin types. The scale classifies skin types, ranging from type I, the palest skin, to type VI, the darkest skin (Table 1.1)[246]. This can be used to determine the extent to which an individual develops an erythemal skin response to UVR exposure. Skin colour is determined by the amount of the pigment melanin in the skin[243]. As melanin protects from UVR, individuals with the lightest skin are broadly more susceptible to sunburn and UVR-mediated skin damage.

Table 1.1 | Fitzpatrick phototyping scale

Fitzpatrick skin phototype	**Reaction of skin to UVR**
Type I	Always burn, never tan
Type II	Usually burn, tan less than average (with difficulty)
Type III	Sometimes mild burn, tan about average
Type IV	Rarely burn, tan more than average
Type V	Brown skin
Type VI	Black skin

Human behaviour can also greatly impact how much UVR an individual is exposed to. Two individuals who both live in the same region of the world can each be exposed to very different amounts of UV each day[247]. For example, one individual may be exposed to UV in very low doses for short periods daily, while carrying out everyday tasks outdoors. Another may spend a longer period outdoors, e.g. due to working outside, and thus be exposed to much higher levels of UV, which is considered more harmful.

1.4.3 Impact of UVR on skin immunity

Importantly, exposure to UV is an environmental factor that is known to alter immune sensitivity at the skin, ranging from immunosuppression to inflammation[223]. As mentioned, the immunosuppressive capabilities of UV exposure can be used to treat some autoimmune skin conditions. However, UV exposure can also trigger other inflammatory conditions, such as systemic lupus erythematosus[248]. Clearly the effect UV exposure has on skin immunity is multifactorial and context dependent.

The early response to UV exposure in the skin, as detailed in Section 1.4.2, is inflammatory and is governed by the innate immune response. Interestingly, the profile of the innate response to UV exposure in the skin appears to be dependent on the dose of UVR *in vivo*[240]. A single harmful exposure to the skin of mice, modelling sunburn in humans, appears to induce a strong inflammatory state in the damaged skin. Some aspects of this response are similar to that observed in normal skin following a mosquito bite[232,240]. In both cases, skin is characterised by an increase in expression of inflammation-associated cytokines and chemokines, including IL-6, TNF-α, CCL2 and CXCL2, with a corresponding increase in the presence of neutrophils and macrophages at the site. Interestingly, the opposite appears to be true following repeated low doses of UV, a model of daily, tanning exposures[240]. Here, the skin is characterised by thickening of the epithelium and an upregulation of antimicrobial peptides, including β-defensins and PRRs, suggesting that the organ is in a primed state. This is perhaps not surprising as infection of UV-blistered skin, in which barrier function is compromised, is common without intervention. In addition, numerous dying cells must be cleared by phagocytes to prevent inflammatory necrosis. Therefore, immune responses in UV-exposed skin, e.g. during infection, may be different based on the dosage of UV the skin has been exposed to.

1.4.3.1 Altered infection outcomes following UV exposure

The changes to immune responses following UV exposure discussed in the previous section can impact on host susceptibility to infection. UV-induced immunosuppression can reactivate latent HSV and varicella zoster virus (VZV) infections, two skin-associated infections[249,250]. UVR exposure also appears to stunt immunity to fungal and bacterial infections, including *Candida albicans*

and *Borrelia burgdorferi*[251,252]. Interestingly though, UV exposure has also been associated with protection from infection with both influenza and *Mycobacterium tuberculosis* at tissues remote from the skin[253,254]. This variability between individual pathogens is likely due to the differences in host response that mediate host resistance to infection. Skin immune microenvironment that is modified by UV exposure may offer resistance against one pathogen, but may not be conducive to protection against another. Differences in local (UV exposed) and systemic (not UV exposed) responses to UV may also explain these findings, as e.g. influenza infects internal mucosal tissue, remote from the skin. Despite the relevance of UV light as a potential environmental factor that modulates arbovirus infection outcome, this remains to be investigated.

1.5 Inflammatory diseases

As previously mentioned, the presence of pre-existing inflammation at the skin has the potential to modulate host susceptibility to subsequent arbovirus infection. Another example of this, is inflammation that results from a pre-existing inflammatory disease. There are a large group of inflammatory skin disorders, including psoriasis which are characterized by chronic, dysregulated inflammation in the skin. Furthermore, other systemic inflammatory conditions, which have effects throughout the body, such as systemic sclerosis, also impact the inflammatory environment at the skin. Both conditions involve dysregulation of type I IFN responses. As type I IFN responses are critical for clearance of arbovirus infection, the inflammatory profile of these conditions have the potential to alter arbovirus infection outcomes in these patients.

1.5.1 Psoriasis

Psoriasis is a common chronic inflammatory autoimmune condition, which affects nearly 2% of the population globally[255]. The disease is caused by the uncontrolled expansion of keratinocytes in the outer layer of the skin, the epidermis[199]. This is driven by a prolonged state of inflammation caused by an infiltrate of immune cells at the site[256]. The most common clinical presentation of this expansion takes the form of inflamed skin lesions or ‘psoriatic plaques’ which are red and scaly in appearance[257]. However, the disease can vary greatly in terms of severity between patients.

1.5.1.1 Immune pathogenesis of psoriasis

The pathogenesis of psoriasis appears to be dependent on complex interactions between immune cells, their positioning and their production of cytokines. The inflammatory infiltrate present at the site of lesions is composed of a number of innate leukocytes, dermal DCs, macrophages and neutrophils but also includes T cells[257]. In particular, it is thought that a perpetuating inflammatory cycle involving dermal DCs and keratinocytes drives psoriasis pathology[258]. Once established, this cycle is driven by a pro-inflammatory Th17 immune response[259]. Much of the pathogenesis driving psoriasis has been elucidated based on which immunosuppressive drugs work to stifle the symptoms of the disease. For example, anti-IL-17 and anti-IL-23 treatments have been particularly effective in the clinic[207,260]. The success of blocking these Th17 cytokines therapeutically gives evidence that these cytokines support the perpetuation of an inflammatory state in the skin of psoriatic patients[261].

Psoriasis can develop when a genetically predisposed individual is exposed to one of several possible external insults[262,263]. Proposed triggers for psoriasis include infection, skin injury or certain medications, including β-blockers[264–266]. Whatever the inducing factor, this results in release of host DAMPs, mainly self-nucleotides, in the skin[257]. Recognition of these via TLR7 and TLR9 drives the production of several inflammatory cytokines, including, notably, type I IFNs, by pDCs[267]. pDCs also present self-antigen to CD8+ T cells, driving expansion of this auto-reactive population. Furthermore, the pDC-produced IFN-α and IFN-β activate dermal DCs which produce IL-12 and IL-23[258]. These push T cell differentiation towards a Th1 phenotype and promote the expansion of the Th17 population[259]. This drives the Th1/Th17 axis, a key characteristic of psoriasis[207]. Cytokines produced by these two populations of T cells, IL-17 by Th17 cells and TNF-α by Th1 cells, act on keratinocytes to trigger production of inflammatory cytokines, including more TNF-α, and chemokines, such as the T cell and DC chemoattractant CCL20[268]. Together, this inflammatory milieu promotes keratinocyte proliferation, dilation of and formation of new blood vessels and the recruitment of innate immune cells to the skin[257,269]. The continual amplification of the inflammatory environment creates a self-perpetuating cycle and leads to

the formation of the psoriatic skin lesions observed in patients[258]. This pre-primed inflammatory profile, particularly with regards to type I IFN expression, may be of great relevance in terms of how these patients respond to arbovirus infection.

1.5.2 Systemic sclerosis

Systemic sclerosis is an autoimmune, rheumatic condition in which skin is the major affected organ[270]. Patients experience skin fibrosis, which causes skin tightness and itching. This fibrosis also extends to internal organs, including the lungs. Patients also often experience vasculopathy[271]. This can present as Raynaud's phenomenon, which occurs due to restriction of blood flow to the extremities, leading to these turning pale or blue and feeling painful or numb. Systemic sclerosis is relatively rare but has an extremely high morbidity and mortality rate considering its prevalence. In fact, the disease has the highest mortality rate of any rheumatic condition[272]. There are two main subsets of systemic sclerosis: limited cutaneous and diffuse cutaneous[273]. Disease in patients with limited cutaneous systemic sclerosis is restricted to skin below the elbows and knees and on the face and neck. Diffuse cutaneous systemic sclerosis is more severe, affecting skin all over the body. Following assessment of symptoms, diagnosis of systemic sclerosis is usually confirmed through the identification of auto-antibodies against centromeres, in patients with limited cutaneous systemic sclerosis, or RNA polymerase, in those with diffuse cutaneous systemic sclerosis[274].

1.5.2.1 Immune pathogenesis of systemic sclerosis

Systemic sclerosis is triggered by an as yet unknown environmental factor(s). However, following a stimulus, disease development begins with damage to the vasculature[275]. This leads to thickening of blood vessels which reduces the flow of oxygen to tissues. Endothelial cells in affected vessels upregulate adhesion molecules, including VCAM1 and ICAM, which facilitates the entry of leukocytes to impacted tissues[276]. These create a highly inflammatory environment through production of cytokines, including TGF-β, IL-1 and IL-6, which promote tissue fibrosis[277].

Systemic sclerosis is characterised by a type I IFN signature[278]. In response to TLR-recognition of DAMPs in affected tissues, recruited leukocytes, mainly monocytes, macrophages and pDCs, and tissue-resident fibroblasts all express high levels of ISGs[279,280]. This inflammatory environment activates local fibroblasts. These differentiate into myofibroblasts which overproduce ECM component, such as collagen and fibronectin, causing tissue fibrosis, a hallmark of systemic sclerosis[281,282]. The presence of these molecules stimulates TLR4 on DCs, which drives additional production of IFN-α by these cells, further amplifying disease pathology[277].

Current treatment options are very limited but mainly involve controlling skin-related symptoms through immune suppression e.g. using methotrexate. More recently, targeting pDC production of type I IFN has been identified as a potential therapeutic strategy for controlling systemic sclerosis[283]. In fact, this dysregulation of type I IFN is so linked to systemic sclerosis disease pathology that clinicians can use an IFN score, based on an individual's serum ISG levels, to stratify patient risk of developing severe disease[284]. This key involvement of the antiviral IFN system in systemic sclerosis patients indicates that responses to arbovirus infection may be altered in this cohort.

1.6 Project rationale and aims

1.6.1 Identifying inflammatory factors with the potential to modulate host susceptibility to infection

Mosquito-borne virus infections, or arboviruses, currently present a huge burden to human health globally. However, the number of people at risk of arbovirus infection is only predicted to get worse in coming decades. Transmission zones are continually widening due to expansion of the principal arbovirus vector, the *Ae. aegypti* mosquito. Several arbovirus infections, including DENV, ZIKV and CHIKV, can cause severe, potentially life-threatening disease.

Crucially, factors that contribute to development of severe disease are unclear. The continuing expansion of arboviruses will expose new, immunologically naïve populations to infection. Furthermore, there are no antivirals available to

treat arboviral disease and effective, safe vaccines are only available for a few of these viruses. To enable us to better prepare for the predicted increase of arbovirus cases in the coming years, and for those presently at risk of arbovirus infection, we need to improve our understanding of the pathogenesis of these viruses and how factors, including those deriving from the virus, host and the environment, alter susceptibility to infection.

Previous work has shown that the mosquito bite which transmits virus at the skin enhances arbovirus infection by driving the creation of an inflammatory environment at the skin[120,126]. This includes an influx of virus-permissive monocytes, providing the virus with new targets for infection. Similarly, there are several other pro-inflammatory contexts that have the potential to alter host susceptibility to arbovirus infection. This includes environmental factors, such as UV exposure, to host factors, such as pre-existing inflammatory conditions. Identification of such modulating factors is crucial for better understanding the molecular and cellular basis of host susceptibly to virus. Such insights may also inform better patient management e.g. through more nuanced stratification of patients at risk of severe arboviral disease.

1.6.1.1 UV exposure of skin prior to infection

Critically, arbovirus infections are generally endemic in sub-tropical and tropical regions of the world, where UV light levels are high. However, exposure to UV, and individual sensitivity to this exposure, varies substantially depending on lifestyle, employment and host genetics. As such UV is a key environmental variable, and defining whether host response to such exposure modulates host susceptibility to infection is a key question. Yet there have been no previous studies which have investigated whether UV exposure of the skin has any impact on arbovirus infection outcomes.

In Section 1.4.3, we outlined the way UV exposure of skin in mice modulates innate immune responses. An effective, robust innate response to arbovirus infection is critical for limiting virus replication, dissemination and successful clearance. Therefore, the inflammatory response to UV exposure of the skin, including induction of pro-inflammatory cytokines and chemokines, could impact the ability of the host to respond to arbovirus infection, when virus is transmitted

at UV-exposed skin. Furthermore, previous studies have shown that the profile of innate immune responses in the skin following UV exposure is highly dependent on whether the skin was exposed to a high, erythemal dose of UV or to low, repeated, sub-erythemal doses of UV[240]. Therefore, if UV exposure prior to infection does alter host susceptibility to infection, the extent to which this occurs could also differ based on UV dosage given.

This evidence leads us to present the first hypothesis of this thesis:

We hypothesise that UV exposure of skin prior to infection will modulate antiviral immune responses, making the host more susceptible to SFV infection.

1.6.1.2 An inflammatory environment in the skin due to inflammatory disease

Chronic inflammatory diseases are responsible for over 50% of deaths worldwide, meaning that the majority of individuals will suffer from one of these conditions during their lifetime[285]. Many of these conditions involve the skin in some way and drive inflammation at this tissue as a result. The immune pathogenesis can vary greatly between diseases. However, two that are of great relevance with relation to immunity to arbovirus infections are psoriasis and systemic sclerosis. Despite the disease presentation of each being very different, both conditions are characterised, to varying extents, by dysregulation of type I IFN responses. Effective type I IFN responses are essential for host clearance of arbovirus infections. Therefore, if these responses are pre-primed in the skin of patients with psoriasis or systemic sclerosis, this could mean that they are better able to respond to arbovirus infections.

Interestingly, the inflammatory processes which drive symptoms at the skin in each of these two diseases lead to the production of soluble inflammatory mediators, which can have systemic effects, e.g. in the blood[284,286–288]. Therefore, PBMCs from these patients may also experience an immune-altered state and show resistance to arbovirus infection. Arbovirus dissemination to the blood is a critical stage in the development of severe disease, as it facilitates spread to fragile organs, such as the brain.

Preliminary experimental findings from *ex vivo* human skin models carried out by previous members of our group suggest that lesional skin from psoriasis patients is more resistant to infection by an arbovirus when compared to non-lesional skin. These findings suggest that the immune characteristics observed in psoriasis are somehow beneficial in resisting arboviral infection. However, it remains to be determined which aspects of this immunological profile contributes to this modulation in susceptibility. It is also not known whether PBMCs from psoriasis patients, the monocytes of which are the main target for ZIKV infection in humans, exhibit altered susceptibility to virus. Additionally, we have not carried out any investigations using samples from systemic sclerosis patients.

Therefore, the second hypothesis of this thesis is as follows:

We hypothesise that PBMCs from psoriasis patients and systemic sclerosis patients will be resistant to ZIKV infection due to their dysregulated type I IFN function.

Just as the burden of arbovirus infections is increasing, as is the number of individuals with chronic inflammatory conditions. While historically, the regions in which psoriasis is most prevalent and the transmission zones of arboviruses have had limited overlap, the growth in prevalence of both, combined with a rise in international travel, means there is increasing need to evaluate whether dermatological patients have differing susceptibilities to arbovirus infection. Understanding the impact that the disease state has on outcomes of arbovirus infection will inform not only our understanding of the pathogenesis of arboviruses, but also the molecular processes underlying these inflammatory conditions.

1.6.2 Thesis aims

Overall, host inflammatory responses, and factors which interfere with these, such as the mosquito bite, are clearly vital for determining virus replication in the skin and dissemination to other tissues. So other factors which have the potential to interfere with these could be of great relevance. This makes it important to understand whether either UV exposure, as an environmental

factor, or the presence of pre-existing inflammatory disease, as a host factor, can modulate host susceptibility to arbovirus infection in the skin.

Therefore, the overall aims of this thesis are:

1) **To investigate whether UV exposure of skin modulates the severity of SFV infection in mice**
2) **To characterise the immune response to SFV infection in mice pre-exposed to UV**
3) **To assess whether susceptibility to ZIKV infection is altered in PBMCs from patients with psoriasis or systemic sclerosis**

Chapter 2: Methods

2.1 General reagents and buffers

A number of general reagents and buffers were used throughout this thesis, details of which can be found in Table 2.1.

Table 2.1 | Composition of reagents and buffers used

Reagent or buffer name/type	Composition and/or manufacturer
Cell Lysis Buffer	20 mL Lysis Buffer from PureLink RNA Micro Scale Kit (Invitrogen) and 1% 2-Mercaptoethanol (Gibco).
Flow cytometry Buffer	100 mL PBS (Gibco) with 0.5% fetal bovine serum (FBS) (Gibco) and 2 mM EDTA (Invitrogen).
Hanks Balanced Salt Solution	With calcium, magnesium and glucose (Gibco)
MACS Buffer	100 mL PBS (Gibco) with 1% FBS (Gibco) and 2 mM of EDTA 0.5 M (Invitrogen).
PBS	Dulbecco's Phosphate-Buffered Saline (PBS) without calcium and magnesium (Gibco).
PBSA	100 mL PBS (Gibco) with 1.5g of 15X bovine serum albumin (BSA) (Sigma-Aldrich).
Tissue Digestion Mix	900 µL Hanks' Balanced Salt Solution (HBSS) (Sigma-Aldrich), 100 µL (1 mg/mL) Collagenase D (Roche/Sigma-Aldrich), 50 µL (0.5 mg/mL) Dispase II (Roche) and 8 µL (0.1 mg/mL) of DNase I (Roche).
0.1% Toluidine Blue	0.1 g of Toluidine Blue (Sigma-Aldrich) with 100 mL deionised water.
1% Crystal Violet	10 g Crystal Violet (Fluka Analytical) with 200 mL 100% ethanol (Sigma-Aldrich)

	with 800 mL deionised water.
1% Evan's Blue Dye	1g Evan's Blue powder (Sigma-Aldrich) with 100 mL PBS (Gibco).
1.2% Avicell	6 mL Avicell (Sigma-Aldrich) with 494 mL deionised water.
4% PFA	10 mL of 37-41% paraformaldehyde (PFA) (Fisher Scientific) with 90 mL deionised water.
10% PFA	135 mL of 37-41% paraformaldehyde (Fisher Scientific) with 365 mL deionised water.

2.2 Cell culture

Cell lines were used for plaque assays (Section 2.21), serum neutralisation assays (Section 2.22) and to grow virus stocks. The compositions of the different cell medias used for cell culture are detailed in Table 2.2.

Table 2.2 | Details of cell culture media used

Medium type		**Medium composition**
Dulbecco's Modified Medium (DMEM)		DMEM (Gibco) supplemented with 5% FBS (Gibco), 100 units/mL Penicillin and 0.1 mg/mL Streptomycin (Gibco), 1% Glutamax (Gibco) and 1% Tryptose Phosphate Broth (TPB) (Sigma Aldrich).
Roswell Park Memorial Institute (RPMI)	For use with human cells	RPMI (Gibco) supplemented with 5% FBS (Gibco), 100 units/mL Penicillin and 0.1 mg/mL Streptomycin (Gibco), 1% Glutamax (Gibco).
	For use with murine cells	RPMI (Gibco) supplemented with 5% FBS (Gibco), 100 units/mL Penicillin and 0.1 mg/mL Streptomycin (Gibco), 1% Glutamax (Gibco) and 500 µL Gentamicin.
Leibovitz's (L-15) Medium		L-15 Medium (Gibco) supplemented with 10% FBS (Gibco), 10% TPB (Sigma Aldrich), 200 units/mL

	Penicillin and 0.2 mg/mL Streptomycin (Gibco).
2X Minimal Essential Medium (MEM)	MEM (Temin's Modification) (2X) (Gibco) with 4% FBS (Gibco) and 200 units/mL Penicillin and 0.2 mg/mL Streptomycin (Gibco).

2.2.1 BHK-21 cells

Baby hamster kidney fibroblast (BHK-21) cells were used to grow SFV and ZIKV stocks. Additionally, plaque assays were performed using BHK-21 cells to titre virus stocks and to ascertain *in vivo* viremia. BHK-21 cells were stored in liquid nitrogen long-term. When required, cells were thawed in a water bath at 37 °C before being immediately moved to a 75 cm^2 culture flask (Corning) containing complete DMEM (Table 2.2). BHK-21 cells were incubated at 37 °C, 5% CO_2 in complete DMEM. Cells were passaged when 80% confluence was reached by washing in PBS, then applying 0.25% Trypsin-EDTA (Gibco) for 3-5 mins to detach cells from the surface of the flask. Complete DMEM was then added to inactivate the Trypsin. Cells were split into new flasks in a 1:10 dilution.

2.2.2 C6/36 cells

Aedes albopictus clone C6/36 (C6/36) cells, derived from *Ae. albopictus* mosquitos, were used to grow ZIKV stocks. C6/36 cells were stored in liquid nitrogen long-term. When required, cells were thawed in a water bath at 37 °C before being immediately moved to a 75 cm^2 culture flask (Corning) containing complete L-15 Medium (Table 2.2). C6/36 cells were cultured at 28 °C, 0% CO_2 in complete L-15 Medium. Cells were passaged when 80% confluence was reached. Briefly, cells were washed with PBS, 10 mL of fresh media was added and cells were gently detached by manual cell scraping. Cells were split into new flasks in a 1:10 dilution.

2.3 Viruses

Virus stocks of wildtype SFV4 and recombinant SFV6 containing the genetic marker mCHERRY (SFV6-mCHERRY) were generated from plasmids containing the genomic sequence, kindly provided by Prof. Andres Merits, University of Tartu. Originally, plasmids were electroporated into BHK- 21 cells to generate infectious virus. ZIKV from Recife, Brazil was kindly provided by

Prof. Alain Kohl, University of Glasgow. All viruses were passaged once in C6/36 cells. Cell supernatant was clarified and the titre was determined using plaque assay in BHK-21 cells to determine virus titres. Before storage, virus was snap frozen using liquid nitrogen. Virus was stored short-term for up to 1wk at -80 °C or long-term in liquid nitrogen.

2.4 Mice

C57BL/6 mice were bred in the animal facilities within the Clinical Sciences Building at the University of Leeds campus at St James's University Hospital. *Ifnar*$^{-/-}$ mice, bred on a C57BL/6 background, were originally purchased from Jackson Laboratories, USA. Breeding stocks were maintained in the St James's Biomedical Services (SBS) facilities (University of Leeds). All mice were housed and maintained in the SBS facility under specific pathogen-free conditions in accordance with UK Home Office regulations. All mice were between 4-12 wks old at time of use and were age and sex matched for experiments. All *in vivo* procedures were undertaken following local Animal Welfare and Ethical Review Body (AWERB) and Home Office (HO) approval (Personal License I07376332, Project Licences PA7CF4E75 and PP0258562).

2.5 Mosquito rearing

Ae. aegypti eggs were kindly provided by Dr Emilie Pondeville, University of Glasgow. Eggs on filter paper were placed in trays (Dutscher Scientific) filled with 1.5 cm of temperature-equilibrated tap water kept in an incubator at 28 °C and 80% humidity and left to hatch overnight. Larvae were subsequently fed cat food (GoCat) until pupation, approximately 7 days later. Pupae were transferred to water-filled containers inside BugDorm-1 mosquito cages (Watkins and Doncaster). Adult mosquitos emerged approximately 9-16 days post-hatching and were subsequently fed a 10% sucrose solution in distilled H_2O. By 21 days post-hatching, mosquitos were ready for use in biting experiments.

2.6 UV exposure of mouse skin

Before UV exposure, mice were anesthetised using isoflurane administered via inhalation. The dorsal (upper) side of the foot was placed directly on top of an 8W UVM-28 mid-range lamp (302 nm peak at 1 mW/cm, Ultraviolet Products). 20-30% of the radiation emitted by the lamp is UVA, with the remaining majority

being UVB. Mice were exposed to either 1 or 3 doses of 20 mJ/cm^2 (low or sub-erythemal dose, equivalent to 'tanning' of human skin) at the same region or 1 dose of 400 mJ/cm^2 (high or erythemal dose, equivalent to mild burning of human skin) of UVR. The UV dosage was controlled via the length of time the foot was exposed to radiation, equating to 16 secs exposure time for 20 mJ/cm^2 or 6 mins exposure time for 400 mJ/cm^2. Mice were then left between 24 hours (24h) to 3 wks post-UV exposure before being exposed to biting mosquitos and/or infected with virus (Figure 2.1).

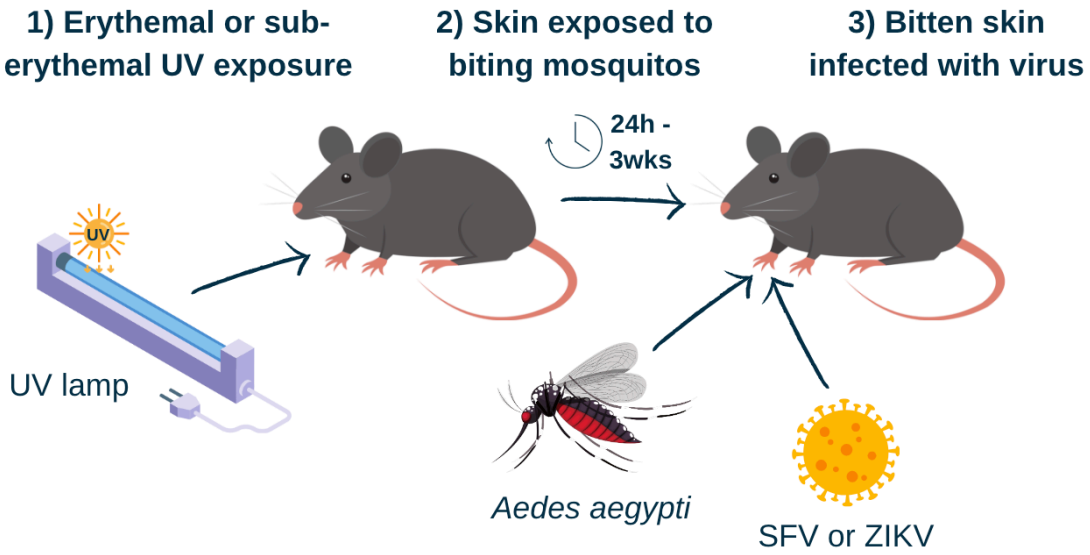

Figure 2.1 | *in vivo* model of UV exposure with mosquito biting and arbovirus infection

2.6.1 Monitoring mice for clinical signs of suffering

For mice kept longer than 24h post-UV exposure, all mice were monitored 3 times a week for clinical signs of suffering (Table 2.3). Any mice displaying more than three clinical signs of suffering were culled.

Table 2.3 | Clinical signs of moderate suffering in mice

Moderate suffering
Body weight loss of up to 20%
Staring coat-marked piloerection
Subdued even if provoked – little peer interaction
Hunched intermittently

Vocalisation if provoked
Oculo-nasal discharge persistent
Intermittent abnormal breathing
Intermittent tremors
Intermittent convulsions
No self-mutilation
Intermittent prostration (less than 1h)

2.7 Vitamin D and steroid treatments

The impact of anti-inflammatory treatments on UV-mediated enhancement of infection were assessed by treating mice with either vitamin D or steroid cream post-UV exposure but prior to virus infection.

2.7.1 Vitamin D treatment

Prior to injection, vitamin D (25(OH) D) (Sigma-Aldrich, H4014-1MG) was reconstituted to 1 mg/mL in 100% ethanol (Sigma-Aldrich) before being further diluted to desired concentration of 5 µg/mL in mineral oil (Sigma-Aldrich, M8410). Mice were then injected subcutaneously (s.c.) with 5 ng of vitamin D at the burn site 1h post-UV exposure or at resting skin in control mice. Vitamin D mixture was mixed thoroughly between each mouse treatment due to the viscose nature of the substance.

2.7.2 Steroid treatment

A thin layer of clobetasol propionate coriticosteroid cream (Dermovate® Ointment, GSK) was applied to the skin at the UV burn site or equivalent site in resting control mice twice daily for 5 days, with the first treatment being applied 1h post-UV exposure.

2.8 Mosquito biting and viral infections of mice

Mice were anesthetised via intraperitoneal (i.p.) injection of Sedator/Ketavet. The dose administered to each mouse was calculated based on body weight (50mg/kg of Ketavet and 0.5mg/kg of Sedator). The upper foot of the foot, the skin of which is naturally hairless and mimics human skin, was placed on top of a mosquito cage containing adult *Ae. Aegypti* female mosquitos and secured using tape. Aluminium foil was used to protect the rest of the body to ensure the

upper foot was the only region of the body exposed to bites. This region of the foot was exposed to 3-5 biting mosquitos until the insects were engorged and their abdomens contained blood. At this point mice were removed from the cage (Figure 2.2). Immediately following this, 1 µl of virus in PBS was injected s.c. into the same region of the upper foot which had been bitten. The titre, measured in plaque forming units (PFU), of each virus used was dependent on experiment based on the virulence of the strain and the mouse model used and is specified throughout this thesis for each individual experiment. Injections were carried out using custom point 4 style 33-gauge microneedles (Hamilton, Switzerland) and a Hamilton syringe. Mice were then either injected with Revertor reversal agent (1mg/kg of body weight) or left to recover from the anaesthesia in a warm room with access to food and water and were monitored hourly.

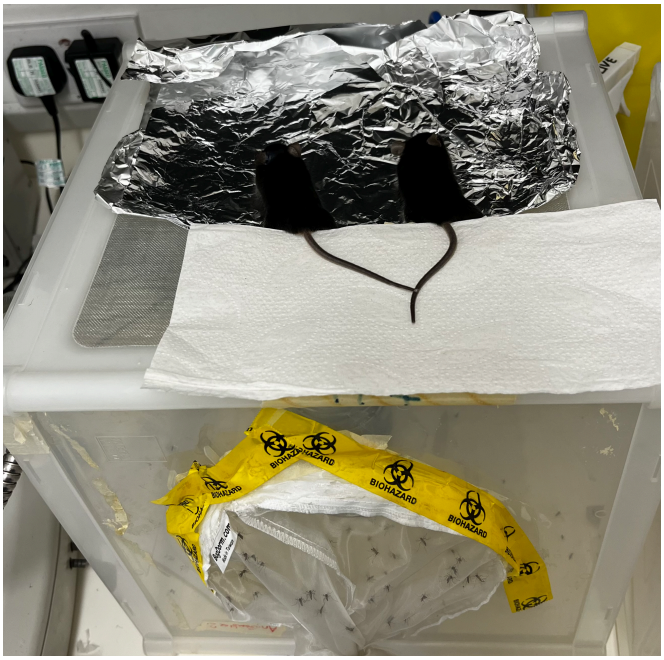

Figure 2.2 | Exposure of mice to bites from *Aedes aegypti* mosquitos

2.9 Measuring skin temperature, mosquito landing and probing time

A Testo 830-T1 Infrared Thermometer (Testo) was used to measure the temperature of UV-exposed or unexposed mouse skin at set time points post-UV exposure. ‘Landing time’ was measured as the time period between when a mouse was set down on top of the mosquito cage with the skin being exposed

to potential mosquito bites to when a mosquito landed on the skin. 'Probing time' was measured as the time period between when a mosquito began probing the mouse skin looking for a blood meal to when the mosquito abdomen was fully engorged with blood and disengaged from the mouse.

2.10 Dissection of mice

Mice were culled via exposure to increasing concentrations of CO_2. Death was confirmed through permanent cessation of the circulation through incision of the vena cava. This also allowed for circulating blood to be collected from the chest cavity and added to a 1.5 mL sterile, RNase-free Eppendorf tube (Eppendorf). Required tissues for the experiment were then dissected; skin from the upper foot, spleen and/or brain. Tissues were either immediately digested to extract cells or kept for RNA extraction in RNAlater (Sigma-Aldrich) for up to 1 week at 4 °C. Blood samples were centrifuged at 12,000 xg for 15 mins at 4 °C to separate the serum from the blood clot. The serum was stored in a 96-well plate at -80 °C until ready for use.

2.11 Oedema quantification

Evan's Blue dye can be used to measure vascular permeability and leakage, and oedema formation at the skin at rest or in response to a stimulus, e.g. UV exposure. The dye binds to albumin in serum and spreads to distant tissues. Usually, albumin cannot pass through selectively permeable barriers, including the endothelial cell barrier. However, increased permeability of vessels allows albumin to pass through this barrier. Therefore, more dye reaches and gathers at tissues, including the skin, allowing the dye to be used as a measure of permeability. Mice were injected s.c. at the scruff of the neck with 200 µl of filter-sterilised 1% Evan's Blue dye (Sigma-Aldrich) at a set time point post-UV exposure. Mice which required mosquito bites were exposed to these 1h post-dye injection. All mice were culled at 3h post-dye injection and blood and skin were collected. Skin was immediately added to 250 µl of formamide (Roche). Blood samples were centrifuged at 12,000 xg for 15 mins to separate serum from the blood clot. Serum was diluted 1:10 in formamide in a 96-well flat bottom plate. Skin and serum samples were incubated in formamide at 4 °C for 24h. Skin samples were then removed from the formamide and the dye-containing formamide was added to separate wells in the plate containing the

serum samples. A 10-fold serial dilution of Evan's Blue dye and formamide was made to form a standard curve. Quantities of dye were assessed using colorimetric measurement at 620 nm using the Cytation 5 Imaging Reader (Biotek). Based on the standard curve, the concentration of dye in each experimental sample was quantified. The concentration of dye from skin samples were normalised to the concentration of dye in the serum sample from the same mouse and used as a measure of vascular permeability and leakage, and oedema in the skin.

2.12 Tissue digestion

Upon harvesting from mice, the tissue was placed in 1 mL complete DMEM (Gibco). The tissue was then moved to 1 mL of digestion enzyme mix, containing 0.9 mL Hanks Balanced Salt Solution (Sigma-Aldrich), 100 µL (1 mg/mL) Collagenase P (Roche), 50 µL (0.5 mg/mL) Dispase II (Roche) and 8 µL (0.1 mg/mL) DNase I (Roche). Tissue was cut into small pieces using dissection scissors to help with digestion. The chopped tissue was incubated in the enzyme mix for 50 mins at 37 °C while being agitated at 1000 rpm on an Eppendorf Thermomixer F1.5 (Eppendorf) to encourage enzymatic breakdown of the tissue and release of cells. Following incubation, 0.5 mL of cold DMEM (Gibco) was added to stop the enzymatic reaction. This solution, including any remaining tissue sections, was then added to a 70 mm cell strainer (Corning) inserted in the top of a 50 mL centrifuge tube (Corning) and pushed through using the plunger section of a 5 mL syringe (BD Plastipak). The strainer was then washed with 3 mL of complete DMEM (Gibco) to collect any cells left attached to the strainer. Cells were counted using Trypan Blue Solution 0.4% (Gibco) and then pelleted by centrifuging at 300 xg for 10 mins at 4 °C. Cells were resuspended to desired concentration for subsequent application based on cell count.

2.13 Assessment of cell proliferation

EdU (5-ethynyl-2'-deoxyuridine), a thymidine nucleoside analogue, was used to assess proliferation of cells extracted from mouse skin using the Click-iT Plus EdU Alexa Fluor 488 Flow Cytometry Assay Kit (Invitrogen, C10632). The manufacturer's protocol was used for this assay. Briefly, following tissue digestion, cells were added to a 96-well flat bottom plate at a concentration of

1x10^6 cells/well in complete DMEM. 10 μM of EdU was added to each well and incubated with the cells at 37 °C for 3h to label proliferating cells. A viability dye was then applied to cells to differentiate between live and dead cells (see Section 2.19.2 for further details). Cells were then washed in PBSA (see Table 2.1 for composition) and fixed in 100 μL of Click-iT fixative for 15 mins at room temperature (RT). After another PBSA wash, cells were resuspended in 100 μL of 1x Click-iT permeabilization and wash reagent and incubated for 15 mins at RT. During the incubation period, the Click-iT Plus Reaction Cocktail was prepared according to the manufacturer's instructions. To detect EdU, 500 μL of the Reaction Cocktail was added to each well once the permeabilization was complete. Cells were incubated with this for 30 mins at RT. Cells were washed in 500 μL of 1x Click-iT permeabilization and wash reagent and resuspended in 200 μL of flow cytometry buffer for subsequent quantification of proliferating cells (EdU-AF488+ cells) using flow cytometry.

2.14 Magnetic Activated Cell Sorting (MACS) separation of cells

MACS (MiltenyiBiotec) separation was used to isolate CD45+ cells from CD45- cells and flow cytometry staining was also applied to cells to confirm successful separation of the two fractions. To do this, cells were resuspended in 90 μL MACS buffer per 10^7 cells. 2 μL of Fc receptor (FcR) Blocking Reagent (MiltenyiBiotec) was then added to each sample and incubated together for 5 mins on ice. 10 μL of CD45 MicroBeads (MiltenyiBiotec) per 10^7 cells were then added, mixed with the sample and incubated for 15 mins at 4 °C. Fluorescent antibodies for flow cytometry analysis (Table 2.4) were then added to cells and left to incubate for 10 mins at 4 °C. Cells were then washed by adding 1 mL of MACS buffer per 10^7 cells and centrifuged at 300 xg for 10 mins. Supernatant was aspirated completely, leaving the cell pellet. Cells were resuspended in 500 μL of MACS buffer. An MS column (MiltenyiBiotec) was placed in the magnetic field of a MiniMACS Separator (MiltenyiBiotec) and a 15 mL centrifuge tube (Corning) was placed underneath the column to collect the flowthrough. The column was prepared by washing with 500 μL of MACS buffer. The cell suspension was then transferred to the column and the unlabelled, or CD45-, cells passed through the column into the collection tube below. The column was then washed three times with 500 μL of MACS buffer to ensure all unlabelled cells were collected. The column was then removed from the magnetic

separator and inserted into a new 15 mL centrifuge tube (Corning) to collect the labelled cell fraction. 1 mL of MACS buffer was added to the column and firmly pushed through the column by using the supplied plunger to flush the labelled, or CD45+, cells into the new collection tube. Cells were then counted and pelleted by centrifuging at 300 xg for 10 mins at 4 °C. Cells were resuspended to desired concentration for subsequent application based on cell count. 10% of total cells were taken for flow cytometry analysis to confirm successful separation of cell populations, with the remaining 90% left for use in subsequent applications. Cells from mice infected *in vivo* were harvested immediately following MACS separation, while cells that were to be infected *in vitro* were plated in 96-well plates.

2.15 Culture and infection of murine skin cells *in vitro*

Following skin digestion (Section 2.12) or cell sorting (Section 2.14), cells were pelleted by centrifuging at 300 xg for 10 mins at 4 °C. Cells were then resuspended at $1x10^6$ cells/mL in complete DMEM (Gibco) with 0.1% Gentamicin (Gibco). 96-well round bottom plate (Corning) were prepared by pre-coating required wells in 100 µL 0.2% Gelatin Solution (Sciencell). The plate was then incubated at 37 °C for 1h and the Gelatin Solution was removed prior to plating of cells. $2.5x10^5$ cells were then added per well. Cells were pelleted by centrifuging the plate at 400 xg for 5 mins and supernatant was discarded. Cells were then infected with 100 µL of SFV4 in PBSA at a multiplicity of infection (MOI) of 2 and incubated at 37 °C for 1h. At the end of the infection period, plates were centrifuged at 400 xg for 5 mins to allow for removal of residual virus by discarding the supernatant following centrifugation. Cells were resuspended in 100 µL complete DMEM with 0.1% Gentamicin and incubated at 37 °C overnight. At 16h post-infection (hpi), the cells and supernatant were harvested for RNA extraction and plaque assay, respectively.

2.16 Harvest of cells and supernatant *in vitro*

Human peripheral blood mononuclear cells (PBMCs) and murine skin cells in 96-well plates were harvested at 16 hpi, unless stated otherwise. Cells were first pelleted by centrifuging the plate at 400 xg for 5 mins. Supernatant was removed and transferred to a new 96-well round bottom plate (Corning). This was stored at -80 °C for use in a plaque assay to test infectious virus titres at a

later date. Cell pellets were resuspended in 250 µL of Lysis Buffer (Invitrogen) with 0.1% 2-Mercaptoethanol (Sigma-Aldrich) to lyse cells. The cell lysate was then added to a QIAshredder (QIAGEN) column and the column was centrifuged at 12,000 xg for 2 mins to homogenise the lysate in preparation for RNA extraction. The lysate was stored at -80 °C.

2.17 Collection of human blood samples and PBMC isolation

For all clinical work, human ethics had already been reviewed and granted prior to commencement of studies by the NHS South Central Hampshire B Research Ethics Committee under reference number 21/SC/0089. Human blood samples were collected in 4 mL EDTA-coated Vacutainer tubes (Becton-Dickenson) from healthy control volunteers by Dr Kave Shams at Chapel Allerton Hospital, Leeds. PBMCs were isolated from blood samples along a density gradient using Ficoll Histopaque-1077 (Sigma-Aldrich), after being mixed 1:1 with PBS supplemented with 1% FCS and 2 mM EDTA. The isolated PBMC fraction was washed three times in this solution. Before the second wash, red blood cells (RBCs) were lysed using eBioscience 1X RBC Lysis Buffer (Invitrogen). Before the third wash, cells were counted using a haemocytometer. After washing steps were complete, cells were resuspended in complete RPMI (Table 2.2).

2.18 *in vitro* infection of PBMCs

Isolated PBMCs were seeded in 96 well plates, with $8x10^5$ cells per well. Cells were either pre- treated with 0.2 µg/mL of imiquimod (Invitrogen), 0.5 µg/mL, 1 µg/mL, 2 µg/mL or 5 µg/mL of poly(dA:dT)/LyoVecTM (Invivogen) 1h pre-infection or left unstimulated. Cells were infected with either BHK-21 cell-derived ZIKV or C6/36 cell-derived ZIKV in complete RPMI at a MOI of either 1, 0.1 or 0.01 for 1h in an incubator at 37 °C, 5% CO_2. After the hour, supernatant was removed, fresh media was added to wells and cells were moved back to the incubator. PBMCs were lysed at 6 hpi and 16 hpi (further details in Section 2.16) for analysis by qPCR.

2.19 Flow cytometry

Cells were stained with fluorescent antibodies to identify cell markers and analysed using flow cytometry to identify cell populations within samples.

2.19.1 Flow cytometry antibodies

A number of antibodies were optimised for use in flow cytometry experiments (Table 2.4).

Table 2.4 | Antibodies used in flow cytometry experiments, including details of their target, clone, fluorophore, target species, manufacturer and optimal dilution

Antibody target	Clone	Fluorophore	Target species	Manufacturer	Dilution
CD16	3G8	BV421	Human	BioLegend	1:50
CD14	HCD14	FITC	Human	BioLegend	1:50
CD123	6H6	PE	Human	BioLegend	1:50
CD19	HIB19	PE-Cy7	Human	BioLegend	1:50
CD3	UCHT1	BV510	Human	BD Biosciences	1:50
CD11c	Bu15	APC	Human	BioLegend	1:50
CD56	5.1H11	APC-Cy7	Human	BioLegend	1:50
IgG2a	Polyclonal	AF-594	Mouse	Invitrogen	1:50 > 1:800
ZIKV E	ZV-54	n/a	ZIKV	Sigma-Aldrich	1:50
IgG2a isotype control	eBM2a	n/a	n/a	Invitrogen	1:50 > 1:800
CD45	30-F11	PeCy5	Mouse	BioLegend	1:50
CD45	30-F11	FITC	Mouse	BioLegend	1:50
CD11b	M1/70	APC	Mouse	Southern Biotec	1:50
CD11b	M1/70	PerCP	Mouse	BioLegend	1:50
Ly6C	HK1.4	PE	Mouse	BioLegend	1:50
Ly6G	1A8	BV421	Mouse	BioLegend	1:50

CD64	S18017D	FITC	Mouse	BioLegend	1:50
MerTK	2B10C42	APC-Cy7	Mouse	BioLegend	1:50
MHC II	MS/114.15.2	APC	Mouse	BioLegend	1:50
CD11c	N418	Pe-Cy7	Mouse	BioLegend	1:50
Vimentin	280618	APC	Mouse	R&D Systems	1:50
CD326 (EP-CAM)	G8.8	APC-Cy7	Mouse	BioLegend	1:50
CD31	MEC13.3	PE	Mouse	BioLegend	1:50

2.19.2 Flow cytometry staining of human PBMCs and mouse skin cells

Extracellular staining of cells was used to identify leukocyte or CD45 cell populations based on cell marker expression. Equal numbers of cells were added to wells in a 96-well round bottom plate. The plate was centrifuged at 400 xg for 5 mins at 4 °C. Supernatant was discarded and cells were resuspended in 250 µL flow cytometry buffer (100 mL PBS (-Ca/Mg), 500 µL FCS, 400 µl EDTA 0.5 M). The plate was centrifuged at 400 xg for 5 mins at 4 °C. Supernatant was discarded and cells were resuspended in 50 µL of Fc block solution. For human samples, the Fc block solution was made using 2 µL of 5% patient-matched plasma and 48 µL flow cytometry buffer per well. The plasma was collected during the PBMC isolation process. For mouse samples, 10 µL of Mouse BD Fc Block (BD Biosciences) was added to each well. Cells were then incubated on ice for 5 mins. 50 µL of antibody mix in flow cytometry buffer was then added to each well. Antibody concentrations can be found in Table 2.4. Cells were incubated at 4 °C for 30 mins protected from light. 150 µL of flow cytometry buffer was then added to wells and cells were pelleted by centrifuging for 5 mins at 400 x g and washed twice in 250 µL of PBS. After the final wash, cells were resuspended in 50 µL of Zombie UV Fixable Viability Stain (BioLegend) and incubated at RT in the dark for 10 mins. 250 µL of flow cytometry buffer was added to wells and cells were pelleted. Cells were fixed in 100 µL of 4% PFA at for 30 mins before being washed twice in 250 µL flow cytometry buffer. Cells were resuspended for a final time in 250 µL flow cytometry buffer and kept in the dark at 4 °C until ready for analysis.

2.19.3 Flow cytometry staining of compensation beads

Compensation beads were used for single stain controls of flow cytometry antibodies to help compensate experiments. Anti-Mouse Ig k/Negative Control Compensation Particles (BD Biosciences) were used for human samples and Anti-Rat/Hamster Ig k/Negative Control Compensation Particles (BD Biosciences) were used for murine samples. Firstly, 1 drop of positive beads and 1 drop of negative beads were incubated in a well with 50 µL of a single antibody/flow cytometry buffer mix, in the same concentration as used to stain cells, for 30 mins in the dark at 4 °C. Beads were then washed twice in 250 µL flow cytometry buffer before being fixed in 100 µL of 4% PFA at RT for 30 mins. Beads were then washed twice more in 250 µL flow cytometry buffer before being resuspended in a final volume of 250 µL flow cytometry buffer. Beads were then stored for up to 1 month in the dark at 4 °C.

2.19.4 Intracellular staining for flow cytometry

Intracellular staining was used to identify cells infected with ZIKV. Cells were stained for intracellular markers and viability as detailed above (Section 2.19.2). Following the incubation of cells with the viability dye, cells were washed twice in 250 µL flow cytometry buffer before being fixed in 100 µL of Cytofix/Cytoperm (BD Biosciences) and incubated for 20 mins at 4 °C. 100 µL of 1X Perm/Wash (BD Biosciences) was added to each well and cells were pelleted by centrifuging for 5 mins at 400 xg. Cells were then washed once in 250 µL 1X Perm/Wash. 50 µL of the primary antibody (anti-Zika E, clone ZV-54) diluted in 1X Perm/Wash was then added to each well (Table 2.4). Cells were incubated at 4 °C for 30 mins in dark conditions. 150 µL of 1X Perm/Wash was then added to wells and cells were pelleted and washed in 250 µL of 1X Perm/Wash. Cells were then resuspended in 50 µL of the secondary antibody (IgG2a) or isotype control diluted in 1X Perm/Wash and incubated 4 °C for 30 mins in dark conditions. 150 µL of 1X Perm/Wash was added to wells and cells were pelleted and washed in 250 µL of 1X Perm/Wash. Cells were resuspended for a final time in 250 µL flow cytometry buffer and kept in the dark at 4 °C until ready for analysis.

2.19.5 Flow cytometry analysis

Measurement of cell marker expression was measured using either the CytoFLEX LX Flow Cytometer (Beckman Coulter) or the CytoFLEX S Flow

Cytometer (Beckman Coulter), depending on the complexity of the fluorescent antibody panel chosen. Gating strategies used are shown in Figures 2.3, 2.4, 2.5 and 2.6. All analysis of flow cytometry data was completed using CytExpert Software 2.5.0.77 (Beckman Coulter).

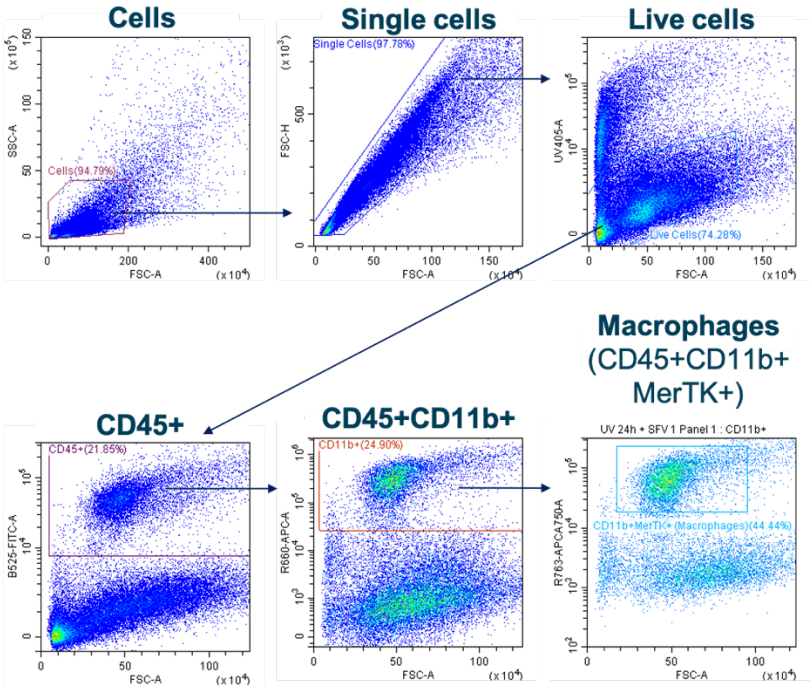

Figure 2.3 | Gating strategy for phenotyping of macrophages in mouse skin using flow cytometry

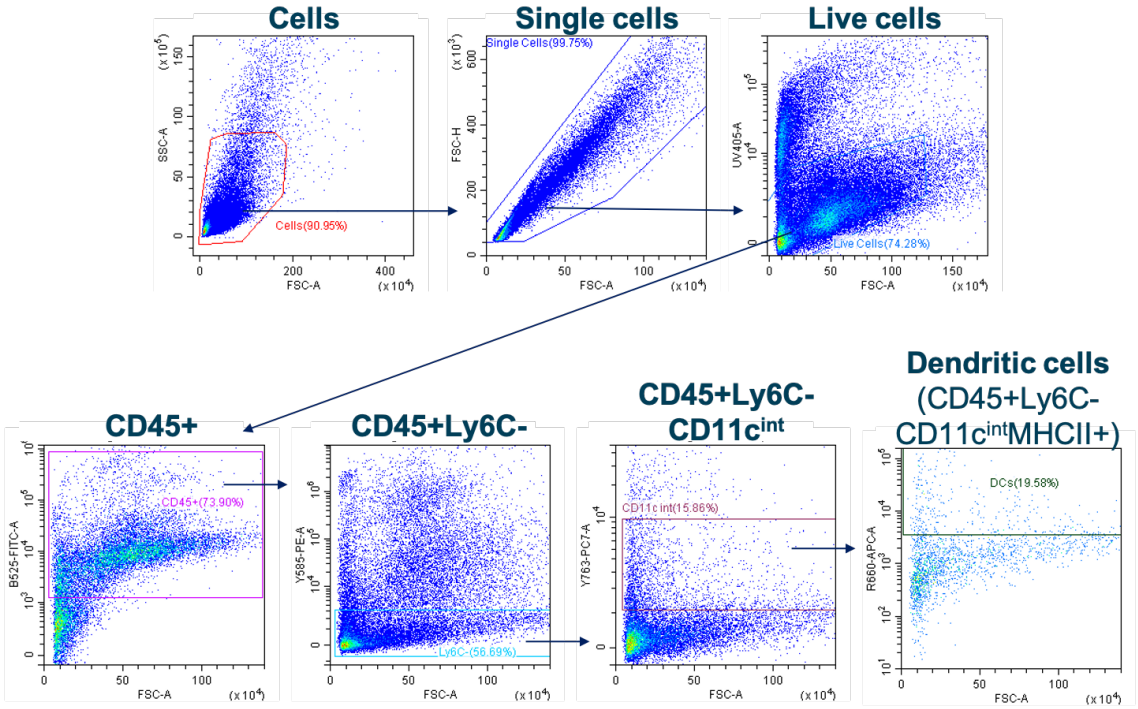

Figure 2.4 | Gating strategy for phenotyping of DCs in mouse skin using flow cytometry

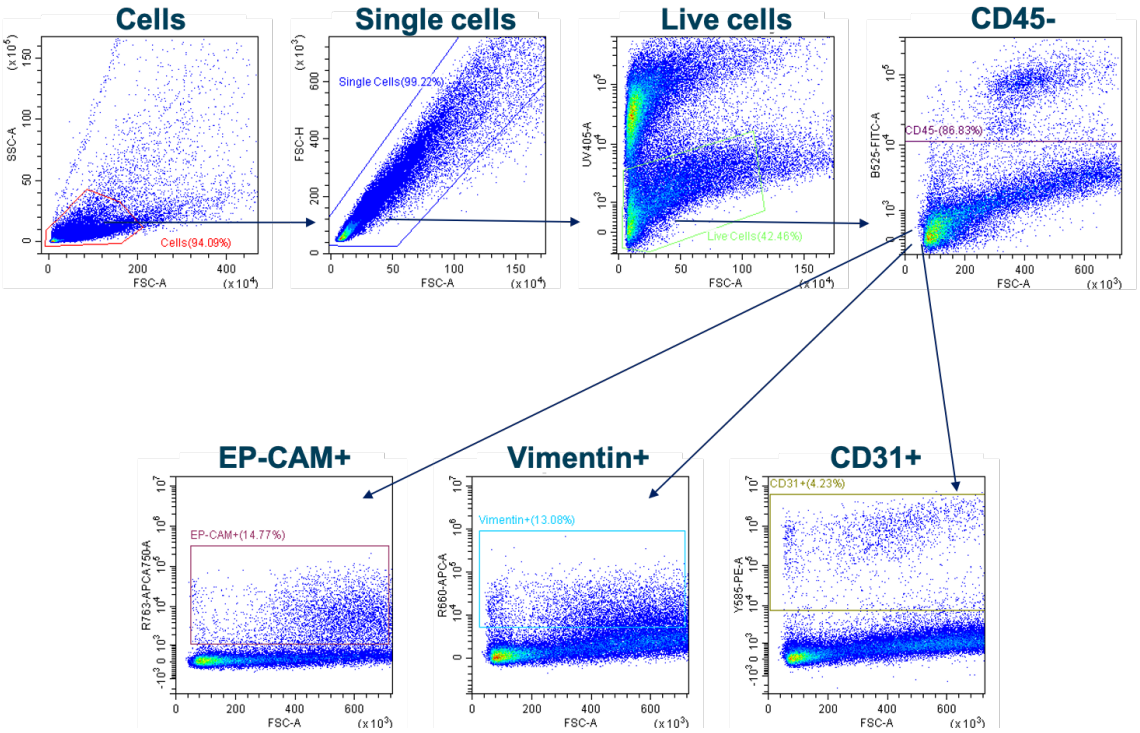

Figure 2.5 | Gating strategy for phenotyping of CD45- cells in mouse skin using flow cytometry

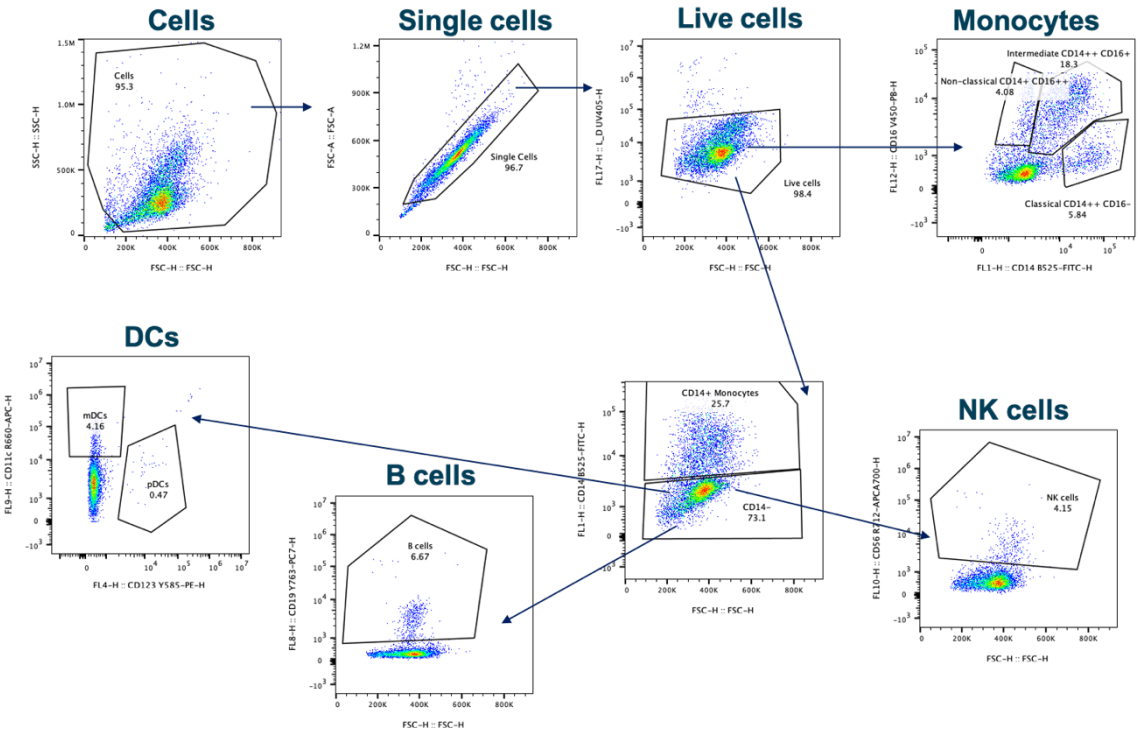

Figure 2.6 | Gating strategy for phenotyping of cell populations within human PBMC samples using flow cytometry

2.20 Gene expression analysis

RNA was extracted from tissues or cells and was then utilised to generate complementary DNA (cDNA) for use in qPCR to examine gene expression. Depending on the experiment, this process was used to analyse expression of human, murine and virus genes.

2.20.1 RNA extraction from tissues

Tissues were dissected from mice and immediately transferred to 1 mL of RNAlater (QIAGEN) in 1.5 mL sterile, RNase-free Eppendorf tube (Eppendorf) to stabilise RNA. Samples were maintained at 4 °C for up to 1 week. To extract RNA, tissues were transferred to 2 mL sterile, RNase-free Eppendorf tubes (Eppendorf) containing 5 mm stainless-steel bead(s) (QIAGEN), one for spleen or two for skin. 1 mL of TRIzol Reagent (Invitrogen) was added to the tube. Samples were homogenised via vigorous shaking for 10 mins at 50 Hz using a TissueLyser LT (QIAGEN). 200 µL of Chloroform (Fisher Chemicals) was added to samples and mixed by inverting each tube 15 times. Tubes were centrifuged for 15 mins at 12,000 xg at 4 °C to separate sample into three phases: the upper aqueous phase containing RNA, the cloudy interphase containing DNA and the pink organic phase containing phenol and proteins (Figure 2.7).

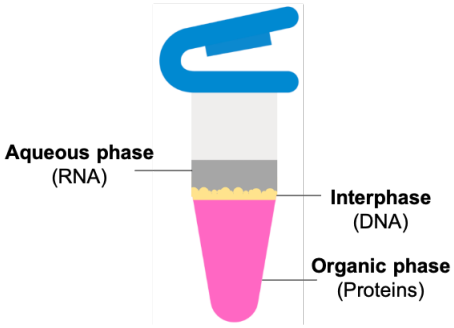

Figure 2.7 | Phase separation during phenol-chloroform RNA extraction Following the addition of chloroform, the sample separates into three layers from which the upper, RNA-containing layer can be removed.

Tubes were removed from the centrifuge carefully, to avoid disruption of these layers, and placed on ice. 500 µL of the RNA layer was pipetted out and added to a fresh 1.5 mL sterile, RNase-free Eppendorf tube containing an equal

volume of 70% ethanol (Sigma-Aldrich). Tubes were then vortexed to mix samples thoroughly. The PureLink RNA Mini Kit (Invitrogen) was used to extract RNA from the homogenised lysate, as per the manufacturer's instructions. 500 µL of the lysate was transferred to Spin Cartridges (Invitrogen) containing a silica membrane which binds nucleic acids. Cartridges were centrifuged at 12,000 xg for 30 secs and flow-through was discarded. This process was repeated to run the remaining 500 µL of lysate through the cartridge. 350 µL of Wash Buffer I (Invitrogen) was added to the cartridge and centrifuged at 12,000 xg for 30 secs. To degrade any genomic DNA contaminants and improve RNA purity, 80 µL of RNase-Free DNase (QIAGEN), consisting of 10 µL of DNase I and 70 µL of RNase-free Buffer RDD, was added directly to the membrane of the cartridge. Samples were incubated with the enzyme at RT for 20 mins. 350 µL of Wash Buffer I (Invitrogen) was added to the cartridge to stop the reaction. The cartridge was then centrifuged at 12,000 xg for 30 secs and flow-through was discarded. The cartridge was then washed twice in 500 µL of Wash Buffer II (Invitrogen) with the flow-through discarded following centrifugation. Following the final wash, the cartridge was centrifuged at 12,000 xg for 2 mins to dry the column. The column section of the cartridge was then removed from the collection tube and inserted into a new 1.5 mL sterile, RNase-free Eppendorf tube (Eppendorf). The original collection tube was discarded. RNase-free water, 60 µL for skin or 100 µL for spleen, was then added directly to the membrane and incubated at RT for 1 min. The cartridge was then centrifuged at 12,000 xg for 2 mins to elute the RNA into the collection tube. The column was then discarded. The eluted RNA was stored long-term at -80 °C.

2.20.2 RNA extraction from cells

Homogenised cell lysates (Section 2.16) were removed from storage at -80 °C and thawed. An equal volume of 70% ethanol (Sigma-Aldrich) was added to the lysate and samples were vortexed. Due to low cell numbers, the PureLink RNA Micro Scale Kit (Invitrogen) was used to extract RNA from the homogenised cell lysate, as per the manufacturer's instructions. Up to 500 µL of sample was transferred to PureLink Micro Kit Columns (Invitrogen) containing a silica membrane which binds nucleic acids. Cartridges were centrifuged at 12,000 xg for 1 min and flow-through was discarded. 350 µL of Wash Buffer I (Invitrogen) was added to the cartridge and centrifuged at 12,000 xg for 1 min. To degrade

any genomic DNA contaminants and improve RNA purity, 20 µL of PureLink On-Column DNase (Invitrogen), consisting of 10 µL of Lyophilized PureLink DNase and 10 µL of Pure-Link On-Column DNase 2X Buffer, was added directly to the membrane of the cartridge. Samples were incubated at RT for 15 mins. 350 µL of Wash Buffer I (Invitrogen) was added to the cartridge to stop the reaction. The cartridge was then centrifuged at 12,000 xg for 30 secs and flow-through was discarded. The cartridge was then washed twice in 500 µL of Wash Buffer II (Invitrogen) with the flow-through discarded following centrifugation. Following the final wash, the cartridge was centrifuged at 12,000 xg for 2 mins to dry the membrane. The column section of the cartridge was then removed from the collection tube and inserted into a new 1.5 mL sterile, RNase-free Eppendorf tube (Eppendorf). The original collection tube was discarded. RNase-free water, 12 µL for murine skin cells or 22 µL for human PBMCs, was then added directly to the membrane and incubated at RT for 1 min. The cartridge was then centrifuged at 12,000 xg for 2 mins to elute the RNA into the collection tube. The column was then discarded. The eluted RNA was stored long-term at -80 °C.

2.20.3 cDNA generation

cDNA, for use in qPCR, was generated from extracted RNA via reverse transcription using the High-Capacity RNA-to-cDNA Kit (Applied Biosystems). RNA extracted from tissue or cells was removed from storage at -80 °C and thawed. Sample RNA was first added to a well in a Non-Skirted 96-Well PCR Plate (STARLAB) at a concentration of 1µg per sample. 11 µL of Reverse Transcriptase (RT) master mix (consisting of 1 µL of 20X RT Enzyme and 10 µL of 2X RT Buffer) was then added to each well. The total volume of each well was made up to 20 µL using Nuclease-free Water (Invitrogen). The contents of each well were mixed thoroughly. The plate was briefly centrifuged to remove any bubbles in the wells. An adhesive Aluminium PCR StarSeal (STARLAB) was then placed over the plate and an applicator was used to seal it. The plate was placed in GeneAmp PCRsystem2700 (Applied Biosystems) and set to run a reverse transcription reaction using the settings detailed in Figure 2.8 to generate cDNA. The cDNA was then stored short-term at -20 °C and long-term at -80 °C.

Figure 2.8 | Cycle settings used on thermocycler for the reverse transcription reaction used to generate cDNA

2.20.4 Primer design

Primers were designed for use in two applications. 'Standard Primers' (Table 2.5) were used to generate sequences of cDNA from target genes of interest or 'standards'. These were then used to generate standard curves for use as a comparison to experimental samples during qPCR to relatively quantify gene expression in the experimental samples. 'qPCR Primers' (Table 2.6) were required for amplification of regions of target genes of interest in experimental samples and the standard curve during qPCR, so that the concentration of each could be compared. Forward and reverse primers for both purposes were designed using NCBI Reference Sequences and the Primer3 Version 0.4.0 software. The following design rules were applied:

- Primers must be between 18 and 23 base pairs (bp) in length.
- Primers must be between 40 and 65% GC content, with 50% being the optimum.
- The melting temperature (Tm) of primers must be within 59.5 °C and 61 °C, with 60 °C being the optimum.
- The maximum self-complementarity score allowed is 2.
- The maximum 3'self-complementarity score allowed is 1.
- The amplicon size must be less than 150 bp for qPCR Primers and less than 800 bp for Standard Primers.
- The standard primers must start at least 20 bp before the start and 40 bp after the end of the qPCR primer target sequence.
- Preferably, there should not be more than two G or C bases in the last 5 bases at the 3' end, known as a GC clamp, of each primer.
- Preferably, there should not be 4 or more G or C bases in a row.

- If no suitable primers are suggested, the maximum self-complementarity score can be relaxed to 3 or the Tm of primers to 59 °C.

All primers were purchased from Integrated DNA Technologies. Prior to use, primers were reconstituted in Nuclease-free Water (Invitrogen) to 100 µM.

Table 2.5 | List of all primers used to generate standard cDNA for use in standard curve, including details of targeted genes, species, orientation, sequence, product size and NCBI reference

Gene name	Species	Orientation	Sequence	Product size (bp)	NCBI reference
CCL5	Human	Forward	GGGGAAGGTTTTTGTAACTGCT	406	NM_002985.3
		Reverse	GGGGAAGGTTTTTGTAACTGCT		
CXCL10	Human	Forward	AGGAACCTCCAGTCTCAGCA	601	NM_001565
		Reverse	AGCAGGGTCAGAACATCCAC		
IFNB1	Human	Forward	AGCACTGGCTGGAATGAGAC	341	NM_002176.4
		Reverse	GCATCTGCTGGTTGAAGAATG		
IFNA1	Human	Forward	CAGAGTCACCCATCTCAGCA	430	NM_024013.3
		Reverse	CTCTCCTCCTGCATCACACA		
18S	Human	Forward	CGTAGTTCCGACCATAAACGA	4443	NR_003278.1
		Reverse	ACATCTAAGGGCATCACAGACC		
RIG-I	Human	Forward	TCCCAGTGTAT	680	NM_00138

			GAACAGCAGAA		5907
		Reverse	TTTGTCTGGCA TCTGGAACA		
MDA5	Human	Forward	TGAAAAGGCTG GCTGAAAAC	371	NM_02216 8.4
		Reverse	GACGAGACCAT AACGGATAACA A		
RSAD2	Human	Forward	ATGCGGCTTCT GTTTCCA	794	NM_08065 7
		Reverse	TGTATTTTCCTC CTCGCTTCA		
cGAS	Human	Forward	TCACTTGAGGT CAGGAGTTTGA	619	NM_13844 1
		Reverse	GCGGAGAGCT GTTTTTCAGT		
IL-36a	Human	Forward	TTTTGCTTCCA GGTCTTTGG	750	NM_01444 0.3
		Reverse	TAGTGTTGGCT TTCCCCAGTT		
RSAD2	Mouse	Forward	CTGTGCGCTGG AAGGTTTTC	583	NM_02138 4.4
		Reverse	CACTGGACCTT GCTCCTCTG		
IFIT1	Mouse	Forward	GCACCTCTATG TTTGAGCAGTT	290	NM_00833 1.3
		Reverse	GCAGAAAAGTC AAGGCAGGAA		
ISG15	Mouse	Forward	GTCCGTGACTA ACTCCATGAC	504	NM_01578 3.3
		Reverse	TCCCAAAAGTC CTCCATACC		
CXCL10	Mouse	Forward	CCTGAGACAAA AGTAACTGCCG	272	NM_02127 4

		Reverse	TGGGAAGATGGTGGTTAAGTTCG		
CXCL2	Mouse	Forward	CGCCCAGACAGAAGTCATAG	484	NM_009140
		Reverse	ACTCACCCTCTCCCCAGAAA		
CCL2	Mouse	Forward	CACCAGCACCAGCCAACT	519	NM_011333.3
		Reverse	GCATCACAGTCCGAGTCACA		
ARG1	Mouse	Forward	CGAGGAGGGGTAGAGAAAGG	389	NM_007482.3
		Reverse	TTCAGGAGAAAGGACACAGGTT		
IFNB1	Mouse	Forward	GGCTTCCATCATGAACAACA	376	NM_010510
		Reverse	TCCCACGTCAATCTTTCCTC		
CCR2	Mouse	Forward	AGGGGAGAGCAGAAGGCTAA	212	NM_009915
		Reverse	CCCAGGAAGAGGTTGAGAGA		
SFV E1	SFV	Forward	AAGTGAAGACAGCAGGTAAGGTG	446	DQ189086
		Reverse	TATGAGTTGCCCCGAGTTTC		
ZIKV E	ZIKV	Forward	AGGCAAACTGTCGTGGTTCT	679	KX197192.1
		Reverse	TCAGACCCAACCACATCAGC		

Table 2.6 | List of all primers used for qPCR, including details of targeted genes, species, orientation, sequence, product size and NCBI reference

Gene name	Species	Orientation	Sequence	Product size (bp)	NCBI reference
CCL5	Human	Forward	GCCAACCCAGAGAAGAAATG	115	NM_002985.3
		Reverse	ACAAGAGCAAGCAGAAACAGG		
CXCL10	Human	Forward	TAAAACCAGAGGGGAGCAAA	81	NM_001565
		Reverse	GTAGGGAAGTGATGGGAGAGG		
IFNB1	Human	Forward	CATTACCTGAAGGCCAAGGA	134	NM_002176.4
		Reverse	CAGAGGCACAGGCTAGGAGA		
IFNA1	Human	Forward	GCTGCTCTCTGGGCTGTG	134	NM_024013.3
		Reverse	GTTGCCATCAAACTCCTCCT		
18S	Human	Forward	GACTCAACACGGGAAACCTC	124	NR_003278.1
		Reverse	TAACCAGACAAATCGCTCCAC		
RIG-I	Human	Forward	GGATGCCAAAAACACAGATGA	108	NM_001385907
		Reverse	TGCTCCAGTTCCTCCAGATT		
MDA5	Human	Forward	GAGGAATCAGCACGAGGAATAA	118	NM_022168.4
		Reverse	TCAGATGGTGGGCTTTGACT		
RSAD2	Human	Forward	TGCTTGGTGCCTGAATCTAAC	97	NM_080657

		Reverse	GGTCCTTCCGTCCCTTTCT		
cGAS	Human	Forward	CGGGAGGCTTAGACATGAGA	73	NM_138441
		Reverse	GCAGTGGTGCCATCTTGAC		
IL-36a	Human	Forward	ACTGTGGCTTGGGACTGACT	99	NM_014440.3
		Reverse	TCCATTGTGGTGGTGTTGTT		
RSAD2	Mouse	Forward	TGAAGCGTGGCGGAAAGTAT	73	NM_021384.4
		Reverse	TCCTTCCCATCTCAGCCTCA		
IFIT1	Mouse	Forward	TTGCACCACACTAGCTTGCA	96	NM_008331.3
		Reverse	GGGATGGAAGCACTCACAGT		
ISG15	Mouse	Forward	CGCAGACTGTAGACACGCTTA	80	NM_015783.3
		Reverse	CTCGAAGCTCAGCCAGAACT		
CXCL10	Mouse	Forward	GCTCAAGTGGCTGGGATG	111	NM_021274
		Reverse	GAGGACAAGGAGGGTGTGG		
CXCL2	Mouse	Forward	AAGTTTGCCTTGACCCTGAA	129	NM_009140
		Reverse	TCTCTTTGGTTCTTCCGTTG		
CCL2	Mouse	Forward	CTCACCTGCTGCTACTCATTCA	153	NM_011333.3
		Reverse	CCATTCCTTCTTGGGGTCA		

ARG1	Mouse	Reverse	TGGAAGAGTCAGTGTGGTGCT	138	NM_007482.3
		Forward	CTGGTTGTCAGGGGAGTGTT		
IFNB1	Mouse	Forward	CACAGCCCTCTCCATCAACT	152	NM_010510
		Reverse	GCATCTTCTCCGTCATCTCC		
CCR2	Mouse	Forward	TGTGGGACAGAGGAAGTGG	130	NM_009915
		Reverse	GGAGGCAGAAAATAGCAGCA		
SFV E1	SFV	Forward	CGCATCACCTTCTTTTGTG	173	DQ189086
		Reverse	CCAGACCACCCGAGATTTT		
ZIKV E	ZIKV	Forward	AGATCCCGGCTGAAACACTG	73	KX197192.1
		Reverse	TTGCAAGGTCCATCTGTCCC		

2.20.5 Testing of primers and generation of standard curve template cDNA

A PCR using positive control cDNA was used to test new primers and generate standard curve template cDNA. 2 µL of positive control cDNA was added to a 0.2 mL PCR Tube (STARLAB). 25 µL of ReadyMix Taq PCR Reaction Mix (Sigma-Aldrich) was then added to the tube. 1 µL each of the relevant forward and reverse primers were also added. The total volume of the mixture was brought to 50 µL by adding 21 µL of Nuclease-free Water (Invitrogen). PCR was performed using a GeneAmp PCRsystem2700 (Applied Biosystems); the protocol is detailed in Figure 2.9.

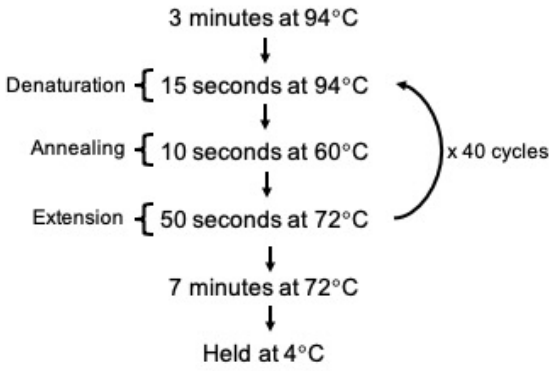

Figure 2.9 | Cycle settings used on thermocycler for the reverse transcription reaction used to generate standard curve template cDNA

PCR products were run on a 2% agarose gel (2 g Agarose Powder (Bioline) and 100 mL distilled H_2O). Briefly, to make the gel the agarose mixture was heated in a microwave in 30 sec increments to fully dissolve the agarose. 2 mL of Ethidium Bromide (Sigma-Aldrich) was added to the 2% agarose and the solution was rapidly cooled by running under cold water. The mixture was then poured into a gel casting cassette with a 12-well comb (BioRad). Once the gel had set it was moved to an electrophoresis tank (BioRad). 1X tris-acetate-EDTA (TAE) buffer (10 mL of 50X TAE Buffer (Serva) and 500 mL of distilled H_2O) was poured over the gel until wells were covered. A 50 bp DNA ladder (Invitrogen) was added to the first well in the gel. 6 µL of PCR product was mixed with 1 µL of TrackIt Cyan/Orange Loading Buffer (Invitrogen) and samples were loaded into subsequent wells. Gels were run at 100 Volts until samples reached the half way mark of the gel. Gels were imaged using ChemiDoc XRS+ gel imager (BioRad) to check that the PCR products were the expected size based on the primer product size and also that they formed a single band, to confirm primer specificity. For PCR products which were to be used as standard template cDNA, the cDNA was purified using the QIAquick PCR Purification Kit (QIAGEN), according to the manufacturer's instructions. Briefly, 250 µL of Buffer PB (QIAGEN) was added to the PCR product and mixed. The sample was then transferred to a QIAquick column and centrifuged for 30 secs at 17,900 xg. Flow-through was discarded. 750 µL of Buffer PE (QIAGEN) was added to the column and centrifuged for 30 secs at 17,900 xg. Flow-through was discarded. The column was centrifuged for a further 1 min at 17,900 xg to dry the membrane. The column was then removed from the collection tube and inserted

into a new sterile, RNase-free 1.5 mL eppendorf tube (Eppendorf). 50 µL of Buffer EB (QIAGEN) was then added directly to the membrane of the column. The column was then centrifuged for 1 min at 17,900 xg to elute the cDNA into the collection tube. This neat solution was kept as a stock and working stocks were made by diluting the cDNA 1:100 in Buffer EB (QIAGEN) for use as standard template cDNA in qPCR. All cDNA was stored short-term at -20 °C and long-term at -80 °C.

2.20.6 qPCR and analysis

qPCR was used to examine relative gene expression of genes of interest compared to a housekeeping gene in our experimental samples, using the standard curve method. The fluorescent dye SYBR Green was used in qPCR to allow for quantification of gene expression. SYBR Green intercalates to cDNA as it is being amplified during qPCR and its fluorescent signal is detected and can be used to quantify gene expression. For qPCR, sample cDNA was diluted 1:5 with Nuclease-free Water (Invitrogen). A standard curve was generated using serial 1:10 dilutions of the working stock solution of standard template cDNA diluted in Nuclease-Free Water (Invitrogen), up to a dilution of 10^{-9}. The qPCR reaction master mix consisted of PerfeCTa SYBR Green FastMix (Quantabio), Nuclease-free Water (Invitrogen) and forward and reverse primers (Integrated DNA Technologies) for the gene of interest. 20 ng of sample cDNA was added to the qPCR master mix to a final volume of 10 µL per well of a 384-well Skirted PCR plate (STARLAB) and repeated in triplicate for each sample. The plate was briefly centrifuged to remove any bubbles in the wells. An adhesive Xtra-Clear Advanced Polyolefin qPCR StarSeal (STARLAB) was placed over the plate and an applicator was used to seal it. The qPCR reaction was run on a Quantstudio 7 Flex Machine (Applied Biosystems) as detailed in Figure 2.10. Quantification of expression of genes of interest was assessed using standard curve analysis. Analysis of data was carried out using Microsoft Excel by calculating the median quantity of the technical replicates and normalising values to the housekeeping gene, *18S*. This method of analysis has previously been validated by our group[289].

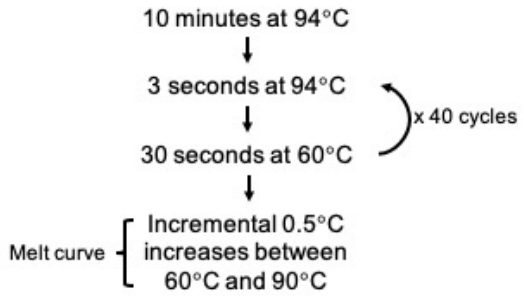

Figure 2.10 | Cycle settings used during qPCR

2.20.7 RNA-seq

Prior to RNA sequencing, RNA was extracted from human PBMCs as detailed in Section 2.20.2. Next-generation RNA sequencing was carried out by the Next Generation Sequencing Facility, University of Leeds. Libraries were created using the TruSeq Stranded mRNA Kit (Illumina) and samples were analysed using a NextSeq 2K (Illumina) with 100 bp per read and 400 million reads per sample. Initial data analysis was carried out by Dr Ian Carr (Next Generation Sequencing Facility, University of Leeds) using R (Version 4.3.1). Subsequent data analysis was carried out by Ailish McCafferty using Microsoft Excel (Version 16.78.3).

2.21 Plaque assay

Plaque assays were used to measure viremia in serum and titre virus stocks. BHK-21 cells were used for all plaque assays. BHK-21 cells were grown to 80% confluency in T75 flasks (Corning). One day prior to beginning the assay (Day 0), media was removed from flask. Cells were then washed in 10 mL PBS twice. 2 mL of 0.25% Trypsin-EDTA (Gibco) was then added for 3-4 mins at RT to dissociate cells from the surface. Cells were monitored under a microscope during this time. Once cells had visibly detached from the surface of the flask, 10 mL DMEM was added to the flask to inhibit the activity of the dissociation reagent and to collect cells. Cell suspension was moved to a 50 mL Falcon Conical Centrifuge Tube (Corning). This cell suspension was centrifuged at 400 xg for 5 mins. Supernatant was discarded, leaving a cell pellet which was resuspended in 50 mL DMEM. 1 mL cell suspension was then carefully administered to each well in a 12-well flat-bottom culture plate (Corning). Plates were left for 30 mins in the tissue culture hood to allow the cells to settle into a monolayer and to avoid clustering before being returned to the incubator (37 °C,

5% CO_2) overnight. Cells were checked the following morning to confirm they had grown to 80% confluency in each well. Serial dilutions of serum or virus stock were then made in 0.75% PBSA. 200 µL of each dilution were added to either two wells to measure viremia or four wells to titre virus stocks. Plates were returned to the incubator for 1h and rocked gently every 10 mins to ensure equal distribution of virus across the cell monolayer. After 1hr, 2 mL of a 1:1 mix of 2XMEM and 1.2% Avicell was added to each well. Plates were then returned to the incubator for 2 days. Following this, the media was removed and cells were fixed in 1 mL of 10% PFA for 1h at RT. 10% PFA was subsequently removed and replaced with 1 mL of 1X Toluidine Blue for 30 mins to stain cells. Toluidine Blue was then washed off with tap water. Plaque assay readout was then performed by choosing a dilution with between 5-20 plaques per well. The number of plaques in the wells with this dilution were then manually counted. The following calculation was used to determine virus titre, measured in PFU/mL:

$$PFU/mL = \frac{average\ number\ of\ plaques\ (across\ replicates)}{volume\ of\ inoculum\ x\ dilution\ factor}$$

2.22 Serum-antibody neutralisation assay

To measure concentrations of virus-neutralising antibody present in mouse serum, the virus killing potential of serum was tested in virus infected BHK-21 cells. Prior to this assay, a plaque assay was used to confirm no residual virus was left in the serum, having likely been neutralised by antibodies *in vivo*. To carry out the neutralisation assay, BHK-21 cells were plated in a 96-well flat bottom plate and grown to 80-95% confluency. Virus-serum mixtures were prepared as follows: serum was diluted 1:10 in PBSA and then serial diluted 1:3. Diluted serum samples were added to the cell culture plate as shown in Figure 2.11. PBSA alone was added to control wells. 10^3 PFU of SFV4 was then added to each well of serum in a volume of 100 µl. The virus-serum mixture was incubated at 37 °C for 1h to allow for any neutralising antibodies present in the serum to neutralise the virus. Following incubation, media was removed from the BHK-21 cells and cells were washed once with PBS. 90 µl of each well of the virus-serum mixture (or the PBSA control) was added to a well of BHK-21

cells and incubated at 37 °C for 1h. After the incubation period, 100 µl of DMEM was added to each well. The infected cells were moved to the incubator and monitored for cytopathic effect, which occurred approximately 2 days later. At this point, cells were fixed in 100 µl of 10% PFA for 1h at RT. After fixing, 100 µl of crystal violet dye was added to cells and incubated for 1h at RT to stain intact cells. Plates were then washed using tap water to remove excess dye. Plates were imaged on the ChemiDoc XRS+ gel imager (BioRad) and analysed using ImageJ. The percentage of each well which was stained and quantified, was used as a readout of protection from virus offered by serum, as lysed cells do not stain with crystal violet dye.

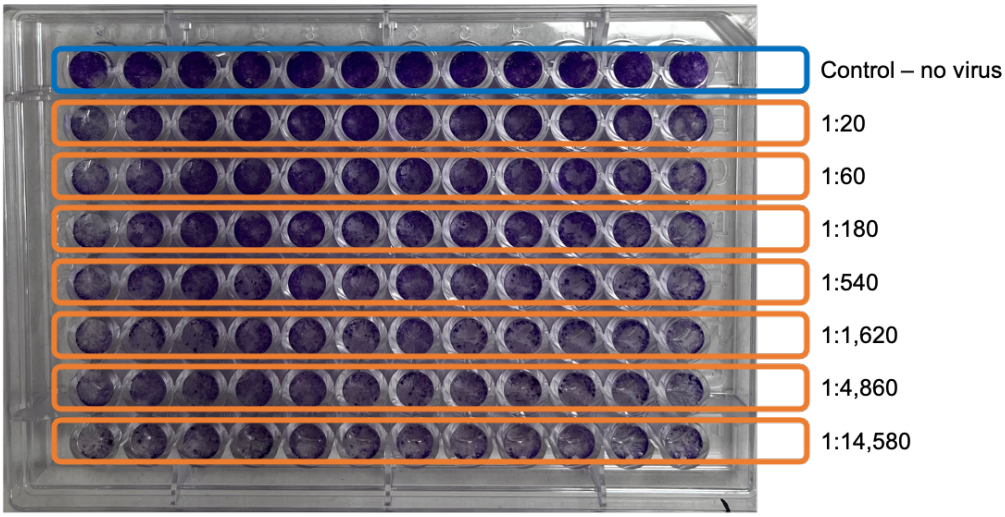

Figure 2.11 | Example plate layout from serum-neutralisation assay showing dilutions of serum used

2.23 Microscopy

2.23.1 *In vivo* procedure, tissue harvest and preparation for microscopy

Mice were anesthetised using isoflurane, administered via inhalation. Mice who were to be exposed to UV on the dorsal region had their fur shaven prior to exposure. Depending on the group of the mice, either the skin on the upper foot or a small region on the lower dorsal region of the torso was placed directly on top of an 8W UVM-28 mid-range lamp (302 nm peak at 1mW/cm, Ultraviolet Products). Mice were exposed to 1 dose of 200 mJ/cm^2 (erythemal dose) of UVR. The UV dosage was controlled via the length of time the foot or dorsal region was exposed to radiation, equating to 6 mins exposure time for 200

mJ/cm^2. Mice were then culled at a set time point post-UV exposure (24h, 1wk, 2wk or 3wk post-UV). For back samples, the fur from the UV-exposed region on the dorsal side of mice was shaved againto ensure tissue samples were hairless. For all samples, skin was carefully dissected from the exposed region (back or foot) to avoid stretching of the tissue. Samples were then unfurled using forceps and moved to 5 mL bijou containers (VWR) containing 10% Buffered Formalin (Statlab Medical Products) for 48h for fixation. Samples were then transferred to 70% ethanol (Sigma-Aldrich) and within 3 days, samples were embedded in paraffin. Paraffin blocks were sectioned, mounted on slides and stained with haematoxylin and eosin (H&E) to visualise the nuclei, ECM and cytoplasm. Sample processing was conducted by the Leeds Institute for Medical Research (LIMR) Histology Service (University of Leeds). Embedded samples were then stored at 4 °C.

2.23.2 Analysis of scanned histology images

Slides were initially imaged using an Olympus BX41 DIC Microscope (Olympus) before being scanned at 20X magnification using the ZEISS AxioScan Z.1 Slide Scanner (ZEISS) by the Faculty of Biological Sciences' Bioimaging and Flow Cytometry Facility (University of Leeds). Scanned images were analysed using the open-source software QuPath v0.3.2 [290]. Measurements of the epidermis, dermis and fatty layer were taken from 10 areas per condition. The epidermis was measured from the top of the section to the basement membrane.

2.24 Statistical analysis

All data was analysed using GraphPad Prism (Version 9.0.0). The Shapiro-Wilk Test was used to determine whether the data was normally distributed. If data was normally distributed, significance was assessed using an unpaired t-test for experiments with two experimental groups or an ordinary one-way ANOVA for experiments with more than two experimental groups. If data was not normally distributed, significance was assessed using Mann-Whitney for experiments with two experimental groups or Kruskal-Wallis test with Dunn's multiple comparison test for experiments with more than two experimental groups. All plots display the median value +/- interquartile range with *$*p < 0.05, **p < 0.01, ***p < 0.001, ****p < 0.0001$*, ns = not significant.

Chapter 3: SFV infection is enhanced *in vivo* at an acute timepoint following an erythemal UV exposure, through recruitment of myeloid cells which are targeted by the virus

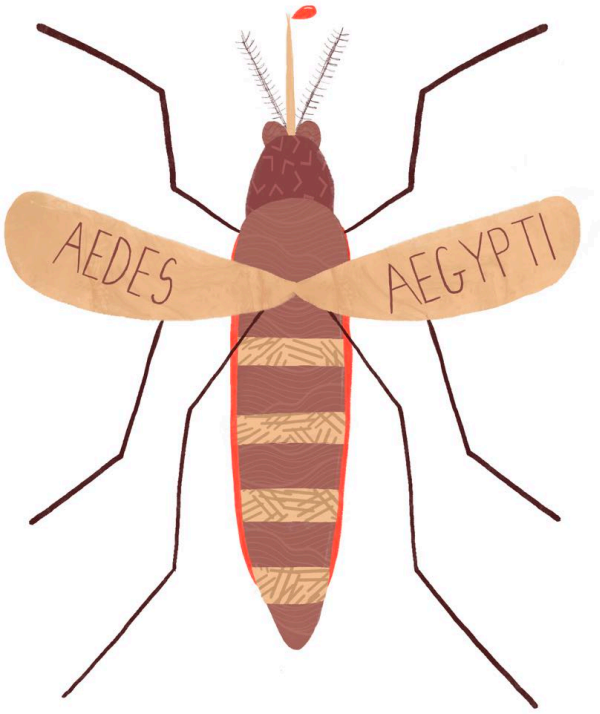

3.1 Introduction

Arbovirus infections have surged in recent years and case numbers continue to rise year-on-year[8]. Although the majority of arbovirus infections cause asymptomatic or mild symptoms, there are a significant proportion of cases that go on to develop severe, potentially life-threatening disease[291]. While there are no antivirals currently available for any arbovirus infection, early intervention, involving rudimentary measures such as administration of fluids and continual monitoring, has been shown to be of some use e.g., to reduce DENV-associated morbidity and mortality[292]. Therefore, it is of vital importance for clinicians to be able to stratify patients based on risk of severe disease development. Furthermore, an awareness of factors that influence host susceptibility to infection can be used to inform public health information or travel advice, particularly during outbreaks.

The factors which underpin this variability in severity between individuals are not clear. However, it is likely that a combination of host, virus, vector and environmental factors are at play. Identifying key factors which contribute to the severe disease phenotype would facilitate the identification of at-risk patients and allow for earlier medical intervention. Preventing the development of severe disease in this way is vital to limit arbovirus-associated deaths. A better understanding of the biology underpinning these infections could also assist in the develop of effective antivirals and/or vaccines.

Our lab group has previously shown that the mosquito bite, which transmits virus at the skin, enhances infection by a number of arboviruses, including SFV[120]. The bite drives a highly inflammatory environment in the skin, including the recruitment of myeloid cells to the site of infection, some of which are subsequently infected by virus. As a result, when virus is inoculated in the skin of C57BL/6 mice alongside a mosquito bite, mice experience higher quantities of virus replication in the skin, increased dissemination of the virus to other tissues and lower survival rates. This led us to consider whether other factors which promote inflammation at the skin have the potential to impact host susceptibility to arbovirus infection.

Exposure to UVR from the sun is an environmental factor which is of upmost relevance during arbovirus transmission, which are transmitted in tropical and sub-tropical regions of the world. Arbovirus transmission zones overlap with regions with high UV indices (UVI), meaning individuals there are exposed both to arbovirus infections but also high levels of UV light from the Sun (Figure 3.1)[35,221]. Additionally, the average global UVI is expected to increase as a consequence of climate change, meaning that people will be exposed to higher levels of UVR in the coming years[293]. At the same time, the gradually warming climate is expanding the regions in which key arbovirus vectors, such as the *Aedes aegypti* mosquito, can live and spread disease to humans[48].

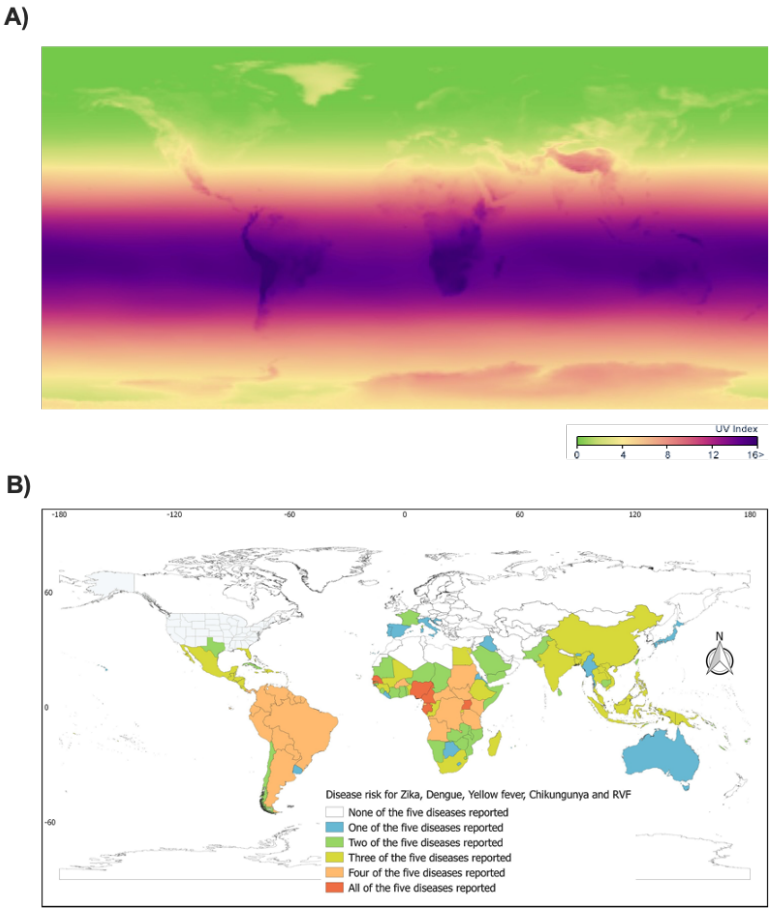

Figure 3.1 | Global arbovirus transmission zones overlap with areas of the world where solar UV exposure levels are highest

(A) Chart from NASA Earth Observations (NEO) showing the UVI distribution across the world in December 2010[221]. The UVI is an indicator of the levels of UVR reaching the Earth's from the Sun in a given area. The UVI peaks at areas around the equator. Green areas have the lowest UVI, 0, and purple areas have the highest UVI, 16+.

(B) Map from Leta et al., 2018 showing global distribution of arbovirus disease risk[35]. The map shows data on five selected arboviruses: ZIKV, DENV, YFV, CHIKV and Rift Valley Fever (RVF). The scale ranges from white areas, which have reported no cases of any of these diseases, to red areas, which have reported cases of all five of these.

UV exposure of the skin has a range of biological impacts, outlined in more detail in Section 1.4. Importantly for this study, UVR can be a potent pro-inflammatory stimulus for skin. Exposure of the skin of C57BL/6 mice to a single, erythemal dose of UVB radiation, measuring 100mJ/cm^2, similar to sunburn in humans, induces a pro-inflammatory state in the skin by 24h post-exposure[240]. This is characterised by expression of a number of inflammatory cytokines, such as TNF-α and IL-6, and also chemokines, such as CCL2 and CXCL2. Erythemal UV exposure drive a similar response in human keratinocytes *in vitro*[294]. Chemokines which are known to attract myeloid cells, such as CCL2 and CXCL2, are also induced in the skin of mice by 24h after an erythemal UV exposure[295]. Correspondingly, neutrophils infiltrate UV-exposed skin by 24h following a higher 500mJ/cm^2 dose of UV[296]. Although whether monocytes are also recruited to UV-exposed skin remains to be determined.

The conditions in UV-exposed skin described here are reminiscent of those induced by the arbovirus-enhancing mosquito bite[120]. In this scenario, neutrophils further deepen the inflammatory state in the skin and monocytes, which are virus permissive, provide the virus with new targets for infection. Therefore, it is possible that UV-exposed skin could also be more susceptible to arbovirus infection as a result. Furthermore, UV exposure not only induces inflammation locally, but drives a cascade of inflammatory cytokine expression, including IL-1β, TNF- α and IL-6, in the blood and kidneys within 24h of the exposure[297,298]. This suggests that dissemination of virus, e.g. to the blood, could also be altered following an erythemal UV exposure.

Thus far, UV exposure has been shown to have very different impacts on infection outcomes based on the pathogen; from reactivating latent HSV and VZV infections and enhancing *Candida albicans* and *Borrelia burgdorferi* infections, to protecting against *Mycobacterium tuberculosis*[299–303]. UV exposure of the skin is a factor of particular relevance to arbovirus infections, both due to

it being an environmental variable in arbovirus transmission zones and because of the impact it has on inflammatory responses at the arbovirus inoculation site, the skin. However, it is not known whether UV exposure impacts host susceptibility to mosquito-borne virus infection.

3.1.1 Hypothesis and aims

Together, the evidence outlined here led us to hypothesise that myeloid cells will be present in the skin of mice by 24h after a single, erythemal UV dose, measuring 100mJ/cm^2. Because some myeloid cells, such as monocytes, are permissive to infection, we hypothesise that mice will be more susceptible to arbovirus infection in UV-exposed skin at 24h-post exposure as a result.

Therefore, the major aims and objectives of this first chapter are to:

1) **Adapt an established *in vivo* mouse model of erythemal UV exposure to include mosquito biting and SFV infection and characterise the physiological impact of erythemal UV exposure on the skin at 24h post-exposure.**
2) **Use this *in vivo* approach to investigate whether erythemal UV exposure of the skin alters host susceptibility to SFV infection at an acute timepoint, 24h post-exposure.**
3) **Investigate the mechanisms driving any observed changes to host susceptibility following erythemal UV exposure at 24h post-exposure.**

3.2 Characterisation of skin 24h after erythemal UV exposure

A previously described mouse model[240] was optimised to investigate the impact of UV exposure on resting skin. For later experiments in this chapter, we incorporated new aspects, mosquito biting and SFV infection, to this established model to investigate arbovirus infection in UV-exposed skin. C57BL/6 mice were exposed to 400mJ/cm^2 of UV light on the skin on the upper side of their left feet. This level of UVR is equivalent to 2 Minimal Erythemal Doses (MED), the minimum dose required to cause erythema, or redness, of the skin. This dosage models a harmful exposure to the sun, or sunburn, in humans. The UV lamp used emits mostly UVB radiation (70-80%), with the remaining light being UVA.

While most studies on UV use only UVB, this model better replicates natural sunlight, which consists of both UVA and UVB. Although the proportions of each type are different, with the UV lamp emitting more UVB than the Sun. However, UVB is responsible for much of the harm caused by UV, including sunburn[304].

Initially, to characterise the phenotype of this model, histology sections from resting skin and mice with a UV burn were examined 24h post-UV exposure. The UV-exposed skin shows a noticeable inflammatory infiltrate to the skin at this timepoint (indicated by the arrow), particularly in the dermis, which is not present in the unexposed skin (Figure 3.2A). Furthermore, the structure of the skin is abnormal and disrupted by 24h post-UV. The epidermis is disrupted and damaged. The thickness of the skin layers was quantified using the imaging software QuPath to further investigate any changes to the tissue structure after exposure to an erythemal dose of UV. Although the depth of the epidermis and the dermis remained the same following a UV exposure, the fatty layer became significantly thinner (Figure 3.2B). Loss of the subcutaneous fat in this way is linked with fibrosis development in mice[305,306]. These findings displayed the marked physiological impact that exposure of the skin to an erythemal dose of UV has on the structure of the tissue.

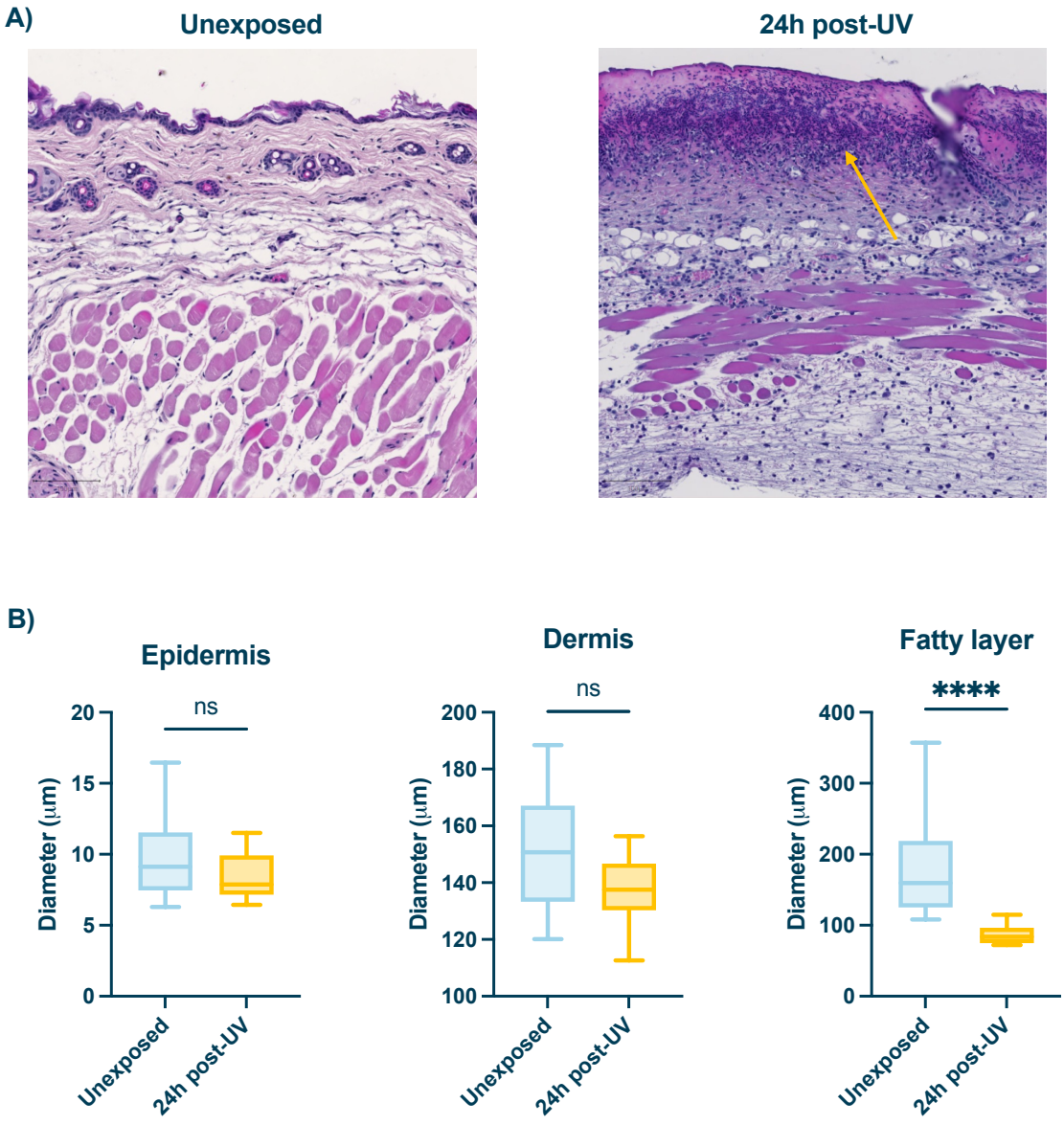

Figure 3.2 | Skin exposed to erythemal UV is characterised by cellular infiltrate at 24h post-exposure

(A) Histology of resting skin or skin exposed to erythemal UV 24h prior, taken from the dorsal region of C5BL/6 mice. Sections stained with H&E. Yellow arrow indicates cell infiltrate. Images shown are representative of the group. Scalebars measure 100 µm. Slides scanned at 20x magnification.

(B) Measurements of epidermis, dermis and fatty layer thickness were taken from 10 areas per condition using QuPath. Plots show the median value ± interquartile range. Data were analysed using unpaired t-test *(*P < 0.05, **P < 0.01, ***P < 0.001, ****P < 0.0001*).

It has previously been shown that both the mosquito bite or mosquito saliva by itself enhances arbovirus infection. Saliva and mosquito bites increase vascular

permeability, and subsequently oedema at the skin, which facilitates entry of virus-permissive myeloid cells to the site[126,134]. As a result, increased oedema is associated with enhanced susceptibility to arbovirus infection. Importantly, one of the earliest symptoms of sunburn in humans is oedema, occurring as a result of UV-induced vasodilation[226,237]. This, together with the link between oedema and enhanced arbovirus infection, made it pertinent to investigate whether erythemal UV exposure increases vascular permeability in mouse skin, by measuring oedema at the skin 24h after a UV burn.

Evan's Blue Dye was used to quantify the amount of oedema and thereby vascular permeability in the UV exposed mice. This dye binds the protein albumin, in blood plasma[307]. At rest, the endothelial barrier does not allow movement of albumin through it. However, inflammation can increase vascular permeability, causing this barrier to lose its integrity and allow larger molecules, such as albumin, to pass through. As a result, the concentration of Evan's Blue Dye in the tissue of interest, e.g. the skin, can be measured as an indication of vascular permeability and oedema at the inflamed site.

To investigate the impact of UV on oedema, Evan's Blue Dye was injected at the scruff of the neck, a site distant from the UV exposed skin in the feet. If required, mice were exposed to mosquito bites at the UV-exposed site 1h after dye had been injected, to determine the magnitude of any effect, with comparison to this known enhancer. Oedema was quantified based on the concentration of dye in the skin 3h after it had been injected.

Compared to resting skin, oedema was increased in mice following a UV burn and this was even higher in mice exposed to a mosquito bite, in addition to a UV burn (Figure 3.3). This characterisation of the skin 24h after an erythemal UV exposure shows that this environmental factor drives a pro-inflammatory response at the skin which may present a favourable environment for arbovirus that promotes more efficient infection.

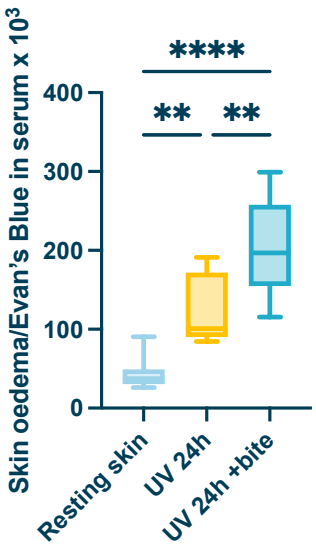

Figure 3.3 | Erythemal UV induces increased vascular permeability, alone and in combination with *Aedes aegypti* bite

Mice were exposed to erythemal UV to upper right foot. 24h later, mice were injected s.c. with Evans blue to scruff of neck, distant from the burn site. Mice were then exposed to mosquito bites at the burn site. The extent of oedema was assessed by quantification of Evan's blue dye leakage into skin at 3 h post-biting via colorimetric assay (n = 8).

Plots show the median value ± interquartile range. Data were analysed using ordinary one-way ANOVA with Tukey's multiple comparisons test (***P < 0.01, ****P < 0.0001*)

3.3 Arbovirus infection is enhanced in mice exposed to erythemal UV 24h prior, despite a robust induction of Type I IFN system during infection

The phenotype of erythemal UV exposed skin 24h after the burn, shown in the previous section, mimic many aspects observed in mosquito-bitten skin, defined by increased oedema and inflammatory infiltrate to the tissue. The mosquito bite and/or mosquito salivary gland extract has been shown numerous times to enhance infection by a range of arboviruses from different virus families[120,126,140,182]. Therefore, hypothesised that erythemal UV exposure would also have the capability to alter host susceptibility to arbovirus infection.

In order to investigate this, the *in vivo* model from Section 3.2 was adapted to include mosquito biting and arbovirus infection. C57BL/6 mice were exposed to an erythemal dose of UV to the dorsal (upper) side of the left foot as described

earlier. Then 24h after the UV exposure, mice were exposed to bites from 2-3 *Aedes aegypti* mosquitos at the UV burn site. Immediately after biting, the same site was inoculated s.c. with 10^4 PFU of the *Aedes* cell-derived arbovirus SFV4 in a total volume of 0.5 μl using a microneedle, as previously described[289]. The microneedle and sub-microlitre volume of inoculum were used in order to mimic the injection of virus-containing saliva via the mosquito proboscis during a blood meal. As a whole, this *in vivo* model aims to replicate natural arbovirus transmission in UV-exposed skin as closely as possible. Mice were culled at 24h post-infection and tissues were collected for analysis. Quantities of virus RNA at the skin were determined using qPCR to measure copy number of the SFV-encoded gene, E1, which codes for a viral membrane protein. Plaque assays were used to quantify quantities of infectious virus in the serum of mice, also known as viremia.

At 24h post-infection, quantities of virus RNA in the inoculation site, the skin, were significantly higher in mice previously exposed to both UV and a mosquito bite than mice with resting skin (Figure 3.4A). Importantly, these mice had more SFV present in the skin than mice exposed to just a mosquito bite, a known enhancer of arbovirus infection[120]. These trends are evident to an even greater extent in the serum of infected mice, with the mice which were exposed to both a bite and a UV burn prior to infection experiencing ~100-fold higher quantities of viremia than mice with no burn or bite. (Figure 3.4B). Together, this data shows that erythemal UV significantly enhances host susceptibility to arbovirus infection, both in terms of quantities of virus RNA at the skin and spread of infectious virus to the blood.

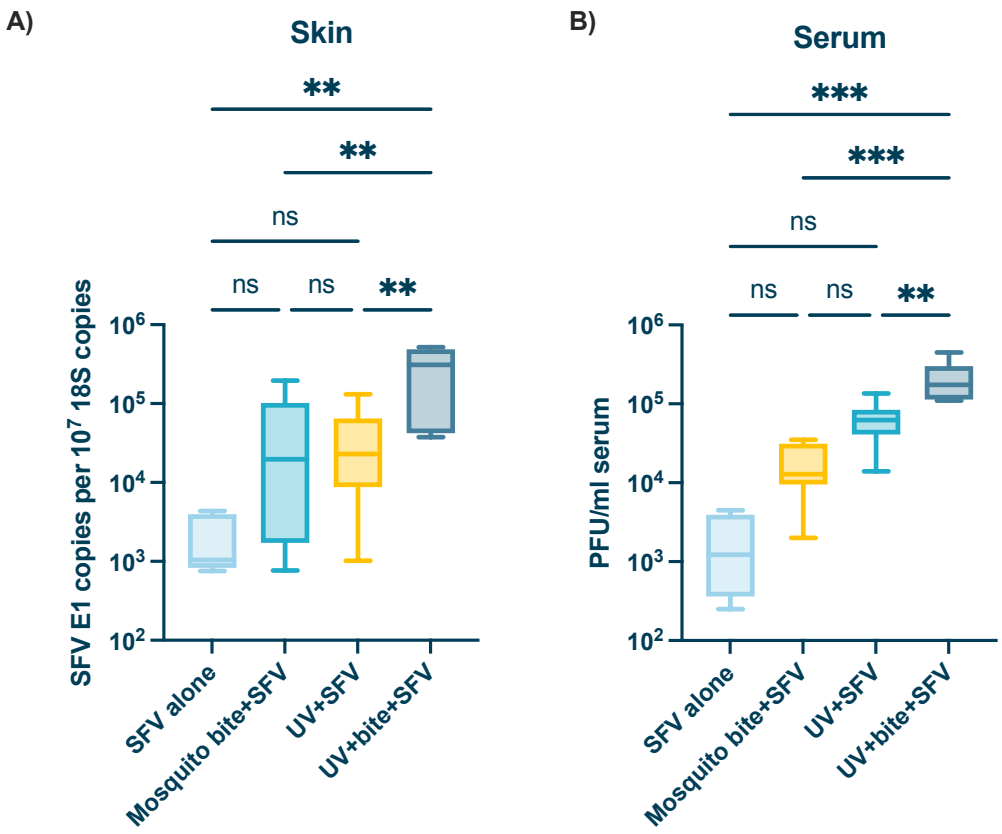

Figure 3.4 | Erythemal UV enhances SFV infection at 24h post-UV

(A-B) SFV RNA (E1 gene) copy number in inoculation site (skin) **(A)** and viral titres in the serum **(B)** 24hpi. Prior to infection, mice were either left unexposed or were exposed to an erythemal dose of UV on the skin on the upper side of the foot. All mice were then infected 24h post-exposure at the same site with 10^4 PFU of SFV4 in the presence or absence of a mosquito bite. (n = 6)

Gene expression measured by qPCR. Titres of virus in serum determined by plaque assay. Plots show the median value ± interquartile range. Data were analysed using ordinary one-way ANOVA with Tukey's multiple comparisons test (*ns = not significant, **P < 0.01, ***P < 0.001*).

Furthermore, there is increasing evidence that UV exposure modulates induction of Type I IFN, locally in the skin and systemically[296,298]. As discussed in Section 1.2.1, the antiviral Type I IFN response is critical for limiting virus infection *in vivo* and their clearance and so any impact UV exposure of the skin has on this system has the potential to contribute to UV-mediated enhancement of infection. Therefore, we sought to define whether IFN and ISG expression are increased in our model of UV exposure. We characterised the Type I IFN response in our erythemal UV exposure model over time, in the absence of virus, to determine whether UV may induce an antiviral environment in the skin

prior to infection. Following UV exposure, skin was collected from mice at 24h, 48h, 72h or 96h post-erythemal UV exposure, with skin taken from resting controls as a comparison. Gene expression was quantified using qPCR.

There was no measurable change in expression of IFN-β, one of the key IFNs in the Type I IFN system (Figure 3.5A). However, IFN-β can be difficult to detect due to its low expression levels even when upregulated in cells[308]. If IFN-β levels are undeterminable, expression of ISGs, which are induced in response to IFN stimulation, can demonstrate Type I IFN activity instead. We choose to study four prototypic ISGs, that have previously been shown to be upregulated by SFV infection in skin[308]. However, expression of these ISGs were also not significantly increased in the skin by 24h post-UV exposure, the timepoint at which mice were infected during previous experiments (Figure 3.5B). Upregulation of skin ISGs at time points beyond 48h are likely too late to modulate overall outcome to virus infection, as virus disseminates systemically within 24hpi. Nonetheless, we found that by 48h, only ISG15 and IFIT1 expression had significantly increased compared to unexposed mice. By 72h post-exposure, expression of RSAD2 and CXCL10 had also significantly increased. This shows that significant induction of the Type I IFN system does not occur until 48h-post-UV. Therefore, the induction of Type I IFNs in response to erythemal UV exposure, although not completely suppressed, is somewhat delayed and so may be of limited benefit in protecting mice from arbovirus infection when transmitted at UV exposed skin at 24h post-UV.

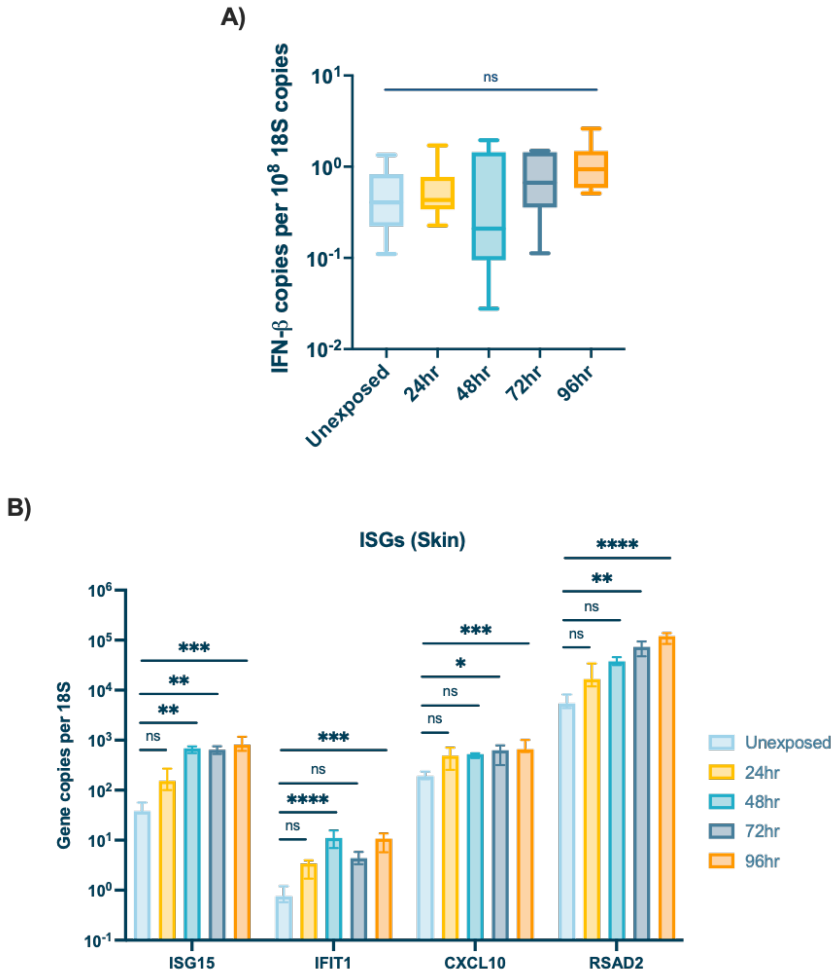

Figure 3.5 | Induction of Type I IFNs post-UV exposure is too late to modulate infection outcome

(A-B) IFN-β **(A)** or ISG **(B)** gene expression in the skin of mice following erythemal UV exposure. Mice were exposed to a single erythemal UV dose and skin was collected at either 24, 48, 72 or 96 hours post UV exposure. Control tissues were taken from unexposed mice. Gene expression was measured in the skin by qPCR. ($n \geq 6$)
Plots show the median value ± interquartile range. Data were analysed using Kruskal-Wallis test with Dunn's multiple comparison test (*ns = not significant, *P < 0.05, **P < 0.01, ***P < 0.001, ****P < 0.0001*).

The robust induction of the Type I IFN response by 48-72h post-UV exposure shown in the last figure led us to consider whether erythemal UV exposure still enhances host susceptibility to arbovirus infection at timepoints later than 24h post-UV exposure, in the presence of these antiviral responses. To investigate this, we infected mice with SFV at either 24h, 48h or 72h post-UV exposure. At 24hpi, quantities of virus RNA in the skin were significantly higher than unexposed mice, as expected (Figure 3.6A). However, virus quantities in the

skin decreased in mice exposed to UV 48h and 72h before infection, the timepoints at which we had shown an increase in expression of antiviral ISGs in the inoculation site, the skin, in response to erythemal UV. As before, virus RNA quantities in the skin were mirrored by infectious virus titres in the blood. Viremia significantly increased in mice exposed to UV 24h prior, before decreasing closer to normal infection quantities in mice exposed to UV 48h and 72h before infection (Figure 3.6B). This shows that virus infection appears to be better controlled at a similar timepoint when ISG expression is induced in response to the erythemal UV exposure, although this could be coincidental.

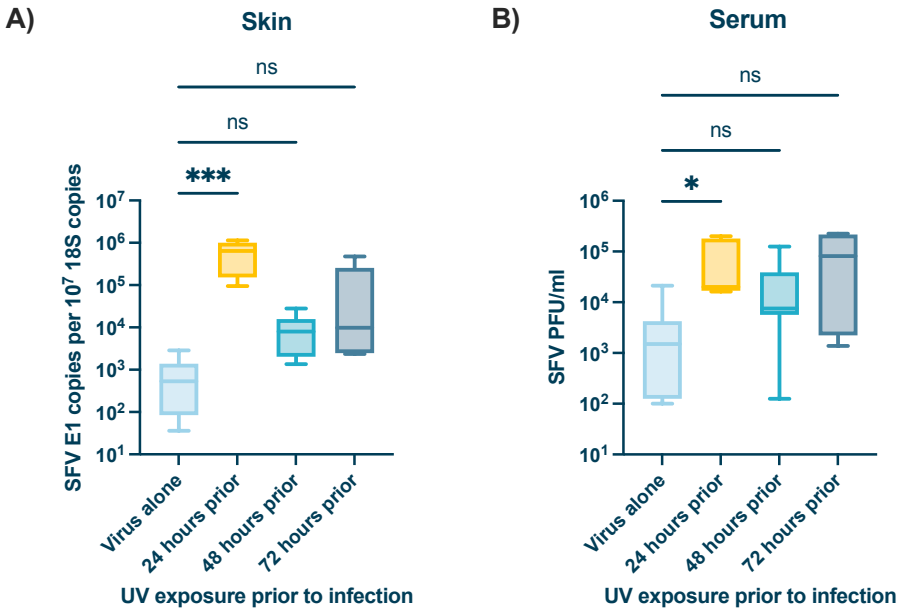

Figure 3.6 | UV-mediated enhancement of arbovirus infection dips at 48h and 72h post-exposure

(A-B) SFV RNA (E1 gene) copy number in inoculation site (skin) **(A)** and viral titres in the serum **(B)** 24hpi. Prior to infection, mice were either left unexposed or were exposed to an erythemal dose of UV on the skin on the upper side of the foot. All mice were then infected at either 24h, 48h or 72h post-exposure at the same site with 10^4 PFU of SFV4 in the presence of a mosquito bite. ($n \geq 6$)

Gene expression measured by qPCR. Titres of virus in serum determined by plaque assay. Plots show the median value ± interquartile range. Data were analysed using Kruskal-Wallis test with Dunn's multiple comparison test (*ns = not significant, *P < 0.05, ***P < 0.001*).

Although we had characterised the Type I IFN response in UV-exposed skin, we postulated that this would likely change with the addition of virus. This led us to

examine expression of a Type I IFN and key antiviral ISGs in the skin of virus infected mice with unexposed skin, or skin which had been exposed to UV 24h, 48h or 72h prior to SFV infection. Interestingly, IFN-β expression was significantly higher in the skin of mice exposed to UV 24h prior to infection, compared to unexposed mice, the timepoint at which susceptibility to arbovirus infection is significantly increased in UV-exposed mice (Figure 3.7A). However, there was no significant difference in expression of IFN-β in mice exposed to UV 48h or 72h before virus infection. This contrasts the results from Figure 3.5, which showed that exposure of skin to erythemal UV did not significantly increase expression of IFN-β between 24-96h post-UV exposure, in the absence of virus. We also quantified expression of some key antiviral ISGs, ISG15, IFIT1, CXCL10 and RSAD2, which act as the effector molecules of the Type I IFN system. These ISGs were all significantly higher in mice exposed to UV 24h before infection, compared to unexposed mice (Figure 3.7B). The exception to this was IFIT1 which was not significantly increased in UV-exposed mice. Again, there was no difference in expression of these ISGs in mice exposed to UV 48h or 72h prior to infection compared to unexposed mice. This differs from the induction of ISGs by 48h and 72h post-UV in the absence of virus shown in Figure 3.5, suggesting that virus may be interfering with this system by later timepoints. Nevertheless, The induction of IFN/ISG expression parallels the quantity of SFV RNA (Figure 3.6A), suggesting that this difference in skin IFN may be driven by quantity of skin virus. This suggests that although ISGs are expressed to a high level during SFV infection in UV-exposed skin at 24h post-UV, this is not enough to control the virus during UV-mediated enhancement of infection at this timepoint.

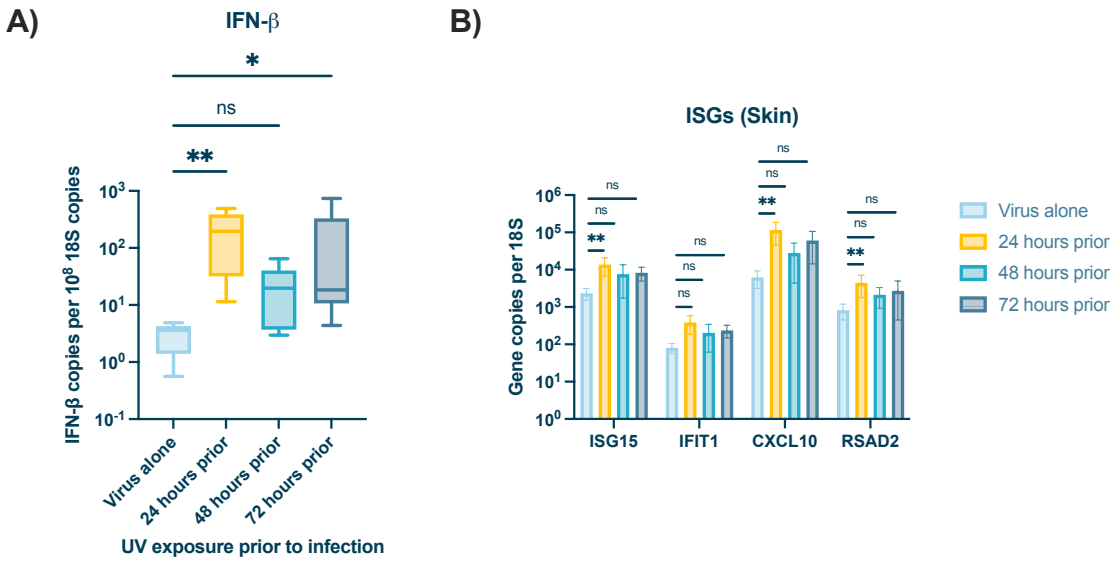

Figure 3.7 | Expression of the type I IFN, IFN-β, and key antiviral ISGs peak at timepoints when UV-mediated enhancement of arbovirus infection is highest

(A-B) IFN-β **(A)** or ISG **(B)** copy number in inoculation site (skin) 24hpi. Prior to infection, mice were either left unexposed or were exposed to an erythemal dose of UV on the skin on the upper side of the foot. All mice were then infected at either 24h, 48h or 72h post-exposure at the same site with 10^4 PFU of SFV4 in the presence of a mosquito bite. ($n \geq 6$)

Gene expression measured by qPCR. Plots show the median value ± interquartile range. Data were analysed using Kruskal-Wallis test with Dunn's multiple comparison test (*ns = not significant, *P < 0.05, **P < 0.01, ***P < 0.001*).

Hypothetically, suppression of IFN function could explain how UV exposure enhances susceptibility to virus. However, due to our findings showing robust Type I IFN induction during infection in UV-exposed mice, we hypothesised that UV-mediated enhancement of infection occurs independently of the Type I IFN system. To definitively determine whether Type I IFN was required for the observed increase in host susceptibility to arbovirus infection in UV exposed mice at 24h post-UV, we used the *Ifnar*$^{-/-}$ mouse strain. These mice lack the Type I IFN receptor and so can't respond to stimulation by IFN-α or IFN-β. These mice were either left unexposed or were exposed to erythemal UV 24h or 48h prior to infection with 500 PFU of SFV4. Due to the immunodeficient status of these mice, a lower dose of SFV was used compared to our previous experiment to minimise the severity of the infection with regards to the welfare of the mice. For the same reason, we did not incorporate a mosquito bite in this

model either, due to the virus-enhancing properties of the bite. At 24hpi, *Ifnar*$^{-/-}$ mice exposed to erythemal UV 24h prior to infection still had significantly higher quantities of virus in the skin compared to unexposed *Ifnar*$^{-/-}$ mice (Figure 3.8A). Despite this, viremia was not significantly different in *Ifnar*$^{-/-}$ mice exposed to erythemal UV 24h prior, although there is an increasing trend (Figure 3.8B). However, *Ifnar*$^{-/-}$ mice exposed to erythemal UV 48h before infection did not have significantly higher quantities of virus RNA in the skin (Figure 3.8C) or infectious virus in the serum (Figure 3.8D) by 24hpi compared to unexposed mice. In summary, since an erythemal UV exposure 24h prior to infection still enhances arbovirus infection in both WT and *Ifnar*$^{-/-}$ mice, which are unable to respond to IFN-α or IFN-β, this suggests that suppression of the Type I IFN system by UV is unlikely to explain the increased susceptibility that occurs at this timepoint.

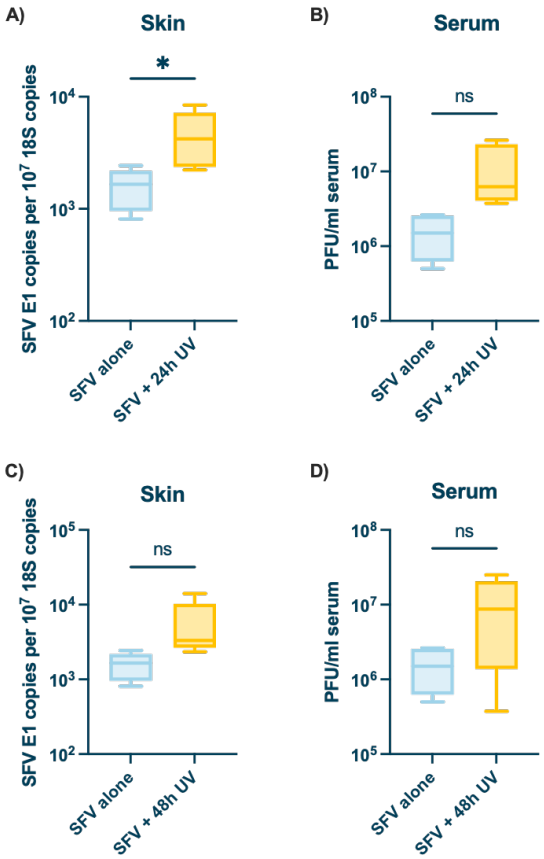

Figure 3.8 | Erythemal UV enhances SFV infection in *Ifnar*$^{-/-}$ mice at 24h post-UV

(A-B) SFV RNA (E1 gene) copy number in inoculation site (skin) **(A, C)** and viral titres in the serum **(B, D)** 24hpi. Prior to infection, *Ifnar*$^{-/-}$ mice were either left unexposed or were exposed to an erythemal dose of UV on the skin on the upper side of the foot. All

mice were then infected 24h **(A, B)** or 48h **(C, D)** post-exposure at the same site with 500 PFU of SFV4. (*n* = 5)

Gene expression measured by qPCR. Titres of virus in serum determined by plaque assay. Plots show the median value ± interquartile range. Data were analysed using Mann-Whitney test (*ns = not significant, *P<0.05*).

3.4 Although there are more proliferating cells present in the skin of mice exposed to erythemal UV 24h prior to infection, SFV does not preferentially infect proliferating cells at this timepoint

The above findings suggest the modulation of the Type I IFN system by UV, as a driving mechanism behind enhancement of arbovirus infection following an acute erythemal UV exposure, is unlikely to explain this phenotype. Therefore, we considered whether the phenotype could be related to other effects that UV exposure has on skin. Some cell types in the skin proliferate in response to UV exposure[232]. Additionally, SFV has been used as an oncolytic virus, due to its ability to replicate more efficiently in proliferating cells[309–311]. Based on this evidence, we considered whether SFV may infect proliferating cells in the skin, of which there may be more due to the prior exposure of the skin to erythemal UV 24h before infection.

First, we simply wanted to determine whether exposure of skin to erythemal UV induces proliferation of cells in the skin at 24h post-UV. To investigate this, we used EdU (5-ethynyl-2´-deoxyuridine) to identify proliferating cells. EdU, a thymidine analogue, incorporates into DNA as it is being synthesised during cell proliferation[312]. Skin cells were collected from mice (24hpi), which had either been exposed to prior erythemal UV (24 hours before virus) and infected with virus, or left unexposed and then infected, or left unexposed and uninfected as a control. These cells were then incubated with EdU *in vitro* for 2 hours, to allow the molecule to bind to the DNA of any proliferating cells. Proliferating cells were then identified by tagging EdU with a fluorescent marker using Click-IT chemistry, for subsequent detection via flow cytometry. In comparison to resting skin, there was no significant difference in the number of proliferating cells in the skin of mice infected with SFV alongside a mosquito bite (Figure 3.9). Importantly, erythemal exposure of mice 24h prior to infection did significantly

increase the proliferation of cells in the skin compared to resting skin. This suggests that erythemal UV exposure of the skin drives proliferation of cells at 24h post-UV.

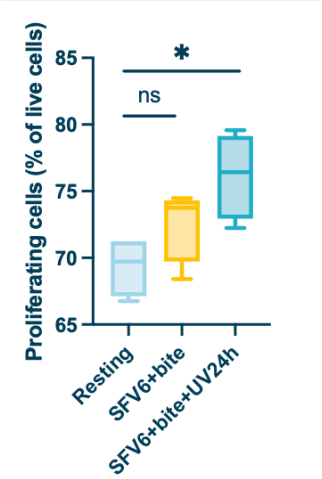

Figure 3.9 | UV exposure drives proliferation of cells at 24h post-UV

EdU+ cells in the skin as a percentage of total live cells. Prior to infection, mice were either left unexposed or were exposed to an erythemal dose of UV on the skin on the upper side of the foot. All mice were then infected 24h post-exposure at the same site with 10^3 PFU of SFV6-mCHERRY in the presence of a mosquito bite. Skin from the exposed site was collected 24h post-exposure and digested to isolate single cells. Cells were incubated with EdU, a thymidine nucleoside analogue, for 2 hours. EdU+ cells were then tagged with a fluorophore using Click-IT chemistry so that proliferating cells could be identified using flow cytometry. (n = 4)

Plots show the median value ± interquartile range. Data were analysed using Kruskal-Wallis test with Dunn's multiple comparison test (*ns = not significant, *P < 0.05*).

As there are more proliferating cells in the skin in UV-exposed mice during infection, we hypothesised that virus would replicate more efficiently in these proliferating cells during UV-mediated enhancement of infection, and that this could contribute to higher quantities of virus observed in UV-exposed mice.

To identify infected cells using flow cytometry, we incorporated a strain of SFV that expresses fluorescent proteins, SFV6-mCHERRY, into the *in vivo* model. Together, this allowed us to identify cells which were both infected and proliferating. We first confirmed by qPCR that SFV6-mCHERRY is enhanced by erythemal UV. There was still an over 100-fold increase in virus RNA in the skin in mice which had been exposed to erythemal UV 24h prior to infection *in vivo*

compared to skin from control mice (Figure 3.10A). Inability to reach statistical threshold was most likely simply due to low number of biological replicates (n=4), and the ability of non-parametric statistical tests, such as the Mann-Whitney test used here, to generate p values of less than 0.05. Nevertheless, we were satisfied that the data followed the same trend as is observed during UV-mediated enhancement of SFV4, and so moved forward with the use of SFV6-mCHERRY as an experimental tool to identify infected cells by flow cytometry.

Next, we quantified the number of cells in the skin which were EdU+ or EdU- and also SFV+ using flow cytometry. To assess whether SFV was preferentially infecting proliferating cells, we analysed all SFV-mCHERRY+ cells, so that the analysis wouldn't be affected by there simply being more proliferating cells in the UV-exposed group. Interestingly, there was no change in the number of infected cells that were also proliferating in the mice exposed to erythemal UV 24h prior to infection, compared to unexposed mice (Figure 3.10B). There was also no difference in the number of infected cells that were classed as 'non-proliferating' (EdU-) (Figure 3.10C). To confirm that SFV does not preferentially infect proliferating cells over non-proliferating cells in mice exposed to erythemal UV 24h prior to infection, we calculated the ratio of 'infected, proliferating cells' to 'infected, non-proliferating cells'. As the ratio is less than 1 for both groups, this confirms that the virus did not disproportionately infect proliferating cells over non-proliferating cells in UV-exposed mice (Figure 3.10D). This was despite there being more proliferating cells present in the skin of UV exposed mice.

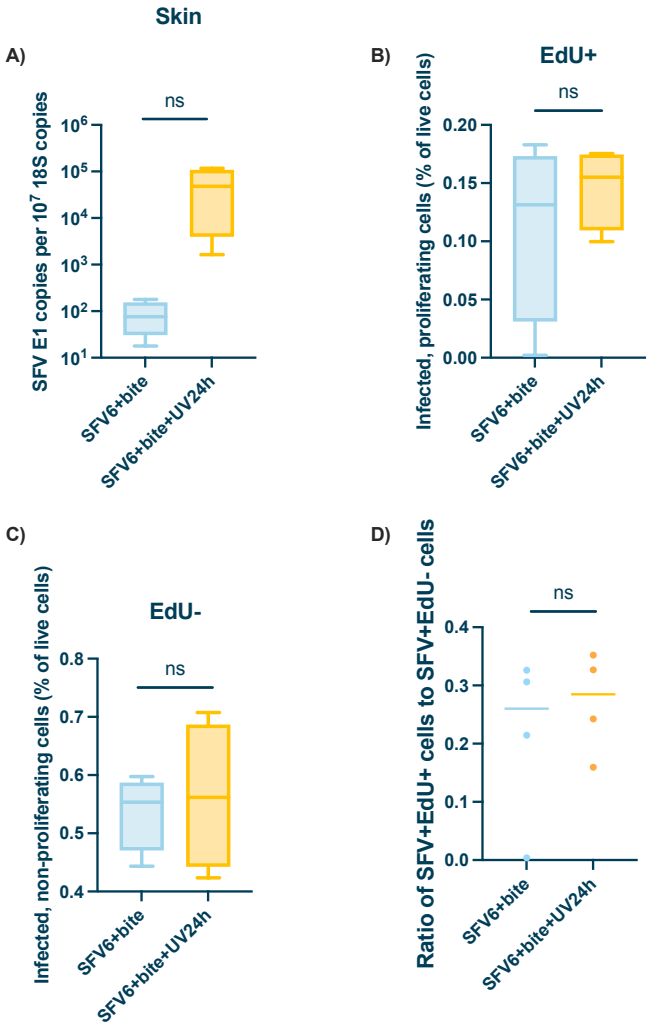

Figure 3.10 | Although there are more proliferating cells in UV exposed skin, SFV does not preferentially infect proliferating cells during UV-mediated enhancement of infection 24h post-UV

(A-D) Prior to infection, mice were either left unexposed or were exposed to an erythemal dose of UV on the skin on the upper side of the foot. All mice were then infected 24h post-exposure at the same site with 10^3 PFU of SFV6-mCHERRY in the presence or absence of a mosquito bite. Skin from the exposed site was collected 24h post-exposure and digested to isolate single cells. Cells were incubated with EdU, a thymidine nucleoside analogue, for 1-2. EdU+ cells were then tagged with a fluorophore using Click-IT chemistry. Proliferating cells (EdU^+) and infected cells ($SFV6\text{-}mCHERRY^+$) could then be identified using flow cytometry. (n = 4)

(A) SFV RNA (e1 gene) copy number in inoculation site (skin) was measured at 24hpi by qPCR.

(B-C) Cells were first gated on SFV^+ and then split into 'infected, proliferating cells' (SFV^+EdU^+) **(B)** or 'Infected, non-proliferating cells' (SFV^+EdU^-) **(C)**.

(D) Ratio of 'infected, proliferating cells' to 'infected, non-proliferating cells'. Ratio of >1 indicates that the virus is preferentially infecting 'proliferating cells'. Ratio of <1 indicates that the virus is preferentially infecting 'non-proliferating cells'.
Plots show the median value ± interquartile range. Data were analysed using Mann-Whitney test (*ns* = *not significant*).

3.5 Immune cell fraction of skin have higher quantities of virus RNA than non-immune cells, during UV-mediated enhancement of infection at 24h post-UV exposure

During mosquito bite-mediated enhancement of infection, SFV infects leukocytes recruited via permeable blood vessels as a result of bite-associated inflammation[289,313]. As there was also evidence of increased oedema and cellular infiltrate at the skin at 24h post-UV, we wanted to determine whether either CD45+ (immune cells) or CD45- (epithelial and stromal cells) were targeted by the virus for replication during infection at 24h post-erythemal UV. To investigate this, we interrogated the quantity of virus RNA in the skin in non-immune cells compared to immune cells in unexposed mice and UV-exposed mice. Mice were exposed to erythemal UV or left resting and then infected with SFV 24h later. At 6hpi, skin from the inoculation site was digested and magnetic separation was used to isolate CD45+ cells from CD45- cells. We used flow cytometry on each fraction to determine the purity of the magnetic separation. While in the CD45+ fraction there were still some $CD45^{lo}$ cells present, almost all $CD45^{hi}$ cells had been effectively removed from the CD45- fraction (Figure 3.11A-B).

Following confirmation of CD45-enrichment in the CD45+ fraction and CD45-depletion in the CD45- fraction, we examined the quantities of virus RNA in each compartment. In mice that had not been exposed to UV prior to infection, there was a relatively equal quantities of virus RNA present in the immune cells compared to the epithelial and stromal cells (Figure 3.11C). Interestingly though, the immune cells which had been isolated from UV-exposed mice had significantly higher quantities of virus RNA compared to the non-immune cells taken from the same mice (Figure 3.11D). This suggests that immune cell fraction exhibit a higher virus burden in the skin during SFV infection in mice exposed to UV 24h prior.

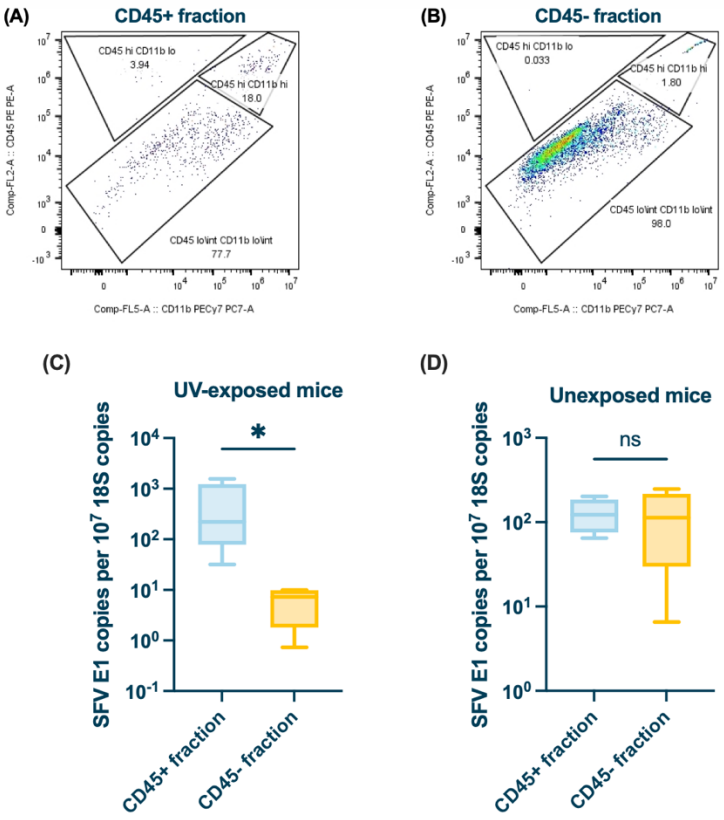

Figure 3.11 | Leukocytes are disproportionately infected by arbovirus during UV-mediated enhancement of infection

(A-D) Mice were either exposed to a single erythemal UV dose or left unexposed. All mice were infected 24 hours post UV exposure with 10^4 PFU of SFV4 in the presence of a mosquito bite. Skin from the inoculation site was collected 6hpi and digested to isolate single cells. Magnetic separation was used to separate cells expressing CD45 (CD45+) from the remaining cells (CD45-). (*n* = 8)

(A, B) Cells from the CD45+ **(A)** and the CD45- **(B)** fractions after CD45+ separation.

(C, D) SFV RNA (*E1* gene) copy number in the CD45+ and CD45- fractions in unexposed **(C)** and UV-exposed **(D)** mice were determined at 6hpi by qPCR.

Plots show the median value ± interquartile range **(C-D)**. Data were analysed using Mann-Whitney test (*ns = not significant, *P < 0.05).*

To uncover what drives the increased quantities of virus RNA in immune cells during UV-mediated enhancement of infection, we next sought to determine whether UV exposure of the skin prior to infection simply makes virus-permissive cells inherently more susceptible to virus infection. If true, this could explain the higher quantities of virus observed in immune cells in the previous figure. We collected and digested resting skin and skin from mice exposed to

UV 24h prior and infected these cells with SFV *in vitro* to determine whether cells from UV-exposed mice would be more permissive to arbovirus infection *ex vivo*. When we quantified the virus RNA in these cells we found that there was no difference in quantities of virus in cells from UV-exposed mice, compared to unexposed mice (Figure 3.12C). This suggests that enhancement of arbovirus infection only occurs *in vivo*. This experiment was then repeated but magnetic separation was used to separate cells into CD45+ and CD45- populations prior to infection, to ascertain whether these was any difference in susceptibility of either cell population to SFV infection *in vitro* after being exposed to UV *in vivo*. We confirmed that the CD45+ fraction was enriched with CD45+ cells and that CD45+ cells had been removed from the CD45- fraction before analysing virus burden in the two compartments (Figure 3.12A,B). Again, there was no difference in quantities of virus RNA in immune cells or non-immune cells from either UV-exposed mice or unexposed mice following *in vitro* infection (Figure 3.12D). This shows that UV does not influence susceptibility to arbovirus infection on a cell-by-cell basis.

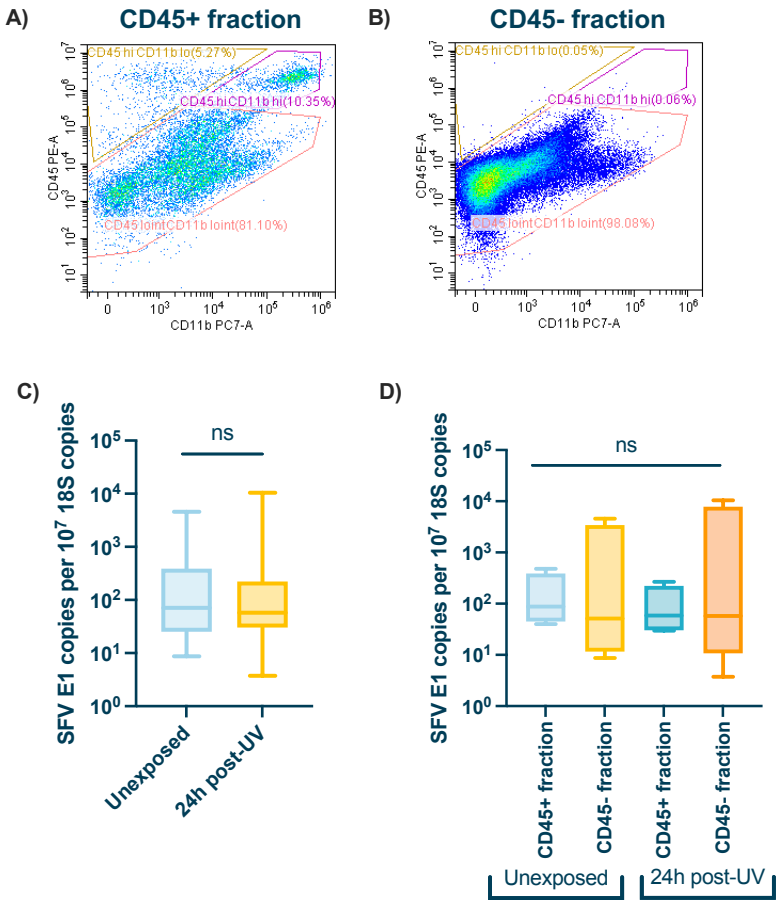

Figure 3.12 | No inherent difference in permissiveness of cells to arbovirus infection 24h after erythemal UV exposure

(A-D) Mice were either exposed to a single erythemal UV dose or left unexposed. Skin from the exposed site was collected 24h post-exposure and digested to isolate single cells. Cells were then infected with SFV4 *in vitro* either immediately, or following magnetic separation into immune cell (CD45+) and stromal or epithelial cells (CD45-) compartments. Quantities of virus RNA were analysed at 16hpi. (*n* = 8)

(A, B) Cells from the CD45+ **(A)** and the CD45- **(B)** fractions after CD45+ separation. **(C)** SFV RNA (*E1* gene) copy number in all cells taken from skin of UV-exposed mice compared to unexposed mice at 16hpi *in vitro*. **(D)** SFV RNA (*E1* gene) copy number in CD45+ and CD45- fractions from unexposed **(C)** and UV-exposed **(D)** mice at 16hpi i*n vitro*.

Gene expression measured by qPCR. Plots show the median value ± interquartile range **(C-D)**. Data were analysed using Mann-Whitney test **(C)** or Kruskal-Wallis test with Dunn's multiple comparison test (*ns* = *not significant*).

3.6 Arbovirus-permissive leukocytes are recruited to the skin in higher numbers in mice exposed to erythemal UV 24h prior to infection

Next, we sought to understand whether erythemal UV-mediated enhancement of infection at 24h post-UV could be driven by similar mechanisms to those which cause increased susceptibility of mice when infected alongside a mosquito bite. Following a bite, neutrophils and monocytes are recruited to the skin *in vivo*[120]. While neutrophils promote an inflammatory state in the skin, monocytes are also permissive to arbovirus infection. This, together with the evidence shown in Figure 3.11 that immune cells have higher quantities of virus RNA during UV-mediated enhancement of infection, led us to investigate whether leukocyte recruitment is altered during UV-mediated enhancement of arbovirus infection at 24h post-UV in a similar way to what we see following a mosquito bite.

The most prominent chemokines which attract neutrophils and monocytes to the skin are CXCL2 and CCL2 respectively, and so we examined expression of these gene transcripts in the skin of mice to see if levels change in response to

erythemal UV. Initially, we assessed chemokine gene expression in the skin of mice 24h, 48h, 72h or 96h and compared this to unexposed skin, in the absence of SFV infection. There was no significant increase in expression of either CCL2 or CXCL2 by 24h post-UV exposure (Figure 3.13A). Both chemokines were significantly upregulated by 48h post-exposure and this increase was maintained up to 96h post-exposure. However, when we quantified expression of these chemokines in the skin of SFV infected mice exposed to UV 24h, 48h, 72h or 1wk prior to infection, we found that CCL2 was significantly upregulated in mice exposed to UV 24h or 1wk prior to infection. These were the two timepoints at which susceptibility to virus infection peaks following UV exposure, compared to mice with no UV exposure (Figure 3.13B). Contrastingly, the neutrophil chemoattractant, CXCL2, was only significantly increased in mice exposed to UV 72h or 1wk prior to infection compared to resting mice. Expression of this gene in mice exposed to UV 24h or 48h before infection did not change significantly. However, it should be noted that although chemokine expression was not significantly upregulated at some of these timepoints, there is a clear overall trend for increased expression with UV. Infection with virus increases this trend with more substantial upregulation of CCL2 in UV exposed skin by 24hpi.

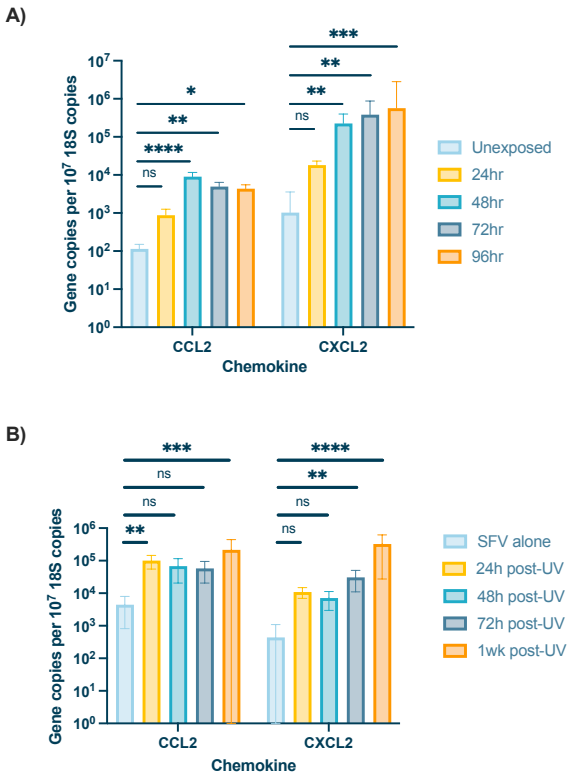

Figure 3.13 | Erythemal UV exposure drives expression of myeloid cell chemoattractants

(A-B) Chemokine gene expression in the skin of mice exposed to a single erythemal UV dose. **(A)** Skin was collected at either 24, 48, 72 or 96 hours post UV exposure. Control tissues were taken from unexposed mice. **(B)** Mice were infected with SFV4 at either 24, 48, 72 or 1wk post UV exposure or at rest and skin was collected 24hpi. (*n* = 6)

Gene expression measured by qPCR. Plots show the median value ± interquartile range. Data were analysed using Kruskal-Wallis test with Dunn's multiple comparison test (*ns = not significant, *P < 0.05, **P < 0.01, ***P < 0.001, ****P < 0.0001*).

CXCL2 and CCL2 are known to recruit neutrophils and monocytes, respectively. Therefore, we hypothesised that the increased expression of CCL2 in mice exposed to UV 24h prior to infection would lead to more monocytes being recruited to the UV-exposed skin during arbovirus infection. To assess this, we used flow cytometry to phenotype and count neutrophils and monocytes present in the skin of mice 16h after infection with 10^4 PFU of SFV4 in the presence or absence of a mosquito bite. 24h prior to infection, mice had been left unexposed or exposed to erythemal UV. This allowed us to compare the cell profile during infection following erythemal UV to that following a mosquito bite, which is known to bring in monocytes[120].

Neutrophil numbers were increased by 16hpi in both groups of mice exposed to erythemal UV 24h prior to infection, compared to non-UV exposed mice (Figure 3.14A-B). This mirrors the trend in increased CXCL2 expression, suggesting leukocyte recruitment has been activated (Figure 3.13). Similarly, monocyte numbers were significantly higher by 16hpi in UV-exposed mice compared to unexposed mice. Therefore, there are more monocytes and neutrophils in UV-exposed mice during infection.

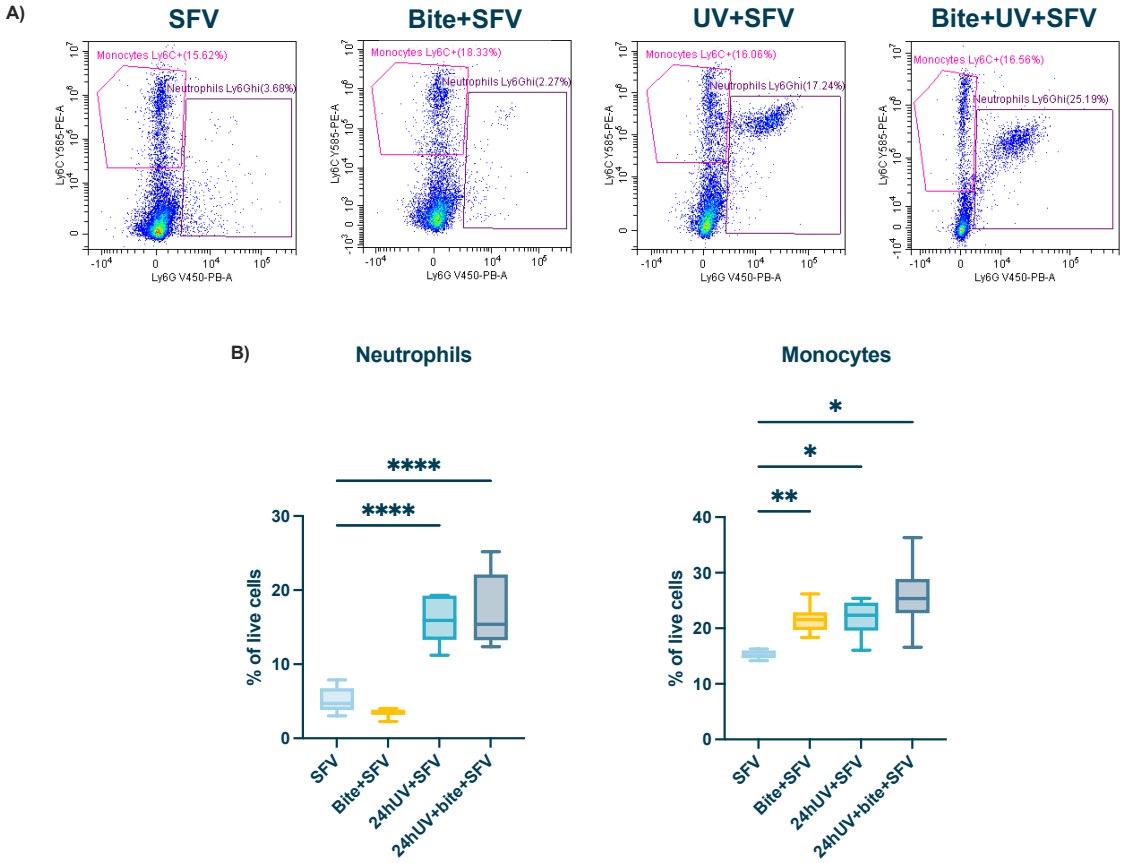

Figure 3.14 | Myeloid cells are recruited to UV-exposed skin in higher numbers during infection

(A) Neutrophil ($CD45^+CD11b^+Ly6G^{hi}$) and monocyte ($CD45^+CD11b^+Ly6C^+$) migration to skin measured by flow cytometry at 16hpi. **(B)** Numbers represent percent of $Ly6C^+$ or $Ly6G^{hi}$ cells of all live cells. Prior to infection, mice were either left unexposed or were exposed to an erythemal dose of UV on the skin on the upper side of the foot. All mice were then infected 24h post-exposure at the same site with 10^4 PFU of SFV4 in the presence or absence of a mosquito bite. *(n = 6)*

Plots show the median value ± interquartile range. Data were analysed using Kruskal-Wallis test with Dunn's multiple comparison test (*ns = not significant, *P < 0.05, **P < 0.01, ***P < 0.001, ****P < 0.0001*).

Monocytes are not the only leukocytes which are permissive to arbovirus infection, and therefore of relevance in terms of their presence in the skin during UV-mediated enhancement of infection 24h post-UV. Macrophages and DCs have also been shown to be targets of infection by a number of arboviruses, including SFV, ZIKV, and CHIKV[119,120,141,142,314]. For this reason, we next interrogated the number of macrophages and DCs in the skin, following an erythemal UV exposure, both in response to the burn alone and also during

arbovirus infection. Mice were either exposed to erythemal UV exposure or left resting. 24h after the UV exposure, mice were infected with SFV or left uninfected. All mice were culled 16hpi. This experiment was designed in such a way that we could compare leukocyte numbers following UV exposure in the presence or absence of virus.

SFV infection in non-UV exposed skin does not significantly increase the number of macrophages by 16hpi, compared to resting, uninfected skin (Figure 3.15A). More importantly, there were significantly more macrophages in UV-exposed skin compared to resting skin. Although there were not significantly higher numbers of macrophages in the skin of infected, UV-exposed mice, there was an increasing trend in the number of these cells. A trend for reduced numbers of macrophages in both SFV-infected groups could be attributed to the lytic replication cycle of SFV causing cell death in infected macrophages. There was no significant difference in the number of DCs in the skin between any of the groups (Figure 3.15B).

This data shows that there are more macrophages present in UV-exposed skin 24h after erythemal UV exposure, suggesting that macrophages are recruited to the skin in response to the burn, or differentiate from recruited monocytic cells. Since some macrophages are susceptible to arbovirus infection, these cells, along with the increased numbers of monocytes shown in Figure 3.14, could provide new cellular targets for virus replication, leading to increased quantities of virus RNA present in the skin of mice exposed to erythemal UV 24h prior to infection.

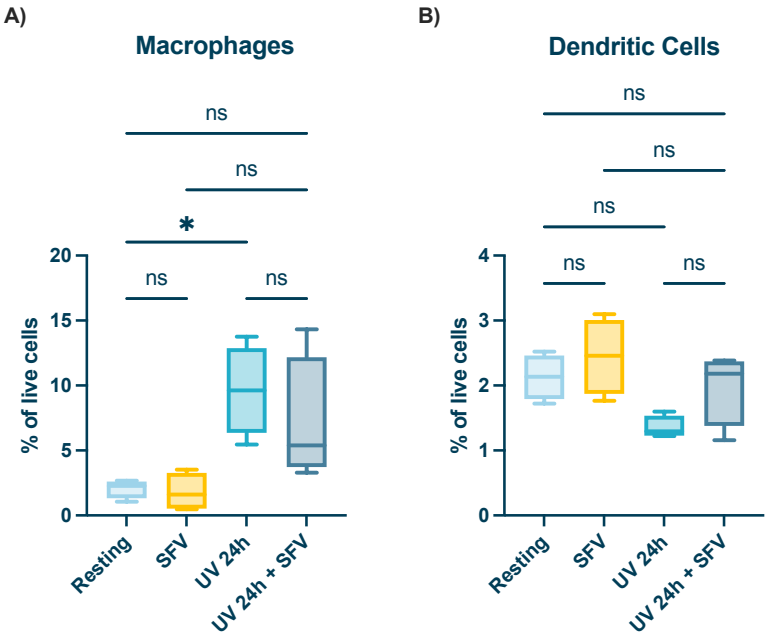

Figure 3.15 | Increased numbers of macrophages in skin exposed to erythemal UV 24h prior

(A-B) Macrophage ($CD45^+Ly6G^-CD11b^+MerTK^+$) **(A)** and DC ($CD45^+Ly6C^-CD11c^{int}MHCII^+$) **(B)** migration to skin measured by flow cytometry at 16hpi. Gating strategy used during analysis outline in Section 2.19.5. Numbers represent percent of indicated cell type of all live cells. Prior to infection, mice were either left unexposed or were exposed to an erythemal dose of UV on the skin on the upper side of the foot. Mice were then left resting or infected post-exposure at the burn site with 10^4 PFU of SFV4. *(n = 4)*

Plots show the median value ± interquartile range. Data were analysed using Kruskal-Wallis test with Dunn's multiple comparison test (*ns = not significant, *P < 0.05*).

Despite the results of Figure 3.11 showing that SFV disproportionately infects immune cells during UV-mediated enhancement of arbovirus infection at this acute timepoint, we have previously found evidence of SFV infection in keratinocytes and fibroblasts[119]. Additionally, UV exposure also drives keratinocytes proliferate in mice[315]. Therefore, we decided to assess numbers of three CD45- cell populations, endothelial cells, fibroblasts and epithelial cells, in the skin following an erythemal UV exposure, both in response to the burn alone and also during arbovirus infection, following the same protocol as the previous experiment.

Interestingly, the numbers of fibroblasts and epithelial cells, which include keratinocytes, were significantly reduced in the skin of mice exposed to UV and SFV infection by 16hpi, compared to resting, uninfected mice (Figure 3.16B-C). Additionally, endothelial cells were significantly reduced in the UV-exposed mice following SFV infection, compared to uninfected, UV-exposed mice (Figure 3.16A). This may reflect changes in cell division, or that leukocyte entry into tissue will also alter apparent cell number when expressed as a percentage.

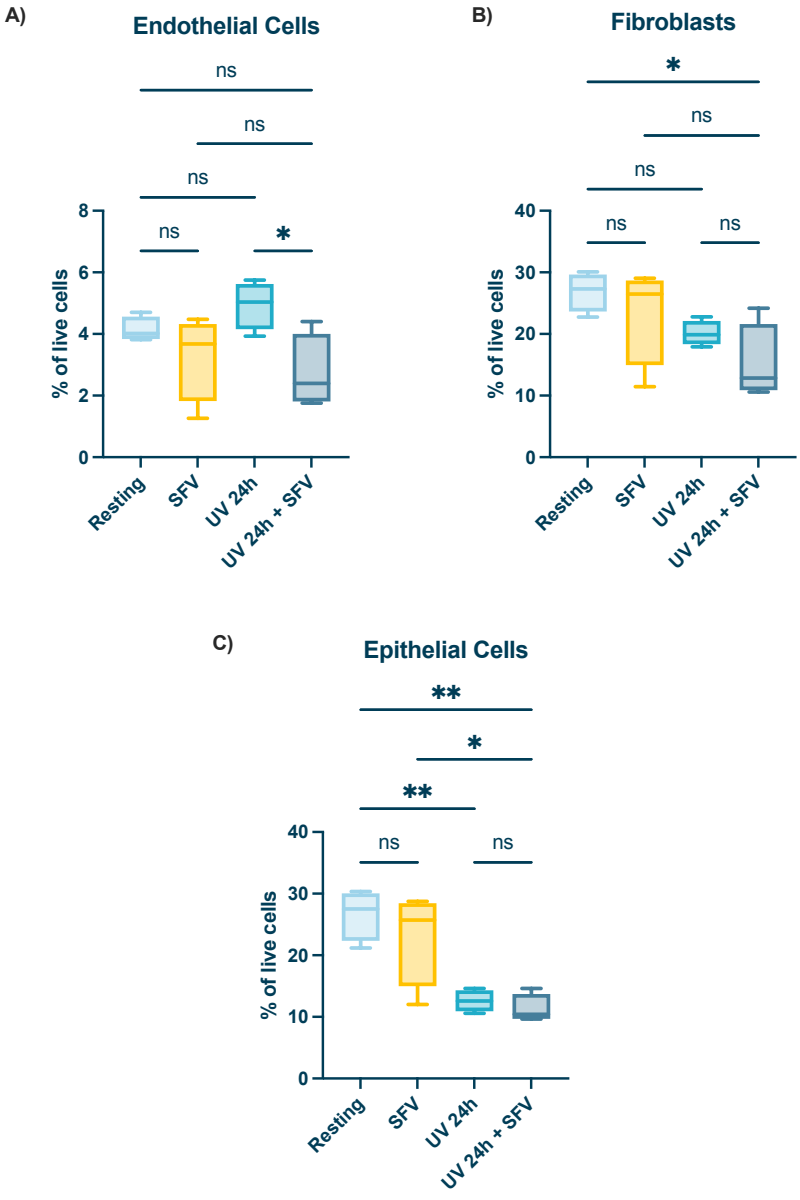

Figure 3.16 | Reduction in CD45- cell numbers during UV-mediated enhancement of infection at 24h post-exposure

(A-C) Endothelial cell ($CD45^{-}CD31^{+}$) **(A)**, fibroblast ($CD45^{-}Vimentin^{+}$) **(B)** and epithelial cell ($CD45^{-}EP\text{-}CAM^{+}$) **(C)** numbers in skin measured by flow cytometry at 16hpi. Gating strategy used during analysis outline in Section 2.19.5. Numbers represent percent of

indicated cell type of all live cells. Prior to infection, mice were either left unexposed or were exposed to an erythemal dose of UV on the skin on the upper side of the foot. All mice were then infected 24h post-exposure at the same site with 10^4 PFU of SFV4 in the presence or absence of a mosquito bite. *(n = 4)*

Plots show the median value ± interquartile range. Data were analysed using Kruskal-Wallis test with Dunn's multiple comparison test (*ns = not significant, *P < 0.05, **P < 0.01*).

3.7 Infection of leukocytes recruited in response to erythemal UV exposure drives UV-mediated enhancement of arbovirus infection at 24h post-UV exposure

In the previous section, we had shown that there are significantly more monocytes and macrophages in the skin of UV-exposed mice, compared to resting skin. We had also shown that the virus disproportionately infected immune cells in UV-exposed skin. Together, our data led us to hypothesise that erythemal UV exposure results in recruitment of immune cells, both monocytes and macrophages, which are virus-permissive and that SFV then uses these cells for virus replication, contributing to the enhanced susceptibility observed in UV-exposed mice.

To determine whether this was true, we aimed to identify which cell types are infected by SFV and whether virus burden in these cells is different during UV-mediated enhancement of infection at 24h post-UV. To do this, we infected mice with SFV6-mCHERRY, the fluorescent strain of SFV which we had previously used. We again examined the three main innate immune cells which are both permissive to arbovirus infection and also involved in the antiviral response during the first 24h of SFV infection: monocytes, macrophages and DCs. We found that by 16hpi there are significantly more infected monocytes and macrophages in the skin of mice exposed to UV 24h prior to infection (Figure 17.A,B). However, there is no change in the number of infected DCs in the skin of these same mice (Figure 17.C). This shows that SFV infects monocytes and macrophages which are brought to UV-exposed skin by 24h post-UV.

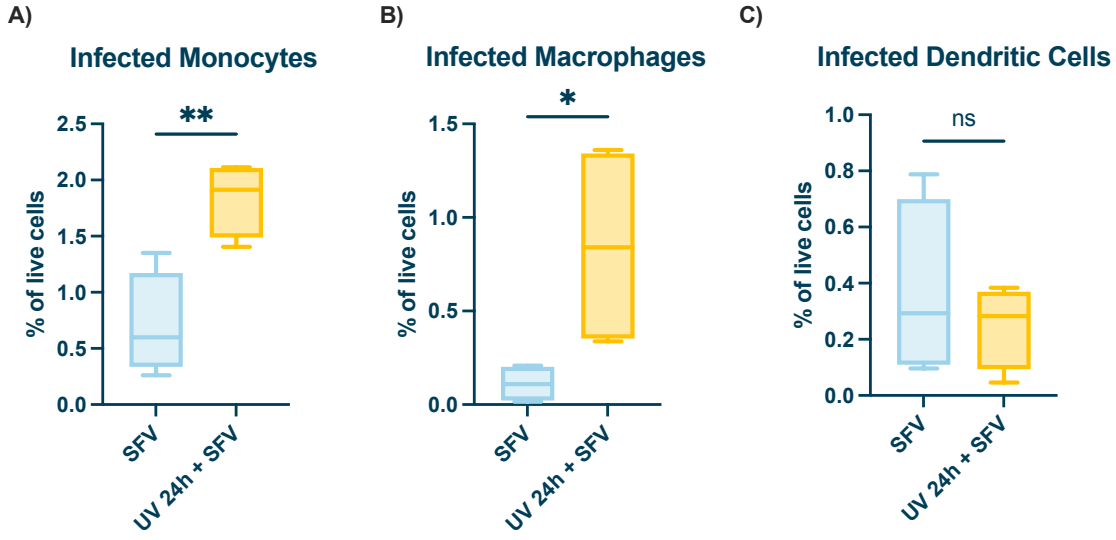

Figure 3.17 | Arbovirus replicates in cells which were recruited in response to erythemal UV exposure

(A-C) Number of infected monocytes ($CD45^+Ly6C^-CD11c^-MHCII^+$) **(A)**, macrophages ($CD45^+Ly6G^-CD11b^+MerTK^+$) **(B)**, DCs ($CD45^+Ly6C^-CD11c^{int}MHCII^+$) **(C)**, measured by flow cytometry at 16hpi. Gating strategy used during analysis outline in Section 2.19.5. Numbers represent percent of indicated SFV6-mCHERRY$^+$ infected cell type of all live cells. Prior to infection, mice were either left unexposed or were exposed to an erythemal dose of UV on the skin on the upper side of the foot. All mice were then infected 24h post-exposure at the same site with 10^3 PFU of SFV6-mCHERRY in the presence or absence of a mosquito bite. *(n = 4)*

Plots show the median value ± interquartile range. Data were analysed using a Mann-Whitney test (*ns = not significant, *P < 0.05, ** P < 0.01*).

We had shown in Figure 3.16 that there was a reduction in the number of two key CD45- cell types, fibroblasts and epithelial cells, in the skin of UV-exposed mice during SFV infection. Additionally, Figure 3.11 showed an increased virus burden in immune cells, rather than CD45- cells, in UV-exposed mice. These findings suggest that CD45- cells are not the source of increased virus replication in the skin of mice exposed to erythemal UV 24h prior to infection, and therefore, not critical for enhancement of arbovirus infection in UV-exposed mice at this timepoint. Nevertheless, we interrogated the number of SFV6-mCHERRY infected epithelial cells, endothelial cells and fibroblasts present in the skin 16hpi to definitively rule this out.

As expected, while there was evidence of infected cells belonging to all three lineages of CD45- cell in the skin by 16hpi in all groups of mice, there were no change in the number of infected endothelial cells, fibroblasts or epithelial cells in the skin of mice which had been exposed to erythemal UV 24h prior to infection, compared to unexposed mice (Figure 18.A-C). This confirms the results from Figure 3.11 which found that SFV does not disproportionately infect CD45- cells in UV exposed mice 24h post-UV. Therefore, it is unlikely that a change in virus burden within this population of cells is responsible for the increase in susceptibility to arbovirus infection in mice exposed to erythemal UV 24h prior.

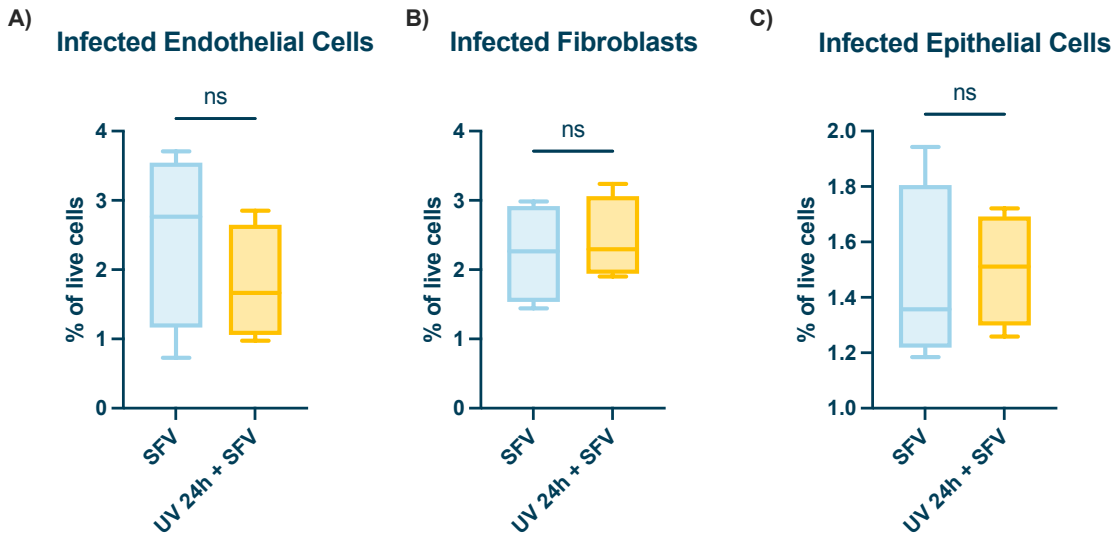

Figure 3.18 | Arbovirus does not preferentially infect CD45- cells during UV-mediated enhancement of infection at 24h post-UV

(A-C) Number of infected endothelial cells ($CD45^-CD31^+$) **(A)**, fibroblasts ($CD45^-Vimentin^+$) **(B)** and epithelial cells ($CD45^-EP\text{-}CAM^+$) **(C)**, measured by flow cytometry at 16hpi. Gating strategy used during analysis outline in Section 2.19.5. Numbers represent percent of indicated SFV6-mCHERRY$^+$ infected cell type of all live cells. Prior to infection, mice were either left unexposed or were exposed to an erythemal dose of UV on the skin on the upper side of the foot. All mice were then infected 24h post-exposure at the same site with 10^3 PFU of SFV6-mCHERRY in the presence or absence of a mosquito bite. *(n = 4)*

Plots show the median value ± interquartile range. Data were analysed using a Mann-Whitney test (*ns = not significant*).

3.8 *Aedes aegypti* mosquitos are more likely to bite UV-exposed skin

Finally, we sought to explore the impact erythemal UV exposure may have on skin temperature and whether this in turn impacts mosquito behaviour towards UV-exposed skin. Mosquitos display heat-seeking behaviours in order to find a blood meal and so any change in skin temperature due to UV exposure has the potential to significantly alter the likelihood of a mosquito feeding from the host[316–318].

It was first important to define whether UV exposure alters the temperature of mouse skin, as this was not known. An infrared thermometer was used to measure the temperature of the burn site every 24h after the UV burn was administered. The temperature of skin increased by almost 1.5°C 24h after the erythemal UV exposure (Figure 3.19). The temperature rise peaked at this timepoint before gradually falling between 48-72h post-UV and returning to normal by 96h post-UV.

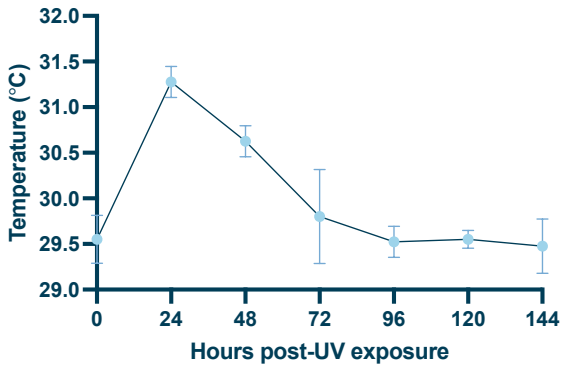

Figure 3.19 | Erythemal UV raises temperature of skin

Mice were shaved before being exposed to erythemal UV on their dorsal regions. Temperature of the burn site was then measured using an infrared thermometer every 24h post-UV exposure (n = 8).

Plots show the median value ± interquartile range.

Following on from this, we observed *Aedes aegypti* feeding behaviour on mice which had been exposed to erythemal UV 24h prior compared to unexposed mice to determine whether mosquitos were more likely to land or probe on UV-exposed skin. We hypothesised that the increase in the temperature of the skin

following a UV exposure would lead to mosquitos being more likely to interact with UV-exposed skin. Unexpectedly, there was no difference in the time it took for a mosquito to land on UV exposed skin compared to resting skin (Figure 3.20A). However, a higher number of mosquitos landed and probed the UV-exposed mice (Figure 3.20B). Additionally, once a mosquito had landed on the skin, they spent significantly longer probing the skin for a blood meal on the UV-exposed mice (Figure 3.20C). Therefore, mosquitos are more likely to be attracted to UV-exposed skin and show increased probing times when trying to take a blood meal from this skin.

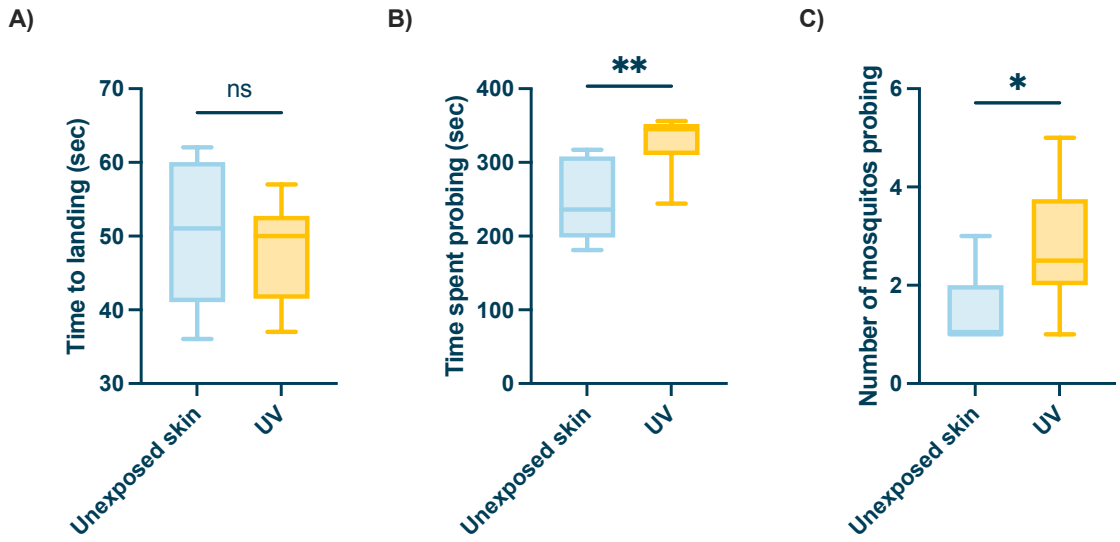

Figure 3.20 | Mosquitos show more interest in and spend more time probing UV-exposed skin

(A-C) Mice were exposed to an erythemal UV dose to upper right foot. 24h later mice were exposed to mosquito bites at the burn site. **(A)** Time from when mouse skin was exposed to cage to when first mosquito landed on the skin. **(B)** Number of mosquitos probing each mouse were counted. **(C)** Time from when mosquitos began probing to when they were engorged with blood was measured. (n = 8).

Plots show the median value ± interquartile range. Data were analysed using unpaired t-test (*ns = not significant, *P < 0.05, **P < 0.01*).

3.9 Summary and conclusions

Gaining a better understanding of factors which determine host susceptibility to arboviral infection outcomes could facilitate the stratification of patients at-risk of developing severe, potentially life-threatening disease and improve outcomes. Exposure of the skin to high levels of UVR from the Sun is a key environmental

variable in the tropical and sub-tropical regions of the world where arboviruses are transmitted[35,221]. UV exposure has long been known to impact the immune system at the skin. Others have shown that a single, erythemal dose of UVR drives a highly inflammatory state at the skin by 24h post-exposure[232,240]. We had previously shown that the mosquito bite drives a similar response but that this facilitates enhancement of arbovirus infection, rather than aiding the antiviral response[120,126]. However, there is relatively little known about whether this altered inflammatory state in UV-exposed skin impacts immune responses to infections which are transmitted at the skin, such as arboviruses. Therefore, we hypothesised that erythemal UV exposure of the skin would alter host susceptibility to subsequent arbovirus infection.

The aim of this chapter was to characterise the effect of an erythemal UV exposure on mouse skin and then to determine whether erythemal UV exposure of the skin modulates host susceptibility to subsequent arbovirus infection at 24h post-UV exposure. To achieve this, we set up an *in vivo* mouse model of UV exposure which could be adapted for experiments involving virus infection by inoculating the burn site 24h post-UV exposure with our model arbovirus, SFV, in the presence or absence of mosquito bites.

Before examining any impact that UV exposure has on host susceptibility, we sought to identify the physiological effects of erythemal UV on mouse skin, in the absence of virus. We found that erythemal UV exposure of skin resulted in an increase in vascular permeability at the skin 24h after the UV exposure, in addition to the increase caused by a mosquito bite (Figure 3.3). Our group have previously shown that a key mechanism behind mosquito bite-mediated enhancement of arbovirus infection is through this promotion of vascular permeability and oedema at the skin[126]. An increase in vascular permeability can increases the efficiency of leukocyte entry, some of which are susceptible to arbovirus infection, providing the virus with new targets for infection. The increase in vascular permeability following UV-exposure offers the first indication that exposure of the skin to an erythemal dose of UV prior to infection may allow the entry of virus-permissive cells, such as monocytes and increase host susceptibility to arbovirus infection as a result.

Upon examination of histology images from these mice, we found that UV exposure drove a substantial inflammatory infiltrate in the skin of UV-exposed mice by 24h (Figure 3.2). Although we did not identify which cell types made up the infiltrate, it is likely that these entered the skin more easily due to the increased vascular permeability apparent at this timepoint (Figure 3.3). Previous studies using different doses of UV, have found that UV drives an inflammatory infiltrate between 24-48h, in a similar manner to what we have shown here[232,240,296]. It is likely that the influx of nucleated cells are leukocytes and this is further supported by our later findings that UV exposure drives monocyte and neutrophil entry to the skin. These initial findings show that erythemal UV drives a highly pro-inflammatory state at the skin by 24h. Furthermore, as some leukocytes, including monocytes, are virus permissive, this initial observation from the histology images provided a preliminary indication that UV-exposed skin may be more susceptible to a subsequent arbovirus infection.

Subsequently, we found that mice exposed to UV at the inoculation site 24h prior to infection were more susceptible to arbovirus infection than mice infected at resting skin or at mosquito-bitten skin (Figure 3.4). This was evidenced by increased virus replication in the skin and viremia by 24hpi. Spread of virus to the blood is of particular relevance to the clinical course of disease, as high quantities of virus in the blood are critical for the virus to cause severe disease[319]. Viremia also facilitates further transmission of the virus to biting insects[320].

We initially hypothesised that this enhancement of arbovirus infection may be due to interference with the antiviral Type I IFN system. There are multiple examples of arboviruses, from a range of virus families, with viral proteins which act to limit host Type I IFN responses as a way of evading immune clearance[321–323]. Additionally, *Ifnar*$^{-/-}$ mice, which lack the Type I IFN receptor and so can't respond to Type I IFN, are highly susceptible to mosquito-borne alphaviruses and flaviviruses[145–147,324]. Furthermore, our group has previously shown that therapeutic induction of Type I IFN pathways at an early timepoint post-arbovirus infection significantly reduces viral dissemination and increases survival in mice[119]. Together, this pre-existing evidence makes it clear that Type I IFN is a critical host defence mechanism against arboviral infection. Therefore,

if UVR has suppressive effects on Type I IFN, this could explain the increase in susceptibility observed in UV-exposed mice.

When we characterised induction of the Type I IFN response following a UV exposure, we found that significant induction of ISGs did not occur until 48h post-UV (Figure 3.5). This is likely to be of limited use in protecting mice from virus infection at 24h post-UV, the timepoint at which infection is enhanced. Other studies have found that UVB induces ISGs and IFN-β by 24h post-UV exposure[325,326]. However, these studies used different doses of UVB exposure from our model. Therefore, it may be that induction of the Type I IFN system varies depending on UV dose. Importantly, we found that susceptibility to infection, although elevated compared to UV unexposed skin, does not reach statistical significance at 48h and 72h post-UV exposure (Figure 3.6). This suggests that Type I IFNs, which are induced by 48h post-UV, may offer some protection at this timepoint.

It was also important to assess the Type I IFN response in the skin during UV-mediated enhancement of infection to determine whether the response was suppressed in UV-exposed skin during virus infection, thereby facilitating increased viral replication. However, this did not appear to be the case. Expression of both IFN-β and multiple ISGs during SFV infection in UV exposed mice was significantly upregulated in mice exposed to UV 24h prior to infection, the timepoint at which mice experience heightened susceptibility to infection (Figure 3.7). This suggests that UV does not impair the induction of Type I IFNs in response to virus, but that this antiviral response is not sufficient to protect from UV-mediated enhancement of infection in UV-exposed skin at these timepoints. This point was backed up by the evidence that SFV infection is still enhanced in the skin of *Ifnar*$^{-/-}$ mice, which can't respond to Type I IFN, exposed to erythemal UV 24h prior to infection (Figure 3.8). Together, this suggests that UV-mediated enhancement of infection is independent of the Type I IFN system.

It is important to note that male and female mice have been shown to have different Type I IFN responses following UV exposure of skin, with Type I IFN being induced to a higher level in female mice early following UV-exposure[325]. We solely used female mice throughout this thesis and so did not investigate

any sex-based differences in response to UV. However, as we had largely ruled out the role of Type I IFN in the enhancement of arbovirus infection, we do not expect these differences between male and females to have an impact on our phenotype.

Once the involvement of Type I IFN in driving enhanced susceptibility to infection following UV-exposure had been eliminated, we hypothesised that UV may be driving proliferation of cells in the skin and that SFV may then be targeting these cells for infection, due to the virus's oncolytic nature. UVR has a variable effect on cell proliferation. Early following exposure, cell replication is halted due to DNA damage[327]. There is also a high occurrence of p53-mediated apoptosis of damaged cells, peaking at 24h post-UV in mouse skin[232]. However, UV exposed skin is also characterised by the expansion of the tissue due to cellular proliferation, known as hyperplasia, particularly as a result of keratinocyte proliferation by 48h post-UV[232]. Interestingly, SFV A7(74) replicates less efficiently in some differentiated 'mature' cells e.g. neurons, and some strains of SFV have been studied as an experimental oncolytic virus due to their ability to preferentially replicate within immortalised immature cells[309–311,328]. Oncolytic viruses preferentially infect tumour cells, which are characterised as being highly proliferative[329,330].

We found that there were more actively proliferating cells in the skin by 24h post-UV, as expected following an inflammatory insult (Figure 3.9). However, when we used a fluorescent strain of SFV, SFV6-mCHERRY, to identify infected cells, we found that there were not more SFV-infected, proliferating cells in the skin, disproving our initial hypothesis (Figure 3.10). It is mostly keratinocytes which proliferate in response to UV between 24-72h post-UV exposure[232]. Since SFV does not seem to be preferentially infecting proliferating cells at this acute timepoint post-UV, it is unlikely that keratinocytes are responsible for the higher quantities of virus present in the skin of UV-exposed mice at this timepoint. Instead, the virus could be replicating in CD45- cells, such as endothelial cells or fibroblasts, or immune cells recruited in response to the UV burn at this acute timepoint post-UV exposure. To definitively confirm this, it would be necessary to carry out a further flow cytometry experiment to phenotype proliferating cell

types based on cell marker expression, which we plan to do before publication of this work.

However, to explore this idea further we assessed whether either CD45+ (immune cells) or CD45- cells (epithelial cells and CD45- cells) were disproportionately infected during UV-mediated enhancement of infection, a previously established approach[289]. We found that in mice exposed to UV 24h prior to infection CD45+ cells had significantly higher quantities of virus than CD45- cells (Figure 3.11). We considered whether this increased virus burden in immune cells may be due to UV making these cells more susceptible to infection. However, when we isolated CD45+ and CD45- cells from the skin of UV-exposed mice and infected them *in vitro*, there was no enhancement of infection in cells from UV-exposed mice and, importantly, no difference in virus burden between immune cells and epithelial and stromal cells (Figure 3.12). This shows that UV does not impact the inherent permissiveness of cells to SFV infection at this timepoint. The result of this experiment also confirms the importance of carrying out our investigation in to enhancement of virus in UV-exposed skin *in vivo*, as the effect does not occur *in vitro*. However, it is worth noting that the harshness of the magnetic separation process may have impacted some cell populations more than others and therefore the fractions may not include all populations which would be present *in vivo*.

An alternative explanation for the higher quantities of virus in immune cells in UV-exposed mice is that there may be more virus-permissive leukocytes present in the skin in response to UV, at the time of infection. When we characterised the skin 24h after erythemal UV exposure, we noted the similarities between the inflammatory state following erythemal UV exposure and following a mosquito bite. Recruitment of pro-inflammatory neutrophils and virus-permissive monocytes is essential for mosquito-bite enhancement of infection[120]. Therefore, we considered whether recruitment of these two cell types contributes to increased susceptibility to arbovirus infection 24h post-erythemal UV exposure. We found that erythemal UV drives expression of neutrophil and monocyte chemoattractants, CXCL2 and CCL2 respectively, in the skin (Figure 3.13). This increase in expression subsequently translated into higher numbers of neutrophils and monocytes in the skin of UV-exposed mice

during infection (Figure 3.14). We also found more macrophages in the skin of UV-exposed mice, another leukocyte type which is susceptible to arbovirus infection (Figure 3.15). While macrophages and monocytes have the potential to be beneficial to the host in terms of protecting from infection, they may also present the virus with new targets for infection. This may contribute to increased host susceptibility to infection that we see at 24h post-erythemal UV exposure. Additionally, while neutrophils are not permissive to SFV infection, they do drive to an inflammatory programme that enhances monocyte entry, and so could contribute to the enhanced susceptibility to infection in this way.

Interestingly, there were significantly fewer fibroblasts and endothelial cells in the skin of UV-exposed mice, when expressed as a percentage of all live cells (Figure 3.16). This reduction is likely due to a combination of the destruction of tissue and apoptosis caused by UVR[232,240], and the influx of leukocytes that would skew % values to show an apparent decrease in number. Since there was no increase in any of the non-immune cell types by 24h post-erythemal UV and there was no evidence of an increase in virus burden in CD45- cells, as shown earlier, it is unlikely that these cells contribute to the higher quantities of virus RNA in these mice at this timepoint. However, it would be worth investigating the quantity of infectious virus produced by individual cell types, as even a small number of infected cells could be responsible for high rates of virus production and so contribute disproportionately based on their population size.

When we identified the phenotype of infected cell types using SFV6-mCHERRY, we found that there were more infected monocytes and macrophages in the skin of UV-exposed mice (Figure 3.17). However, there was no change in the number of infected DCs, endothelial cells, fibroblasts or epithelial cells (Figures 3.17 and 3.18). This suggests that macrophages and monocytes are recruited to the skin in response to UVR and these cells then provide the virus with new targets for infection in UV-exposed skin. This key finding highlights an important mechanism by which host susceptibility to arbovirus infection is enhanced in mice 24h after being exposed to an erythemal UV dose. Additionally, an increase in infected monocytes and macrophages in the skin has the potential to drive arbovirus dissemination and cause disease, as the virus can transit to

other tissues via infected leukocytes, as is the case in WNV infection[331]. In the future, we plan to definitively assess whether monocytes and macrophages are critical during enhancement at this timepoint by investigating whether susceptibility to virus is still enhanced following UV exposure in *Ccr2*$^{-/-}$ mice, which do not effectively recruit monocytes to tissues.

After characterising the altered immune response which occurs during UV-mediated enhancement of infection, we concluded our investigation in to the impact of UV exposure at 24h post-UV by considering whether mosquitos behave differently towards UV-exposed skin. The attraction of mosquitos towards host skin is critical both for the mosquito to find a blood meal but also for the insect to pass on virus to the host as it feeds. Therefore, any factor which may impact these behaviours could have profound effects on virus transmission by the insect. Mosquitos, including *Aedes aegypti*, have heat and humidity sensors in their antennae, which drive mosquito behaviour in a number of ways. For example, these sensors facilitate blood feeding by allowing the insect to detect nearby hosts based on body temperature[316]. *Aedes aegypti* in particular display thermotaxis, allowing them to identify objects which are warmer than the environmental temperature e.g. humans, and actively seek these out[317]. These insects also show increased activity on warmer surfaces[332]. Exposure of human skin to UVB radiation increases skin temperature, with UV-exposed skin being warmer by 24h post-exposure compared to non-exposed skin[333]. Therefore, if erythemal UV exposure of skin raises skin temperature, this may increase the likelihood of a mosquito landing on and probing UV exposed skin compared to resting skin.

We found that UV exposure increases the temperature of skin between 24-72h (Figure 3.19). This increase in temperature of mouse skin following a UV exposure tracks with what happens in human skin, with UV-exposed back skin of humans also rising ~1.5°C in temperature by 24h post-exposure[333]. However, it is worth noting that the same study found that the degree to which skin temperature increased following exposure did differ depending on the part of the body which was exposed, with UV-exposed forearms only increasing by ~0.5°C by the same timepoint. During our experiment, we experienced difficulties getting a consistent temperature reading of skin temperature on the

upper foot using the infrared thermometer. Therefore, we conducted the experiment on the dorsal region instead, where readings were consistent. As such, it should be noted that the change in temperature of the skin of the upper foot following UV exposure may differ in magnitude from that of the dorsal region.

Following on from this, when we looked at whether UV exposure affects mosquito feeding behaviour at UV exposed skin, we reached a number of conclusions. Unexpectedly, mosquitos did not reach the skin of UV exposed mice any quicker than that of unexposed mice, even though *Aedes aegypti* utilise heat-seeking to find hosts to feed on (Figure 3.20A)[316,317]. However, it has previously been shown that *Aedes aegypti* seek out objects within very specific temperature ranges, matching mammalian body temperatures[317]. Therefore, since the UV-exposed skin still sat within these temperature parameters this may explain why the slight increase in skin temperature did not alter the seeking behaviour of the mosquitos. In addition, the mosquitoes were caged and already placed close to mouse skin. It may be that UV inflamed skin may have more of an attractive effect in real world conditions in which mosquitoes are not already crowded in close proximity to the mammalian host.

Nevertheless, we found that more *Aedes aegypti* were attracted to UV-exposed skin and, once at the skin, they spent longer probing. This longer probing time was unexpected as UV drives blood vessel dilation[334]. Therefore, it would be expected that this would make it easier for the insect to feed as reduced probing times have previously been associated with increased blood vessel availability[335]. However, it may be that UV-induced tissue destruction could explain this reduced efficiency to obtain a blood meal. Nevertheless, this finding is of particular importance as *Aedes aegypti* saliva has been well characterised as making arbovirus infection worse[126,134,182]. Therefore, the longer mosquitos spend probing, the more virus-enhancing saliva they will inject into the skin. In addition, longer probing times may result in higher titre of virus inoculated into the skin during a feed, as has been shown for DENV infection[336]. Therefore, these changes to mosquito behaviour at UV exposed skin may also contribute to enhancement of arbovirus infection in a natural infection.

However, we cannot definitively attribute this change in mosquito behaviour to the increase in skin temperature alone. UV exposure may have other impacts on the skin which drive these alterations to the insect behaviours. For example, UV exposure may also change the bacterial composition of the skin. While we did not investigate this, such an effect could also affect *Aedes aegypti* biting behaviour towards the exposed skin, as has been previously shown for the malaria vector, *Anopheles gambiae*[337]. In spite of this, we have shown that more mosquitos are attracted to UV-exposed skin compared to resting skin and that once they have landed on UV-exposed skin they spend longer probing.

In summary, this chapter has illustrated that erythemal UV exposure of the skin has profound impacts on host immunity to arbovirus infection. By 24h post-exposure, mice are more susceptible to SFV infection, experiencing increased virus replication and viremia. This is likely mediated via the recruitment of monocytes and macrophages to the UV burn site by 24h, which are then infected by the virus. Additionally, the arbovirus vector *Aedes aegypti* is more likely to be attracted to UV-exposed skin and spends longer probing the skin, injecting virus-enhancing saliva while it does so. Together, these two effects of UV exposure of the skin have the potential to have profound consequences on host outcomes to arbovirus infection.

Chapter 4: Increased host susceptibility to SFV at 1 week post UV exposure is driven by preferential infection of replicating skin fibroblasts *in vivo*

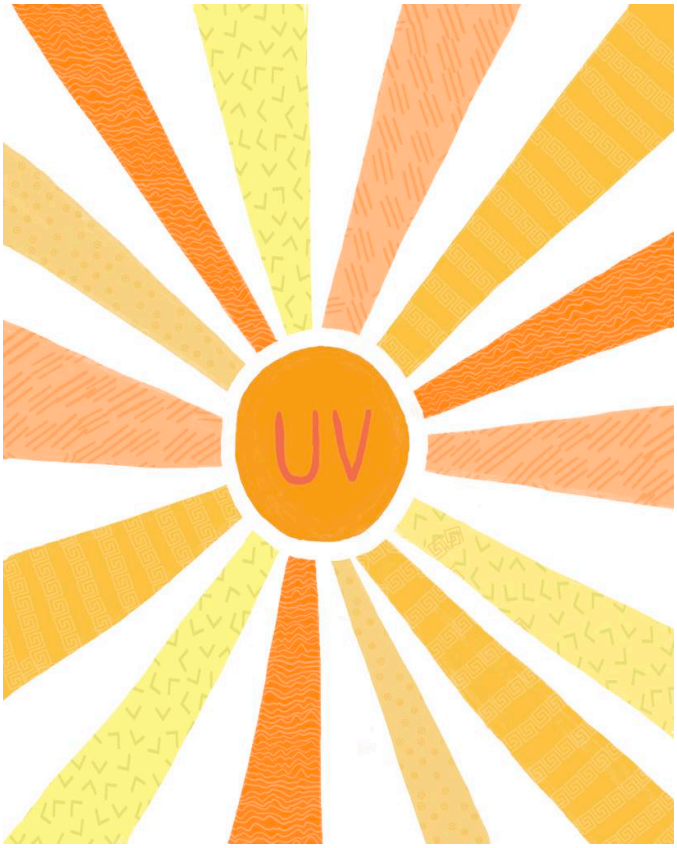

4.1 Introduction

The skin undergoes many profound changes following exposure to erythemal UV, or sunburn; from the time immediately following the administration of the burn, when the skin appears red and swollen, through to the process of wound healing, when the top layer of the skin peels, culminating in the point when the burn has resolved[304]. Although much of the acute tissue damage following an erythemal exposure resolves within 1-2 weeks, sunburn can have long-term consequences for the skin, particularly in terms of DNA damage[338]. These changes can lead to the development of skin cancer, wrinkles and skin-aging long after the causative exposure occurred[339–341]. Indeed, an individual who has experienced ≥5 cases of sunburn in their life is twice as likely to develop skin cancer[342]. Therefore, it is necessary to considering whether these changes could impact susceptibility to arbovirus infection at later timepoints post-UV exposure, even once the obvious damage has healed e.g. by 3 weeks post-burn.

As discussed in the previous chapter, due to the extreme impact UV has on the biology of the skin following sunburn, we hypothesised that UV exposure could impact susceptibility of the host to arbovirus infection, when transmitted at UV-exposed skin. However, as the different stages of sunburn progression post-exposure exhibit distinct features, we hypothesised that the effects on immunity would be different based on the timepoint post-UV when the host was infected. Therefore, we sought to understand whether arbovirus infection is also enhanced at later timepoints post-UV, from 1-week onwards.

By 1-week post-UV exposure the skin has likely moved past the initial acute phase of sunburn, which is highly inflammatory, and moved into an anti-inflammatory, wound-healing process[295,304]. As a result, any mechanisms modulating host susceptibility to arbovirus infection at this timepoint are likely to be different at 24h post-UV. There is limited knowledge around how sunburn inflammation and damage resolves. However, it is known that following an initial burst of keratinocyte apoptosis following a UV burn, keratinocytes in the epidermis proliferate, driving a thickening of this skin layer, termed hyperplasia, which protects from future exposures[315,343]. This is one of several photoadaptations that occurs, a list which also includes increased melanocyte

frequency[344]. Additionally, expression of inflammatory cytokines, such as TNF-α and IL-6, in the epidermis and the dermis of mice return to basal levels by 8 days post-erythemal UV exposure[240]. However, outside of these few published findings, the molecular processes taking place by 1-week post-UV, during healing of an erythemal UV burn, are yet to be fully investigated.

Instead, we can look to what is known about wound healing more generally for a guide on what may happen post UV exposure. A number of models have been used to investigate wound healing, including punch biopsies and scalding using a water bath[345,346]. Together, these have allowed researchers to put forward a picture of the processes underlying tissue repair following a skin wound, as detailed below. However, it is important to note that there are likely variations to this consensus when it comes to how a UV burn heals, due to the added dynamic of UVR being a mutagenic agent which causes DNA damage. Nevertheless, the core wound healing processes likely have some similarities.

The tissue micro-environment in the skin as a wound begins to heal is largely anti-inflammatory. Macrophages coordinate the cutaneous tissue repair, making them the most critical immune cell during the wound-healing process in skin. Their depletion in mice leads to severely impaired tissue repair[347,348]. During the acute stage of the process, soon after the injury has occurred, recruited monocyte-derived macrophages display a highly inflammatory phenotype, similar to *in vitro* derived macrophages that are referred to as M1, which enables them to clear any infection associated with the breaking of the skin barrier and to phagocytose apoptotic cell debris[208,349]. However, once any initial threats have been dealt with, the damaged tissue must be repaired. Therefore, after playing their initial role, macrophages in the skin switch to a phenotype similar to M2 macrophages, which are largely anti-inflammatory and promote wound healing[350,351]. These are the most prominent macrophage type in the skin by day 5 following a wound[219]. These cells facilitate tissue repair through a number of means, including dampening inflammation at the skin, promoting proliferation of fibroblasts, epithelial and endothelial cells, producing ECM remodelling molecules and driving angiogenesis[348349]. Expression of arginase (ARG1) has long been closely associated with these so called M2 macrophages[352]. This molecule breaks down L-arginine into L-ornithine, which

drives downstream cell proliferation and collagen production, both of which are critical to wound healing[206]. Fibroblasts, keratinocytes and epithelial cells have also been shown to express ARG1 during wound healing, developing a 'macrophage-like' phenotype, however, there is less well understood[353,354]. The wound-healing process ends with the formation of the ECM over the damaged site, which forms a scaffold for the newly formed blood vessels and for macrophages, fibroblasts and endothelial cells to cover and close the wound[218].

4.1.1 Hypothesis and aims

It is clear that the immunological landscape in the skin during wound healing is very different to that which characterises the acute phase of a wound. Therefore, we hypothesised that mouse skin will exhibit differential susceptibility to virus during wound repair, as compared to the initial 24 hours post UV. The mechanisms driving these hypothesised changes in host susceptibility to arbovirus infection are also likely to be quite distinct from those which were shown to contribute to host susceptibility to virus at 24h post-UV.

Therefore, this chapter aims to:

1) **Define host susceptibility to virus from 1 week to 3 weeks post UV exposure**
2) **Characterise the physiological changes to the skin at 1-week post-UV, during the wound-healing stage of the UV burn**
3) **Determine whether the mechanism modulating any change in host susceptibility to virus infection at 1-week post-UV is linked to processes associated with wound-healing**

4.2 UV exposed skin at 1-week post UV is characterised by hyperplasia and high levels of oedema

The mouse model was adapted to investigate the impact on tissue architecture of UV exposure on skin up to 3 weeks post exposure to UV. For the purposes of generating tissue samples that can be easily sectioned for histology, we used back skin of C57BL/6 mice, exposed to 400mJ/cm^2, an erythemal dose, of UVR and samples were collected 1-week, 2 weeks or 3 weeks post-UV.

Initially, to examine any structural changes in the skin during the wound-healing process following a UV burn, we examined histology sections taken from the burn site of mice exposed to UV 1 week, 2 weeks or 3 weeks before, and compared this to resting skin. Hyperplasia of the skin layers at 1-2 weeks post-UV is evident in the images (Figure 4.1A). The structure of the skin appears to return to normal by 3 weeks post-UV. These observations were confirmed by measuring the layers of the skin using the quantitative imaging software QuPath. All three layers were significantly expanded by 1-week post-UV (Figure 4.1B). The layers did not begin to reduce back to normal thickness until 3 weeks after the UV burn had been administered. Thus, the skin undergoes substantial gross pathological changes following UV exposure, resulting in substantially thickened skin, which is mostly resolved by 3 weeks post-exposure.

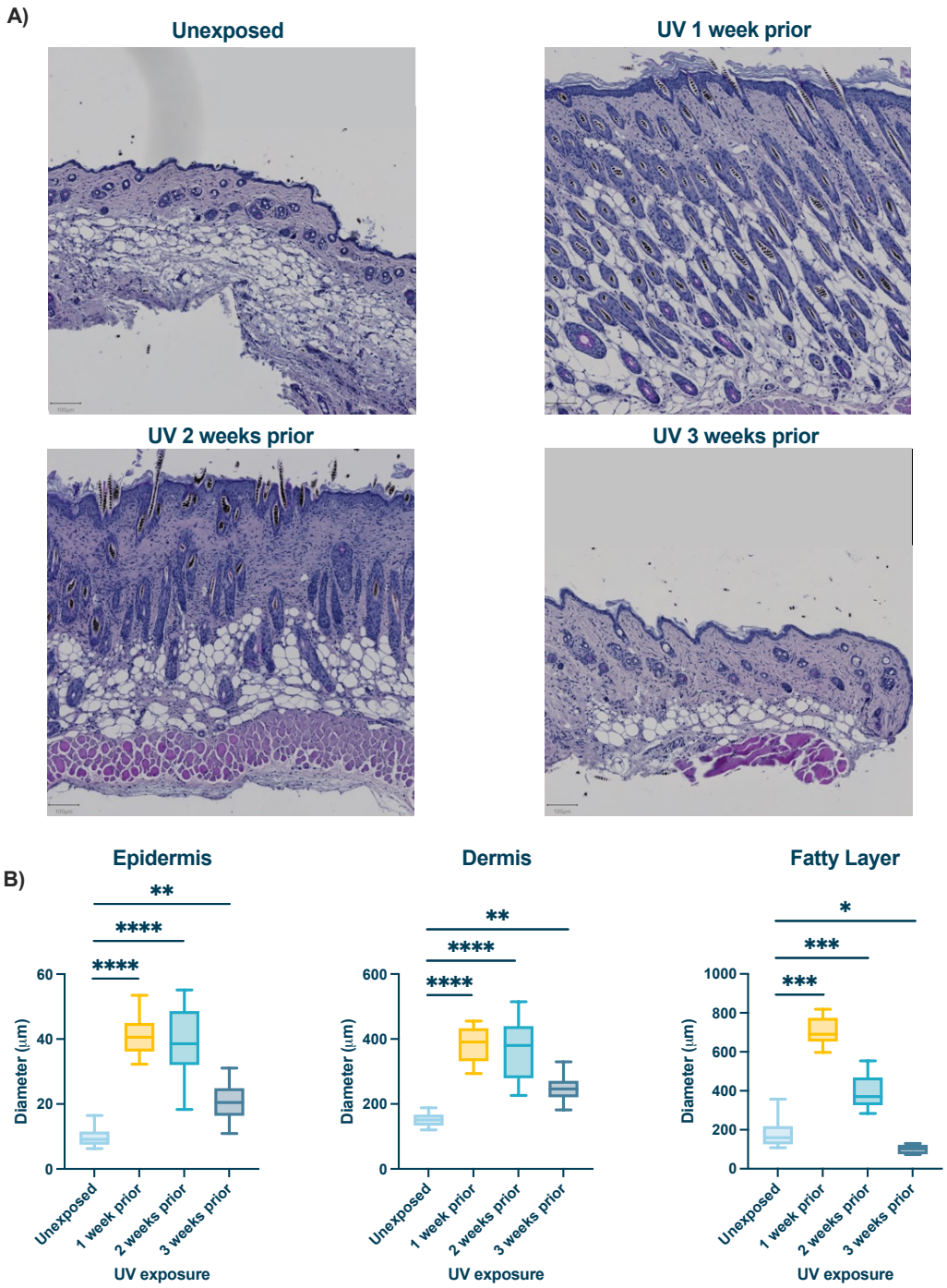

Figure 4.1 | Skin layers expanded in thickness in skin exposed to erythemal UV up to 2 weeks prior, before returning to normal at 3 weeks

(A) Histology of resting skin or skin exposed to erythemal UV 1 week, 2 weeks or 3 weeks prior, taken from the dorsal region of C5BL/6 mice. Sections stained with H&E. Images shown are representative of the group. Scalebars measure 100 µm. Slides scanned at 20x magnification.

(B) Measurements of epidermis, dermis and fatty layer thickness were taken from 10 areas per condition using QuPath. Plots show the median value ± interquartile range. Data were analysed using ordinary one-way ANOVA with Tukey's multiple comparisons test (**P < 0.05, **P < 0.01, ***P < 0.001, ****P < 0.0001*).

We also sought to determine whether vascular permeability is increased at the skin 1-week post-UV, as it was at 24h. As discussed previously, increased vascular permeability can enhance entry of virus-permissive immune cells and that this enhances arbovirus infection, both in mosquito-bitten mice[120] and mice exposed to UV 24h prior to infection (Chapter 3). Therefore, an increase in oedema at the skin by 1-week post-UV exposure could indicate the propensity of UV-exposed tissue to be more susceptible to arbovirus infection at this timepoint. Evan's Blue Dye was injected s.c. in the scruff of the neck of mice which had been exposed to erythemal UV to the foot skin 1 week before. Quantities of dye that had diffused to the burn site by 3h post-injection could then be used as a readout of oedema at this skin and, therefore, vascular permeability in the tissue.

Mice which had been exposed to UV 1 week prior had significantly more oedema in UVR exposed skin, compared to mice with resting skin (Figure 4.2A). Interestingly, the addition of a mosquito bite, a known rapid inducer of skin oedema, in UV-exposed mice did not significantly further increase oedema, compared to UV-exposure alone. Importantly, oedema is driven to a higher level in the skin of mice exposed to UV 1-week prior, compared to 24h prior, the timepoint which was shown to significantly enhance arbovirus infection in Chapter 3 (Figure 4.2B). Therefore, erythemal UV exposure drives an increase in vascular permeability at the exposed skin up to 1 week after the UV exposure. Together, Figure 4.1 and 4.2 show that the skin environment is still highly dysregulated at 1-week post-erythemal UV burn and this does not likely return to normal until 3 weeks post-UV exposure.

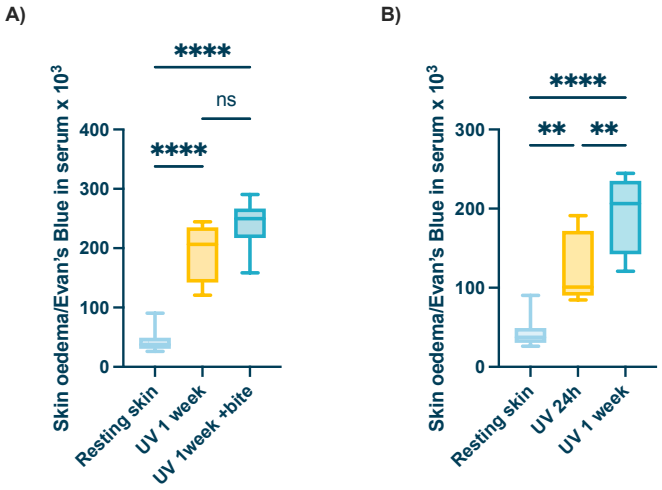

Figure 4.2 | Erythemal UV exposure induces increased vascular permeability up to 1-week post-UV exposure

(A-B) Mice were exposed to erythemal UV to upper right foot. 1 week **(A,B)** or 24h **(B)** later, mice were injected s.c. with Evans blue to scruff of neck, distant from the burn site. Mice were then exposed to mosquito bites at the burn site. The extent of oedema was assessed by quantification of Evan's blue dye leakage into skin at 3 h post-biting via colorimetric assay (n = 8).

Plots show the median value ± interquartile range. Data were analysed using Kruskal-Wallis test with Dunn's multiple comparison test (***P < 0.01, ****P < 0.0001*).

4.3 Susceptibility to arbovirus infection peaks in UV-exposed mice at 1-week post-UV

Due to the changes observed in the skin by 1-week post-UV, we hypothesised that mice would be more susceptible to SFV infection 1 week after an erythemal UV exposure, as we had shown earlier at 24h post-UV. Skin and blood were collected 24hpi from mice infected with 10^4 PFU of SFV4 in the skin of the upper foot. This skin had either been left resting or had been exposed to erythemal UV 24h or 1-week prior to infection. qPCR was used to determine the quantities of the SFV4 E1 gene in the skin at 24 hpi, to indicate virus replication at the inoculation site. Titres of virus in the serum at 24 hpi were also quantified by plaque assay, to measure viremia of each mouse.

As expected, mice which had been exposed to an erythemal dose of UV 24h prior to exposure had significantly more virus in the skin by 24hpi compared to unexposed mice (Figure 4.3A). Interestingly, the mice with the highest quantities of virus RNA in the skin were those which had been exposed to UV 1 week prior

to infection, with ~1000-fold more virus RNA than unexposed mice. This was reflected in the quantities of virus present in the blood by 24hpi also (Figure 4.3B). Again, mice exposed to UV 1 week prior to infection had the highest quantities of viremia. Therefore, susceptibility to SFV infection is increased in mice exposed to an erythemal dose of UV 1-week prior to infection and this occurs to an even greater extent than the enhancement observed at 24h post-UV.

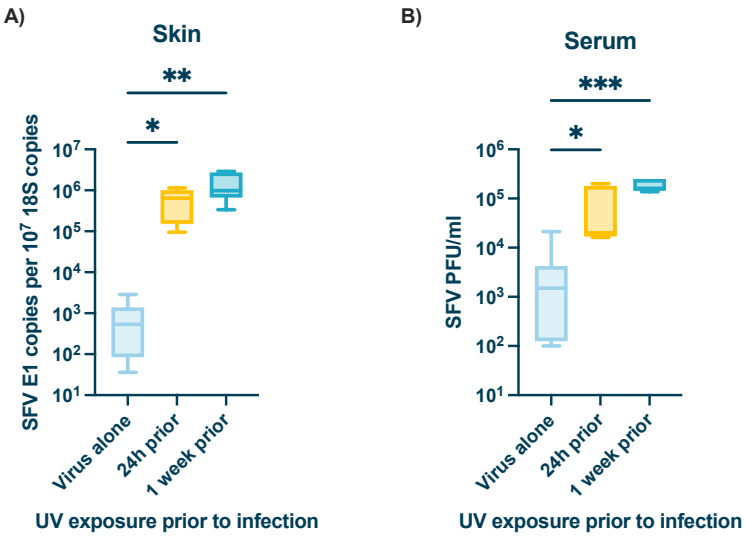

Figure 4.3 | Erythemal UV enhances SFV infection at 1wk post-UV

(A-B) SFV RNA (E1 gene) copy number in inoculation site (skin) **(A)** and viral titres in the serum **(B)** 24hpi. Prior to infection, mice were either left unexposed or were exposed to an erythemal dose of UV on the skin on the upper side of the foot. All mice were then infected at either 24h or 1 week post-exposure at the same site with 10^4 PFU of SFV4 in the presence of a mosquito bite. (*n* = 6)

Gene expression measured by qPCR. Titres of virus in serum determined by plaque assay. Plots show the median value ± interquartile range. Data were analysed using Kruskal-Wallis test with Dunn's multiple comparison test (*ns = not significant, *P < 0.05, **P < 0.01, ***P < 0.001*).

After establishing that host susceptibility to SFV infection occurs at both 24h and 1-week post-UV, As outlined in the introduction, UV exposure of the skin can have long-term effects, including photoaging, even after the visible burn has healed. Furthermore, we had shown in Figure 4.1 that dysregulation of the skin structure was still evident 2 weeks post-UV exposure. Therefore, we set out to

investigate whether this UV-mediated enhancement impacts mice at timepoints later than 1-week post-UV.

As expected, mice exposed to erythemal UV 1-week prior to infection had significantly higher quantities of virus RNA in the skin and viremia by 24hpi, compared to mice infected at resting skin (Figure 4.4A-B). Interestingly though, there was still significantly more virus in the skin and the blood in mice exposed to erythemal UV 2 weeks before the infection took place, although lower than at 1-week post-UV. However, quantities of virus RNA and titres of infectious virus in serum returned to normal quantities in mice exposed to erythemal UV 3 weeks prior to infection. Together, this shows that susceptibility to arbovirus infection is significantly higher in mice exposed to erythemal UV at the inoculation site up to 2 weeks before infection, with susceptibility returning to normal by 3 weeks post-UV.

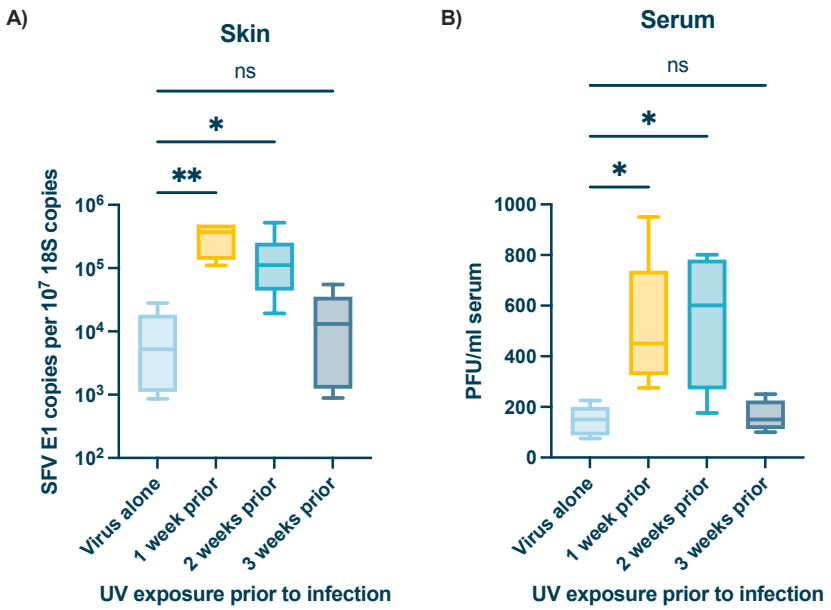

Figure 4.4 | UV-mediated enhancement of arbovirus infection persists up to 2 weeks post-UV exposure

(A-B) SFV RNA (E1 gene) copy number in inoculation site (skin) **(A)** and viral titres in the serum **(B)** 24hpi. Prior to infection, mice were either left unexposed or were exposed to an erythemal dose of UV on the skin on the upper side of the foot. All mice were then infected at either 1 week, 2 weeks or 3 weeks post-exposure at the same site with 10^4 PFU of SFV4 in the presence of a mosquito bite. (n = 6)

Gene expression measured by qPCR. Titres of virus in serum determined by plaque assay. Plots show the median value ± interquartile range. Data were analysed using

Kruskal-Wallis test with Dunn's multiple comparison test (*ns = not significant, *P < 0.05, **P < 0.01*).

While SFV makes an excellent model arbovirus for studying immune responses in mice, the virus does not pose a significant threat to human health. While the virus is able to infect and replicate in humans, there have been a limited number of cases of SFV infections in humans, and symptoms are generally mild[115,355]. Therefore, we sought to understand whether UV-exposed skin is more susceptible to a more medically relevant virus, such as ZIKV. Another member of our lab group had previously shown that ZIKV infection is also significantly enhanced in mice exposed to erythemal UV 24h prior to infection (data not shown). This led us to consider whether susceptibility to infection with this more medically relevant virus would also be increased when mice are infected at UV-exposed skin 1-week post-burn.

Studying ZIKV infection *in vivo* requires an immunodeficient mouse model, such as *Ifnar-/-* mice, as ZIKV does not cause disease in immunocompetent mice[128]. To investigate the impact of UV exposure on ZIKV infection, we exposed *Ifnar-/-* mice, which can't respond to Type I IFN, to erythemal UV or left them resting and infected both groups with 10^3 PFU of ZIKV 1-week post-UV. We used a lower virus dose than that used in the SFV experiments due to the immunodeficient status of the mice. Mice were regularly monitored for clinical signs. At 24hpi, mice were culled and skin, spleen and blood were collected. Quantities of the ZIKV Env gene, encoding the virus envelope protein, were measured in the skin and the spleen using qPCR and a plaque assay was carried out using the serum samples to assess viremia.

Interestingly, relatively low quantities of ZIKV RNA were found in the skin at this timepoint and there was no difference in the quantity of virus RNA between the UV-exposed mice and the unexposed mice by 24hpi (Figure 4.5A). However, there was a high virus burden in the spleen and the blood of both groups of mice, suggesting the virus had spread from the skin rapidly post-infection (Figure 4.5B-C). However, the quantities of virus in the spleen and blood were similar between the mice exposed to UV 1-week prior to infection and the unexposed mice. Despite this, during clinical monitoring of the mice, all mice in

the ZIKV-infected, UV-exposed group displayed clinical signs of disease, including subdued behaviour and hunched posture, by 24hpi (Figure 4.5D). None of the mice who did not receive UV exposure prior to infection with ZIKV displayed these signs. Therefore, although ZIKV quantities in the skin, spleen and blood did not differ between UV-exposed mice and unexposed mice, mice which had been exposed to UV 1 week prior to infection experienced a more clinically severe form of ZIKV infection.

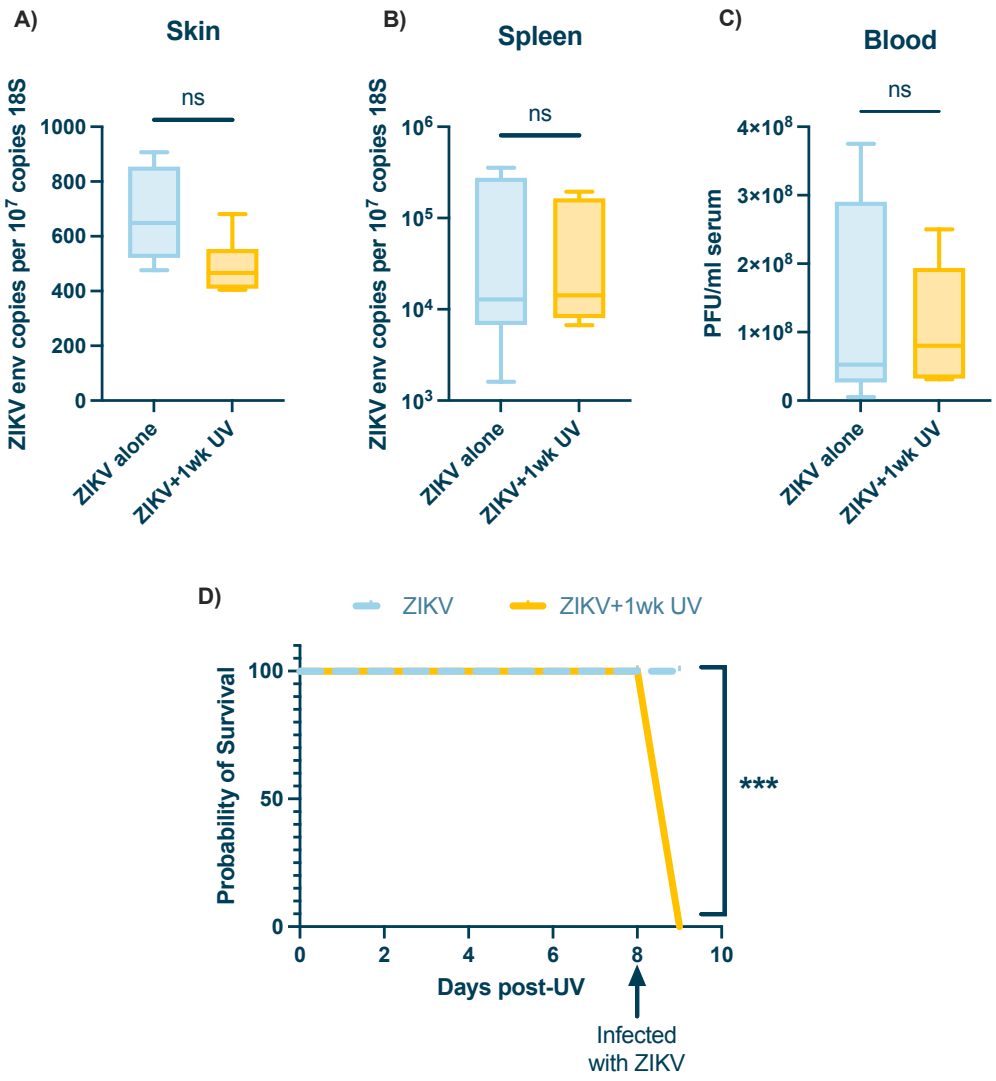

Figure 4.5 | Erythemal UV exposure causes more clinically severe ZIKV infection 1-week post-exposure

(A-D) ZIKV RNA (Env gene) copy number in inoculation site (skin) **(A)** or spleen **(B)** or viral titres in the serum **(C)** 24hpi. Prior to infection, *Ifnar-/-* mice were either left unexposed or were exposed to an erythemal dose of UV on the skin on the upper side of the foot. All *Ifnar-/-* mice were then infected at 1-week post-exposure at the same site with 10^3 PFU of ZIKV in the presence of a mosquito bite. Mice were monitored

post-UV exposure and post-infection for clinical signs, as outline in Section 2.6.1, with those mice that reach clinically defined thresholds of suffering removed from study, and classed as succumbed to infection **(D)**. ($n \geq 6$)
Gene expression measured by qPCR. Serum titres measured by plaque assay. Plots show the median value ± interquartile range. Data were analysed using Mann-Whitney test (*ns = not significant, ***P < 0.001*).

Once we had determined that susceptibility to SFV infection was increased in mice up to 2-weeks post UV exposure, and that mice exposed to UV 1-week prior to ZIKV infection experience more clinically severe outcomes, we next sought to investigate the mechanism behind this enhanced infection phenotype. Initially, we hypothesised that this effect could be due to impairment of the antiviral Type I IFN response, which is critical for fighting arbovirus infections. However, the evidence from Figure 4.5, showing that UV exposure of mice 1 week prior to ZIKV infection led to more clinically severe signs in *Ifnar-/-* mice, which lack the Type I IFN receptor, suggested that UV-mediated enhancement of arbovirus infection at 1 week occurs independently of Type I IFN. Nevertheless, we characterised Type I IFN expression in mice exposed to UV 1 week prior to infection, to determine whether this is blunted, and could potentially allow the virus to replicate more efficiently.

Gene expression of the Type I IFN, IFN-β, and a number of ISGs, the antiviral effector molecules of the Type I IFN system, were measured using qPCR in the skin of mice at 24hpi with 10^4 PFU of SFV4, a known inducer of type I IFNs in immunocompetent mice. Mice had either been unexposed or exposed to erythemal UV 1-week, 2 weeks or 3 weeks prior to infection at the inoculation site. Based on above data, we hypothesised that UV exposure might suppress induction of IFN expression, as UV caused enhanced virus infection. However, we found expression of IFN-β was significantly increased by 24hpi in mice exposed to erythemal UV 1-week prior to infection, compared to infected, unexposed mice (Figure 4.6A). Correspondingly, those exposed mice had significantly higher levels of expression of several key ISGs, IFIT1, ISG15, RSAD2 and CXCL10 (Figure 4.6B). Interestingly, mice exposed to UV 2 weeks before infection had significantly higher levels of ISGs as well, despite no significant increase in IFN-β by this timepoint (Figure 4.6A-B). Expression of both IFN-β and these ISGs was not significantly different in mice exposed to UV

3 weeks prior to infection. Together, this data shows that the Type I IFN response was not impaired during UV-mediated enhancement of infection 1-week post-UV. In fact, UV-exposed mice 1-week post-UV had a particularly strong induction of both IFN-β and several important antiviral ISGs. However, despite this enhanced induction of IFN, this does not seem to be enough to protect them from increased susceptibility to arbovirus infection caused by UV exposure.

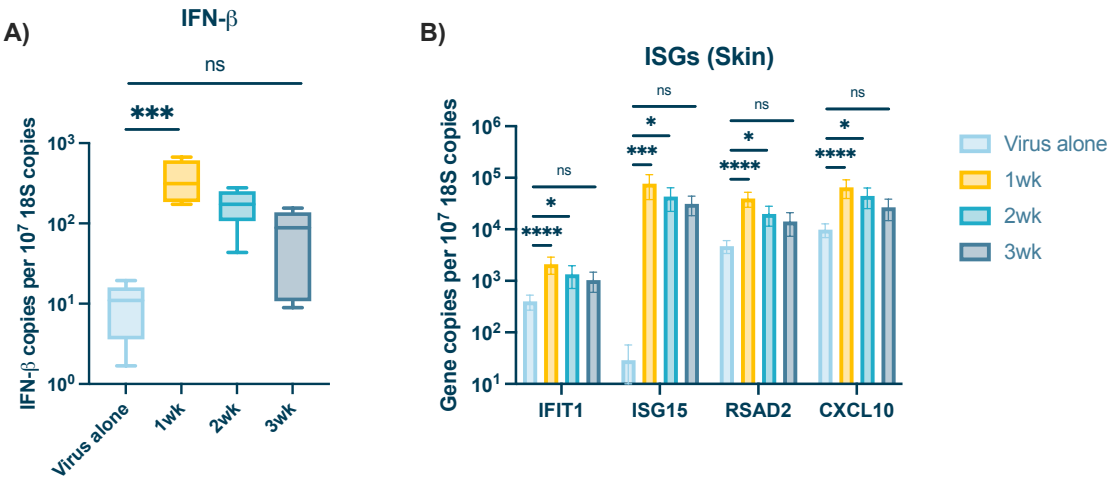

Figure 4.6 | Expression of antiviral ISGs induced during UV-mediated enhancement of infection 1-2wks post-UV exposure

IFN-β **(A)** or ISG **(B)** copy number in inoculation site (skin) 24hpi. Prior to infection, mice were either left unexposed or were exposed to an erythemal dose of UV on the skin on the upper side of the foot. All mice were then infected at either 1 week, 2 weeks or 3 weeks post-exposure at the same site with 10^4 PFU of SFV4 in the presence of a mosquito bite. ($n \geq 6$)

Gene expression measured by qPCR. Plots show the median value ± interquartile range. Data were analysed using Kruskal-Wallis test with Dunn's multiple comparison test (*ns = not significant, *P < 0.05, **P < 0.01, ***P < 0.001, ****P < 0.0001*).

4.4 Erythemal UV exposure drives proliferation of cells in skin at 1-week post-UV and SFV preferentially infects these proliferating cells

As introduced in Chapter 3, UV exposure is known to drive proliferation of cells at various stages post-UV and SFV, infects actively proliferating cells and has been used as an experimental oncolytic agent for this reason[232,309,310]. During wound-healing in skin, the tissue becomes highly proliferative, for example, with

macrophages driving the proliferation of structural cell types to rebuild the tissue[349]. UV also causes photoadaptation, including epidermal thickening and melanin production, that involves proliferation of cells in the skin[315,356]. We witnessed signs of hyperplasia, characterised by proliferation of cells, in the skin of mice 1-week post-UV (Figure 4.1). While the last chapter explored this at 24h post-UV, we also wanted to examine whether UV drives proliferation at 1-week post-UV, thereby providing SFV with more cellular targets for infection. As before, we used EdU, which incorporates into DNA as cells proliferate, to quantify levels of proliferating cells. Skin was taken from resting mice, or from mice infected with SFV at a mosquito bite, or from mice exposed to UV 1 week prior and then infected in mosquito bitten skin. The cells from this skin were then collected at 24hpi and cultured with EdU *in vitro* for 2 hours, giving time for this nucleoside analogue to incorporate into proliferating cells. EdU was then detected using a fluorescent tag, allowing us to identify proliferating cells using flow cytometry. There were significantly more proliferating cells in mice exposed to UV 1 week prior to infection, compared to resting skin (Figure 4.7). Interestingly, SFV infection itself did not drive a significant increase in proliferation compared to resting skin. Therefore, erythemal UV exposure drives proliferation of cells in the skin of mice by 1-week post-UV.

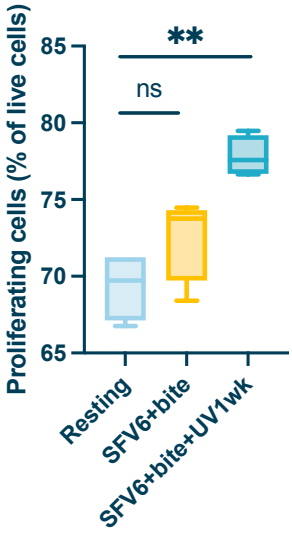

Figure 4.7 | UV exposure drives proliferation of cells at 1-week post-UV

EdU+ cells in the skin as a percentage of total live cells. Prior to infection, mice were either left unexposed or were exposed to an erythemal dose of UV on the skin on the upper side of the foot. All mice were then infected 1 week post-exposure at the same site with 10^3 PFU of SFV6-mCHERRY in the presence of a mosquito bite. Skin from the

exposed site was collected 24h post-exposure and digested to isolate single cells. Cells were incubated with EdU, a thymidine nucleoside analogue, for 2 hours. EdU+ cells were then tagged with a fluorophore using Click-IT chemistry so that proliferating cells could be identified using flow cytometry. (n = 4)
Plots show the median value ± interquartile range. Data were analysed using Kruskal-Wallis test with Dunn's multiple comparison test (*ns = not significant, **P < 0.01*).

Once the proliferative nature of skin at 1-week post-UV had been demonstrated, and the assay to measure this established, we next sought to determine whether SFV was preferentially infecting these proliferating cells, thereby providing one mechanism by which UV drives more robust virus infection in mice exposed to UV 1 week before. To investigate this, we used a modified strain of SFV which encodes the fluorescent protein mCHERRY, SFV6-mCHERRY. Initially, we confirmed that SFV6-mCHERRY infection is still enhanced in mice exposed to UV 1 week prior to infection, as we had shown repeatedly with SFV4 infection. We used qPCR to quantify virus quantities in the skin of these mice and found that there was significantly more virus present at the inoculation site by 24hpi in mice infected 1-week post-UV, compared to unexposed mice (Figure 4.8A).

After confirming that host susceptibility to SFV6-mCHERRY at 1 week post UV exposure was substantially enhanced, we next used this strain of virus to facilitate the identification of virus-infected cells present in the skin at 24hpi, using flow cytometry. We infected either unexposed mice or mice which had been exposed to erythemal UV at the inoculation site 1-week earlier with 10^3 PFU of SFV6-mCHERRY. At 24hpi, skin was collected and digested to a single cell suspension. All skin cells were then cultured with EdU for 2 hours, at which point EdU+ cells were fluorescently tagged, as before. This meant that we could identify cells which were both infected with virus and actively proliferating by 24hpi, to determine whether SFV was targeting proliferating cells in the skin of mice exposed to erythemal UV 1 week prior to infection.

When we examined the proportion of SFV-infected cells which were actively proliferating by 24hpi, there were significantly more infected, proliferating cells in mice exposed to UV 1-week before infection, compared to infected, unexposed mice (Figure 4.8B). Furthermore, there were significantly less

infected, non-proliferating cells in the skin of UV-exposed mice compared to unexposed mice (Figure 4.8C). To confirm this finding that there are more infected, proliferating cells in the mice exposed to UV 1-week prior to infection compared to the non-UV exposed mice, we calculated the ratio of infected, proliferating cells to infected, non-proliferating cells in each group. The mice which had been exposed to UV 1-week before infection had a ratio of greater than 1, meaning that there were more infected, proliferating cells in that group than infected, non-proliferating cells (Figure 4.8D). However, the same ratio for the infected, unexposed mice was less than 1, confirming that there were more infected, non-proliferating cells in these mice. Together, this data suggests that UV drives proliferation of cells in the skin by 1-week post-UV and that SFV preferentially infects proliferating cells during UV-mediated enhancement of infection 1-week post-UV.

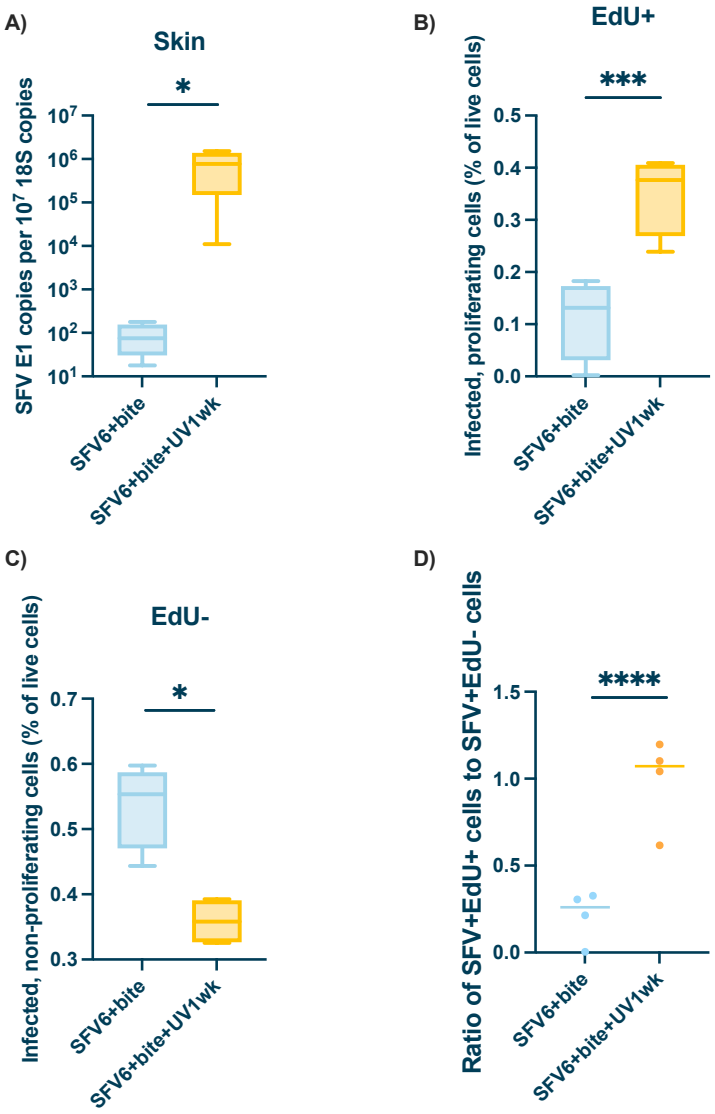

Figure 4.8 | SFV preferentially infects proliferating cells during UV-mediated enhancement of infection 1-week post-UV

(A-D) Prior to infection, mice were either left unexposed or were exposed to an erythemal dose of UV on the skin on the upper side of the foot. All mice were then infected 1 week post-exposure at the same site with 10^3 PFU of SFV6-mCHERRY in the presence of a mosquito bite. Skin from the exposed site was collected 24h post-infection and digested to isolate single cells. Cells were incubated with EdU, a thymidine nucleoside analogue, for 1-2. EdU^+ cells were then tagged with a fluorophore using Click-IT chemistry. Proliferating cells (EdU^+) and infected cells (SFV6-$mCHERRY^+$) could then be identified using flow cytometry. (n = 4)

(A) SFV RNA (E1 gene) copy number in inoculation site (skin) was measured at 24hpi by qPCR.

(B-C) Cells were first gated on SFV^+ and then split into 'infected, proliferating cells' (SFV^+EdU^+) **(B)** or 'Infected, non-proliferating cells' (SFV^+EdU^-) **(C)**.

(D) Ratio of 'infected, proliferating cells' to 'infected, non proliferating cells'. Ratio >1 = virus preferentially infecting 'proliferating cells'. Ratio <1 = virus preferentially infecting 'non-proliferating cells'.

Plots show the median value ± interquartile range. Data were analysed using unpaired t-test **(A)** or Mann-Whitney test **(B-D)** (*ns = not significant, *P < 0.05, ***P < 0.001, ****P < 0.0001*).

4.5 UV-exposed skin at 1-week post-exposure possesses multiple characteristics of wound healing phenotype, including macrophage recruitment and increased ARG1 expression

Others have found that in similar mouse models of sunburn, healing begins after 1-week post-UV in mice, primarily characterised in the first instance by hyperplasia[232]. Our earlier data in Figure 4.1 concurred with this, showing the expansion of skin depth 1-2 weeks after the burn took place and the wound having healed by 3 weeks post-UV. Endothelial cells and fibroblasts proliferate during the wound-healing process in skin[210]. Additionally, macrophages are critical for rebuilding damaged tissue at the wound site[351]. Since SFV appears to be infecting proliferating cells during UV-mediated enhancement of infection at 1-week post-UV, it was vital for us to understand the cellular profile of UV-exposed skin at this timepoint, both before and after infection. Therefore, we set out to investigate whether the proportions of any key cell population changed.

First, we wanted to examine expression of two important chemokines, CCL2 and CXCL2, which attract monocytes and neutrophils respectively. This is relevant as monocytes and their progeny can be infected and replicate some arboviruses, including SFV. Importantly, expression of these genes is increased in the skin at 24h post-UV (Chapter 3) and following a mosquito bite; we believe this is critical to enhancement of arbovirus infection under both of these conditions[120]. Therefore, we used qPCR to quantify the levels of expression of CCL2 and CXCL2 in the skin of mice infected with 10^4 PFU of SFV4 in resting skin or skin exposed to erythemal UV 1-week, 2 weeks or 3 weeks prior. At 24hpi, the monocyte chemoattractant, CCL2, was significantly upregulated during infection of mice exposed to UV 1-week or 2 weeks before, compared to infected, non-UV exposed mice (Figure 4.9). However, levels of CCL2 had returned to normal in mice exposed to UV 3-weeks before being infected. Similarly, expression of CXCL2, the neutrophil-attracting chemokine, was significantly increased by 24hpi in mice exposed to UV 1-week prior to infection compared to unexposed mice but did not change in mice that were 2 weeks or 3 weeks post UV when the infection took place. Together, this shows that there is increased expression by 1-week post-UV of CCL2 and CXCL2, two chemokines which bring in cell types known to facilitate enhancement of infection at 24h post-UV and in mosquito-bitten skin.

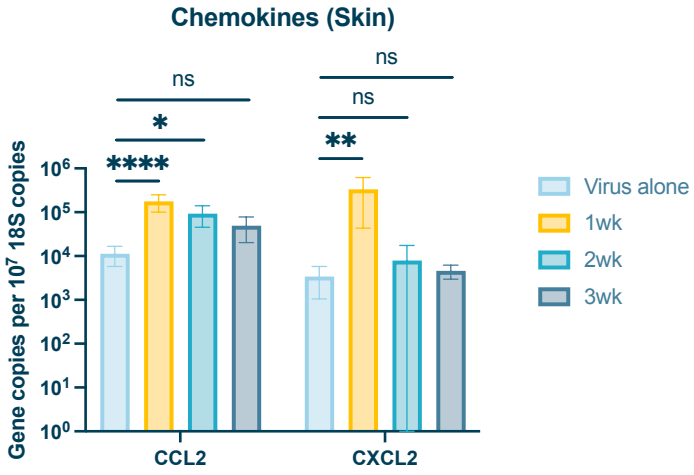

Figure 4.9 | Expression of myeloid cell chemoattractants induced during UV-mediated enhancement of infection 1-2wks post-UV exposure

Chemokine copy number in inoculation site (skin) 24hpi. Prior to infection, mice were either left unexposed or were exposed to an erythemal dose of UV on the skin on the upper side of the foot. All mice were then infected at either 1 week, 2 weeks or 3 weeks

post-exposure at the same site with 10^4 PFU of SFV4 in the presence of a mosquito bite. ($n \geq 6$)
Gene expression measured by qPCR. Plots show the median value ± interquartile range. Data were analysed using Kruskal-Wallis test with Dunn's multiple comparison test (*ns = not significant, *P < 0.05, **P < 0.01, ****P < 0.0001*).

The increased expression of CXCL2 and CCL2 by 1-week post-UV, when enhancement of infection peaks, suggests that there may be more neutrophils and monocytes present in the skin during infection, as a result of being recruited by these chemokines. To investigate this, we used flow cytometry to assess the number of neutrophils and monocytes in the skin of mice by 16hpi with 10^4 PFU of SFV4 and how this changed with the addition of a mosquito bite or an erythemal UV exposure 1-week prior to infection, or with the combination of both. There were significantly more neutrophils in the skin by 16hpi in both groups of UV-exposed mice compared to non-exposed mice (Figure 4.10A-B). However, the only group which experienced an increase in the number of monocytes was the mosquito bite alone group. Both groups of mice which had been exposed to UV 1-week prior to infection did not have a change in the number of monocytes in the skin by 16hpi, compared to normal SFV infection. Importantly and surprisingly, the addition of UV-exposure alongside a mosquito bite reversed the increase in the number of monocytes brought in by the mosquito bite alone, suggesting UV exposure 1 week before may suppress monocyte recruitment to SFV infection at mosquito bites.

Collectively, this data shows that although there is an increase in expression of monocyte and neutrophil chemoattractants during infection of mice exposed to UV 1-week prior, this only translated into more neutrophils, but not monocytes, being present in the skin of UV-exposed, infected mice.

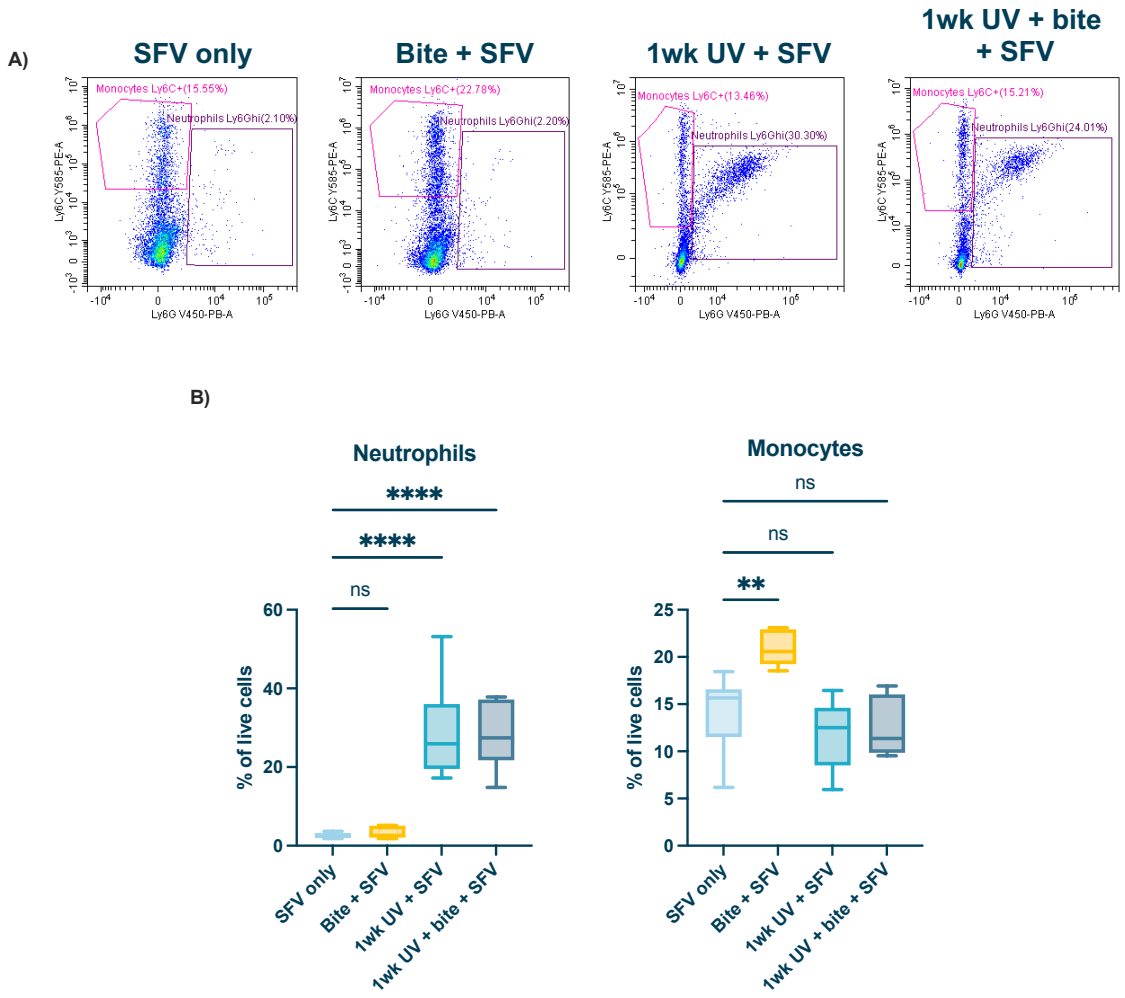

Figure 4.10 | Increased numbers of neutrophils, but not monocytes, at the skin during arbovirus infection at 1-week post-UV exposure

(A-B) Skin on the upper left feet of mice were either exposed to a single erythemal UV dose or left unexposed. All mice were infected 1 week post UV exposure with 10^4 PFU of SFV4 at the exposed site in the presence or absence of a mosquito bite. Skin was collected 16hpi and digested to isolate single cells.

(A) Cells were stained with antibodies against CD45, CD11b, Ly6C and Ly6G and analysed using flow cytometry.

(B) Monocyte ($Ly6C^+$) and neutrophil ($Ly6G^{hi}$) migration to skin measured by flow cytometry at 16hpi. Numbers represent percent of $Ly6C^+$ or $Ly6G^{hi}$ cells of all live cells. Plots show the median value ± interquartile range. Data were analysed using Kruskal-Wallis test with Dunn's multiple comparison test (*ns = not significant, **P < 0.01, ****P < 0.0001*).

As covered in the introduction to this chapter, macrophages are critical for tissue repair during wound healing and are present in the wounded area in high numbers[219]. While far less is known about the role of DCs in wound-healing,

these cells are also phagocytes and in addition to their antigen presenting/immune surveillance roles, also contribute to e.g. apoptotic cell clearance, albeit to a lesser extent than macrophages[357]. DC also contribute to tissue repair through the secretion of important factors/effector molecules, such as growth factors[357]. Importantly, when dermal DCs are depleted, wound healing in the skin is delayed in mice by day 5 post-wound, suggesting that they play an important role[358].

As such, it was important to assess whether numbers of both macrophages and DCs in UV-exposed skin at 1-week post-UV were altered, especially since these phagocytes are permissive to SFV infection. Using flow cytometry, we found that the proportion of macrophages was significantly higher in UV-exposed skin at 1-week post-UV, compared to resting mouse skin (Figure 4.11A). However, in mice infected with SFV 1-week post-UV, there were significantly less macrophages in the skin, compared to UV-exposed mice alone. This group had a similar proportion of macrophages to the resting mice and those infected with SFV in the absence of UV. Interestingly, there was no significant change in the proportion of DCs present in the skin in UV-exposed mice, even during infection (Figure 4.11B). Therefore, UV exposure drives an increase in the number of macrophages, but not DCs, in the skin by 1-week post-UV. However, this population contracts during SFV infection of UV-exposed skin.

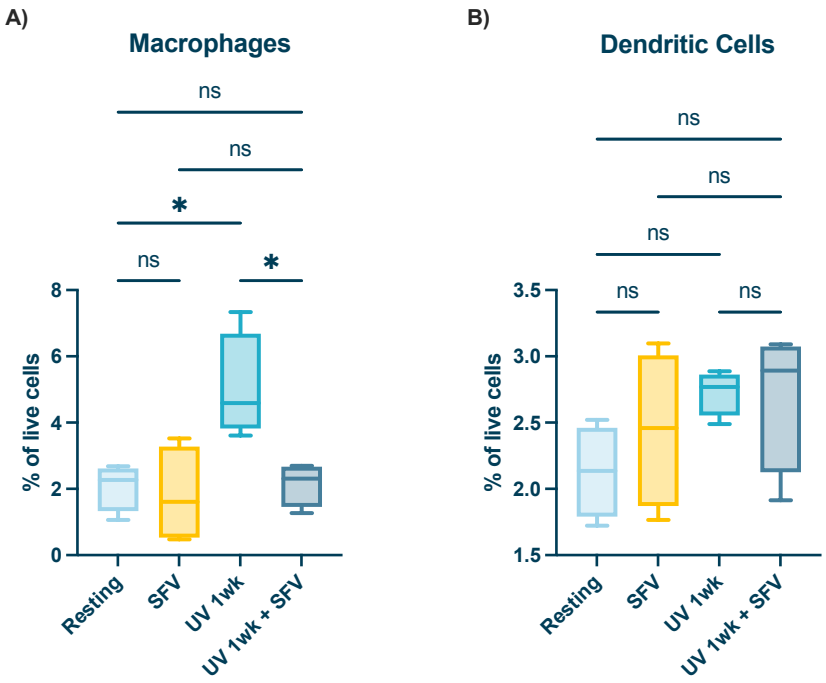

Figure 4.11 | Erythemal UV exposure drives recruitment of macrophages to the skin at 1wk post-UV but numbers reduce during UV-mediated enhancement of infection

(A-B) Macrophage ($CD45^+Ly6G^-CD11b^+MerTK^+$) **(A)** and DC ($CD45^+Ly6C^-CD11c^{int}MHCII^+$) **(B)** migration to skin measured by flow cytometry at 16hpi. Gating strategy used during analysis outline in Section 2.19.5. Numbers represent percent of indicated cell type of all live cells. Prior to infection, mice were either left unexposed or were exposed to an erythemal dose of UV on the skin on the upper side of the foot. All mice were then infected 1wk post-exposure at the same site with 10^4 PFU of SFV4 in the presence or absence of a mosquito bite. *(n = 4)*

Plots show the median value ± interquartile range. Data were analysed using Kruskal-Wallis test with Dunn's multiple comparison test (*ns = not significant, *P < 0.05*).

The replication and differentiation of endothelial cells, keratinocytes and fibroblasts in the skin are a critical for the efficient healing of damaged skin. Together, these CD45-ve cells form the core components of the tissue, including the ECM, epithelium and vasculature[359]. Due to their core structural role in the skin, these cells face a lot of the damage caused by UV exposure of the skin during sunburn and, therefore, proliferation and regeneration of these populations is required to restore the tissue to homeostasis[209,360]. These cells are also susceptible to SFV infection[308]. Therefore, we also sought to define their quantities in the skin 1 week after erythemal UV exposure, both in response to the burn alone and also during arbovirus infection. When these three cell populations were assessed using flow cytometry, we found that there were significantly more endothelial cells in the skin of mice 1-week post-UV exposure, compared to resting mice (Figure 4.12A). However, this population as a percentage of all live cells was reduced back to normal levels in UV-exposed mice by 16hpi. Unexpectedly, there was no significant change in the proportion of fibroblasts or endothelial cells 1-week post-UV exposure and/or SFV infection (Figure 4.12B-C). Despite the requirement for CD45- cell proliferation during tissue regeneration, we found no increase in epithelial cells or fibroblasts, and the increase in endothelial cells in the skin observed at 1-week post-UV was reversed with the addition of SFV infection. However, this could be due to expansion in numbers of other cell types in the skin, e.g. macrophages, which may lead to the CD45- compartment not appearing any larger. The expansion of

the skin layers (Figure 4.1) indicates that there are many more cells overall in the skin following UV-exposure.

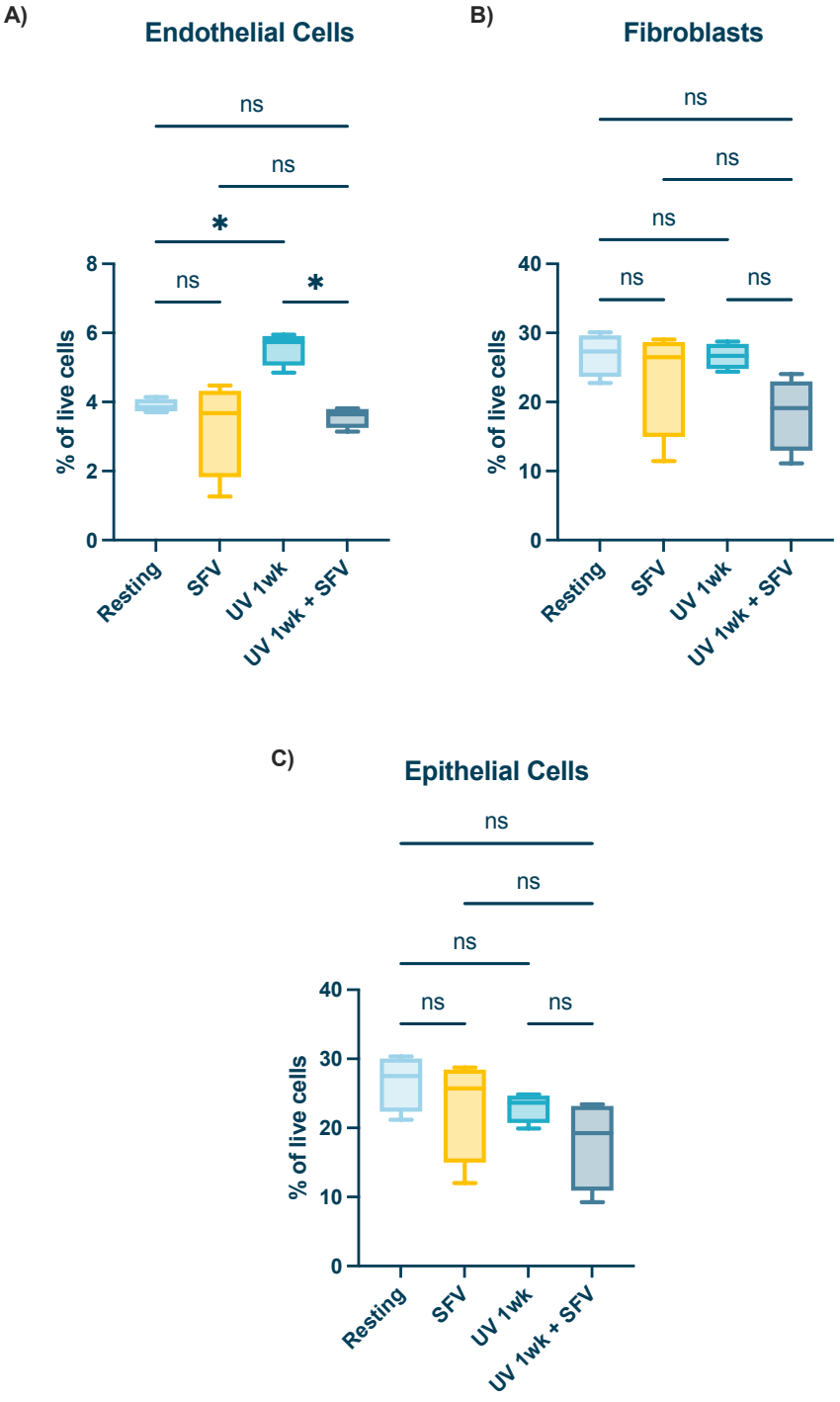

Figure 4.12 | UV-exposed skin, 1wk post-UV, exhibits higher numbers of endothelial cells

(A-C) Endothelial cell ($CD45^{-}CD31^{+}$) **(A)**, fibroblast ($CD45^{-}Vimentin^{+}$) **(B)** and epithelial cell ($CD45^{-}EP\text{-}CAM^{+}$) **(C)** numbers in skin measured by flow cytometry at 16hpi. Gating strategy used during analysis outline in Section 2.19.5. Numbers represent percent of indicated cell type of all live cells. Prior to infection, mice were either left unexposed or

were exposed to an erythemal dose of UV on the skin on the upper side of the foot. All mice were then infected 1wk post-exposure at the same site with 10^4 PFU of SFV4 in the presence or absence of a mosquito bite. *(n = 4)*
Plots show the median value ± interquartile range. Data were analysed using Kruskal-Wallis test with Dunn's multiple comparison test (*ns = not significant, *P < 0.05*).

ARG1 encodes the Arginase 1 protein, a hallmark of the wound-healing M2 macrophages. To further characterise the wound-healing phenotype of the skin at 1-week post-UV, we investigated expression of the ARG1 gene using qPCR. Levels of ARG1 were first assessed in the skin from mice infected with 10^4 PFU of SFV4 at resting skin or in skin exposed to UV between 24h-1 week prior. There was no significant increase in ARG1 expression in the skin until 1-week post-UV exposure, at which point levels of the gene had increased 100-fold compared to infected, resting skin (Figure 4.13A). However, there was an increasing trend in ARG1 expression over time post-burn, which was particularly apparent by 72h post-UV exposure. When we investigated ARG1 expression in mice infected with SFV at later timepoints post-UV, we found that levels of ARG1 begin to return to normal in mice infected 2 or 3 weeks post-UV (Figure 4.13B).

While ARG1 is strongly associated with M2 macrophages, fibroblasts have also been shown to express ARG1 during wound-healing. Therefore, we set out to identify whether the increase in ARG1 expression observed at 1-week post-UV was due to expression by immune cells or CD45- cells, which include fibroblasts. To investigate this, we separated out CD45+ and CD45- cells from the skin of mice infected *in vivo* with 10^4 PFU of SFV4 1-week post-UV and used qPCR to quantify the levels of ARG1 expression in each cellular compartment. As expected, there was significantly higher levels of ARG1 expression in immune cells in the skin of mice exposed to UV 1-week before infection compared to infected, unexposed mice (Figure 4.13C). Interestingly though, the CD45- compartment in the skin of UV-exposed mice had also significantly upregulated ARG1, compared to the same cells in the unexposed mice (Figure 4.13D). Together, the data from this figure shows that ARG1 expression is increased in the skin of mice 1-week post-erythemal UV

exposure, and that this is observed in both immune cells and CD45- cells, including fibroblasts.

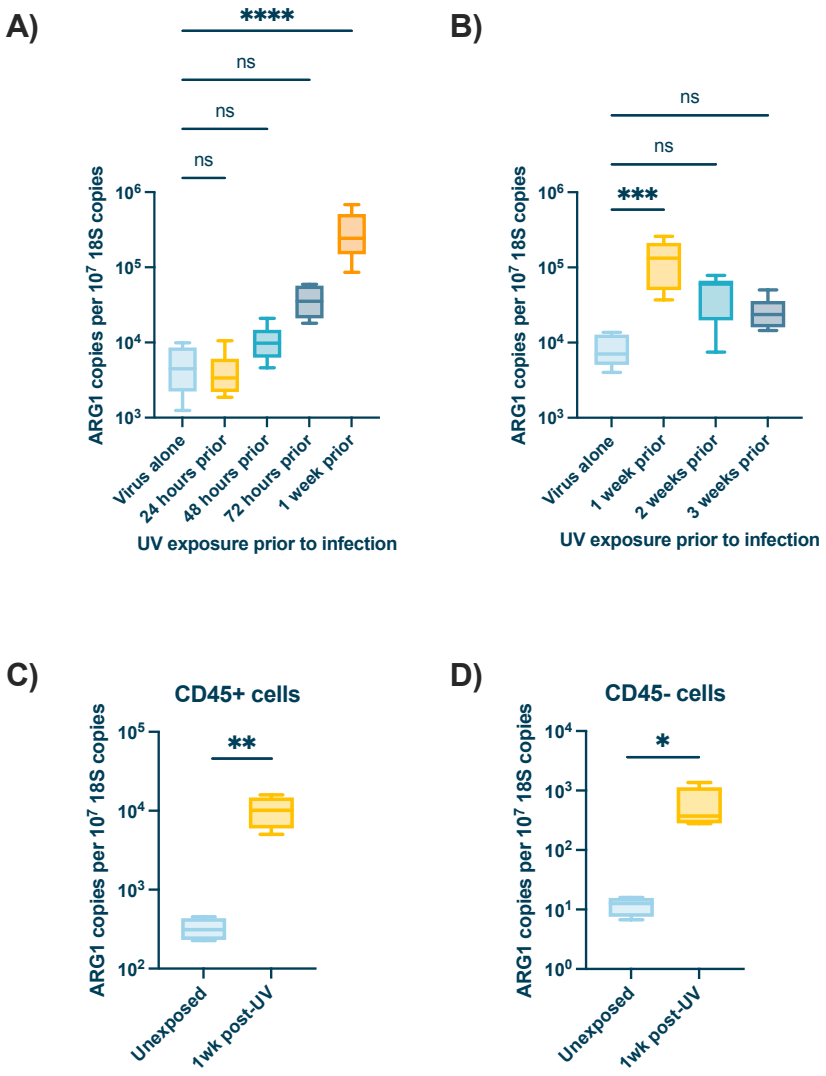

Figure 4.13 | CD45+ and CD45- cells in the skin express more ARG1, a key signalling molecule involved in wound-healing, at 1wk post-UV exposure

(A-B) ARG1 copy number in inoculation site (skin) 24hpi. Prior to infection, mice were either left unexposed or were exposed to an erythemal dose of UV on the skin on the upper side of the foot. All mice were then infected at either 24h, 48h, 72h or 1 week post-exposure **(A)** or 1 week, 2 weeks or 3 weeks post-exposure **(B)** at the same site with 10^4 PFU of SFV4 in the presence of a mosquito bite. ($n \geq 6$)

(C-D) ARG1 copy number in CD45+ **(C)** or CD45- cells **(D)** isolated from infected unexposed or UV-exposed mice. CD45+ and CD45- fractions were separated using MACS separation.

Gene expression measured by qPCR. Plots show the median value ± interquartile range. Data were analysed using Kruskal-Wallis test with Dunn's multiple comparison

test **(A-B)** or Mann-Whitney test **(C-D)** (*ns = not significant, *P < 0.05, **P < 0.01, ***P < 0.001*).

4.6 SFV does not preferentially target either CD45- or CD45+ cells during UV-mediated enhancement of infection 1-week post-UV

In Figures 4.11 And 4.12 we had found that there were significantly more macrophages and endothelial cells in the skin by 1-week post-UV and that this expanded frequency was seemingly reversed during SFV infection of UV-exposed skin, suggesting that the cells may have been infected and killed by virus, or that expression of specific cell markers used for gating had been altered. Therefore, we next investigated whether either immune cells (CD45+) or CD45- cells were disproportionately infected with virus during UV-mediated enhancement of infection in mice exposed to UV 1 week prior. Mice were infected with 10^4 PFU of SFV4 in unexposed skin or skin which had been exposed to erythemal UV 1-week prior. Cells from this skin were then isolated and separated into CD45+ and CD45- populations. Flow cytometry was used on a sample of each of these populations to confirm that the CD45+ fraction was enriched with CD45+ cells and the CD45- fraction had all CD45+ cells removed (Figure 4.14a-B). qPCR was used to quantify quantities of virus RNA present in each of these fractions. We found no significant difference in the quantities of virus between immune cells and CD45- cells in either unexposed mice or mice infected 1-week post-UV (Figures 4.14C-D). However, while this approach can be useful to easily identify changes in virus burden, there are many distinct cell types within both the CD45+ and CD45- fractions. Thus, small changes in virus quantities in one cell type e.g. macrophages (CD45+) or fibroblasts (CD45-), could be masked by all of the other cell types contained within that fraction.

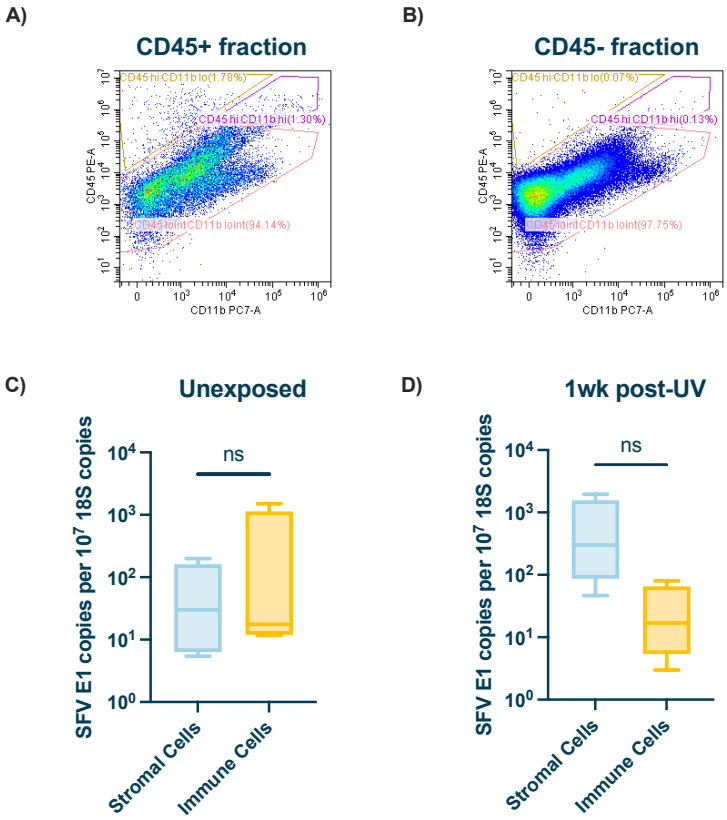

Figure 4.14 | Virus burden in leukocytes is comparable to that in CD45- cells during enhancement of infection at 1-week post-UV exposure

(A-D) Skin on the upper left feet of mice were either exposed to a single erythemal UV dose or left unexposed. All mice were infected 1 week post UV exposure with 10^4 PFU of SFV4 at the exposed site in the presence of a mosquito bite. Skin from the inoculation site was collected 6hpi and digested to isolate single cells. Magnetic separation was used to separate cells expressing CD45 (CD45+) from the remaining cells (CD45-). (*n* = 8)

(A, B) Cells from the CD45+ **(A)** and the CD45- **(B)** fractions were stained with antibodies against CD45 and CD11b and analysed using flow cytometry. Numbers represent percentage of total live cells. Plots contain data from one individual but are representative of all samples and show the gating strategy used throughout.

(C, D) SFV RNA (*E1* gene) copy number in the CD45+ and CD45- fractions in unexposed **(C)** and UV-exposed **(D)** mice were determined at 6hpi by qPCR.

Plots show the median value ± interquartile range **(C-D)**. Data were analysed using Mann-Whitney test (*ns = not significant, *P < 0.05, ***P < 0.001*).

UV exposure of skin makes several changes to individual cells over time, including mutations to DNA which can lead to skin cancer[338,340,341]. Therefore, we considered whether such changes on a cell-by-cell (cell autonomous) basis could make cells more susceptible to arbovirus infection, 1 week after UV

exposure of the skin. While we had shown that this was not the case at 24h post-UV (Chapter 3), this timepoint may have been too early for any changes caused by UV to alter the inherent permissiveness of cells to become infected and replicate virus.

To investigate this at 1-week post-UV, we collected skin from resting mice or mice exposed to UV 1 week before. The skin was digested to collect the cells from the tissue. These cells were infected *in vitro* and RNA was extracted at 16hpi to analyse the quantities of virus RNA present in the cells using qPCR. The quantities of virus by 16hpi were similar in the cells taken from unexposed mice compared to those taken from mice exposed to UV 1-week prior to infection (Figure 4.15C). We then repeated this experiment but separated the skin cells into CD45+ and CD45- populations and infected each population separately, to determine whether either individual population was more susceptible following UV exposure. Separation of the two fractions was confirmed using flow cytometry (Figure 4.15A-B). When we examined quantities of virus RNA in each cellular compartment, we found that there was no significant difference in the virus burden by 16hpi between immune cells and CD45- cells from either UV-exposed mice or unexposed mice (Figure 4.15D). Additionally, there was no difference in the quantities of SFV RNA in immune cells from unexposed mice compared to immune cells from mice exposed to UV 1-week prior to infection. The same was true for CD45- cells. SFV infection was not enhanced *ex vivo*, suggesting that cells are not made more inherently susceptible by UV exposure at 1-week post-UV, and that the mechanism driving this effect only occurs *in vivo.*

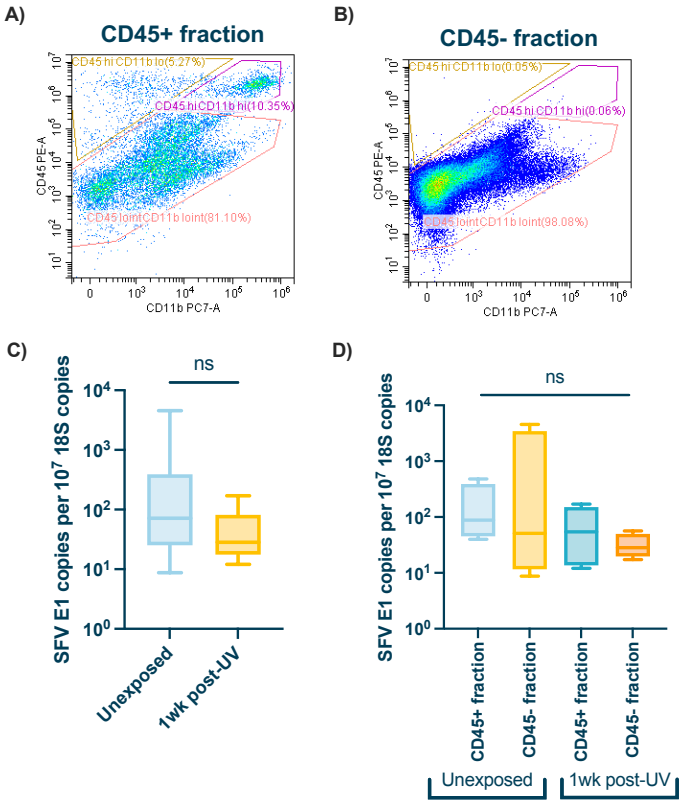

Figure 4.15 | No inherent difference in permissiveness of cells to arbovirus infection 1 week after erythemal UV exposure

(A-D) Mice were either exposed to a single erythemal UV dose or left unexposed. Skin from the exposed site was collected 1wk post-exposure and digested to isolate single cells. Cells were then infected with SFV4 *in vitro* either immediately, or following magnetic separation into immune cell (CD45+) and stromal cell (CD45-) compartments. Quantities of virus RNA were analysed at 16hpi. (n = 8)

(A, B) Cells from the CD45+ **(A)** and the CD45- **(B)** fractions after CD45+ separation. **(C)** SFV RNA (*E1* gene) copy number in all cells taken from skin of UV-exposed mice compared to unexposed mice at 16hpi *in vitro*. **(D)** SFV RNA (*E1* gene) copy number in CD45+ and CD45- fractions from unexposed **(C)** and UV-exposed **(D)** mice at 16hpi i*n vitro*.

Gene expression measured by qPCR. Plots show the median value ± interquartile range **(C-D)**. Data were analysed using unpaired t-test (**C)** or Kruskal-Wallis test with Dunn's multiple comparison test **(D) (***ns = not significant*).

4.7 An increase in infected fibroblasts present in mice exposed to UV 1-week prior to infection

While the results from Figure 4.14 showed that there is no difference in the virus burden in immune cells vs CD45- cells of UV-exposed mice, we still did not have an explanation for the reduction in macrophage and endothelial cell

numbers in the skin between mice exposed to UV 1 week prior and mice infected with SFV at UV-exposed skin 1-week post-UV. One explanation for this reduction could be that these cell types had been infected with SFV, resulting in cell lysis and death. Therefore, we used a fluorescent strain of SFV, SFV6-mCHERRY, and flow cytometry to identify infected cell types in mice infected with SFV in resting skin or in skin exposed to UV 1-week prior. We first looked at the three main immune cell types which are infected by SFV within the first 24h of infection. Surprisingly, we did not find any change in the number of SFV-infected monocytes, macrophages or DCs in mice exposed to UV 1-week prior to infection, compared to infected, unexposed mice (Figure 4.16A-C).

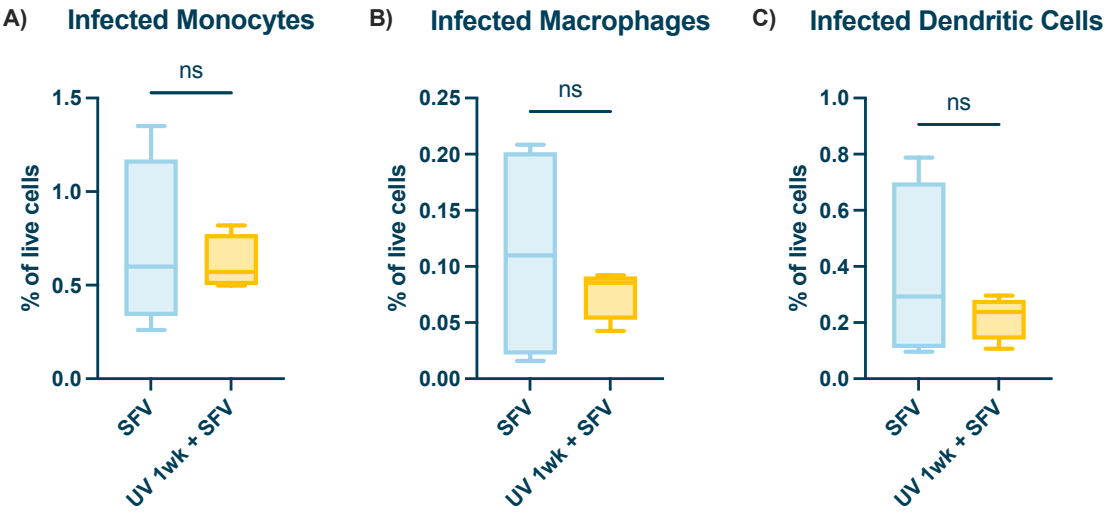

Figure 4.16 | No difference in virus burden in leukocytes during UV-mediated enhancement of infection 1wk post-UV

(A-C) Number of infected monocytes ($CD45^+Ly6C^-CD11c^-MHCII^+$) **(A)**, macrophages ($CD45^+Ly6G^-CD11b^+MerTK^+$) **(B)**, DCs ($CD45^+Ly6C^-CD11c^{int}MHCII^+$) **(C)**, measured by flow cytometry at 16hpi. Gating strategy used during analysis outline in Section 2.19.5. Numbers represent percent of indicated SFV6-mCHERRY$^+$ infected cell type of all live cells. Prior to infection, mice were either left unexposed or were exposed to an erythemal dose of UV on the skin on the upper side of the foot. All mice were then infected 1wk post-exposure at the same site with 10^3 PFU of SFV6-mCHERRY in the presence or absence of a mosquito bite. *(n = 4)*

Plots show the median value ± interquartile range. Data were analysed using Mann-Whitney test (*ns* = *not significant*).

We next assessed SFV6-mCHERRY infection of key CD45- cell populations, endothelial cells, fibroblasts and epithelial cells. Interestingly, there was no

significant increase in the number of infected endothelial cells between UV-exposed mice and unexposed mice, despite this being the cell type which had been shown to be ablated following SFV infection of UV-exposed mice earlier in this chapter (Figure 4.17A). There was also no difference in the number of infected epithelial cells between the two groups (Figure 4.17C). However, there were significantly more infected fibroblasts in UV-exposed mice by 16hpi, compared to unexposed mice (Figure 4.17B).

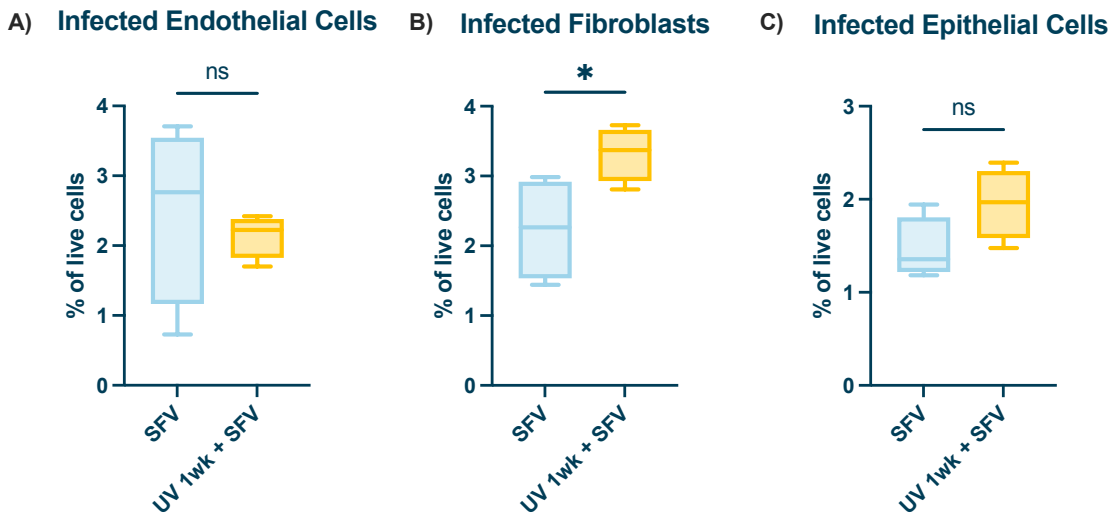

Figure 4.17 | SFV preferentially infects fibroblasts in UV-exposed skin during UV-mediated enhancement of infection 1wk post-UV

(A-C) Number of infected endothelial cells ($CD45^-CD31^+$) **(A)**, fibroblasts ($CD45^-Vimentin^+$) **(B)** and epithelial cells ($CD45^-EP\text{-}CAM^+$) **(C)**, measured by flow cytometry at 16hpi. Gating strategy used during analysis outline in Section 2.19.5. Numbers represent percent of indicated SFV6-mCHERRY$^+$ infected cell type of all live cells. Prior to infection, mice were either left unexposed or were exposed to an erythemal dose of UV on the skin on the upper side of the foot. All mice were then infected 1wk post-exposure at the same site with 10^3 PFU of SFV6-mCHERRY in the presence or absence of a mosquito bite. *(n = 4)*

Plots show the median value ± interquartile range. Data were analysed using Mann-Whitney test (*ns = not significant, *P < 0.05*).

4.8 Summary and conclusions

As introduced earlier, the inflammatory state at the skin early following a cutaneous wound switches to a largely anti-inflammatory, wound healing environment at later timepoints to facilitate tissue repair[361]. This involves

changes mediated by both leukocytes and CD45-ve cells, including fibroblasts, endothelial cells and epithelial cells. Therefore, it is likely that the cellular and molecular environment in the skin is extremely different at 1-week post-UV, compared to 24h post-UV. This led us to hypothesise that mice would be more susceptible to arbovirus infection at 1-week post-UV and that the mechanisms driving this are distinct from those which contribute to the enhanced arbovirus infection observed at 24h post-UV.

We first set out to characterise any changes to the skin's architecture between 1-3 weeks after an erythemal UV exposure, in the absence of virus, by examining skin histology and vascular permeability. We found that the layers of the skin are much thicker in mice exposed to UV 1-week or 2 weeks prior, compared to resting skin, before returning to normal thickness by 3 weeks post-exposure (Figure 4.1). This corroborates findings by other groups, which have shown that hyperplasia is clear by 1-week post-exposure, before beginning to resolve around 2 weeks post-UV in mice[232,240,360]. Hyperplasia is not only a hallmark of UV exposure in mice, but humans also[362,363] and involves the proliferation of keratinocytes and other cell types to better protect the skin from further UV exposures[232,343]. Keratinocyte proliferation in particular is also required to rebuild the epidermal layer[210].

Upon examination of the vascular permeability in UV-exposed skin at 1-week post-UV, we found that oedema was increased compared to rest, but also to an even higher level than mice exposed 24h prior, with no additional effect observed following the addition of a mosquito bite, a known inducer of permeability itself (Figure 4.2). This increased oedema is associated with an observed increase in virus RNA quantity at 1 week compared to infection at 24 hours post UV (Figure 4.3). During wound healing, macrophages produce a number of effector molecules, including VEGF, which act on endothelial cells to induce vascular permeability[364]. Although we did not examine VEGF expression in UV-exposed skin, it is likely that the mechanism driving vascular permeability is different at 1-week post-UV than 24h post-UV, which may explain the differing levels of permeability between the two timepoints. Regardless of the molecular driver, increased vascular permeability in the skin, like that observed at 1-week post-UV, can allow for more efficient entry of leukocytes, some of which may be

permissive to arbovirus infection and/or drive programs that increase cellular permissiveness to infection.

In addition to the quantitative measurements made based on the skin of mice exposed to UV 1-week prior, anecdotally, during skin collection we also noted the visual appearance of the UV-exposed skin to be flaky and peeling by this timepoint with the skin stretched tightly over the limb, causing restriction in the motility of the foot joint. Visible erythemal inflammation of the skin, readily observable at 24h post-UV, was no longer observed at 1 week. This observation is also indicative of the wound going through the healing process. Together, the changes to the skin of mice exposed to UV 1-week prior shown here indicate that the skin is undergoing wound-healing by 1-week post-UV and possesses features that may modulate susceptibility to virus infection.

Subsequently, we demonstrated that susceptibility to SFV infection is significantly higher in mice exposed to UV 1-week prior to infection, with increased quantities of virus in the skin and blood by 24hpi (Figure 4.3). Interestingly, mice are still more susceptible to infection when infected 2 weeks post-UV but this abates by 3-weeks post-UV (Figure 4.4). This mirrors the resolution of the burn wound by 3 weeks post-UV shown in Figure 4.1, suggesting that the processes taking place in the skin during wound healing at 1-week post-UV are linked to the increase in susceptibility observed in these mice at this timepoint.

Next, we investigated whether infection with a more medically relevant virus, ZIKV, is also enhanced 1-week post-UV exposure. While quantities of virus in the skin, spleen and blood of mice were the same between non-UV exposed mice and those exposed to an erythemal dose of UV 1-week prior, the UV exposed mice did experience a much more clinically severe course of infection (Figure 4.5).

We had to use the immunodeficient mouse model, *Ifnar-/-* in order to study ZIKV *in vivo*. However, the use of *Ifnar-/-* mice does bring with it some limitations which may explain the results observed here. In both groups, there were very low quantities of virus in the skin but high quantities in the spleen and blood,

and these were much higher than comparative experiments with SFV in WT mice. This suggests that the virus rapidly spread from the inoculation site in both groups. However, this was not enhanced at these sites with the addition of UV. The lack of difference between the two groups may be attributed to the extreme susceptibility of *Ifnar-/-* mice to virus infection, because they lack the capacity to respond to Type I IFN, the antiviral system[365]. This could negate any impact that UV exposure may have on an immunocompetent model at 1-week post-UV. However, as ZIKV does not cause clinical disease in WT mice, this cannot be studied. Nevertheless, the virus only caused clinical signs in mice which had been exposed to UV 1-week before. It is important to note that all mice were clinically well following the UV exposure and only deteriorated following virus infection, suggesting that it was not the UV exposure alone which was causing the illness. These results may indicate that UV exposure drives an increase in the spread of virus to the brain, as viral encephalitis is the main cause of pathology following ZIKV infection. However, during the planning of the experiment we chose not to collect the brain as we believed 24hpi would be too early for the virus to spread to the brain. Therefore, this experiment will need to be repeated and the brains examined for virus RNA to definitively conclude this.

The components of the immune system at the skin during wound healing are characterised as being anti-inflammatory, as resolution of the inflammatory response is critical for efficient repair and closure of the wound. Therefore, we considered whether suppression of the antiviral immune response in the skin at 1-week post-UV may explain the increase in susceptibility to infection observed at this stage. When we interrogated the expression of genes associated with the Type I IFN system, including IFN-β and several prototypic anti-viral ISGs, during SFV infection of mice exposed to UV 1-3 weeks prior, we found that there was a robust induction of these at timepoints where virus quantities also peak, in mice 1-week or 2 weeks post-exposure (Figure 4.6). In fact, this occurs to a much higher level than during SFV infection in non-UV exposed mice. This suggests that the Type I IFN is not suppressed in UV-exposed skin during arbovirus infection, however, it is not nonetheless powerful enough to overcome the impact of erythemal UV exposure on raising susceptibility to arbovirus infection.

As shown in Section 4.2 of this chapter, the skin possesses characteristics of wound healing at 1-week post-UV. This led us to consider whether related processes could be contributing to the enhanced susceptibility to virus infection observed at this timepoint. Proliferation of a range of cells, including fibroblasts, epithelial and endothelial cells is essential for rebuilding damaged cutaneous tissue[210]. As SFV is also considered an oncolytic virus, with a characteristic ability to preferentially replicate within proliferating cells, we decided it would be insightful to examine the presence of proliferating cells in the skin of UV-exposed mice at 1-week post-UV. Consequently, we found that there are more proliferating cells in the skin of mice exposed to UV 1-week prior (Figure 4.7). Additionally, there are more infected, proliferating cells than infected, non-proliferating cells present in the skin of these mice during infection, suggesting that SFV targets proliferating cells during UV-mediated enhancement of infection at 1-week post-UV (Figure 4.8). Importantly, this was not found to be the case, in the previous chapter, during infection at 24h post-UV, despite there being more proliferating cells in those mice also (Section 3.4). This suggests that SFV utilises proliferating cells for replication at 1-week post-UV and, since there are more of them, this could be contributing to enhanced virus infection in UV-exposed skin at this timepoint. The reason why SFV infects proliferating cells at 1-week post-UV but not at 24h post-UV is yet to be explained. However, this could be due to the phenotype of the proliferating cell types. This may mean that the cell types which are highly proliferative during wound-healing, fibroblasts, endothelial cells and keratinocytes, may be targeted by the virus. Whereas, leukocytes, which are generally terminally differentiated once they reach the skin, may not be targeted by the virus at 1-week post-UV[208]. However, it is worth noting that macrophages have been shown to proliferate locally in the tissue, rather than migrating from the blood during Th2-associated inflammatory responses[366]. Therefore, it is also possible that some of these proliferating cells are macrophages. However, based on our results alone we cannot definitively conclude the cell identities of the proliferating cells. This could be elucidated by combining the EdU assay, used to identify proliferating cells, with a multi-parameter flow cytometry panel to stain for cell markers to allow for the identification of proliferating cell types.

We also sought to identify changes to the frequency of key cell types present in the skin at 1-week post-UV. Initially, we identified an increase in the expression of both CXCL2 and CCL2, which attract neutrophils and monocytes respectively (Figure 4.9). However, this did not necessarily correspond to an increase in the numbers of these cells present in the skin. In fact, while there were significantly more neutrophils present in UV-exposed mice at 16hpi, compared to infected, non-UV exposed mice, there was no change in the number of monocytes (Figure 4.10). While neutrophils can contribute to inflammation in the skin, through the production of cytokines, they are not permissive to SFV infection. Therefore, they can't act as cellular targets for SFV replication or as a reservoir for the virus, and so won't be directly responsible for the increase in virus replication observed in the skin of UV-exposed mice at 1-week post-UV. Nevertheless, they can contribute to altered immunity at the skin in an indirect way.

Although neutrophils are commonly associated with the rapid response to a skin barrier breach to clear infection and debris, they are also recruited in the skin at later timepoints during wound healing[367]. In UV-exposed skin specifically, they have been found at 8-days post-exposure, which supports our findings here that they are also present during infection in UV-exposed skin at 1-week post-UV. [240]. At this stage of wound healing, they can contribute to the resolution of inflammation and are a vital component of the process, with *Cxcr2-/-* mice, which are unable to recruit neutrophils to the injury site, experiencing impaired cutaneous wound healing [368]. Of great relevance here is the role neutrophils play in producing chemokines to recruit monocytes and macrophages to the damaged tissue, to coordinate the wound healing process[369]. This suggests that the increase in neutrophils observed in the skin of mice during infection 1-week post-UV may lead to a corresponding increase in the number of virus-permissive macrophages, despite finding no change in the number of monocytes.

As introduced earlier, macrophages are the master coordinators of the wound healing response. As such, macrophages are one of the most abundant cell types present in wounded skin[370]. These cells are also susceptible to SFV infection, making their abundance in the skin during wound healing a potential

contributory factor to enhanced susceptibility to arbovirus infection. However, their presence during the wound-healing phase of an erythemal UV burn at 1-week post-UV had not been investigated. Interestingly, when we interrogated macrophage numbers in the skin, UV increases the number of macrophages by 1-week post-UV, in the absence of virus infection (Figure 4.11). This corresponds with findings from Cela *et al.,* who found large granulomas filled with macrophages in skin histology of mice by 8 days post-UV[240]. However, when we looked at macrophage numbers in infected, UV-exposed mice, this population was ablated back to resting levels (Figure 4.11). This could represent a reduction in the number of macrophages due to infection, as SFV does infect macrophages. Alternatively, these macrophages could have changed their cell marker expression in response to virus infection. Similar to our findings here, a reduction in Lyve1+ macrophages following SFV infection in mosquito-bitten skin has previously been shown[289]. However, whether this is due to a change in marker expression or due to lytic infection remains to be seen.

DCs are the primary antigen presenting cell in the skin and, therefore, are mainly responsible for bridging the innate and adaptive response during wound healing and infection[371]. Interestingly though, we found no change in the number of DCs in the skin 1 week after an erythemal UV exposure compared to resting skin, either in the absence or presence of virus (Figure 4.11). This might be expected, as tissue residency of these cells are highly dynamic e.g. with activated skin DC migrating to lymph nodes, while inflammatory chemokine expression attracts new DC progenitors.

The increased number of macrophages shown in Figure 4.11 may explain the increase in proliferating cells shown in Figure 4.7, as macrophages produce growth factors that drive proliferation of cells, including keratinocytes, endothelial cells and epithelial cells, during wound healing[206]. SFV has also been shown to preferentially infect proliferating cell types, and so we sought to interrogate their presence in the skin of UV-exposed mice. There were more endothelial cells in the skin by 1-week post-UV (Figure 4.12). Angiogenesis, the formation of new blood vessels, is required to fully repair damaged tissue[216]. For this to happen, endothelial cells must proliferate to form new vessels[372]. Therefore, the expansion of this population in UV-exposed skin observed here

is expected. However, this population was reduced when UV-exposed mice were infected with SFV, similar to what was observed with the macrophage population following infection in UV-exposed skin. Again, this could be due to endothelial cells being infected with virus, leading to cell death.

Unexpectedly, there was no change in the number of epithelial cells or fibroblasts in the skin of mice exposed to UV 1-week prior, regardless of virus infection (Figure 4.12). Expansion of both of these cell populations is essential for effective wound healing as these cells are required to rebuild the damaged tissue[209,373]. We would expect the number of keratinocytes, a type of epithelial cell, in particular to have increased in UV-exposed mice, as the histology images taken from these mice, shown in Figure 4.1, had shown massive expansion of the tissue, which is driven by keratinocyte proliferation. However, this unexpected finding could be due to there being more CD45+ cells present in the skin of UV-exposed mice, skewing the proportion of these CD45- cell populations to appear smaller in comparison. Although the live cell count was consistent across groups and so this should not have affected the result significantly as proportions were calculated based on the total live cells in each sample. However, it is possible that some cells have been lost during the digestion process used to isolate cells from skin for flow cytometry.

When we explored expression of the key wound healing-associated molecule ARG1, we found that levels of ARG1 in the skin gradually increase over time following an erythemal UV burn, and which reached statistical significance at 1-week post-UV (Figure 4.13). We found that expression of ARG1 in UV-exposed skin returns to basal levels by 2-3 weeks post-UV, tracking with the resolution of the burn by this timepoint shown in skin histology by us, in Figure 4.1, and by others[232]. ARG1 is traditionally associated with M2 macrophages, prevalent in the skin during tissue repair, and has long been a marker of this population[352]. At timepoints earlier than this post-UV, macrophages are likely to be skewed towards the pro-inflammatory M1 phenotype, which express inducible Nitric Oxide Synthase (iNOS), the antagonist of ARG1, rather than ARG1[374]. The trending increase in expression observed between 48-72h post-UV in our model likely tracks with the phenotype switch of these macrophages, signalling that the skin environment is progressing away from the acute inflammatory phase post-

burn into the wound-healing phase by 1-week post-UV[375]. ARG1 kickstarts several downstream processes which culminate in collagen production and cellular proliferation, two vital processes to repair damaged tissue[206].

It has been shown that M2 macrophages are not the only cell type to express ARG1 during tissue repair; fibroblasts also express ARG1 during wound healing[353]. Correspondingly, when we interrogated expression of ARG1 in CD45- cells, containing fibroblasts, and CD45+ cells, containing macrophages, taken from skin exposed to UV 1-week prior, we found that both cell populations significantly upregulated expression of ARG1 compared to rest by 1-week post-UV exposure (Figure 4.13). This further confirms that the skin is undergoing wound healing at this timepoint post-UV and suggests that some fibroblasts may have developed the 'macrophage-like' wound healing phenotype by 1-week post-UV.

Interestingly, it has been argued that polarisation of macrophages towards an M2 phenotype may be of harm to the host during viral infection. Whereas M1 macrophages are highly phagocytic and produce anti-viral type I IFNs, the anti-inflammatory state driven by the M2 macrophage may be of great benefit to the virus in terms of avoiding immune clearance. In fact, some viruses, including HCMV and SARS-CoV-2, actively drive or are associated with M2 polarisation[376,377]. Additionally, M2 macrophages have been shown to be ineffective in controlling respiratory syncytial virus (RSV) *in vitro*, while M1 macrophages were able to reduce quantities of the virus [378]. Although, deletion of ARG1 in macrophages and neutrophils in mice led to enhanced clearance of the two arthritogenic arboviruses CHIKV and RRV in the joints of mice, the tissues where these viruses cause pathology[379]. Furthermore, the role of M2 macrophages, or ARG1 expression more generally, during arbovirus infection in the skin remains to be elucidated. Therefore, it is not clear what affect the increased expression of ARG1, be it by macrophages or fibroblasts, in the skin of UV-exposed mice at 1-week post-burn may have on the increased susceptibility to arbovirus infection observed in our study.

Based on our earlier observations, from Figure 4.11 and 4.12, that macrophage and endothelial cell numbers were reduced following SFV infection at UV-

exposed skin, we considered whether this drop could be due to these cell types being infected by virus. Therefore, we investigated whether either CD45- cells, which include endothelial cells, or CD45+ cells, which include macrophages, were disproportionately infected by virus during UV-mediated enhancement of infection at 1-week post-UV. Although, we found that the quantities of virus were equal between the two populations (Figure 4.14). Alternatively, if both macrophages and fibroblasts are infected, this would lead to equal virus burden between CD45+ and CD45- cells, as observed here. Additionally, we ruled out the idea that UV was simply making cells more permissive to infection on a per cell basis, by showing that cells from UV-exposed mice were not more susceptible to arbovirus infection when infected *in vitro* (Figure 4.15). Together, this led us to hypothesise that the increase in susceptibility to arbovirus infection in mice exposed to UV 1 week prior, may be partially explained by the presence higher numbers of virus-permissive cells in UV-exposed skin during infection, due to the ongoing wound-healing process.

Therefore, we concluded our investigations into the mechanism driving enhancement of infection at this timepoint by examining whether there were any differences in the numbers of specific cell populations infected with SFV, in UV-exposed mice compared to non-exposed mice. While we were most interested in macrophages and endothelial cells, due to our earlier findings that these populations dropped in number following SFV infection of UV-exposed skin, we explored several other cell populations, both within the CD45+ and CD45- fractions. However, there was no change in the number of infected monocytes, macrophages, DCs, endothelial cells or epithelial cells by 16hpi in the skin of mice exposed to UV 1-week prior to infection, compared to infected, non-exposed mice (Figure 4.16 and 4.17). Interestingly though, there were more infected fibroblasts in UV-exposed skin during infection, compared to infected, non-exposed mice. While these results were not as we had expected based on the findings from Figures 4.11 and 4.12, it is possible that we missed the timepoint at which macrophages and endothelial cells are infected. These cells may have been infected earlier post-infection and have died by 16hpi, explaining the reduction observed in their numbers following infection. Further studies at different time points could therefore be informative, although due to

effort required to undertake such experiments, were outside the scope of this study.

Nevertheless, the presence of more infected fibroblasts in the UV-exposed mice suggests that infection of these could be contributing to the enhanced infection phenotype observed at 1-week post-UV. Additionally, fibroblasts are one of the key proliferative cell types in the skin during tissue repair. Therefore, it may be that the proliferative cells that are targeted by the virus, as shown in Figure 4.8, are fibroblasts and that this targeting of proliferating cells by SFV during the healing of the UV burn is contributing to the higher quantities of virus observed in these mice. However, further investigation to phenotype the infected, proliferating cells must be done to determine whether this is true.

Overall, this chapter has shown that mice exposed to an erythemal dose of UV 1-week prior to infection are much more susceptible to arbovirus infection. Although there is limited existing knowledge around the kinetics of healing of a UV burn, we have shown that UV-exposed skin at this timepoint is characterised by several features of wound healing, including increased cell proliferation and ARG1 expression. Furthermore, we have found evidence that SFV benefits from this wound healing environment, by infecting proliferating cells and fibroblasts.

Chapter 5: Repeated sub-erythemal UV exposure *in vivo* is sufficient to increase host susceptibility to SFV infection

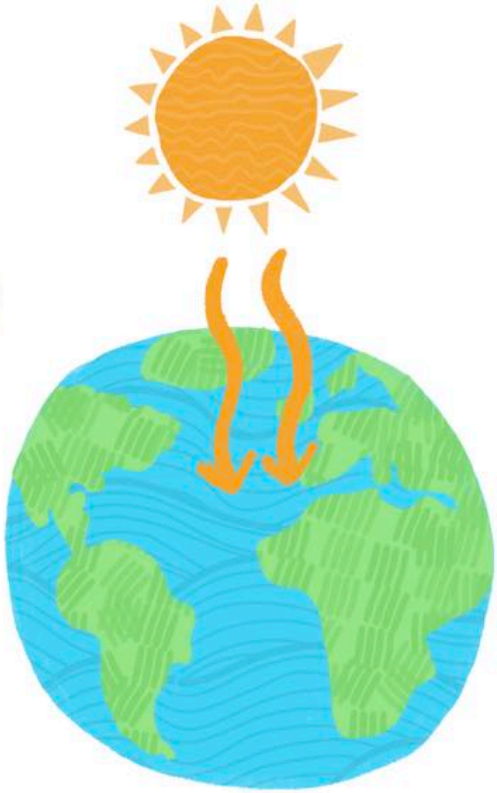

5.1 Introduction

The first two results chapters of this thesis have explored the impact of a single erythemal UV exposure on host susceptibility to arbovirus infection. However, people are exposed to varying quantities of UV from the environment. This most commonly takes the form of regular repeated exposures to lower quantities of UV. Typically, this occurs as individuals carry out general daily tasks outdoors. This type of exposure leads to photoadaptation, including thickened skin and tanning, or melanisation, of the skin[220].

Exposure to UV purposely, either outdoors or via tanning beds, with the aim of getting a suntan is a common practice in many parts of the world, particularly in Western nations[380]. Despite common misconceptions, exposure of the skin to tanning doses of UV is not safe, as the cellular processes that result in the tanned appearance of the skin, or melanisation, are driven by UV-induced DNA and cell damage[220]. As such, recreational tanning still puts an individual at higher risk of UV-associated conditions, such as skin cancer[381].

The extent of UV exposure that an individual experiences is highly variable and depends on a number of factors. For one, this can differ based on the region of the world a person lives in and the daily activities they partake in[224,247]. For example, an individual who works outdoors in Australia, a country with a high UV index, is exposed to more UV on average than an individual who works indoors in England, where the UV index is much lower[224]. Furthermore, individual UV exposure is estimated to increase by 30% when an individual is on holiday in a sunny climate[382]. A person's ability to tan following a UV exposure also largely depends on their skin tone, with the palest tones being more likely to burn than tan[220,383]. Thus, the level of exposure that a specific individual experiences is highly variable, as is their response to UV exposure, which is largely driven by genetics. Together, this makes exposure to UV a key environmental variable that may have the potential to assist in risk stratification of patients infected with mosquito-borne viruses. As such, it is key that we better define how differing intensities of UV exposure alters host susceptibility to virus.

While the impact of higher dose UV exposures on immunity at the skin have been studied, there is relatively little understanding about the impact that repeated, sub-erythemal doses of UV have in this capacity. However, it has been shown that the impact of a single, erythemal UV exposure, of the kind we investigated in Chapters 3 and 4, and repeated, low level UV exposures on immune responses, particularly the innate component, are very different[240]. Repeated low doses of UV have limited impact on upregulating the expression of pro-inflammatory cytokines or inducing myeloid cell recruitment. Instead, the most obvious cutaneous changes include a thickening of the epithelium and an upregulation of antimicrobial peptides. Furthermore, exposure of mice to a sub-erythemal UV dose prior to infection with the *Leishmania* parasite has been shown to alter innate immune components during subsequent infection, including an increase in mast cells[384]. However, whether these changes following sub-erythemal UV exposure of skin impacts *Leishmania* infection outcomes remains to be seen.

5.1.1 Hypothesis and aims

In summary, due to the large variability in individual exposure to UV, we thought it vital to investigate whether host susceptibility to arbovirus infection is also altered following sub-erythemal dose(s) of UV. Based on our observed findings that type I IFNs are induced over time in UV exposed skin and the findings of Cela *et al.* that suggests skin adopts a photoadaptive state, lacking prototypic pro-inflammatory signature (e.g. myeloid cell recruitment), following repeated, sub-erythemal UV exposures[240], we hypothesised that susceptibility to arbovirus infection would not be enhanced in the skin following this type of exposure.

Therefore, this short chapter aims to:

1) **Determine whether repeated, sub-erythemal doses of UV are sufficient for enhancing subsequent SFV infection**
2) **Characterise the inflammatory profile of the skin during infection in skin previously exposed to repeated, sub-erythemal doses of UV**
3) **Determine the lower limits of the UV dose required for UV-mediated enhancement of infection**

5.2 Exposure of skin to repeated, sub-erythemal doses of UV drives epidermal thickening but does not induce oedema

To determine whether a lower, sub-erythemal dose of UV exposure has an impact on arbovirus infection outcome, we adopted a previously developed *in vivo* model[240], in which the skin on the upper side of the left foot of C57BL/6 mice were exposed to a sub-erythemal dose of UV, measuring 20mJ/cm^2, three times every 48-hours, before being culled or infected 24h after the final dose. Each of these doses of UVR was equivalent to 0.1 MEDs. This regimen of exposures models a tanning exposure to UV in humans, rather than sunburn we had modelled in previous chapters.

Before investigating whether this type of UV exposure impacts host susceptibility to arbovirus infection, we sought to characterise any changes to the structure of the skin following these exposures, as we had done previously 24h and 1-week after exposure to an erythemal dose of UV. We hypothesised that repeated exposure to sub-erythemal doses of UV would not have as extreme effects on the structure of the skin as an erythemal dose had been shown to have in previous chapters. To investigate this, we examined skin histology taken from these mice at the end of the treatment regime, 24h after the final dose. The UV-exposed skin shows some evidence of an inflammatory cell infiltrate in the dermis (indicated by the arrow), compared to the unexposed skin (Figure 5.1A). Furthermore, the epidermis appears to be thicker following UV-exposure. This observation was confirmed via measurements of the skin layers using the imaging software QuPath (Figure 5.1B). This analysis also showed that the subcutaneous fatty layer was considerably thinner in the UV-exposed mice. These results indicated that repeated, sub-erythemal exposures of the skin to UV does drive epidermal thickening and an infiltrate of cells, although smaller than that observed 24h after an erythemal exposure.

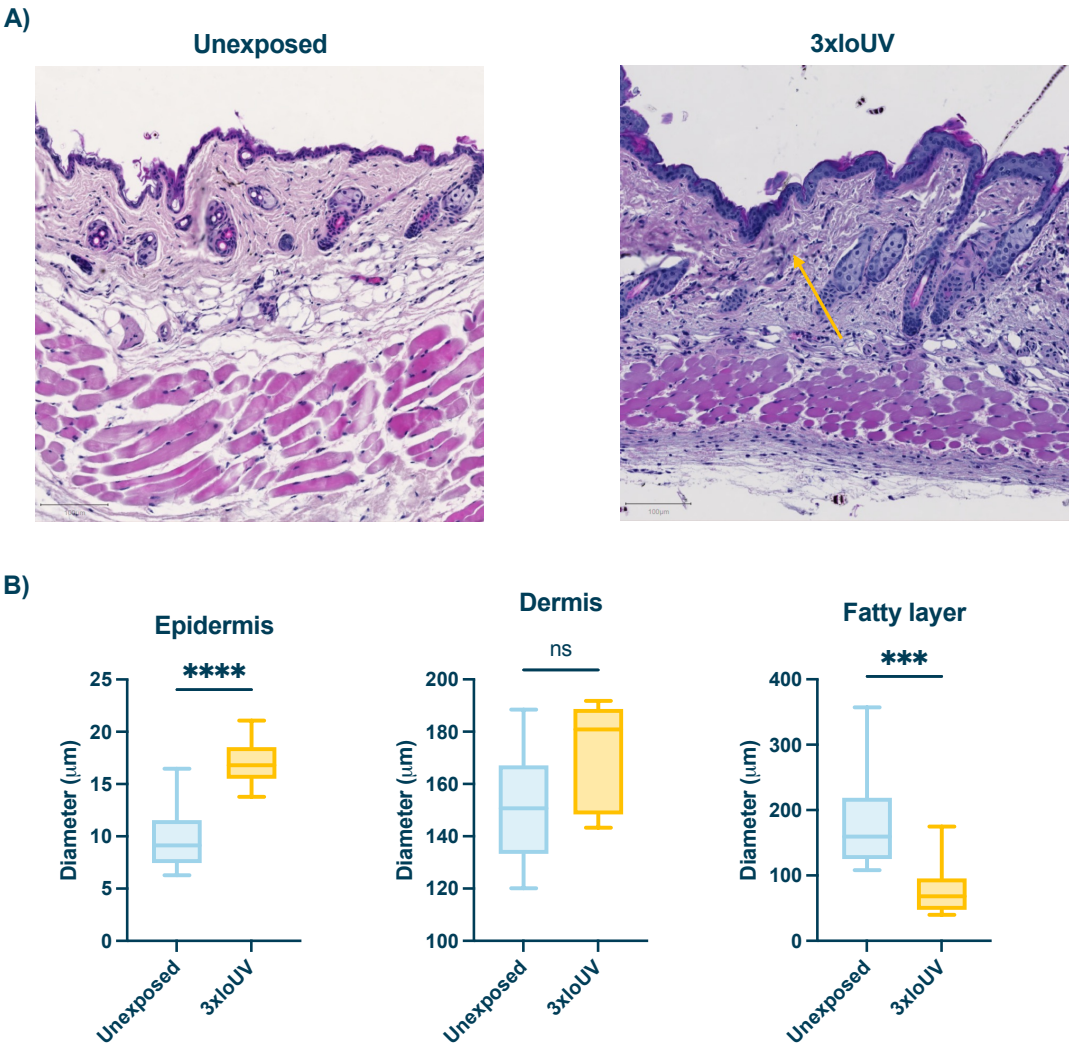

Figure 5.1 | Repeated sub-erythemal UV exposure causes epidermal thickening and cellular infiltrate

(A) Histology of resting skin from dorsal region of C57BL/6 mice or skin exposed to a sub-erythemal UV dose to dorsal region three times at intervals of 48 hours. Skin collected 24h after final exposure. Sections stained with H&E. Yellow arrow indicates cell infiltrate. Images shown are representative of the group. Scalebars measure 100 µm. Slides scanned at 20x magnification.

(B) Measurements of epidermis, dermis and fatty layer thickness were taken from 10 areas per condition using QuPath (n = 3). Plots show the median value ± interquartile range. Data were analysed using Mann-Whitney test (*ns = not significant, ***P < 0.001, ****P < 0.0001).*

As discussed in earlier chapters, induction of vascular permeability is a key mechanism by which arbovirus infection is enhanced by a mosquito bite[126,134]. The resultant increase in oedema associated with vascular permeability can be

measured and can be used to indicate whether a factor has the potential to modulate susceptibility to arbovirus infection. As before, we used Evan's blue dye to quantify the level of oedema in the skin and measured this in the skin of resting mice or following repeated, sub-erythemal UV exposures alone or with the addition of a mosquito bite at the end of the treatment regime. Interestingly, there was no difference in oedema at the skin in UV-exposed mice, compared to resting mice (Figure 5.2). However, when UV-exposed mice were also exposed to mosquito biting, there was a significant increase in levels of oedema compared to both resting mice and non-bitten, UV-exposed mice. Therefore, since oedema was only increased in mice exposed to a mosquito bite, as well as UV, it is likely that this is being driven by the bite, a known inducer of vascular permeability.

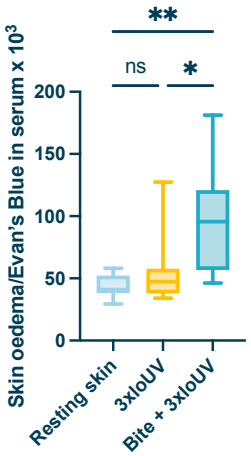

Figure 5.2 | Vascular permeability is only induced in skin following repeated, sub-erythemal UV exposure, when exposed skin is also bitten by *Aedes aegypti*

Mice were exposed to a sub-erythemal UV dose to upper left foot three times at intervals of 48 hours. 24h after the final UV exposure, mice were injected s.c. with Evans blue to scruff of neck, distant from the UV-exposed site. Mice were then exposed to mosquito bites at the UV-exposed site. The extent of oedema was assessed by quantification of Evan's blue dye leakage into skin at 3 h post-biting via colorimetric assay (n = 8).

Plots show the median value ± interquartile range. Data were analysed using Kruskal-Wallis test with Dunn's multiple comparison test (*$P < 0.05$, **$P < 0.01$).

5.3 Repeated, sub-erythemal doses of UV only enhanced subsequent arbovirus infection in combination with *Aedes aegypti* bite

Since repeated sub-erythemal UV exposure did not induce extreme structural changes or oedema in skin, we hypothesised that the outcome of arbovirus infection in these mice would not be significantly altered. To examine this, we exposed mice to a sub-erythemal dose of UV every 48 hours, three times, and then, 24h after the final exposure, infected mice at the UV-exposed site with 10^4 PFU of SFV4 at mosquito bitten skin. To determine whether infection was enhanced in these mice, we collected skin, from the inoculation site, and serum at 24hpi. To detect the presence of SFV in the skin, we used qPCR to quantify expression of the virus gene, E1. There was significantly more virus RNA by 24hpi in the skin of mice exposed to repeated, sub-erythemal doses of UV prior to infection and exposed to mosquito bites during infection, compared to unexposed mice infected alongside a mosquito bite alone (Figure 5.3A). A plaque assay was used to quantify the quantities of infectious virus in the serum by 24hpi. Viremia followed the same trend as had been observed in the skin; UV-exposed mice, infected alongside a bite, had significantly higher quantities of infectious virus in the serum by 24hpi than non-UV exposed mice, which were also exposed to biting mosquitos (Figure 5.3B). This data disproved our hypothesis, showing that exposing mice to repeated, sub-erythemal doses of UV prior to infection causes an increase in host susceptibility to arbovirus infection, in the presence of a mosquito bite.

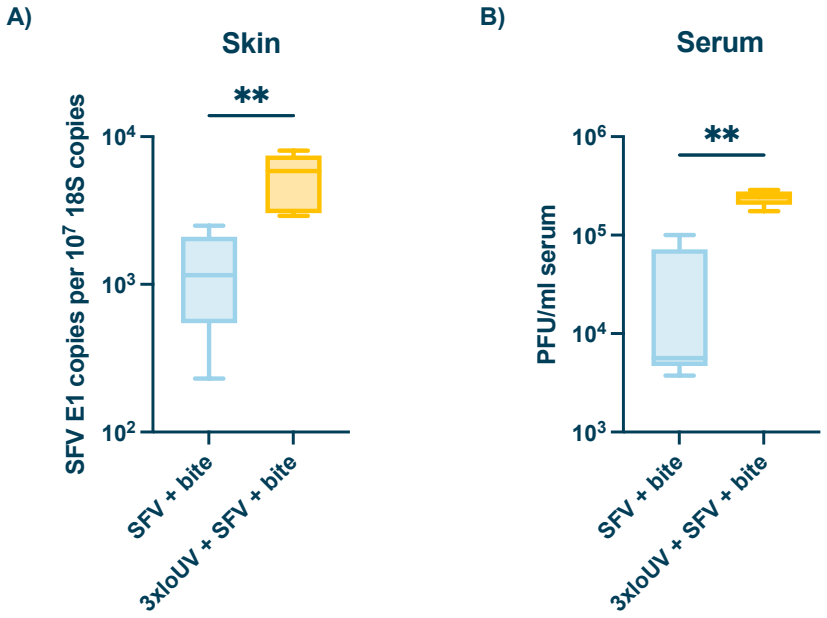

Figure 5.3 | Repeated sub-erythemal UV exposure results in enhancement of arbovirus infection, in combination with *Aedes aegypti* bite

(A-B) SFV RNA (E1 gene) copy number in inoculation site (skin) **(A)** and viral titres in the serum **(B)** 24hpi. Prior to infection, mice were either left unexposed or had the skin of their left upper foot exposed to a sub-erythemal UV dose three times at intervals of 48 hours before being infected with 10^4 PFU of SFV4 in the presence of a mosquito bite. ($n \geq 6$)

Gene expression measured by qPCR. Plots show the median value ± interquartile range. Data were analysed using Mann-Whitney test (*$^{**}P < 0.01$*).

In our previous experiments looking at the impact of erythemal UV on arbovirus infection at 24h and 1-week post-UV, we had found that erythemal UV exposure was able to enhance arbovirus infection in the presence or absence of a mosquito bite. However, the mosquito bite is a known enhancer of arbovirus infection. Additionally, in our last experiment which found that infection is also enhanced following sub-erythemal UV exposures, both groups of mice had been exposed to mosquito bites, with the only variable between the groups being the addition of repeated, sub-erythemal UV exposures. Therefore, we wanted to determine whether susceptibility to arbovirus infection could be modulated by this low dose UV regime alone. To investigate this, mice were exposed to repeated, sub-erythemal doses of UV, as before, and then infected 48h after the final exposure with 10^4 PFU of SFV4 at the exposed site. However, this time we did not include mosquito bites in the infection step and so could determine whether repeated, sub-erythemal UV exposure is able to

enhance infection by itself. Surprisingly, when we examined quantities of virus RNA in the skin by 24hpi, we found that the UV-exposed mice had significantly less virus present, compared to infected, unexposed mice (Figure 5.4A). There was no difference in the quantities of virus RNA in the spleen between the two groups, which both exhibited very low quantities of virus RNA in this organ (Figure 5.4B). Most importantly in terms of clinical disease, the quantity of infectious virus in the serum by 24hpi was not significantly different, as determined by plaque assay (Figure 5.4C). Together with our studies above, this demonstrates that repeated, sub-erythemal UV exposures only enhance host susceptibility to arbovirus infection when the infection takes place alongside a mosquito bite.

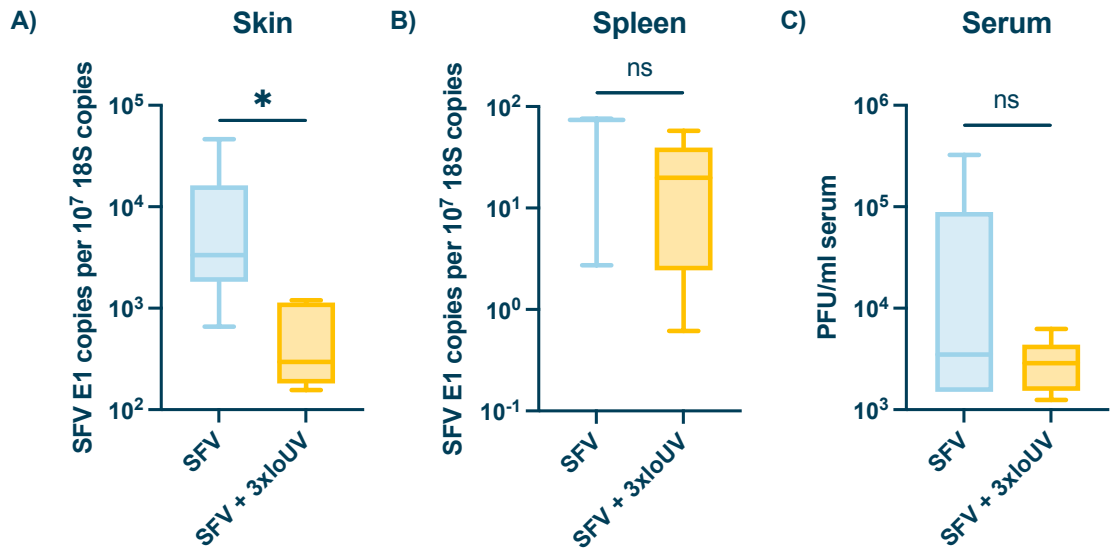

Figure 5.4 | *Aedes aegypti* bite required for increased susceptibility to arbovirus infection in mice exposed to repeated sub-erythemal UV prior to infection

(A-C) SFV RNA (E1 gene) copy number in inoculation site (skin) **(A)** or spleen **(B)** and viral titres in the serum **(C)** 24hpi. Prior to infection, mice were either left unexposed or had the skin of their left upper foot exposed to a sub-erythemal UV dose three times at intervals of 48 hours before being infected with 10^4 PFU of SFV4 24h after the final exposure. ($n \geq 6$)

Gene expression measured by qPCR. Plots show the median value ± interquartile range. Data were analysed using Mann-Whitney test (**$P < 0.01$).

5.4 Exposure of skin to repeated, low doses of UV drives monocyte recruitment and ISG induction during arbovirus infection

Next, we wanted to explore the molecular processes that may be driving the enhanced susceptibility to arbovirus infection observed in mice exposed to repeated, sub-erythemal UV exposures prior to infection. To investigate the mechanism, all experiments included mosquito biting in the protocol, to ensure we were investigating the enhanced phenotype following repeated, sub-erythemal UV exposures, as observed in Figure 5.3.

Initially, we set out to characterise the Type I IFN response in these mice, to determine whether suppression of this system may be involved. We used qPCR to assess expression of the Type I IFN, IFN-β, and several prototypic ISGs in the skin of infected mice, during enhancement of infection at 24hpi. Levels of IFN-β in the skin during infection were significantly higher in mice exposed to repeated, sub-erythemal UV exposures prior to infection, compared to unexposed mice (Figure 5.5A). Correspondingly, this led to an increase in expression of the ISGs IFIT1 and CXCL10, and a trending increase in expression of two others, ISG15 and RSAD2 (Figure 5.5B). Therefore, the Type I IFN system appears to be effectively induced during infection in these mice and is not suppressed. However, despite the presence of this antiviral response, mice are still more susceptible to SFV infection.

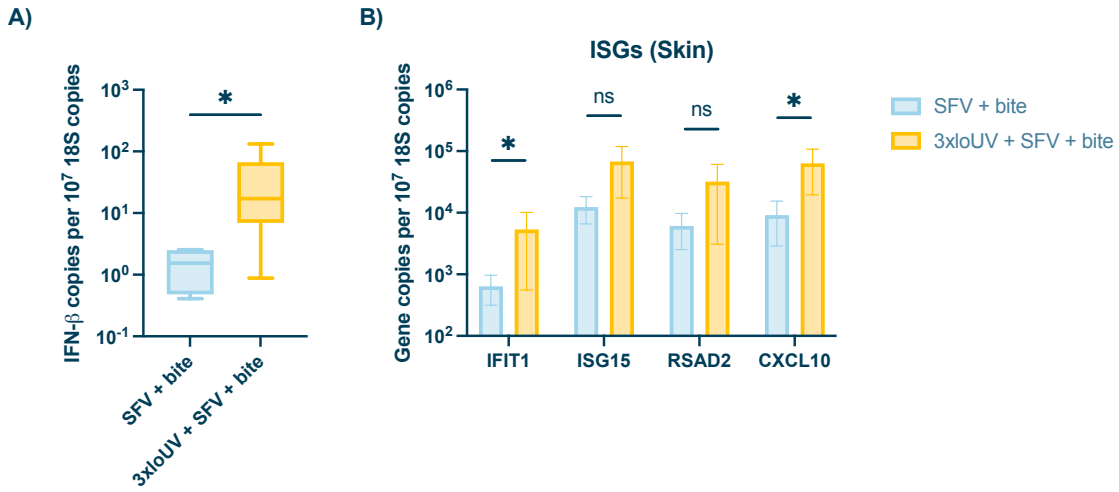

Figure 5.5 | Expression of IFN-β and ISGs induced during infection of mice exposed to repeated sub-erythemal doses of UV

(A-B) IFN-β **(A)** or ISG **(C)** gene expression in inoculation site (skin) 24hpi. Prior to infection, mice were either left unexposed or had the skin of their left upper foot exposed to a sub-erythemal UV dose three times at intervals of 48 hours. Mice were infected with 10^4 PFU of SFV4 in the presence of a mosquito bite 24 hours after the final UV exposure. Gene expression was measured in the skin by qPCR. (*n* = 6)
Plots show the median value ± interquartile range. Data were analysed using Mann-Whitney test **(***ns = not significant, *P < 0.05*).

We had put forward, in Chapter 3, that recruitment of myeloid cells in response to an erythemal UV exposure contribute to UV-mediated enhancement of infection by 24h post-UV. Therefore, it was important to investigate whether neutrophil and/or monocyte numbers change following repeated, sub-erythemal UV exposures as well. We had shown in Figure 5.2 that oedema was increased in mice exposed to repeated, sub-erythemal UV exposures, together with mosquito bites, and increased vascular permeability facilitates the entry of myeloid cells to the skin[126]. Therefore, we hypothesised that there may also be an increase in myeloid cells in the skin of these mice as well. To begin with, we quantified the expression of the two main chemokines which attract myeloid cells to the skin; CXCL2 which is the chemoattractant for neutrophils and CCL2 which attracts monocytes. However, there was no significant difference in the expression of either of these by 24hpi in the skin of mice exposed to repeated, sub-erythemal doses of UV prior to infection, compared to unexposed mice (Figure 5.6A). Nevertheless, increased expression of these chemokines could have occurred earlier than the timepoint we looked at. Consequently, we still investigated the numbers of neutrophils and monocytes in the skin by 16hpi using flow cytometry (Figure 5.6B). Interestingly, there was no significant difference in the number of neutrophils between UV-exposed mice and unexposed mice by this timepoint (Figure 5.6C). However, there were significantly more monocytes in the skin of UV-exposed mice by 16hpi compared to unexposed mice (Figure 5.6D). Therefore, while there was no change in the number of neutrophils, mice which had been exposed to multiple, sub-erythemal doses of UV prior to infection had more monocytes in the skin during infection, and as these cells are virus-permissive, this could be contributing to the enhanced infection observed in these mice.

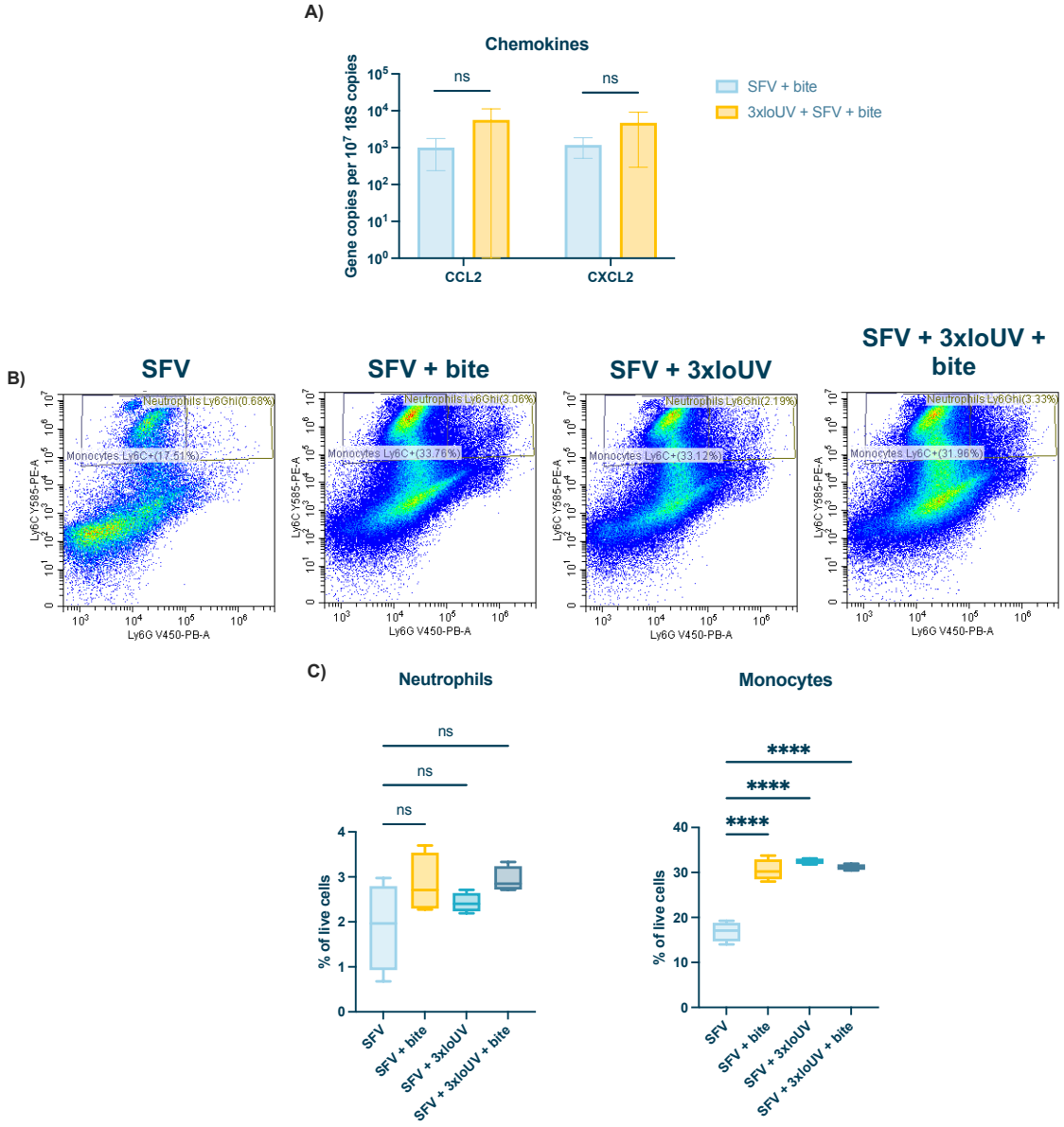

Figure 5.6 | Repeated sub-erythemal UV exposure does not change expression of myeloid cell chemoattractants but does increase recruitment of monocytes

(A) Chemokine gene expression in inoculation site (skin) 24hpi. **(B)** Neutrophil ($CD45^+CD11b^+Ly6G^{hi}$) and monocyte ($CD45^+CD11b^+Ly6C^+$) migration to skin in these mice, measured by flow cytometry at 16hpi. **(C)** Numbers represent percent of $Ly6C^+$ or $Ly6G^{hi}$ cells of all live cells. Prior to infection, mice were either left unexposed or had the skin of their left upper foot exposed to a sub-erythemal UV dose three times at intervals of 48 hours. Mice were infected with 10^4 PFU of SFV4 in the presence of a mosquito bite 24 hours after the final UV exposure. (*n* = 4-6).

Gene expression measured by qPCR. Plots show the median value ± interquartile range. Data were analysed using Mann-Whitney test **(A)** or Kruskal-Wallis test with Dunn's multiple comparison test **(C)** (*ns = not significant, ****P < 0.0001*).

Earlier in this thesis, we had found that there are more proliferating cells in the skin by 1-week post-erythemal UV and that SFV preferentially infects these cells, which likely contributes to UV-mediated enhancement of infection at this timepoint. Therefore, it was important to determine whether there is any change to cellular proliferation in the skin of mice exposed to repeated, sub-erythemal UV exposures to see if this exposure regimen also drives cellular proliferation. We used the fluorescently tagged DNA binding agent EdU to detect and count proliferating cells in these mice, using flow cytometry. Although there was no significant difference in the number of proliferating cells in the skin of UV-exposed mice, compared to bite-alone mice or resting mice, there was a clear trending increase in EdU+ cells (Figure 5.7). Therefore, exposure of the skin to multiple, sub-erythemal doses of UV appears to drive proliferation of cells in the skin.

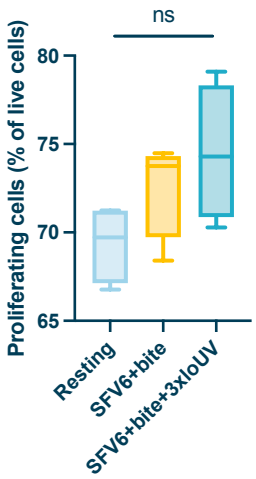

Figure 5.7 | Proliferation of cells does not change in skin exposed to repeated sub-erythemal doses of UV

EdU+ cells in the skin as a percentage of total live cells. Prior to infection, mice were either left unexposed or were exposed to a sub-erythemal UV dose three times at intervals of 48 hours. All mice were then infected 24h after the final exposure at the same site with 10^3 PFU of SFV6-mCHERRY in the presence of a mosquito bite. Skin from the exposed site was collected 24h post-exposure and digested to isolate single cells. Cells were incubated with EdU, a thymidine nucleoside analogue, for 2 hours. EdU+ cells were then tagged with a fluorophore using Click-IT chemistry so that proliferating cells could be identified using flow cytometry. (n = 4)

Plots show the median value ± interquartile range. Data were analysed using Kruskal-Wallis test with Dunn's multiple comparison test (*ns = not significant).*

As there was a trending increase in proliferating cells in the skin of mice exposed to repeated, sub-erythemal doses of UV, SFV could be targeting the population of proliferating cells that are present at this timepoint and contributing to enhancement of infection in this way. Therefore, it was important to assess whether there were more infected, proliferating cells in the skin of mice exposed to multiple, sub-erythemal doses of UV prior to infection. To do this, we infected UV-exposed mice with a strain of SFV, mCHERRY-SFV6, which encodes a fluorescent protein and so can be detected using flow cytometry. This allowed us to identify cells that were proliferating and whether they express virus encoded gene products. First, we confirmed that this strain of SFV is also enhanced by repeated, sub-erythemal UV exposures. These mice did have significantly higher quantities of virus RNA in the skin compared to non-exposed mice (Figure 5.8A). When we counted the number of infected, proliferating cells, there was no difference in the number of these cells present in the skin of mice exposed to repeated, sub-erythemal doses of UV prior to infection and unexposed mice (Figure 5.8B). Furthermore, there is no change in the number of infected, non-proliferating cells between UV-exposed and unexposed mice (Figure 5.8C). To confirm that SFV does not preferentially infect proliferating cells in this model, we calculated the ratio of infected, proliferating cells to infected, non-proliferating cells. As expected, we found that the ratio was less than 1 (Figure 5.8D). Together, this data suggests that SFV does not preferentially infect proliferating cells during UV-mediated enhancement of infection in mice exposed to multiple, sub-erythemal doses of UV prior to infection.

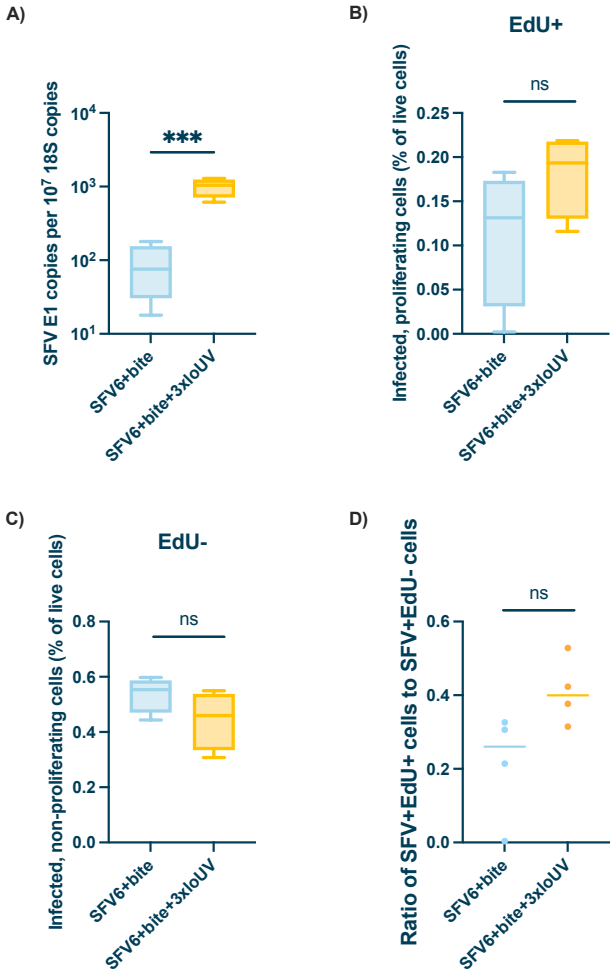

Figure 5.8 | SFV does not preferentially infect proliferating cells during UV-mediated enhancement of infection following repeated sub-erythemal doses of UV

(A-D) Prior to infection, mice were either left unexposed or were exposed to a sub-erythemal UV dose three times at intervals of 48 hours. All mice were then infected 24h post-exposure at the same site with 10^3 PFU of SFV6-mCHERRY in the presence or absence of a mosquito bite. Skin from the exposed site was collected 24h post-exposure and digested to isolate single cells. Cells were incubated with EdU, a thymidine nucleoside analogue, for 1-2. EdU+ cells were then tagged with a fluorophore using Click-IT chemistry. Proliferating cells (EdU+) and infected cells (SFV-mCHERRY+) could then be identified using flow cytometry. (n = 4)

(A) SFV RNA (E1 gene) copy number in inoculation site (skin) was measured at 24hpi by qPCR.

(B-C) Cells were first gated on SFV+ and then split into 'infected, proliferating cells' (SFV+EdU+) **(B)** or 'Infected, non-proliferating cells' (SFV+EdU-) **(C)**.

(D) Ratio of 'infected, proliferating cells' to 'infected, non proliferating cells'. Ratio >1 = virus preferentially infecting 'proliferating cells'. Ratio <1 = virus preferentially infecting 'non-proliferating cells'.

Plots show the median value ± interquartile range. Data were analysed using Mann-Whitney test (*ns = not significant, P < 0.05*).

5.5 A single sub-erythemal UV exposure is sufficient for enhancement of arbovirus infection

Following the unexpected finding that repeated sub-erythemal exposure to UV resulted in increased susceptibility to SFV infection, we considered whether just one exposure to this sub-erythemal dose of UV can enhance infection. Here, we exposed mice to a single sub-erythemal dose of UV, rather than repeating the sub-erythemal doses, and then infected the mice 24h after this single UV exposure with 10^4 PFU of SFV4 at the UV-exposed site alongside a mosquito bite. Interestingly, the UV-exposed mice had significantly more virus RNA in the skin by 24hpi, compared to unexposed mice (Figure 5.9A). However, the timing of the infection post-UV exposure appears to be critical in terms of deciding whether susceptibility to arbovirus infection is increased or not. As, when mice were infected 1-week after the single sub-erythemal UV dose, there was no significant difference in the quantities of virus RNA in the skin by 24hpi, although there was still an increasing trend (Figure 5.9B). Therefore, although a single sub-erythemal dose of UV at the skin is sufficient to enhance subsequent arbovirus infection, the time period post exposure does not extend up to 1 week.

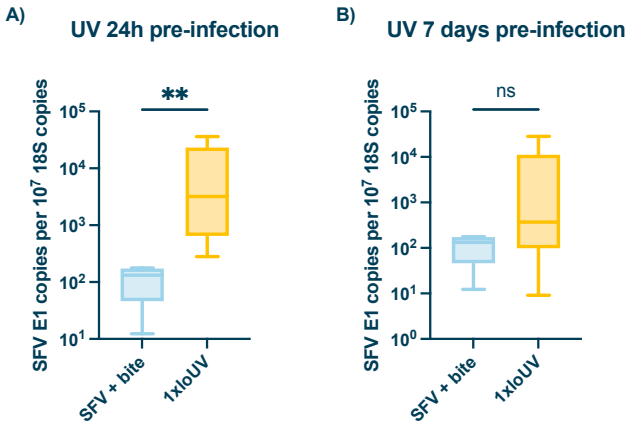

Figure 5.9 | Susceptibility to arbovirus is increased 24h after a single sub-erythemal dose of UV

(A, B) SFV RNA (E1 gene) copy number in inoculation site (skin) 24hpi. Prior to infection, mice were either left unexposed or had the skin of their left upper foot

exposed to a single sub-erythemal UV dose 24h **(A)** or 7 days **(B)** before being infected with 10^4 PFU of SFV4 in the presence of a mosquito bite. ($n \geq 6$)
Gene expression measured by qPCR. Plots show the median value ± interquartile range. Data were analysed using Mann-Whitney test (*ns = not significant, **P < 0.01*).

Often, individuals are only exposed to UV on areas of their skin not covered by clothing. Therefore, to conclude our work exploring the extent to which UV exposure can enhance arbovirus infection, we wanted to understand whether recurring exposure to low levels of UV at one uncovered site could result in enhancement of subsequent infection at a distant unexposed site. This aims to define whether there is a systemic difference in host susceptibility to virus by UV. To investigate this, the right feet of mice were repeatedly exposed to low doses of UV and the opposite feet, which had been left unexposed, were then infected with SFV4 24h after the final UV exposure. When we quantified quantities of virus RNA at the inoculation site, we found that there was no difference in the quantity of SFV in the skin by 24hpi in the UV-exposed mice, compared to unexposed mice (Figure 5.10A). Additionally, there was no difference in quantities of viremia between the two groups of mice either (Figure 5.10B). Therefore, this suggests that repeated, sub-erythemal UV does not appear to have a systemic effect as enhancement does not extend to infections that are transmitted at unexposed sites.

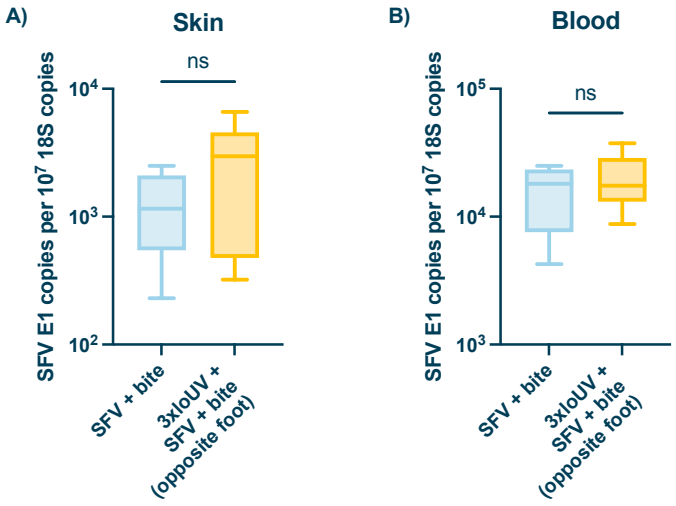

Figure 5.10 | Enhancement of infection is localised to the UV exposed site
(A, B) SFV RNA (E1 gene) copy number in inoculation site (skin) **(A)** and viral titres in the serum **(B)** 24hpi. Prior to infection, mice were either left unexposed or were exposed to a sub-erythemal dose on their right upper foot, three times at intervals of 48

hours. All mice were then infected at the opposite foot 24 hours post UV exposure with 10^4 PFU of SFV4 in the presence of a mosquito bite.

Gene expression measured by qPCR. Titres of virus in serum determined by plaque assay. (n ≥ 6) for all experiments. Plots show the median value ± interquartile range. Data were analysed using Mann-Whitney test (*ns* = *not significant*).

5.6 Summary and conclusions

In this short chapter, we set out to understand whether enhancement of arbovirus infection only occurs following erythemal UV exposure, or whether lower, sub-erythemal doses of UV can cause increased susceptibility to arbovirus infection also. To begin with, we set out to understand the impact this type of UV dose had on vascular permeability and skin histology, as we had done previously following an erythemal exposure to UV in Chapters 3 and 4. Interestingly, oedema was not significantly increased in mice exposed to repeated, sub-erythemal exposures only, but was higher in UV-exposed mice which had also been bitten by mosquitos at the same site (Figure 5.2). We have previously shown that mosquito bites are potent enhancers of oedema[120,126]. Therefore, as repeated, sub-erythemal UV exposures are not enough to induce oedema alone, this suggests that it is actually the bite driving vascular permeability at the skin, rather than the exposure to this regimen of UV. This differs greatly from what we witnessed following an erythemal dose of UV, where oedema was increased in the skin up to 1-week post-UV, in the presence or absence of a bite.

Although changes to the skin histology of mice exposed to repeated, low doses of UV were less extreme than those following an erythemal dose, shown in earlier chapters, the skin had undergone epidermal thickening, similar to 1-week after an erythemal dose (Figure 5.1). This is a known consequence of UV exposure of skin[385]. Driven by keratinocyte hyperplasia, this is thought to protect the skin from subsequent exposures[356]. Although we did not assess melanin production, melanogenesis likely also occurs at this timepoint, causing a tanned appearance of the skin following low dose exposures[344,386]. Of further note, was the appearance of an inflammatory infiltrate in the skin, although there were less cells present than observed following an erythemal exposure. Although we did not phenotype the cells present in this influx, these nucleated cells are likely

leukocytes. This is further supported by our later findings that monocytes are recruited to the skin of these UV-exposed mice. As monocytes are permissive to SFV infection, this influx could be critical to the enhancement of virus infection in these mice.

Interestingly, a reduction in the thickness of the subcutaneous fatty layer in the UV-exposed skin was also observed. This has been linked with fibrosis, especially in mouse models of the fibrotic skin condition systemic sclerosis[305,306]. Skin fibrosis induces the activation and proliferation of resident fibroblasts[387]. In Chapter 4, we demonstrated that fibroblasts are targeted by the virus during UV-mediated enhancement of infection at 1-week post-UV. Therefore, if this skin fibrosis following repeated, sub-erythemal doses of UV also leads to an increase of virus-permissive fibroblasts, this could enhance host susceptibility in this scenario also. Although, we did not assess fibroblast numbers or infected cell types in this chapter and so this would need to be worked on in the future.

Together, these observations were our first indication that exposure to repeated, low doses of UV does cause some changes to the skin, including driving an inflammatory infiltrate, but not to the same extent as a single, erythemal dose has.

Subsequently, we demonstrated that susceptibility to SFV infection is increased in mice exposed to repeated, sub-erythemal UV exposures prior to infection and then exposed to mosquito bites, evidenced by higher quantities of virus in the skin and blood (Figure 5.2). Furthermore, this effect was in addition to the enhancement already known to occur when virus is transmitted alongside a mosquito bite only. Crucially though, when we investigated whether this enhancement occurs when mice are only exposed to UV, and not also bitten by mosquitos, we found that enhancement no longer occurs (Figure 5.4). In fact, quantities of virus RNA in the skin are lower in UV-exposed mice than unexposed mice in this case. Therefore, it appears that enhancement following repeated, sub-erythemal UV doses only occurs in bitten skin. Nevertheless, this is still of great importance as natural infections are transmitted by mosquitos, and so the infection would never occur outside of this scenario anyway.

However, this can provide some indication as to the mechanisms that may be driving this effect. It is possible that low level UV exposure primes the skin for more exaggerated responses to mosquito biting, and it is this indirect effect that enhanced virus infection. This links back to our initial finding in this chapter that repeated, low doses of UV exposure of the skin alone did not induce oedema, but did when combined with a mosquito bite. It is well documented that induction of oedema contributes to mosquito-bite enhancement of arbovirus infection by facilitating the entry of virus-permissive cells to the inoculation site[120,126,134]. Arbovirus infection is also potently enhanced at both timepoints post erythemal UV exposure. Therefore, it could be that this mechanism of cell entry via permeable vessels is essential for UV-mediated enhancement of infection as well. Furthermore, since repeated, low-dose UV exposure of skin is not sufficient for induction of oedema without the addition of a bite, this may explain why susceptibility to arbovirus infection is not increased in these mice in the absence of a mosquito bite.

These UV-exposed mice still have robust induction of the antiviral Type I IFN system, evidenced by an increase expression in IFN-β and several ISGs during infection. Therefore, it is unlikely that this low dose UV exposure is suppression the Type I IFN system, allowing the virus to escape immune clearance. Rather, this antiviral defence mechanism is activated but is not sufficient at controlling the virus in UV-exposed skin. This is similar to what was observed during UV-mediated enhancement of infection in skin exposed to an erythemal dose of UV. These mice also had robust induction of a range of prototypic antiviral ISGs, however this did not aid the mice in controlling virus replication.

Furthermore, when we interrogated myeloid cell recruitment during infection of mice previously exposed to regular, sub-erythemal UV doses prior to infection, we found that there was no change in the number of neutrophils present in the skin during infection (Figure 5.6). This varies greatly from what was observed in mice exposed to erythemal UV either 24h or 1-week prior to infection, where there was an increase in neutrophil numbers. Importantly though, we found that there are more monocytes in the skin of UV-exposed mice, compared to unexposed mice, despite there being no change in expression of the monocyte

chemoattractant, CCL2. This finding, together with the data from the previous figure, suggests that susceptibility to arbovirus infection could be increased in mice exposed to repeated, low doses of UV and also mosquito bites due to recruitment of virus-permissive monocytes, despite having a robust Type I IFN response during infection. Furthermore, as enhancement of infection is only observed in mice also exposed to mosquito bites, it appears that these low-level exposures to UV prime the skin for more exaggerated responses to the mosquito bite, including increased leukocyte recruitment, which is of use to the virus. However, further investigation is required to confirm this. In the future, we could phenotype infected cells using the fluorescent strain of SFV we have used previously, SFV6-mCHERRY, to determine whether the increase in monocytes in the skin during infection also leads to more monocytes being infected in UV-exposed skin.

We also discounted the role of hyperproliferation in response to repeated, low doses of UV in driving enhanced infection in these mice. This level of UV exposure did drive a slight increase in cell proliferation but not to the same extent as was observed following an erythemal exposure in earlier chapters. Furthermore, there was no change in the numbers of infected, proliferating cells (Figures 5.7 and 5.8). This further extricates the phenotype of skin exposed to several, low doses of UV from that following a single, erythemal exposure, where UV does drive a large increase in cells proliferation and this appears to contribute to the increase in susceptibility at 1-week post-UV.

Finally, we sought to understand the limit of UV-mediated enhancement of infection by determining what the lowest dose required for this phenotype is. We found that a single, sub-erythemal dose of UV given 24h prior to infection results in increased susceptibility to the virus (Figure 5.9). However, mice were no longer susceptible 1-week after a single exposure. This suggests that while one low dose of UV is sufficient to enhance subsequent arbovirus infection, the exposure must occur soon before the infection takes place. Nevertheless, this display of the effect that this minimal dose of UV can have on arbovirus infection, shows the power of UV exposure of the skin in this capacity. Furthermore, these findings warrant further investigation regarding how long

after a low dose UV exposure enhancement lasts e.g. at 48h or 72h post-exposure.

We concluded this chapter by determining whether UV-mediated enhancement of infection following repeated, low doses of UV is localised to the UV-exposed site. Interestingly, the increase in susceptibility is confined to the skin where the UV exposure occurred (Figure 5.10). This suggests that, if this work translates to humans, enhancement of infection could be avoided by using protective interventions to avoid sunburn, either by covering exposed skin in clothing or by using sunscreen to block UVR reaching the skin. However, it is worth noting this chapter has made it clear that a single, erythemal dose of UV appears to have more extreme effects than the course of repeated, sub-erythemal doses of UV do. Therefore, we will also need to test whether the enhanced infection observed in mice exposed to an erythemal dose of UV is localised to the burn site in the same way, as it is more likely that the more severe exposure will drive a systemic effect.

The data reported in this chapter illustrates that exposure to even low doses of UV can lead to enhancement of subsequent arbovirus infection. This presents a novel risk posed by UV exposure in addition to those already known. However, we also showed that UV exposure only enhances local infection at the skin site where UV exposure occurs, as this effect was not observed when the infection site was distant from the site of UV exposure. This suggests that the threat, at least from low-dose exposure, can be mitigated by protecting the skin from UV exposure e.g. covering exposed regions of skin when outdoors in sunny environments.

The findings in this chapter are perhaps even more important in terms of public health than what we have shown in previous chapters, as people in areas of endemicity are repeatedly exposed to daily, sub-erythemal doses of UV. Furthermore, individuals often believe that tanning of the skin, through intermittent exposure to lower doses of UV, is less dangerous than more extreme UV exposure which causes sunburn, with some individuals even partaking in deliberate tanning[388–390]. Therefore, this could significantly increase

the risk of developing more severe disease if infected at UV exposed skin for either locals or those visiting, in areas where these viruses circulate.

Chapter 6: Treatment of UV burn with anti-inflammatory steroid cream offers some protection from UV-mediated enhancement of infection *in vivo*

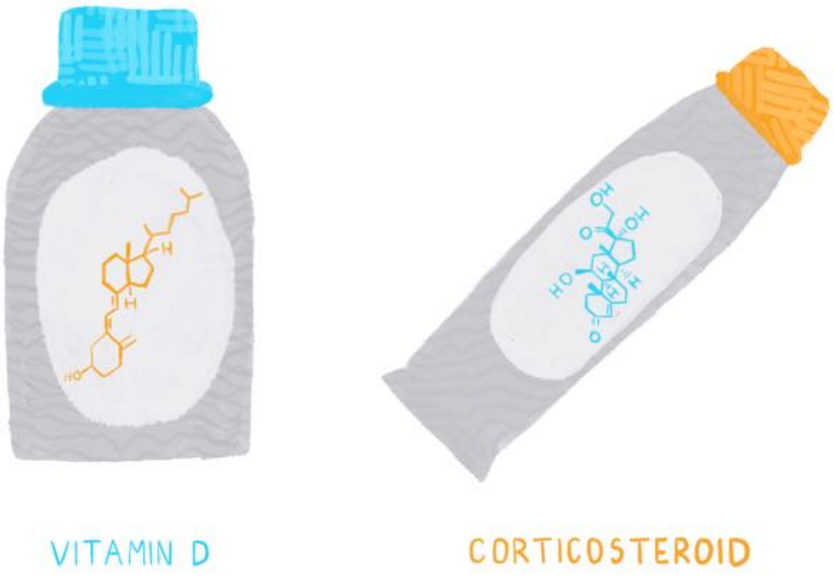

6.1 Introduction

Our findings in the previous chapters suggest that the inflammatory processes in UV-exposed skin likely contribute to UV-mediated enhancement of infection in mice. This led us to consider whether therapeutically dampening inflammation in the skin of UV-exposed mice would attenuate the increase in susceptibility to arbovirus infection observed in these mice. For this, we turned to two treatments which limit inflammation in UV exposed skin: topical steroids and vitamin D injections.

In most cases, sunburn does not require treatment and resolves by itself. Instead, pain and discomfort can be managed e.g. by cooling the affected skin[226]. Patients with more severe cases of sunburn, such as those that cover large areas, or exposure that causes blistering, can be treated with topical immunomodulators. Due to their anti-inflammatory effect, the standard of care for these patients is topical corticosteroid treatment, applied to the burn at least twice a day[391]. However, the evidence of the efficacy of steroids against sunburn is limited[226]. Multiple studies have shown that they have limited effect, evidenced by failure to either reduce the time to recovery or improve symptoms[392,393]. Nevertheless, they are still commonly used to reduce the pain and oedema associated with the burn.

Much of the research done on evaluating steroids as a sunburn treatment have focused on observations of their effects on reducing symptoms in humans e.g. erythema and oedema, rather than investigating the impact they have on the molecular processes in the skin following sunburn. However, steroids are known to have a number of effects, including as anti-inflammatories. They bind the glucocorticoid receptor in the cytoplasm, leading to interactions with glucocorticoid response elements in the genome, which drives upregulation of an anti-inflammatory gene expression programme, and the inhibition of pro-inflammatory transcription factors, including NFkB[394]. As well as these directly immunosuppressive effects, they also limit proliferation and exhibit vasoconstrictive activity, largely through histamine inhibition[395]. They are regularly used in the treatment of a number of anti-inflammatory skin conditions as a result, including eczema and sometimes in psoriasis[258,396]. These anti-

inflammatory effects inform the rationale behind treating sunburn with topical steroids.

More recently, experimental vitamin D injections have been suggested as a treatment for sunburn. In mice, i.p. injection of a type of vitamin D, calcifediol, the precursor to the active form of vitamin D, after an erythemal UV exposure, significantly reduced inflammation compared to untreated mice, resulting in the UV skin damage healing more quickly[397]. It was suggested that this effect was a result of promoting the anti-inflammatory activity of M2 macrophages by driving autophagy, the process by which cells recycle cellular structures and proteins, in these cells. When a similar intervention was trialled in humans, vitamin D drove lower expression of inflammatory cytokines in the skin, decreased skin erythema and increased expression of the anti-inflammatory, M2 macrophage-linked gene ARG1[398]. However, not all patients who were given vitamin D responded to the treatment in this way. Nevertheless, these studies together suggest that vitamin D injection can dampen inflammation in the skin following an erythemal exposure.

6.1.1 Hypothesis and aims

Based on the evidence put forward here, we hypothesised that treatment with either a vitamin D injection or topical steroids at the burn site following an erythemal UV exposure would reduce inflammation and protect from UV-mediated enhancement of infection at 1-week post-UV as a result.

To fully investigate this, this chapter aims to:

1) **Characterise the skin of mice treated with either a vitamin D injection or topical steroids at the burn site following an erythemal UV exposure to determine whether either treatment dampens inflammation in the skin**
2) **Determine whether either of these treatments alter host susceptibility to SFV infection in mice exposed to UV 1-week prior to infection**
3) **Investigate the mechanism driving any alterations to susceptibility observed in treated mice**

6.2 Development of an *in vivo* model to test treatments to reverse UV-mediated enhancement of infection

We adapted our original *in vivo* UV exposure model used in previous chapters to test the impact of either vitamin D treatment or steroid treatment on UV-mediated enhancement of infection. To investigate vitamin D treatment, mice were exposed to an erythemal dose of UV, equivalent to 2 MED or 400mJ/cm^2, on the back (for histology) or the upper side of the left foot (for all other experiments). 1h after the UV exposure, mice were injected with 5ng of vitamin D in the 25-hydroxy vitamin D_3 form s.c. at the burn site (Figure 6.1A). This form of vitamin D is the inactive vitamin D precursor which requires minor enzymatic processing to generate the active form[399]. We chose to inject s.c. instead of i.p. with the aim of localising any anti-inflammatory effect the vitamin D may have to our site of interest, the skin. Following one week of treatment, mice were exposed to biting mosquitos and infected with SFV at the burn site. We choose this time point as it has been demonstrated that vitamin D treatment shows some efficacy in reducing UV-induced inflammation by day 5 post-UV and onwards[397]. Therefore, we chose to inject vitamin D 1h after the burn had been administered, as had been done in the previous study, but waited to infect the mice until 1-week post-UV. Additionally, this was the same timepoint investigated in Chapter 4, when host susceptibility to arbovirus infection peaks post-UV. This allowed us to explore whether the treatment was effective at reversing UV-mediated enhancement of arbovirus infection.

We also developed an adapted version of the standard of care treatment for sunburn in humans, a regimen of topical corticosteroids at the burn site, to treat the UV-exposed mice. Following an erythemal UV exposure, as described above, clobetasol propionate corticosteroid cream (Dermovate® Ointment, GSK) was applied to the burn site twice daily for 5 days, with the first treatment taking place 1h post-UV (Figure 6.1A). This treatment regimen was developed under the guidance of a clinical dermatologist to best model the human treatment course. When virus infections were required, mice were exposed to

mosquito bites at the burn site and infected with SFV s.c. at the same site, 1-week post-UV exposure.

When we piloted each of these treatments in a small number of mice, in the absence of virus, we observed that the mouse treated with vitamin D post-UV appeared to have a slightly smaller burn lesion than the untreated, UV-exposed mouse (Figure 6.1B). Yet, the steroid treatment seemed to have the most significant effect on reducing the size of the wound and helping it to heal more quickly. This indicated that these treatments may successfully reduce inflammation at the burn site and, as a result, potentially limit UV-mediated enhancement of infection.

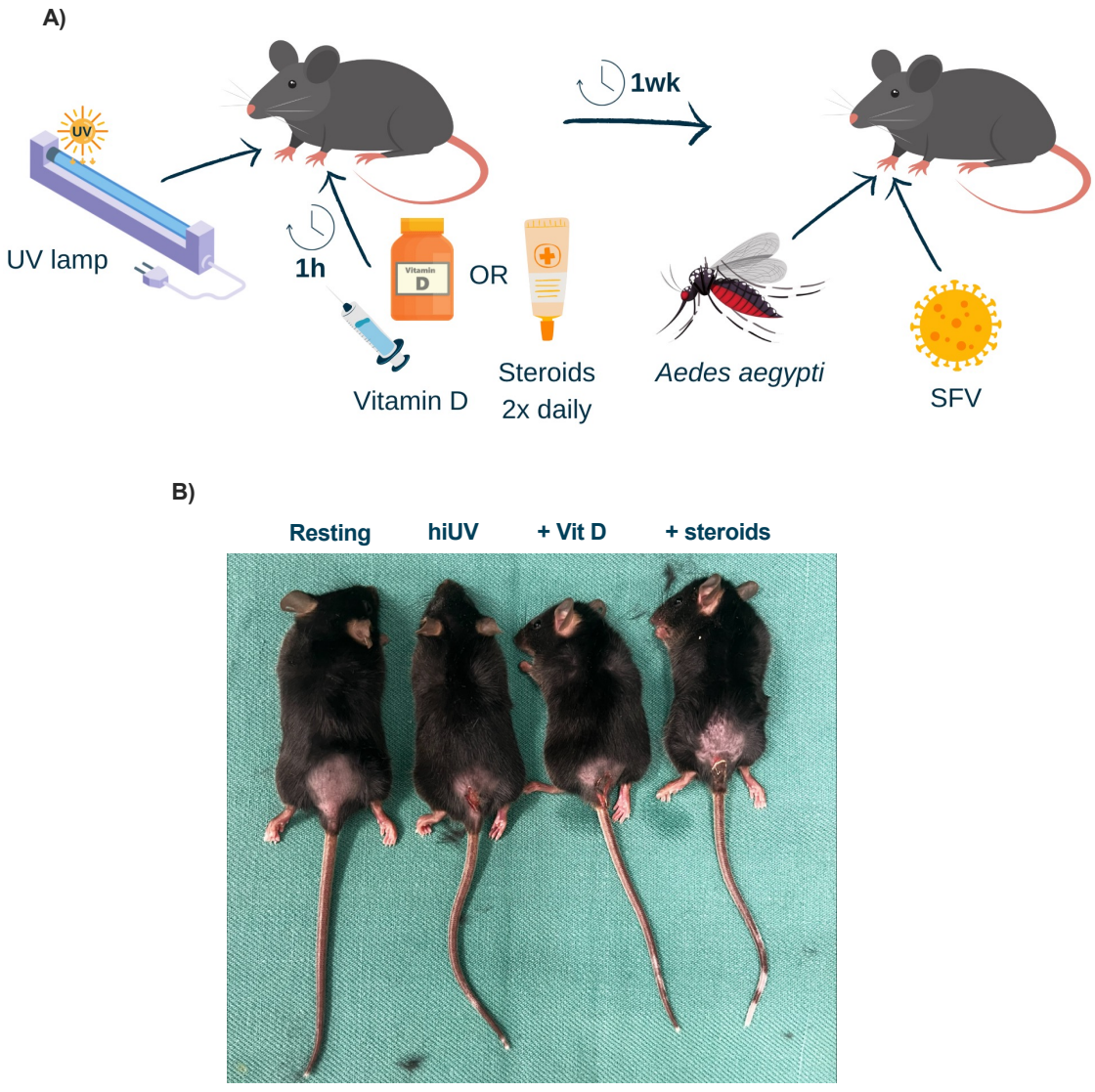

Figure 6.1 | Treatment of UV burn with Vitamin D or steroids visibly improved burn lesion in mice

(A) Graphical depiction of treatment regime. Mice were exposed to erythemal dose of UV and either injected s.c. at the burn site with 5ng of Vitamin D in mineral oil 1h post-exposure or the burn site was treated with topical steroids twice daily for 5 days with the first treatment administered 1h post-exposure, to replicate human sunburn treatments. For infection models, 1wk after the UV exposure, the burn site was exposed to biting mosquitos and injected s.c. with 10^4 PFU SFV4.
(B) Picture showing resting skin or the UV burn sites of mice which had been UV exposed ± Vitamin D or steroid treatment.

6.3 Vitamin D injections post-UV do not reverse UV-mediated enhancement of infection

Once the *in vivo* treatment model was established we first set out to investigate the impact of vitamin D on UV-exposed skin, in the absence of virus. We began by examining skin histology to confirm whether the changes observed in the appearance of the burn site following treatment were supported with evidence of structural changes in response to treatment. Skin histology from mice treated with vitamin D after UV-exposure shared appeared to be more similar to skin from untreated, UV-exposed mice than resting skin (Figure 6.2A). The layers of the skin were measured to investigate this further in an unbiased manner. Vitamin D treatment significantly reduced the thickness of the epidermis of UV-exposed skin back to normal thickness (Figure 6.2B). Additionally, there was a decreasing trend in the thickness of the dermis also. However, the inflammatory expansion of the fatty layer in UV-exposed skin persisted even after vitamin D treatment. Furthermore, there appeared to be an increase in nucleated cells in the dermis and fatty layer of UV exposed mice and this was not alleviated following vitamin D treatment. These nucleated cells were likely leukocytes. However, further investigation was needed to confirm this, e.g. using flow cytometry. Nevertheless, a single injection of vitamin D following an erythemal UV exposure limited the thickening of the epidermis observed in the skin by 1-week post-UV.

The weight of the mice was also regularly monitored following UV exposure ± vitamin D injections to assess the clinical signs of UV exposure and response to treatment. The weight of mice given vitamin D injections did not differ from untreated mice (Figure 6.2C). Together, this indicates that the treatment was

well tolerated by the mice and significantly reduced epidermal thickening, a marker of inflamed, UV-exposed skin. This suggested that vitamin D treatment had some ability to suppress the inflammatory responses in UV-exposed skin and may therefore also modulate UV-mediated enhancement of infection as a result.

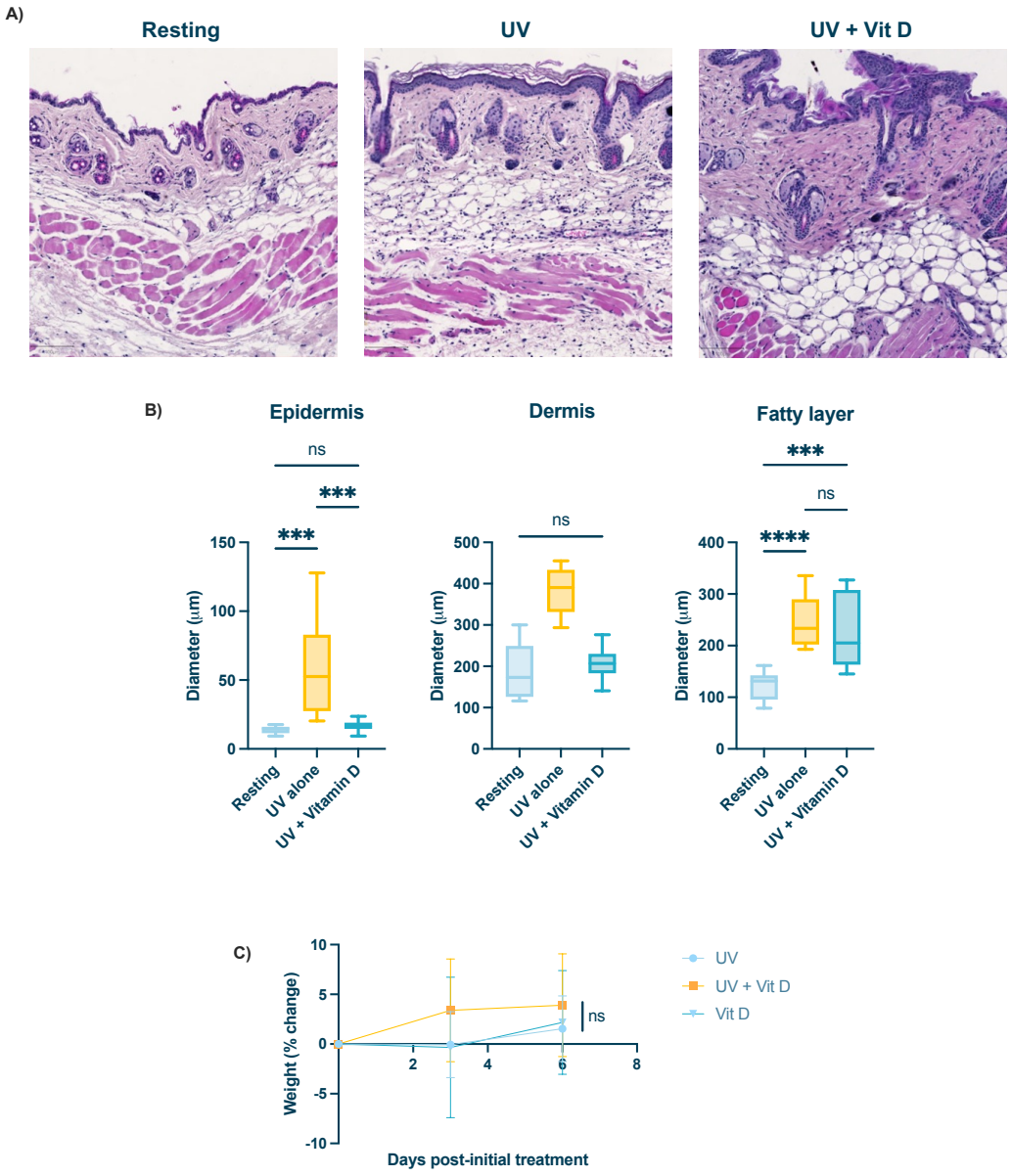

Figure 6.2 | Vitamin D treatment of UV burn reversed epidermal thickening, a hallmark of inflammation, and was well tolerated

(A) Histology of resting skin or skin exposed to erythemal UV ± Vitamin D injection 1h post-UV. Skin taken from the dorsal region of C5BL/6 mice 1-week post-UV exposure. Sections stained with H&E. Images shown are representative of the group. Scalebars measure 100 µm. Slides scanned at 20x magnification.

(B) Measurements of epidermis, dermis and fatty layer thickness were taken from 10 areas per condition using QuPath.

(C) Percentage weight change after treatment of mice in each treatment group, based on initial weight.

Plots show the median value ± interquartile range. Data were analysed using Kruskal-Wallis test with Dunn's multiple comparison test (*ns = not significant, ***P < 0.001, ****P < 0.0001*).

Another important feature of UV-exposed skin by 1-week post-UV, shown in Chapter 4, was the change to myeloid cell number by this timepoint. There was an increase in the number of neutrophils, which contribute to the inflammatory processes taking place during wound-healing, and a reduction in the number of monocytes, compared to skin exposed to a mosquito bite alone. This led us to investigate how vitamin D treatment impacts the numbers of these two cell types in the skin 1-week post-UV exposure using flow cytometry (Figure 6.3A). As expected, there were significantly more neutrophils in UV exposed mice irrespective of vitamin D treatment. This correlates with the evidence of the inflammatory infiltrate observed in the skin of these mice in Figure 6.2. Monocyte frequency in the skin of mice exposed to UV and mosquito bites was slightly reduced, although this might not reflect an absolute decrease in numbers, but rather relative decrease in frequency, due to large infiltrate of neutrophils (Figure 6.3B). Importantly, Vitamin D treatment did not have any significant effect on numbers of either neutrophils or monocytes in the skin.

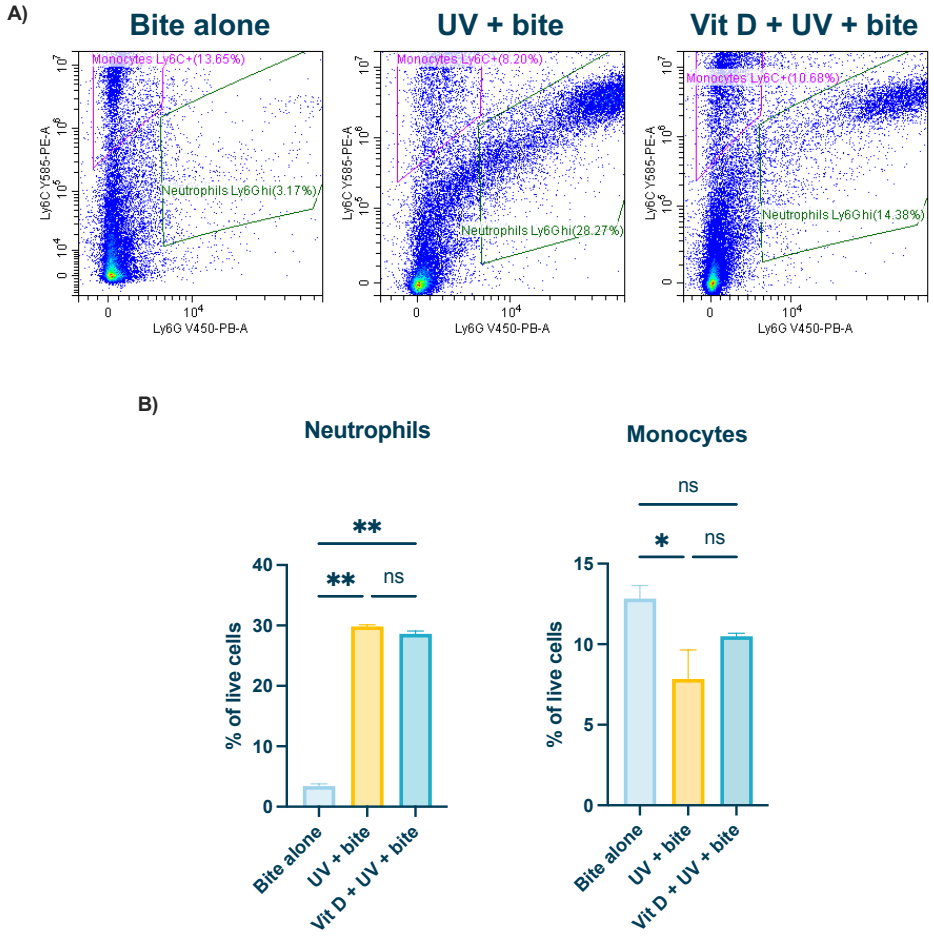

Figure 6.3 | Vitamin D does not impact recruitment of myeloid cells in response to UV burn

(A-B) Skin on the upper left feet of mice skin exposed to erythemal UV ± Vitamin D injection 1h post-UV. Burn site was exposed to biting mosquitos 1 week after UV exposure. Skin was collected 16hpi and digested to isolate single cells. (n=3).

(A) Cells were stained with antibodies against CD45, CD11b, Ly6C and Ly6G and analysed using flow cytometry.

(B) Monocyte ($Ly6C^+$) and neutrophil ($Ly6G^{hi}$) migration to skin measured by flow cytometry at 16hpi. Numbers represent percent of $Ly6C^+$ or $Ly6G^{hi}$ cells of all live cells. Plots show the median value ± interquartile range. Data were analysed using Kruskal-Wallis test with Dunn's multiple comparison test (*ns = not significant, **P < 0.01*).

Despite there being no change in myeloid cell numbers, the amelioration of inflamed skin size/depth by 1-week post-UV, shown in the Figure 6.2, led us to hypothesis that vitamin D treatment following UV-exposure may have some effect in preventing UV-enhancement of SFV infection. To investigate this, we infected mice with 10^4 PFU of SFV4 at the burn site 1-week post-UV and/or vitamin D injection. Quantities of virus RNA in skin by 24hpi were assessed

using qPCR. Mice exposed to erythemal UV 1-week prior to infection had significantly higher quantities of virus RNA in the skin, as expected (Figure 6.4A). Unexpectedly though, there was no significant difference in virus quantities in mice treated with vitamin D following UV exposure, compared to untreated, UV-exposed mice. However, interestingly there was a significant reduction in SFV RNA in the skin of control mice treated with vitamin D 1-week prior to infection, compared to mice infected at resting skin.

To further assess any potential impact vitamin D treatment has on arbovirus infection in UV-exposed skin, a plaque assay was used to quantify the quantities of infectious virus in the serum of mice by 24hpi. The same trends were observed in the quantities of viremia of these mice, as had been detected in the skin. There was more infectious virus in the serum of mice exposed to UV 1-week prior to infection (Figure 6.4B). Quantity of virus in the serum of vitamin D treated, UV-exposed mice were not significantly different from untreated, UV-exposed mice. Again, there was a significant reduction in serum virus of control mice treated with vitamin D 1-week prior to infection, compared to mice infected at resting skin.

Together, this shows that, despite the reduction in skin thickness shown in Figure 6.2, treatment of the UV burn with vitamin D, did not reduce quantities of virus in the skin or viremia in UV-exposed mice, therefore offering no protection from UV-mediated enhancement of arbovirus infection.

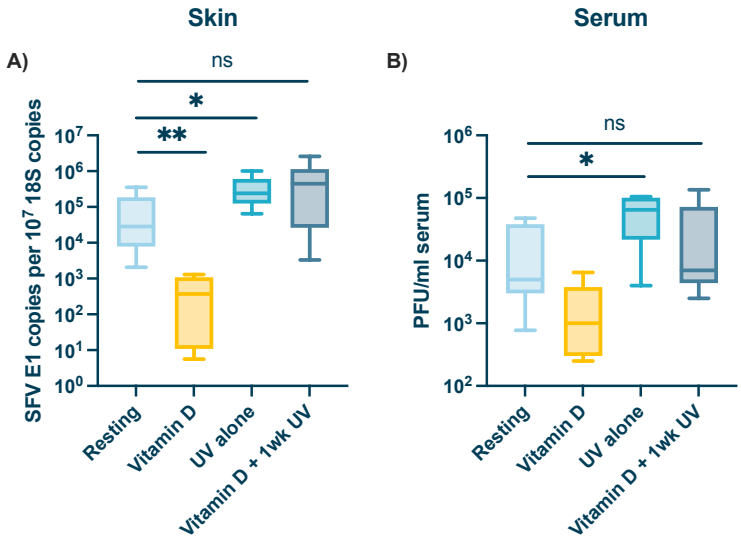

Figure 6.4 | Vitamin D treatment of UV burn did not reverse UV-mediated enhancement of infection but did protect from SFV infection in resting skin

(A-B) SFV RNA (E1 gene) copy number in inoculation site (skin) **(A)** and viral titres in the serum **(B)** 24hpi. Prior to infection, mice were either left unexposed or were exposed to an erythemal dose of UV on the skin on the upper side of the foot and treated with 5ng of vitamin D s.c. 1h post-UV. All mice were then infected 1wk post-exposure at the same site with 10^4 PFU of SFV4 in the presence of a mosquito bite. (*n* = 6)

Gene expression measured by qPCR. Titres of virus in serum determined by plaque assay. Plots show the median value ± interquartile range. Data were analysed using Kruskal-Wallis test with Dunn's multiple comparison test (*ns = not significant, *P<0.05, **P < 0.01*).

6.4 Topical steroid treatment of UV burn limits its ability to enhance viremia

Once we had established that vitamin D treatment of the UV burn did not affect the increase in host susceptibility to SFV infection observed at 1-week post-UV, we moved on to investigate whether steroid treatment of the UV-exposed site may have an impact. First, it was important to establish whether our topical corticosteroid regime reduced inflammation at UV-exposed skin, in the absence of virus. In Section 6.2, we observed that the steroid-treated burn looked significantly less red than the untreated burn. We explored this further by assessing skin histology from these mice 1-week post-UV to identify whether treatment resulted in any structural changes. These images showed that steroid treated, UV-exposed skin looks more similar to resting skin than untreated, UV-exposed skin (Figure 6.5A). We confirmed this by measuring the thickness of each skin layer. The thickening of the epidermis and fatty layers of the skin observed in UV-exposed mice at 1-week post-UV had been ablated back to normal levels following steroid treatment (Figure 6.5B). There was also a trend for decreasing thickness of the dermis following steroid treatment. This suggests that treatment of the UV burn with topical corticosteroids reversed much of the structural damage done to the skin by the erythemal UV exposure, as assessed at 1-week post-UV.

We also assessed health by weighing the mice daily. Unexpectedly, we noted that steroid treatment alone caused significant weight loss in mice, although not

enough to provoke welfare concerns (Figure 6.5C). Therefore, while steroid treatment reduced signs of inflammation in the skin to a greater extent than vitamin D treatment did, the repeated treatment with topical corticosteroids, which have known effects on multiple cellular pathways, appeared to be less well tolerated by mice.

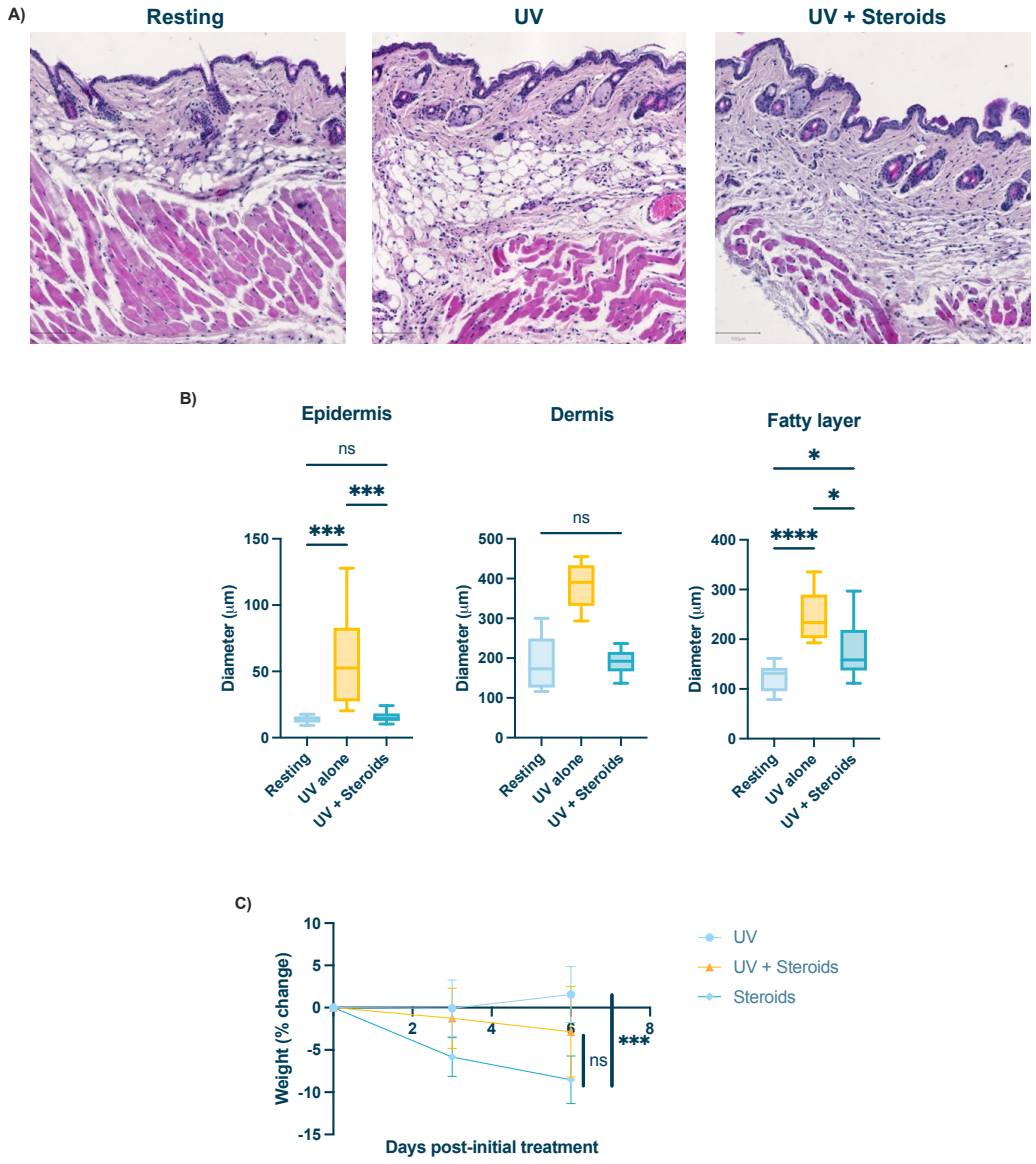

Figure 6.5 | Topical steroid treatment of UV burn limited the damage done to skin by erythemal UV exposure but did cause weight loss

(A) Histology of resting skin or skin exposed to erythemal UV ± topical steroid treatment of burn twice daily, starting 1h post-UV. Skin taken from the dorsal region of C5BL/6 mice 1 week post-UV exposure. Sections stained with H&E. Images shown are representative of the group. Scalebars measure 100 µm. Slides scanned at 20x magnification.

(B) Measurements of epidermis, dermis and fatty layer thickness were taken from 10 areas per condition using QuPath.

(C) Percentage weight change after treatment of mice in each treatment group, based on initial weight.

Plots show the median value ± interquartile range. Data were analysed using Kruskal-Wallis test with Dunn's multiple comparison test (*ns = not significant, ***P < 0.001, ****P < 0.0001*).

Since treating an erythemal UV burn with topical steroid cream reversed some of the UV-associated damage in the skin by 1-week post-UV, we hypothesised that steroid treatment of UV-exposed skin may also protect from the increase in susceptibility to arbovirus infection observed in these mice by 1-week post-UV. To explore this, we infected mice at the steroid treated or untreated burn site with 10^4 PFU of SFV4, alongside mosquito bites, and assessed virus quantities in the skin at 24hpi using qPCR. As expected, quantities of virus RNA in the skin were significantly increased in mice exposed to UV 1-week prior (Figure 6.6A). However, steroid treatment of the UV burn did not significantly reduce SFV quantities in the skin compared to untreated, UV-exposed mice. However, quantities of virus RNA were sufficiently decreased by steroids to a level which was not significantly elevated compared to control, non-UV exposed skin. Interestingly, when we assessed virus dissemination to the blood, using a plaque assay, we found that viremia was significantly reduced in mice treated with steroids post-UV, compared to untreated, UV-exposed mice (Figure 6.6B). Therefore, this treatment regimen protects from UV-enhanced dissemination of virus to the blood in these mice.

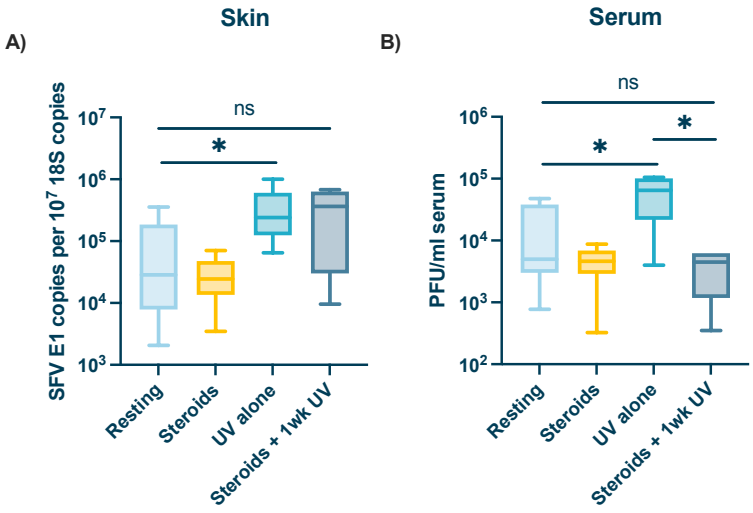

Figure 6.6 | Steroid treatment of UV burn protected mice from viremia associated with UV-mediated enhancement of infection

(A-B) SFV RNA (E1 gene) copy number in inoculation site (skin) **(A)** and viral titres in the serum **(B)** 24hpi. Prior to infection, mice were either left unexposed or were exposed to an erythemal dose of UV on the skin on the upper side of the foot and treated with topical steroids twice daily, starting 1h post-exposure. All mice were then infected 1wk post-exposure at the same site with 10^4 PFU of SFV4 in the presence of a mosquito bite. (*n* = 6)

Gene expression measured by qPCR. Titres of virus in serum determined by plaque assay. Plots show the median value ± interquartile range. Data were analysed using Kruskal-Wallis test with Dunn's multiple comparison test (*ns = not significant, *P<0.05*).

Steroids are known to be highly anti-inflammatory and can affect the ability of cells to proliferate, which has been suggested earlier in this thesis as a potential driving mechanism behind UV-mediated enhancement of infection at 1-week post-UV. Therefore, we considered whether the protection against UV-mediated enhancement of infection following treatment of the UV burn with topical corticosteroids could be due to a change in the number of myeloid cells present in the skin at 1-week post-UV. When we quantified these cells using flow cytometry, however, there was no significant difference in the number of neutrophils or monocytes between steroid-treated, UV-exposed skin and untreated, UV-exposed skin (Figure 6.7A-B).

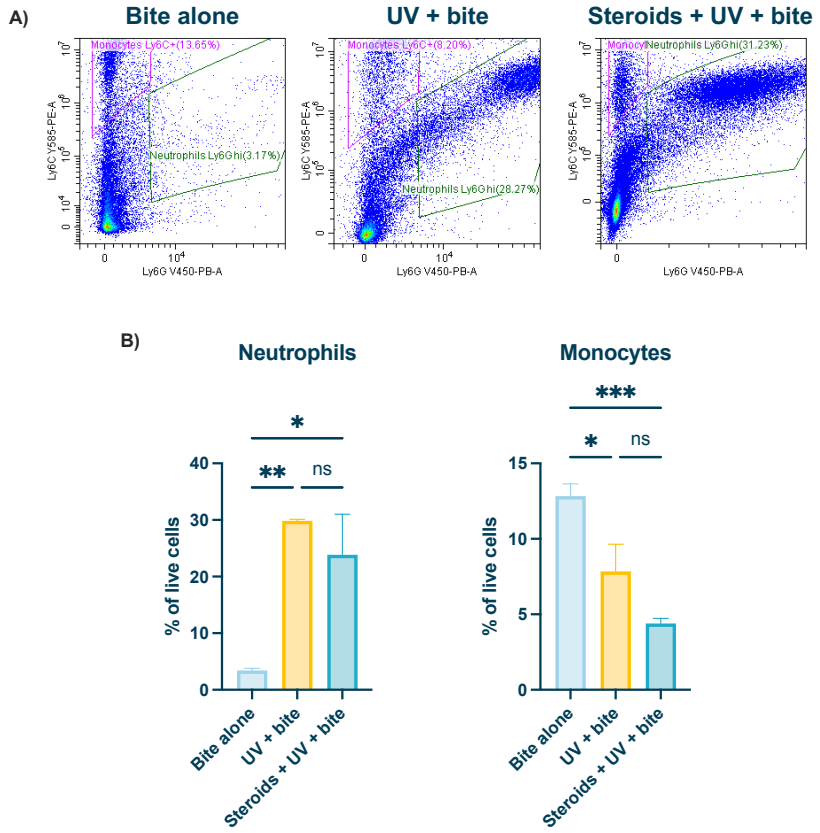

Figure 6.7 | Steroid treatment does not impact recruitment of myeloid cells in response to UV burn

(A-B) Skin on the upper left feet of mice skin exposed to erythemal UV ± topical steroid treatment of burn twice daily, starting 1h post-UV. Burn site was exposed to biting mosquitos 1 week after UV exposure. Skin was collected 16hpi and digested to isolate single cells. (n=3).

(A) Cells were stained with antibodies against CD45, CD11b, Ly6C and Ly6G and analysed using flow cytometry.

(B) Monocyte ($Ly6C^+$) and neutrophil ($Ly6G^{hi}$) migration to skin measured by flow cytometry at 16hpi. Numbers represent percent of $Ly6C^+$ or $Ly6G^{hi}$ cells of all live cells. Plots show the median value ± interquartile range. Data were analysed using Kruskal-Wallis test with Dunn's multiple comparison test (*ns = not significant, *P < 0.05, **P < 0.01*).

Type I IFNs are critical for limiting spread of SFV away from the inoculation site[117]. Therefore, we next sought to characterise whether the antiviral Type I IFN response was modulated by application of steroids, and if so whether this could shed light on the mechanism driving steroid-mediated protection against viremia in UV-exposed mice. We quantified expression of IFN-β and the

prototypic ISG, RSAD2 in the skin of mice. However, there was no change in the expression of either gene between experimental groups (Figure 6.8A-B), suggesting that topical steroid did not modulate host IFN response to virus and/or UV.

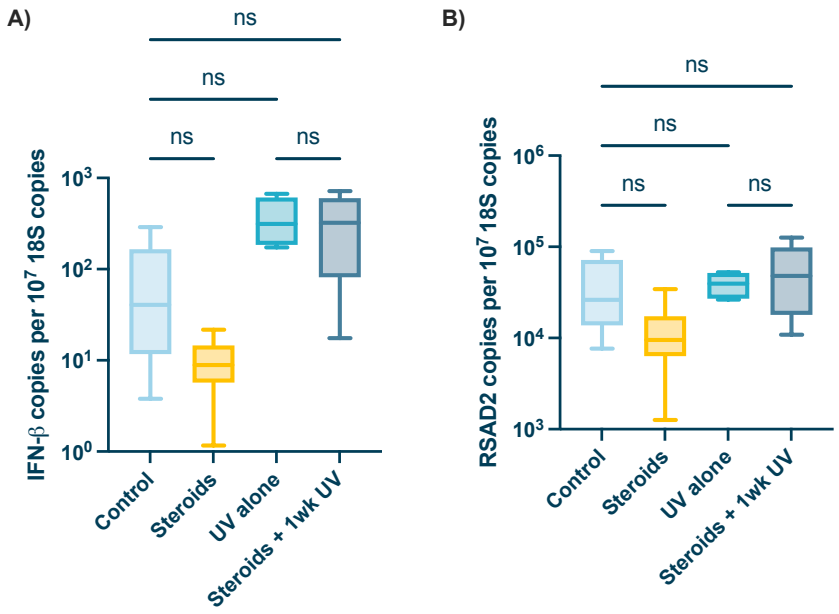

Figure 6.8 | Steroid treatment of UV-exposed skin does not drive expression of IFN-β or key antiviral ISG, RSAD2, during UV-mediated enhancement of infection

(A-B) IFN-β **(A)** or RSAD2 **(B)** copy number in inoculation site (skin) 24hpi. Prior to infection, skin on the upper left feet of mice was exposed to erythemal UV ± topical steroid treatment of burn twice daily, starting 1h post-UV. All mice were then infected at 1 week post-exposure at the same site with 10^4 PFU of SFV4 in the presence of a mosquito bite. ($n \geq 6$)

Gene expression measured by qPCR. Plots show the median value ± interquartile range. Data were analysed using Kruskal-Wallis test with Dunn's multiple comparison test (*ns = not significant, *P < 0.05*).

Following the finding that steroid treatment of the burn prior to infection limits viremia in Figure 6.6, we considered whether the treatment, although localised to the skin, may have systemic effects throughout the body and that this was what was restricting the spread of the virus to the blood. Therefore, we hypothesised that, if the steroid treatment was having a systemic effect to protect from virus, then steroid treatment of the burn site may protect from infection at a distant inoculation site, separate from the UV-exposed, steroid

treated site. To investigate this, we exposed mice to an erythemal dose of UV on the upper side of the left foot and then treated the burn with topical corticosteroids, as before. However, when it came to infecting the mice 1-week post-UV, we administered the infection i.p., rather than at the burn site. Serum was then collected from mice 24hpi to assess whether steroid treatment provided systemic protection from arbovirus infection, or whether the effect was localised to the treatment site. Here, untreated, UV-exposed mice and steroid-treated, UV-exposed mice had significantly lower quantities of infectious virus present in the serum by 24hpi (Figure 6.9). Therefore, it appears that while UV exposure drives an increase in susceptibility to arbovirus infection at the burn site, the exposure appears to result in protection from arbovirus infection when the virus is inoculated i.p., separate from the burn site. As the steroid treated, UV-exposed mice experienced a similar effect, steroids did not significantly modulate this protection from virus.

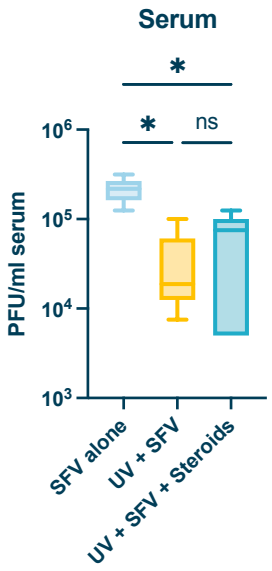

Figure 6.9 | UV exposure protects from virus inoculated intra-peritoneally, and is not modulated significantly by topical steroids

Skin on the upper left feet of mice skin exposed to erythemal UV ± topical steroid treatment of burn twice daily, starting 1h post-UV. Mice were infected with 10^4 PFU of SFV4 i.p. 1 week after UV exposure. Serum was collected to measure systemic spread of virus. Titres of virus in serum determined by plaque assay.

Plots show the median value ± interquartile range. Data were analysed using Kruskal-Wallis test with Dunn's multiple comparison test (*ns = not significant, *P < 0.05*).

6.5 Steroids partially protect against systemic spread of SFV during UV-mediated enhancement of infection

Arboviruses must spread to the blood in order to disseminate to other tissues, such as the brain, and cause disease, including arboviral encephalitis[101,118–120,400]. While we had identified in Chapters 3 and 4 that there is an increase in dissemination of virus to the blood in mice exposed to UV either 24h or 1-week prior to infection, we had not investigated whether this drives an increase in dissemination to other tissues as a result. Therefore, we hypothesised that mice exposed to UV prior to infection would have higher quantities of virus present in remote tissues. Furthermore, since steroid treatment of a UV burn had been shown to protect from UV-mediated enhancement of viremia by 24hpi, in Figure 6.6, we considered whether this would protect mice from the systemic spread of SFV to other tissues at later stages of infection. To investigate this, mice were exposed to an erythemal dose of UV to the upper side of the left foot and the burn was either left untreated or was treated with topical corticosteroids for 5 days, as before. The burn site was infected with SFV4, alongside mosquito bites, at 1-week post-UV. However, as the virus takes time to spread systemically to remote tissues; when SFV4 infection takes place alongside a mosquito bite, the virus disseminates to the brain by 3 days p.i.[120]. Therefore, rather than cull the mice at 24hpi as we had previously done, mice were culled at 3 days p.i. instead and samples were collected.

We monitored the weight of the animals each day post-infection, as a sudden drop in weight can be indicative of the onset of severe disease. However, none of the mice lost more than 20%, the limit of the humane endpoint for this study, and there was no significant difference in the weight change between any of the groups 3 days p.i. (Figure 6.10A). We also measured virus at the inoculation site, the skin, to determine whether there was a difference in residual virus, as an indicator of quantities of virus replication at this site. While there was still detectable virus in the skin of all three groups of mice by 3 days p.i., there was no significant difference between the groups (Figure 6.10B). Finally, we assessed quantities of virus in the blood, spleen and brain, by 3 days p.i., to interrogate any impact steroid treatment has on virus dissemination around the body. Interestingly, there were no plaques formed when we performed a plaque assay using the serum from any of the three experimental groups, meaning that

there was no infectious virus present in the serum taken from these mice. This suggests that any virus left in the blood had likely been neutralised, e.g. by antibodies or complement, by 3 days p.i. When we assessed virus RNA present in two remote tissues, the spleen and the brain, we found evidence of SFV in both tissues taken from all groups (Figure 6.10C-D). However, there was no difference in the quantities of virus in the spleen or brain between untreated, UV-exposed mice and steroid treated, UV-exposed mice or untreated, unexposed mice. Therefore, there does not seem to be any difference in the systemic spread of virus in UV-exposed mice, either steroid treated or untreated, by 3 days p.i., compared to the normal course of infection.

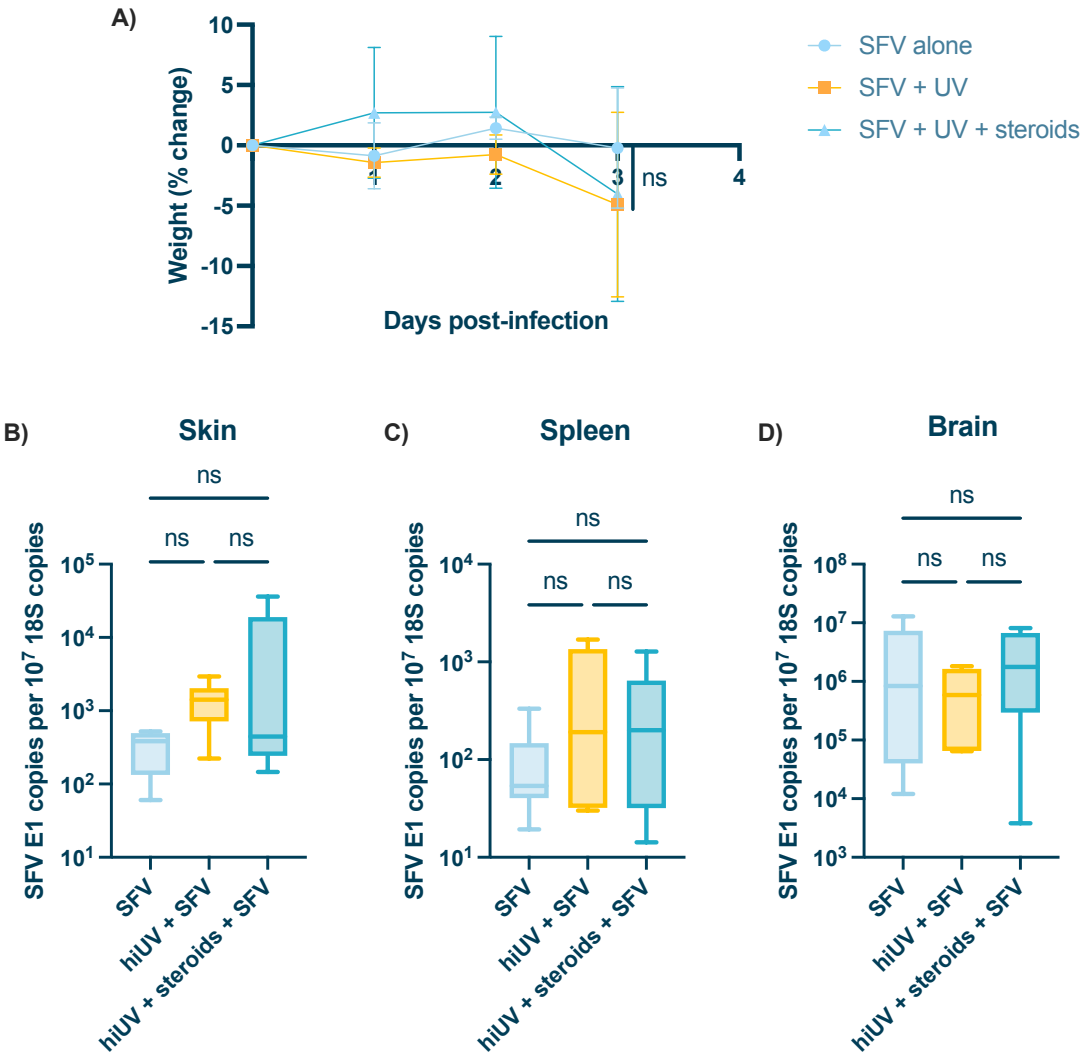

Figure 6.10 | No difference in systemic spread of virus by 3 days p.i. in UV-exposed mice

(A-D) Skin on the upper left feet of mice exposed to erythemal UV ± topical steroid treatment of burn twice daily, starting 1h post-UV. The burn site was exposed to biting

mosquitos and infected with 10^4 PFU of SFV4 s.c. 1 week after UV exposure. Mice were monitored and culled 3 days p.i. (n=6)

(A) Percentage weight change after infection of mice in each treatment group, based on weight on day of virus inoculation.

(B-D) SFV RNA (e1 gene) copy number in inoculation site (skin) **(B)**, spleen **(C)** or brain **(D)** 3 days p.i.

Gene expression measured by qPCR. Plots show the median value ± interquartile range. Data were analysed using Kruskal-Wallis test with Dunn's multiple comparison test (*ns* = *not significant*).

The findings of the previous figure led us to consider whether 3 days p.i. was too early a timepoint to observe any differences in terms of systemic spread of the virus, driven by UV exposure alone or following steroid treatment of the burn. Accordingly, we repeated the experiment but culled the mice 1 day later, at 4 days p.i. instead. As before, there was no discernible change in the weight of the mice over time following infection (Figure 6.11A). When we assessed virus quantities in the skin, we found that there was significantly more SFV left at the inoculation site by 4 days p.i. in mice exposed to UV 1-week prior to infection (Figure 6.11B). Interestingly, quantities of virus in the skin were higher in steroid treated, UV-exposed mice compared to untreated, unexposed mice. However, treatment of the burn with steroids did significantly reduce the quantities of virus RNA in the skin compared to untreated, UV-exposed mice. In the spleen, there was no significant difference in quantities of virus by 4 days p.i. between mice exposed to UV prior to infection and unexposed mice (Figure 6.11C). However, mice treated with steroids post-UV did have significantly less virus in the spleen compared to untreated, unexposed mice. Most importantly, mice exposed to erythemal UV 1-week prior to infection had significantly more virus RNA in the brain by 4 days p.i., compared to non-UV exposed mice (Figure 6.11D). Furthermore, quantities of virus RNA in the brains of mice which had received steroid treatment following UV exposure were not significantly different from untreated, UV-exposed mice.

Together, this shows that an erythemal UV exposure of mice 1-week prior to SFV infection results in enhanced dissemination of the virus to the brain by 4 days p.i. Additionally, while corticosteroid treatment of the burn protects from the increase in viremia observed in UV-exposed mice by 24hpi (Figure 6.6), this

does not translate in to a reduction in the spread of virus by 4 days p.i. to the brain, a site of great clinical relevance during arbovirus infection. This is perhaps not surprising considering that SFV4, when inoculated at a mosquito bite, is a highly neurotropic virus and replicates very efficiently in the brain[289]. Therefore, in this one aspect, it may not be that representative of most arbovirus infections transmitted to people. Nevertheless, steroid treatment did result in lower quantities of virus in the spleen and inoculation site by this timepoint. Therefore, steroids appear to offer partial protection against UV-mediated enhancement of infection.

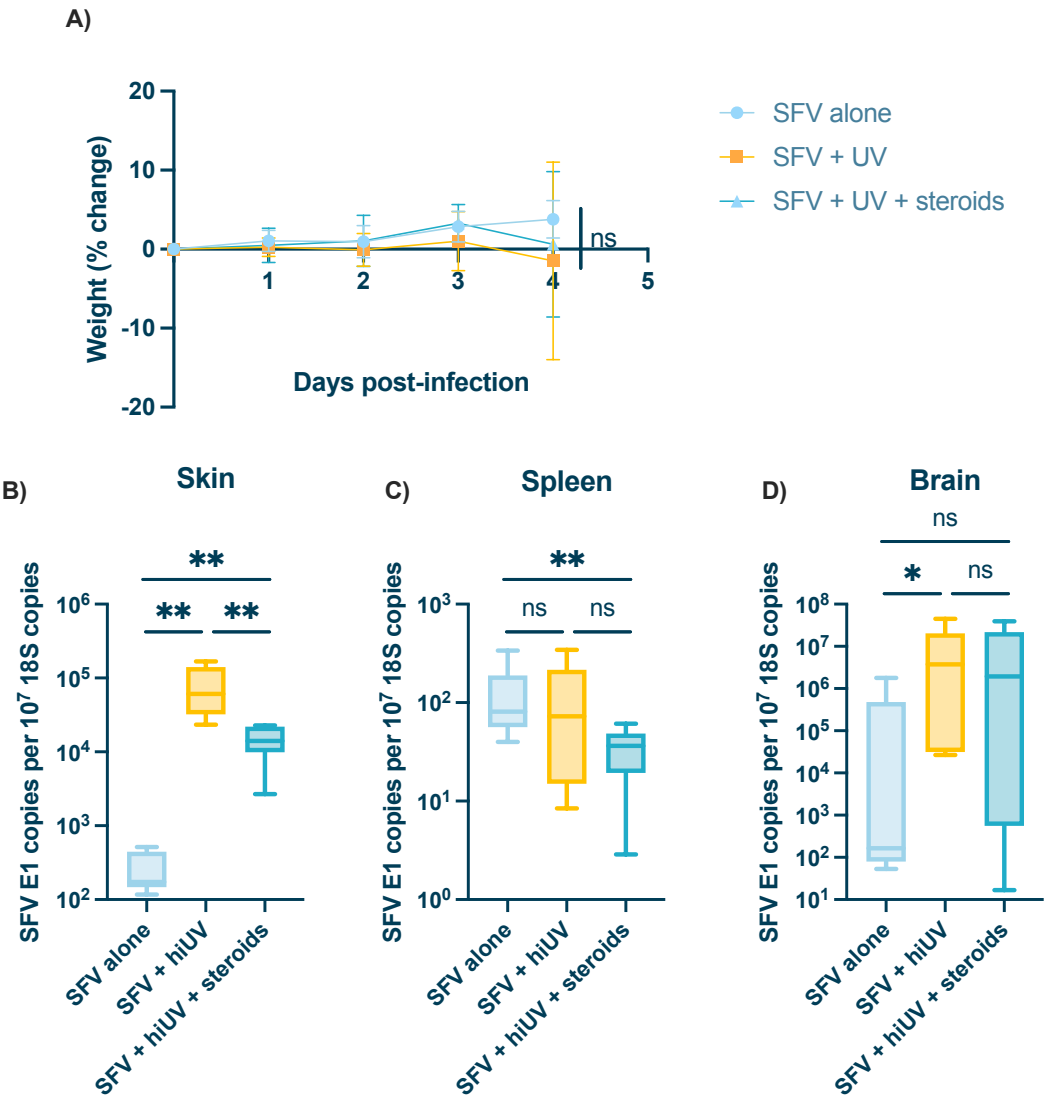

Figure 6.11 | UV exposure results in higher quantities of viral RNA in brain by 4 days p.i. and steroids do not protect from this

(A-D) Skin on the upper left feet of mice exposed to erythemal UV ± topical steroid treatment of burn twice daily, starting 1h post-UV. The burn site was exposed to biting

mosquitos and infected with 10^4 PFU of SFV4 s.c. 1 week after UV exposure. Mice were monitored and culled 4 days p.i. (n=6)

(A) Percentage weight change after infection of mice in each treatment group, based on weight on day of virus inoculation.

(B-D) SFV RNA (e1 gene) copy number in inoculation site (skin) **(B)**, spleen **(C)** or brain **(D)** 4 days p.i.

Gene expression measured by qPCR. Plots show the median value ± interquartile range. Data were analysed using Kruskal-Wallis test with Dunn's multiple comparison test (*ns = not significant, *P<0.05, **P < 0.01*).

As mentioned, there was no infectious virus left in the serum by 3 days p.i., suggesting that virus had been effectively neutralised and cleared from the blood by this timepoint. Neutralising antibodies in serum act to limit viremia. Antibodies against virus epitopes are generated during the adaptive immune response against infection[401]. These can protect the host in a multi-pronged manner, both directly and indirectly. Antibodies can bind virus particles, directly blocking them from infecting host cells. They can also assist effector leukocytes identify virus particles through FcR interactions, by coating the virion to amplify the antiviral immune response, a process called opsonisation. Importantly, neutralising antibody in the serum are vital for effective control of viremia, including during SFV infection[402,403].

SFV can traffic via the blood to remote sites, including the brain[404]. As we had shown in the previous figure that there were higher quantities of virus in the brain of mice exposed to UV prior to infection, we decided to investigate whether the generation of neutralising antibodies in the serum was modulated in UV-exposed mice. We also included steroid-treated mice in this experiment to determine whether this treatment could counteract any impact UV exposure has on the neutralising capacity of serum. We used an adapted version of a standard protocol to measure serum-neutralising antibody quantities, in which BHK-21 cells are pre-treated with mouse serum before being infected with SFV4[405]. Assessing whether dilutions of serum protected BHK-21 cells was used as a readout of the quantities of neutralising antibody present in the mouse serum.

We found that the serum of mice exposed to UV 1-week prior to infection, provided a significantly lower level of protection than unexposed, infected mice (Figure 6.12A). This was apparent in UV-exposed mice across multiple dilutions of serum (Figure 6.12B). Additionally, the proportion of protected cells was not significantly different between untreated, UV-exposed mice and steroid treated, UV-exposed mice. These findings suggest that UV exposure of mice prior to infection, limits the generation of serum-neutralising antibodies during subsequent SFV infection and that steroid treatment of the burn prior to infection did not fully restore neutralising antibody production back to normal.

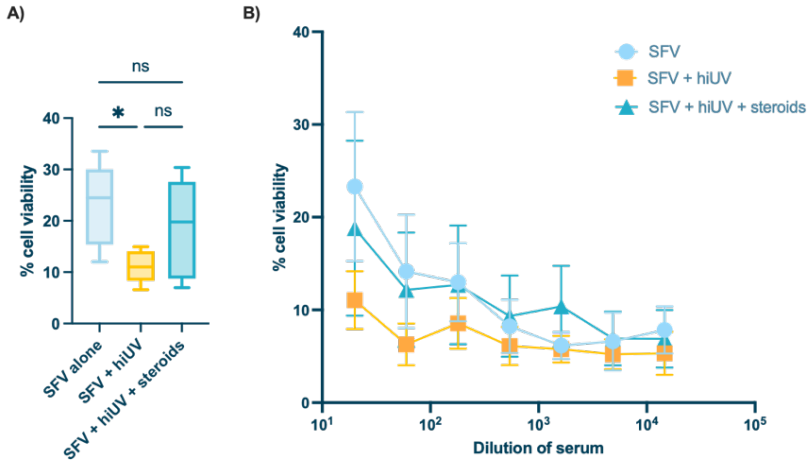

Figure 6.12 | UV exposure limits the generation of neutralising antibodies in serum

Capacity of mouse serum in protecting BHK-21 cells from SFV4 infection *in vitro*, indicating neutralising antibody quantities.

(A-B) BHK-21 cells were pre-treated with serum taken from mice 3 days p.i., at a set serum dilution between 1:20 and 1:14580, before being infected 1h later with $5x10^4$ PFU SFV4. Cells were stained 2 days p.i. with Crystal Violet to identify live cells (% of cells protected by serum). A plaque assay had been carried out using the serum beforehand to confirm there was no residual infectious virus from the *in vivo* infection left in the serum. Plates were then scanned and analysed using ImageJ to calculate the percentage of viable cells as a readout of the protective capacity of the serum.

The mice which the serum was taken from had been exposed to erythemal UV ± topical steroid treatment of burn twice daily, starting 1h post-UV. The burn site was exposed to biting mosquitos and infected with 10^4 PFU of SFV4 s.c. 1 week after UV exposure. Mice were monitored and culled 3 days p.i. (n=6)

Graphs show percentage of viable cells when treated with serum diluted 1:20, a representative dilution, **(A)** or one of a range of dilutions between 1:20 and 1:14580 **(B)**

prior to SFV infection. All cell viability readouts were normalised to background readings from uninfected cells.
Plots show the median value ± interquartile range. Data were analysed using Kruskal-Wallis test with Dunn's multiple comparison test (*ns = not significant, *P<0.05*).

Viral encephalitis is one of the most serious conditions associated with arbovirus infection[406]. If virus crosses the blood-brain-barrier it can cause damage, either directly via infection or indirectly due to the onset of inflammation in response to the pathogen. Here, we have shown that there are higher quantities of virus in the brains of UV-exposed mice by 4 days p.i. (Figure 6.11). As such, this enhanced infection in mice exposed to UV 1-week prior to infection could lead to an increased influx of inflammatory cells into this sensitive organ, which has the potential to cause life threatening pathology. Therefore, we assessed histology of brains from these mice at 4 days p.i. to determine whether there is an increased inflammatory infiltrate to the brain during UV-mediated enhancement of infection. Since steroid treatment of the UV burn appeared to offer partial protection from this enhancement, we sought to understand whether steroids would also impact brain inflammation.

Upon examination of brain histology collected 4 days p.i., we identified blood vessels in the brains of UV-exposed mice with large numbers of nucleated cells surrounding them (Figure 6.13A). As cells can enter tissues via blood vessels, cell clusters at these sites can be indicative of an inflammatory infiltrate. This is a defining feature of arboviral encephalitis. Contrastingly, blood vessels in non-UV exposed mice appeared normal, with limited signs of inflammatory infiltrate. Interestingly, steroid treated mice showed minimal cell infiltrate at the vessels, suggesting that this treatment of the UV burn prior to infection protects from this. To probe this further, we quantified cell density in the cortex of the brain using the imaging analysis software, QuPath. UV-exposed mice had significantly more cells present in the brain by 4 days p.i., compared to untreated, unexposed mice (Figure 6.13B). Interestingly, our analysis confirmed that steroid treatment of the burn did reduce the number of cells back to normal levels. Therefore, the brains of UV-exposed mice showed signs of increased cellular infiltrate at blood vessels and had more cells present in the brain by 4 days p.i. Furthermore, despite not reducing quantities of virus in the brain back

to normal, steroid-treated mice did exhibit reduced cellular infiltrate during infection, compared to untreated, UV-exposed mice, which could be of clinical benefit during the later stages of SFV infection.

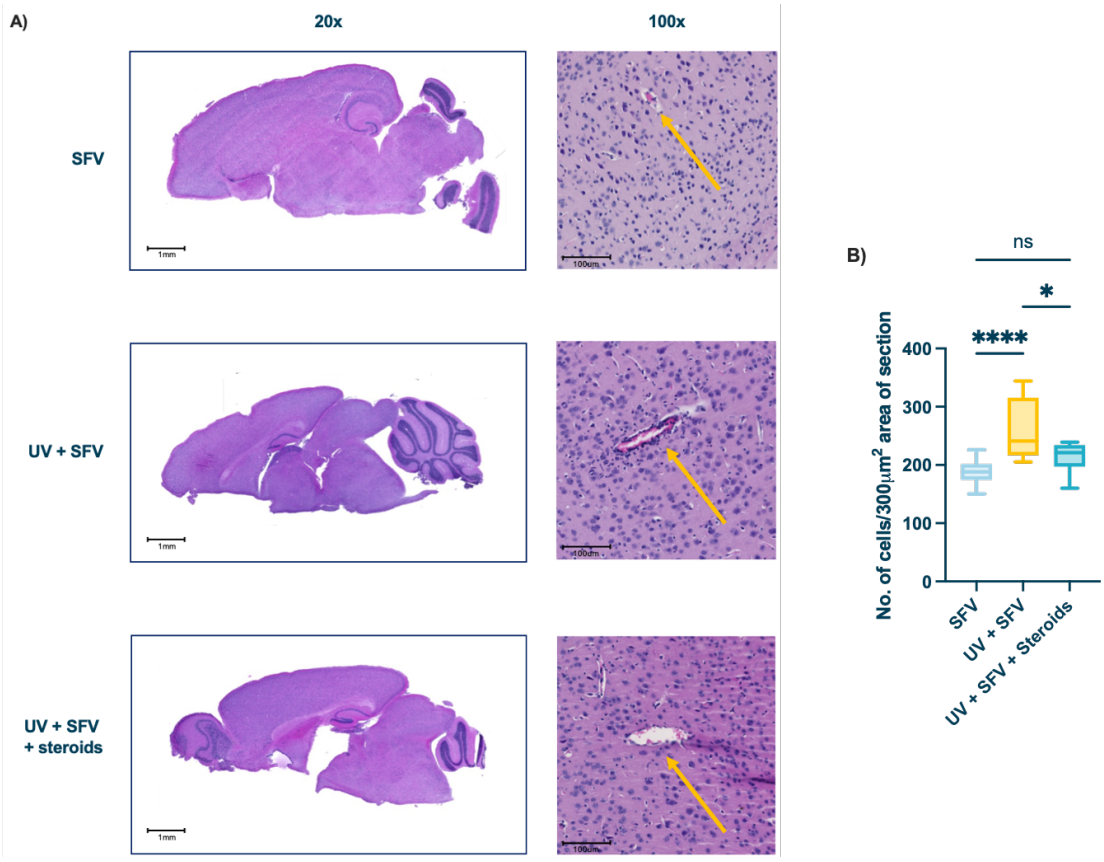

Figure 6.13 | UV drives inflammatory infiltrate to brain at 4 days p.i.

(A) Histology of brains from mice exposed to erythemal UV ± topical steroid treatment of burn twice daily, starting 1h post-UV and infected with 10^4 PFU of SFV4 s.c. in the presence of mosquito bites 1 week post-UV. Brains collected 4 days p.i . Sections stained with H&E. Yellow arrows indicate blood vessels. Images shown are representative of the group. Slides scanned at 20x magnification and displayed at magnification indicated above images. Scalebars measure 100 µm.

(B) Cell counts per 300µm^2 area of section were taken from 10 areas per mouse, from 3 mice per condition using QuPath.

Plots show the median value ± interquartile range. Data were analysed using Kruskal-Wallis test with Dunn's multiple comparison test (*ns = not significant, *P<0.05, ****P<0.0001*).

T cells are critical for the antiviral response in the brain but are also implicated in arboviral encephalitis immunopathology. Therefore, we considered whether

these cells are recruited to the brain as part of the increased inflammatory infiltrate observed in the brains of UV-exposed mice in the previous figure. To investigate this, we analysed expression of the CD8+ T cell chemoattractant CXCL10 in the brain of mice at 3 or 4 days p.i. using qPCR. However, there was no significant difference in expression of CXCL10 by 3 days p.i. between untreated, unexposed mice and untreated, UV-exposed mice or steroid-treated, UV-exposed mice (Figure 6.14A-B). Nevertheless, there was a trending increase in CXCL10 expression in the brains of mice exposed to UV prior to infection by 4 days p.i. and this matches the increase in virus quantities in these mice, shown earlier (Figure 6.11). It is likely that these changes did not reach statistical significance due to the large amounts of variation evident.

The increased quantities of virus in the brains of UV-exposed mice by 4 days p.i. suggests either more efficient dissemination of virus to brain, or perhaps also that there is an inadequate antiviral response in the brains of this mice. Therefore, we also investigated expression of a key antiviral ISG, RSAD2, to interrogate whether perhaps suppression of the antiviral response in the brain during UV-mediated enhancement of infection could explain the higher quantities of virus observed here. RSAD2 was expressed at similar levels in the brain across experimental groups, at days 3 or 4 p.i. (Figure 6.14C-D). However, as Type I IFNs are induced by the presence of virus, it would be expected that there would be higher expression of ISGs in the brains of UV-exposed mice by 4 days p.i. due to the increase in virus RNA in the brain by this timepoint. Therefore, we cannot completely rule out inhibition of the antiviral response in the brain as a mechanism by which susceptibility to arbovirus infection is increased in mice following a UV exposure.

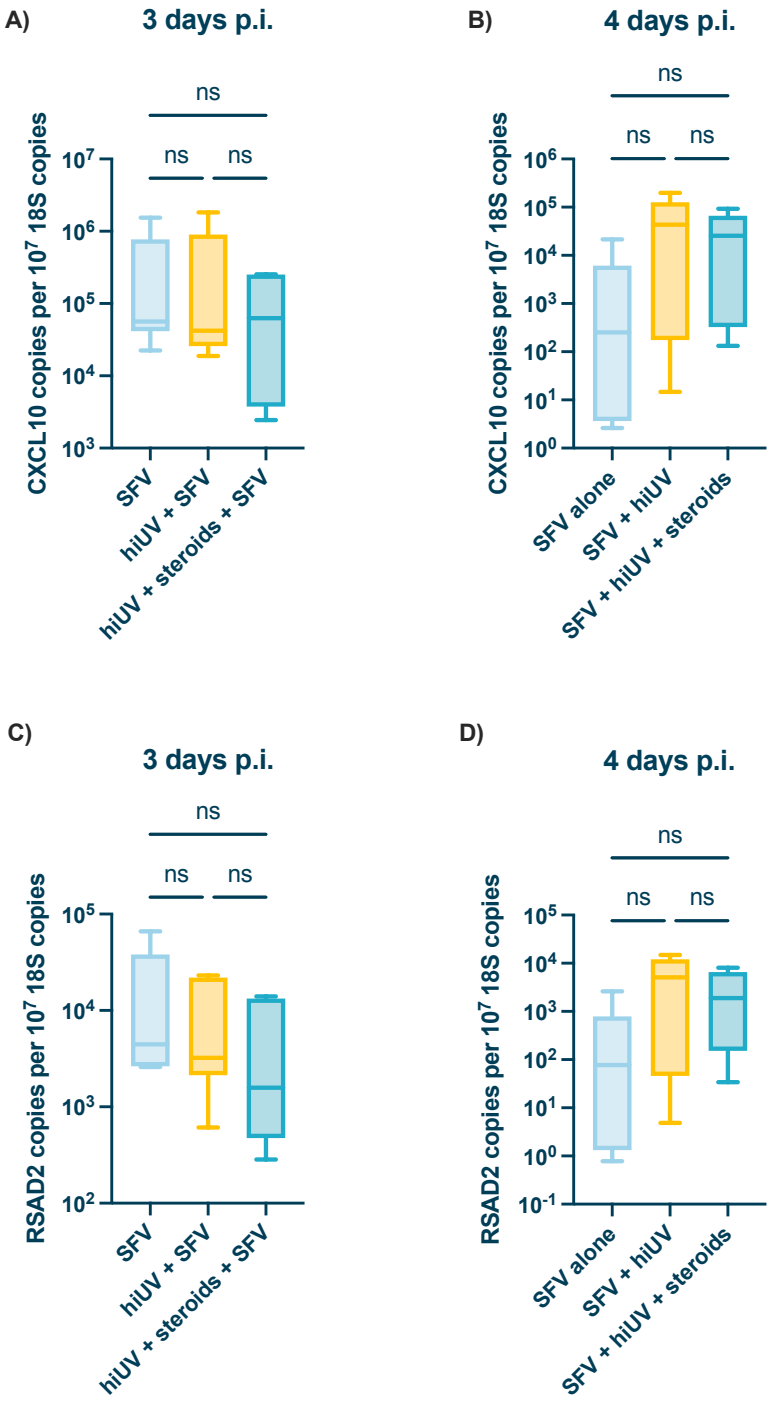

Figure 6.14 | No change in expression of T cell chemoattractant or key antiviral ISG, RSAD2, in brains of UV-exposed mice at 3-4 days p.i.

(A-D) CXCL10 **(A, B)** or RSAD2 **(C, D)** copy number in brain at 3 days p.i. **(A, C)** or 4 days p.i. **(B, D)**. 1 week prior to infection, skin on the upper left feet of mice exposed to erythemal UV ± topical steroid treatment of burn twice daily, starting 1h post-UV. The burn site was exposed to biting mosquitos and infected with 10^4 PFU of SFV4 s.c. 1 week after UV exposure. Mice were monitored and culled 3 or 4 days p.i. (n = 6)

Plots show the median value ± interquartile range. Data were analysed using Kruskal-Wallis test with Dunn's multiple comparison test (*ns* = *not significant*).

6.6 Summary and conclusions

To conclude our investigations into UV-mediated enhancement of arbovirus infection, we sought to understand whether this phenotype could be reversed through the use of anti-inflammatory treatments against sunburn. We initially tested Vitamin D in this capacity. This molecule has been put forward as a new option for treating sunburn, due to the its anti-inflammatory effects on sunburn in mice and humans[397,407]. We hypothesised that this interference by vitamin D in the inflammatory processes following a UV exposure could protect from the UV-mediated enhancement of infection observed in mice in previous chapters. We adapted our existing *in vivo* model of UV exposure to investigate this, by adding a single injection of vitamin D at the burn site 1h after the exposure.

Initial observations of the vitamin D-treated UV burn by 1-week post-UV were promising, as the lesion appeared to be healing more quickly than an untreated UV-burn at the same timepoint (Figure 6.1). This was further supported by our findings that vitamin D treatment of the burn limited epidermal thickening by 1-week post-UV, a key feature of sunburn (Figure 6.2). This reduction in the thickness of the epidermis compared to untreated skin by 1-week post-UV could be critical, as it suggests that vitamin D has driven accelerated wound healing. As we believe that wound healing processes are involved in enhancement of infection in UV-exposed skin at 1-week post-UV, as we postulated in Chapter 4, this was a positive sign that vitamin D treatment of the UV burn may reverse UV-mediated enhancement of infection. Additionally, the treatment was well tolerated by mice, giving it further credence as a potential therapeutic option.

However, vitamin D treatment did not alter the numbers of inflammatory myeloid cells present in the skin by 1-week post-UV (Figure 6.3). As we have shown in previous chapters, we believe that the increased presence of inflammatory leukocytes in the skin post-UV likely contribute to UV-mediated enhancement of infection. Therefore, the persistent presence of these cells in the skin post-UV, despite vitamin D treatment of the UV burn, was the first sign that this treatment may not be effective at reversing UV-mediated enhancement of infection. This theory was confirmed when we infected mice which had been UV-exposed and treated with vitamin D 1-week prior to infection. We found that vitamin D

treatment did not protect from enhanced susceptibility to SFV infection in UV-exposed mice, either in terms of virus RNA in the skin or infectious virus in the blood (Figure 6.4). Therefore, despite the promising changes on the tissue structure in vitamin D treated skin, this treatment had no impact on UV-mediated enhancement of arbovirus infection, disproving our initial hypothesis.

Although surprising, there are several reasons why this may be. Despite causing a measurable reduction in inflammation in the skin, shown in our work here and by Das *et al.* in 2019, when injected 1h post-exposure, this may be too early to have a lasting impact on skin by the time virus infection takes place 1-week later. Additionally, the mice were only given one dose of vitamin D and so repeating the treatment throughout the week between UV exposure and infection may promote the anti-inflammatory effects for longer or heal the wound quicker, which may be of benefit in terms of protecting from infection. In future, we could trial giving the dose later post-exposure or repeating the treatment, as was done with the corticosteroid treatment of the burn. This would further define whether vitamin D treatment is able to curb the increased susceptibility to arbovirus infection observed in UV-exposed mice.

Furthermore, when vitamin D treatment of sunburn had previously been trialled in mice, the molecule had been injected i.p., allowing it to reach the bloodstream and spread systemically. Whereas we injected it s.c. at the burn site as we wanted to concentrate the anti-inflammatory effect here. However, perhaps the systemic impact of vitamin D would have aided the host in terms of protecting from infection.

Nevertheless, our findings may also shed some light on the mechanism driving UV-mediated enhancement of infection at 1-week post-UV. We had discussed, in Chapter 4, the possibility that M2 macrophages may be involved in the phenotype. Vitamin D treatment of sunburn in mice improves anti-inflammatory M2 macrophages[397]. However, as the same treatment regimen does not protect from the increase in susceptibility to arbovirus infection by 1-week post-UV-mediated, these responses may not represent the limiting factor that defines UV-mediated enhancement of infection at this timepoint.

Interestingly, outside of the context of UV-exposed skin, vitamin D did provide protection from SFV infection when the infection took place in resting skin, evidenced by lower quantities of virus in the skin of mice treated with vitamin D 1-week prior to infection (Figure 6.4). Further investigation into the mechanism underlying this is outside the scope of this study. However, since we have shown that other pro-inflammatory factors, such as a mosquito bite[120], enhance arbovirus infection, it could be that the anti-inflammatory environment in the skin following vitamin D treatment benefits the host in terms of immunity against SFV infection.

We next trialled topical corticosteroids in a similar way. Following an initial pilot experiment, we observed that the steroid-treated burn looked much less inflamed and closer to being fully healed than both the untreated UV burn and the vitamin D-treated UV burn (Figure 6.1). This treatment looked even more promising when we analysed skin histology and found that the steroids had limited much of the damage done to the structure of the skin by 1-week post-UV (Figure 6.5).

Based on these findings, we next moved on to testing corticosteroid treatment of the UV burn prior to infection would limit the increase in susceptibility to arbovirus infection experienced by UV-exposed mice by 1-week post-UV. While steroid treatment did not significantly reduce quantities of virus in the skin by 24hpi, during the early stage of UV-mediated enhancement of infection, steroid-treated mice did have significantly lower quantities of infectious virus in serum compared to untreated, UV-exposed mice (Figure 6.6). This suggests the treatment is either stopping virus leaving the skin and spreading to the blood or improving neutralisation of virus in the blood once it gets there, for example through generation of a more effective antibody response.

One way in which viremia could be reduced is through a reduction in the number of myeloid cells, as neutrophils contribute to vascular permeability and monocytes are susceptible to arbovirus infection[408]. As corticosteroids are highly immunosuppressive, we considered whether this could be happening here. However, there was no change in the number of neutrophils or monocytes in UV-exposed skin following steroid treatment (Figure 6.7). However, we had

shown earlier in Chapter 4 that there are a higher number of proliferating cells in the skin by 1-week post-UV and that these are more susceptible to SFV infection. Therefore, examining whether steroid treatment alters the numbers of replicating cells, such as fibroblasts, by 1-week post-UV would be a crucial next step to understanding the impact this treatment has.

We also briefly examined induction of the Type I IFN system at the skin to determine whether this was altered following steroid treatment of the UV burn but there was no difference in expression of IFN-β or of the quintessential ISG, RSAD2 (Figure 6.8). This suggests that interference with the antiviral Type I IFN system is not involved in the changes in viremia observed in steroid-treated mice during UV-mediated enhancement of infection.

Next, we sought to determine whether corticosteroid treatment of the UV burn drives systemic changes which could protect from infection at a site remote from the steroid-treated site, or whether the effect is localised. However, mice that had been UV-exposed on the foot skin and left untreated or steroid-treated at the same site but infected i.p. surprisingly had lower quantities of virus in serum (Figure 6.9). This suggests that UV exposure of the skin can alter the host's systemic susceptibility to arbovirus infection. UV exposure can drive systemic inflammation at sites separate from the UV-exposed area[296]. Importantly, UVB exposure of skin induces a potent type I IFN signature in the blood and remote tissues[298]. Although, this has only been demonstrated up to 24h post-exposure, if this systemic induction of type I IFN continues up to 1-week post-UV, this could be of great benefit to the host in terms of antiviral protection, as observed in our findings here. This could be further investigated by examining type I IFN and ISG expression in unexposed tissues, such as the spleen, and blood from UV-exposed mice at 1-week post-UV, in the absence of virus infection.

Although we had shown repeatedly that virus spreads to the blood at higher quantities in UV-exposed mice, we had yet to determine whether an erythemal UV exposure 1-week prior to infection increases dissemination of arbovirus to other tissues. Additionally, our findings that steroid treatment of the burn following UV exposure limits viremia during subsequent SFV infection

suggested that this treatment may protect from systemic spread of the virus at later timepoints. Initially, when we examined virus RNA in the skin, spleen and brain by 3 days p.i., we found no difference in the quantity of RNA between unexposed and untreated mice, UV-exposed and untreated mice or UV-exposed, steroid treated mice (Figure 6.10). This led us to conclude that we may have looked too early post-infection to see any differences between the groups or that there may have been variation in other factors between mice, such as the magnitude and frequency of mosquito biting, which can be difficult to control.

Therefore, we next examined virus dissemination at 4 days p.i. Of the most clinical relevance, is our finding that showed an increase in virus reaching the brain in mice exposed to UV 1-week prior to infection (Figure 6.11) meaning that UV exposure at the inoculation site results in enhanced dissemination during systemic spread of the virus. As viral encephalitis is one of the most serious, and potentially lethal, consequences of arbovirus infection, the higher quantities of virus in the brain of UV-exposed mice during infection has potentially serious implications for health[118,120,406]. However, SFV is particularly efficient at replicating within the brain, therefore, this effect may not necessarily apply to other arboviruses, such as DENV[117]. Mice with higher quantities of virus in the brain have increased mortality as a result of SFV infection[119,120]. Therefore, it is likely that UV-exposed mice may also experience higher rates of mortality following SFV infection, due to the high quantities of virus in their brains. However, we would need to carry out a survival experiment to confirm this. It would also be useful to repeat this experiment at a lower dose of SFV, as this may allow us to see a greater difference in responses between experimental groups. It is possible that the dose used here was so high that all mice were susceptible to dissemination, therefore making it difficult to discern the enhancing ability of UV exposure in this capacity.

We also found increased quantities of virus RNA in the skin in UV-exposed mice at the later timepoint of 4 days p.i. (Figure 6.11). Importantly, treatment with steroids reduced the quantity of virus RNA in the skin and dissemination to the spleen. Therefore, it seems that the impact steroids have on reducing replication at the inoculation site then prevents dissemination to some remote

tissues, such as the spleen. However, this was not sufficient to prevent this neurotropic virus from disseminating and replicating within the brain. Although it should be noted that quantities of virus in the brain of the steroid treatment group were more variable, suggesting that dissemination of virus to the brain may not be as reproducibly efficient in this group as compared to group not treated with steroids.

Virus can transit to remote tissues via the blood. Therefore, the increase in the quantity of virus reaching the brain in UV-exposed mice, shown in Figure 6.11, suggested that the generation of neutralising antibodies in serum may be somewhat dented in these mice. Accordingly, we found that serum taken from mice exposed to UV 1-week prior to infection offered much lower level of protection compared to unexposed mice (Figure 6.12). As steroid-treatment had lowered quantities of infectious virus in the blood by 24hpi compared to untreated, UV-exposed mice (Figure 6.6), we also considered whether treatment of the UV burn may result in a return to normal antibody production during infection. However, steroid treatment of the burn prior to infection did not restore serum-neutralising antibody levels (Figure 6.12). Together, these results suggest that antibody generation is blunted in UV-exposed mice and is not rescued by steroid treatment. Whether this impairment is due to the generation of a sub-neutralising antibody population or simply a lower antibody titre remains to be determined. Either way, it suggests that UV treatment at least partially interferes with coordination of adaptive immune response to virus.

As neutralisation of the virus in the blood is critical for preventing spread to the brain, this ablation of the antibody response could partly explain the increased spread of virus to the brain by 4 days p.i. in UV-exposed mice, observed in Figure 6.11. Additionally, while antibodies are crucial for initial clearance of the virus, generation of an effective neutralising antibody population can also offer long-term protection against secondary infection. Therefore, secondary immune responses may also be affected in these mice. However, it should be noted that generation of antibodies against some genetically related arboviruses are not necessarily always of benefit to the host. Generation of a sub-neutralising antibody response to DENV, for example, can lead to increased susceptibility to re-infection with other DENV serotypes via ADE of infection[409]. The presence of

bound non-neutralising antibody can facilitate entry of the virus in to target cells which possess FcRs, through binding of the Fc region of the antibody[410]. This has long been associated with DENV, however, there is evidence of this occurring during infection with a number of other arboviruses, including with genetically related ZIKV, and a separately with CHIKV [83,180,411].

As discussed earlier, higher viral loads in the brain are linked with reduced survival during SFV infection in mice. However, the cellular response to virus dissemination to the brain can also cause pathology, leading to arboviral encephalitis. If there is more virus in the brain, as is the case in UV-exposed mice, this may lead to more cells infiltrating this fragile site to help clear the virus and more damage as a result. Therefore, to conclude this chapter we assessed whether the brains of infected, UV-exposed mice had any signs of an increased inflammatory infiltrate. Accordingly, we found evidence of cellular infiltrate around vessels in the brains of mice exposed to UV prior to infection by 4 days p.i., but not in non-UV exposed mice or steroid treated mice (Figure 6.13). This was further supported by our finding that there was a higher number of cells found in the brains of UV-exposed mice during infection, compared to the other two groups. The increase in cells in the brains of UV-exposed mice during infection is likely linked to the higher quantities of RNA present in the organ. Additionally, steroid treatment of the UV burn prior to infection reduced the cellular infiltrate to the brain during infection. To ascertain whether this has an impact on limiting further pathology in these mice, a survival experiment over a longer period of time will have to be carried out.

To identify the recruited cell types, we examined levels of the CD8+ T cell chemoattractant CXCL10. However, there was no change in expression of this in the brain of UV-exposed mice by 4 days p.i. (Figure 6.14). Nevertheless, no change in the expression of the T cell chemoattractant does not rule out the presence of these cells in the cellular infiltrate observed in the brains of UV-exposed mice during enhanced arbovirus infection. However, the timepoint we examined may be too early for this cell type, as CD3+ T cells were shown to infiltrate the brain at 7 days p.i. during infection with another strain of SFV, A7(74)[412]. Further investigation needs to be carried out to phenotype the cellular

infiltrate in the brains of UV-exposed mice, including staining brain histology sections for CD3 using immunohistochemistry.

Expression of Type I IFNs have previously been shown to increase in accordance with SFV quantities in the brain by 3 days p.i.[117]. Therefore, we expected expression of the important ISG, RSAD2, to also be higher in mice exposed to UV prior to infection, due to the higher quantities of SFV RNA evident in the brain by 4 days p.i. (Figure 6.11). However, this was not the case; RSAD2 expression in the brain was no higher in UV-exposed mice than unexposed mice (Figure 6.14). This provides some evidence that the antiviral response to virus in the brain may not be as efficiently induced in UV-exposed mice, which could be contributing to the higher quantities of virus observed in the brain of these mice by 4 days p.i.

Overall, this chapter built on previous findings that UV-exposed mice experience increased susceptibility to arbovirus infection by 24hpi, by showing that mice which are exposed to erythemal UV 1-week prior to infection also undergo enhanced dissemination of virus to remote tissues, including the brain, during systemic SFV infection by 4 days p.i. Additionally, mice had signs of an increased cellular infiltrate to the brain, a sign of arbovirus pathology, and ablated serum-neutralising antibody generation. Together, these findings suggest that UV-mediated enhancement of infection could result in more clinically severe arbovirus infection.

Furthermore, we tested two sunburn treatments, vitamin D and topical corticosteroids, in an attempt to reverse UV-mediated enhancement of infection. We found that vitamin D had no effect in this capacity. However, steroid treatment of the burn prior to infection seemed to offer partial protection from the increase in susceptibility to infection observed in UV-exposed mice. This treatment limited viremia at the skin by 4 days p.i. and this led to protection from spread to the spleen and decreased cellular infiltrate to the brain. Importantly though, this did not limit dissemination to the brain or restore neutralising antibody levels in the blood, and this spread is critical in terms of causing serious diseases. Therefore, it is too early to say whether there are clinical benefits of steroid treatment to protect against UV-mediated enhancement of

infection. Furthermore, the feasibility of using steroid treatment as a means of protecting against UV-mediated enhancement of infection in humans remains questionable. Long-term use of steroids can cause a severe reaction in the skin upon withdrawal, for example in chronic disease like eczema and psoriasis where the treatment is used for long periods of time[413]. Therefore, the regular use of these following sun exposure in areas of arbovirus endemicity regularly may not be advisable as the small benefits may not outweigh the risks in this scenario. Nevertheless, they may be of use short-term in individuals with sunburn as a preventative measure against severe arbovirus infection, if the benefits are supported by further investigation.

Chapter 7: PBMCs from patients with psoriasis, an inflammatory skin condition, exhibit different susceptibility to ZIKV infection

7.1 Introduction

There are numerous factors which have the potential to impact susceptibility of a host to arbovirus infection. These can derive from the environment, such as UVR, or from the virus-transmitting vector, like mosquito saliva. However, these can also result from variability within the host itself. Infection of the skin by arboviruses is the first stage in the virus life cycle in the vertebrate host. We have shown in previous published works and in this thesis that factors which impact inflammation within the skin prior to infection can modulate susceptibility to arbovirus infection[119,120,126]. Therefore, one important host factor to consider in this context, is the presence of pre-existing inflammation at the skin because of inflammatory disease.

There are numerous inflammatory conditions which involve the skin, of which psoriasis is one of the most prevalent. The most common clinical presentation of the disease is the formation of inflamed skin lesions or 'psoriatic plaques'[207]. The pathogenesis of psoriasis is dependent on complex interactions between immune cells, their positioning and their production of cytokines. It is largely thought to be primarily Th1 and Th17 T cell driven, as biologic therapies that target cytokines produced by these cells have proven to be therapeutic in patients with psoriasis[257]. However, the pathogenesis is also characterised by dysregulated type I IFN function, making it of particular relevance to our work investigating arbovirus immunity[267]. Our group previously found that therapeutic induction of type I IFN pathways, at an earlier timepoint following arbovirus infection, significantly reduces arbovirus dissemination[119]. Therefore, the type I IFN dysregulation in psoriasis, although detrimental in terms of causing disease, could actually be of benefit to the host during arbovirus infection through pre-priming of the antiviral response.

The impact inflammatory skin diseases have on susceptibility is highly variable between conditions. For example, patients with eczema, another inflammatory skin condition, are known to have heightened risk of contracting certain infections, including a severe form of HSV infection[414]. However, psoriasis patients are less susceptible to some infections[415,416]. Patients with psoriasis have been shown to be more resistant to virus infection than eczema patients,

suggesting that this disease state may instead offer protection against skin-transmitted viruses[417]. Although whether psoriatic skin is more resistant to infection than healthy control skin remains to be seen. A previous member of our group, Stephen Bryden, found that that explants from lesioned skin from psoriasis patients are less susceptible to ZIKV infection ex vivo than those from patient-matched non-lesioned skin (unpublished data). This suggests the immune characteristics of psoriasis are beneficial to host immunity during arbovirus infection. Although, the specific aspects of this immunological profile, or whether other key cell types infected by virus, such as PBMCs, exhibit similar resistance to infection, remain to be uncovered.

Psoriasis is known to have a widespread impact that reaches far beyond the skin. Most new lesion development occurs in areas of otherwise healthy-looking skin, suggesting a systemic predisposition to develop lesions exists[418]. Furthermore, it should be noted that patients with psoriasis are also more prone to develop a multitude of other diseases, including psoriatic arthritis, cardiovascular disease and inflammatory bowel disease, suggesting a systemic component to the disease[419–421]. Indeed, aberrant cytokine expression in psoriasis patients is not restricted to lesional skin, it also extends to the blood[286]. Transcriptomic analysis of the blood of psoriasis patients has described the gene profile of these samples as inflammatory and particularly enriched in genes associated with the inflammasome and neutrophils, both key components of the innate immune response[288]. In terms of arbovirus infection in blood, monocytes and DCs are the main targets of infection and this can facilitate virus dissemination to remote sites[142,422,423]. Indeed, the most frequent infected cell type in ZIKV-infected patient blood are monocytes. Monocytes and DCs, together with lymphocytes, form the PBMC compartment in blood. Together, this suggests that susceptibility to infection may also be altered in PBMCs in the blood of psoriasis patients.

7.1.1 Hypothesis and aims

The evidence outlined here led us to hypothesise that the systemic immune dysregulation observed in psoriasis patients would provide PBMCs from these patients with more resistance to arbovirus infection, compared to healthy controls.

Therefore, this chapter aims to:

1) **Establish optimal conditions for ZIKV infection of human PBMCs *in vitro***
2) **Investigate susceptibility to ZIKV infection in psoriatic PBMCs compared to healthy PBMCs**
3) **Characterise gene expression in psoriatic PBMCs compared to healthy PBMCs, before and after ZIKV infection**

7.2 Optimisation of ZIKV infection of human PBMCs *in vitro*

To begin with, the protocol for infecting PBMCs with ZIKV was optimised to determine conditions under which to run subsequent experiments. Initially, ZIKV stocks were grown in BHK-21 cells, a common mammalian cell line frequently used to grow arbovirus stocks. This produced robust titers of ZIKV, measured as $4.375x10^8$ PFU/ml via a plaque assay. To ascertain whether this ZIKV stock would infect PBMCs *in vitro*, isolated human PBMCs were infected at an MOI of 1 with BHK-derived ZIKV for 16h. Unexpectedly though, this failed to produce detectable quantities of viral RNA in the cells 16hpi (Figure 7.1A). To test whether infecting the PBMCs with a higher concentration of virus would make them more permissive to infection, cells were infected with 100-fold more virus than previously. However, this still did not result in quantities of virus much higher than the limit of detection. We had stocks of ZIKV that had been grown in C6/36 insect cells, derived from larvae of the Aedes albopictus mosquito, by a previous lab member. The infectivity of this virus derived from C6/36 insect cells in PBMCs was tested. In contrast to BHK-derived ZIKV, when cells were infected with C6/36-derived ZIKV at an MOI of 1, viral RNA was present in high quantities in PBMCs 16hpi. As a result, the decision was made to use C6/36-derived ZIKV in future PBMC infection experiments. Several publications investigating ZIKV infection of PBMCs also use C6/36 cells to generate virus stocks[424–426].

Initially, we set out to determine the optimal MOI of virus to use and length of time to run infections for at which evidence of infection would be clear but cells would not be overloaded with virus. To do this, isolated PBMCs were infected

with ZIKV at a range of MOIs for either 6h or 16h before analysing quantities of viral RNA present within cells. There was no difference in the amount of virus RNA in cells between 6hpi and 16hpi, suggesting that either timepoint would be an effective choice (Figure 7.1B). Additionally, the 10-fold difference in viral RNA quantities observed between cells infected at different MOIs correlates with the 10-fold reduction in the concentration of virus that the cells were infected with. This indicated that any of these three MOIs would be suitable for use in future experiments.

Although this data shows reproducible evidence of ZIKV RNA at both time points, we chose to concentrate on 16hpi as this was most suitable for infecting cells post collection from the clinic. Additionally, the decision was made to undertake future experiments at an MOI of 0.1 and an MOI of 0.01 to allow for the observation of differences in the capacity of cells to support virus replication, thus allowing us to determine differences in susceptibilities between individuals. All ZIKV experiments were run under these conditions.

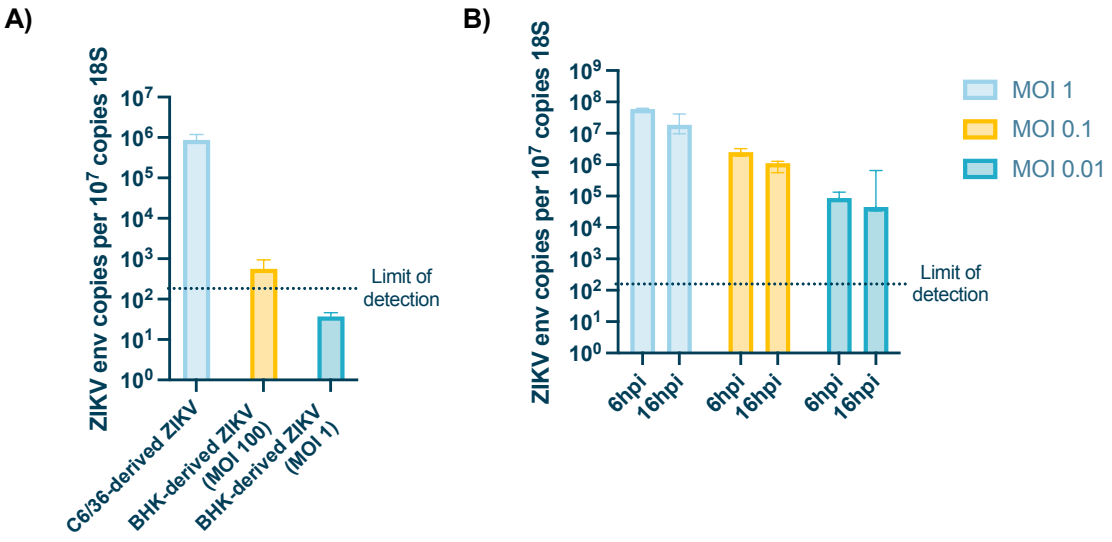

Figure 7.1 | ZIKV derived from a mosquito cell line, but not a mammalian cell line, is able to infect PBMCs

(A) Quantities of viral RNA present in PBMCs 16hpi. PBMCs were infected with either ZIKV grown in C6/36 cells (MOI of 1) or with ZIKV grown in BHK-21 cells (MOI of 1 or 100) for 16h. (*n* = *2*)

(B) Quantities of viral RNA present in PBMCs 6hpi or 16hpi. PBMCs were infected with C6/36- derived ZIKV at a range of MOIs (1, 0.1 or 0.01) for the indicated length of time. (*n* = *3*)

PBMCs isolated from healthy control donor blood samples. ZIKV RNA (*env* gene) copy number was determined by qPCR. Plots show the median value ± interquartile range. Dotted lines represent the assay's limits of detection based on qPCR values taken from samples of uninfected cells.

As a proof of principle, we wanted to explore what impact prior immune stimulation has on ZIKV infection of PBMCs. Therefore, healthy donor PBMCs were pre-treated with the TLR7 agonist, imiquimod, prior to infection. However, pre-treatment with imiquimod had no significant effect on the quantity of viral RNA present in the cells by 16hpi (Figure 7.2A). Subsequently, a second innate immune agonist was tested, poly(dA:dT). This agonist activates both RIG-I, MDA5 and cGAS-STING signaling, receptors which are more widely expressed than TLR7, meaning this treatment works better to model the widespread inflammatory state observed in psoriasis patients. Here, poly(dA:dT) was applied to cells 1h prior to infection with ZIKV at a range of doses to ensure that any effects of the treatment on the infection outcome were not missed by incorrect dosing of the agonist. Interestingly, pre-treatment with poly(dA:dT) significantly reduced quantities of ZIKV RNA present in the PBMCs by 16hpi, when compared to cells that were infected but not stimulated with the agonist (Figure 7.2B). Notably, there was no apparent difference in this effect between doses, suggesting that the effect of poly(dA:dT) stimulation has reached its maximum potential at the doses tested here. Nevertheless, the effect observed here further supports the data already gathered by our group that an inflammatory, primed state prior to infection, whether in psoriatic lesions or modelled in PBMCs using poly(dA:dT), offers resistance to ZIKV infection. Although whether this affects production of infectious virus by these cells remains to be seen.

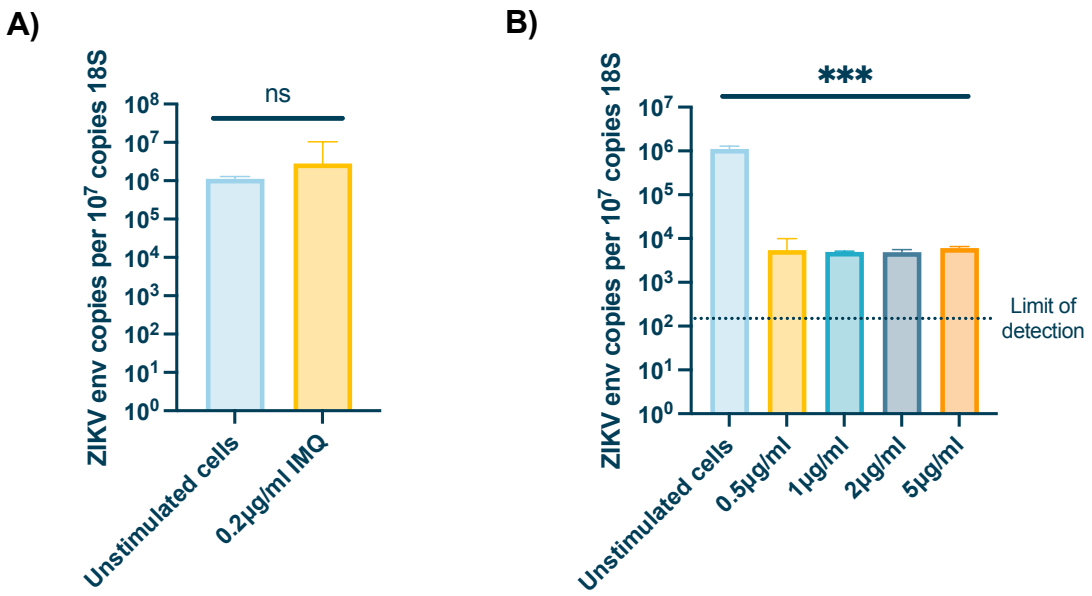

Figure 7.2 | Pre-treatment of PBMCs with an innate immune agonist protects against ZIKV infection

(A, B) Quantities of viral RNA present at 16hpi in PBMCs pre-treated with 0.2µg/ml of imiquimod (IMQ) **(A)** or poly(dA:dT) at a dose of either 0.5µg/ml, 1µg/ml, 2µg/ml or 5µg/ml **(B)** 1h prior to infection with C6/36-derived ZIKV at an MOI of 0.1. PBMCs isolated from healthy control donor blood samples. (*n = 3*)

ZIKV RNA (*env* gene) copy number was determined by qPCR. Plots show the median value ± interquartile range. Dotted lines represent the assay's limits of detection based on qPCR values taken from samples of uninfected cells. Data were analysed using Mann-Whitney test **(A)** or Kruskal-Wallis test with Dunn's multiple comparison test **(B)** (*ns = not significant, ***P < 0.001*).

7.3 PBMCs from psoriasis patients, an inflammatory skin disease, exhibit increased protection from ZIKV infection

Based on our initial finding that pre-priming of healthy PBMCs prior to infection offered cells protection against ZIKV infection, we hypothesised that PBMCs from psoriasis patients may also be less susceptible to ZIKV infection. Although psoriasis primarily affects the skin, the disease can also have profound systemic effects, as covered in the chapter introduction. In particular, the transcriptome of PBMCs from patients with psoriasis shows a high level of dysregulation, characterised by a pro-inflammatory signature. Therefore, this led us to postulate that the systemic inflammatory nature of psoriasis may lead to PBMCs being pre-primed against virus infection. To investigate this, we isolated PBMCs from blood samples taken from psoriasis patients with active

disease or healthy control donors. We accepted patients regardless of their treatment regimen; the individuals in the cohort ranged from not receiving any treatment for their disease to the use of non-biologics, e.g. methotrexate, to biologics, e.g. Adalimumab, a TNF-α inhibitor. Crucially, as all patients had active disease, any treatment used had failed to control disease. The two groups, psoriasis patients and healthy donors, had similar age and sex distribution (Table 7.1).

Table 7.1 | Homogeneity test between experimental and control group

Details of the sex and age distribution in the experimental (psoriasis patient) and control (healthy donor) groups. Chi-squared (χ^2) values and degrees of freedom were used to calculate a *p*-value for each variable to rule out ($P < 0.05$) any statistical difference between the two populations.

Variable	**Category**	**Total (n = 19) N (%) or M ± SD**	**Experimental (n = 12) N (%) or M ± SD**	**Control (n = 7) N (%) or M ± SD**	**χ^2**	***p*-value**
Sex	Male	10 (52.6)	6 (50.0)	4 (57.1)	0.09	0.76
	Female	9 (47.4)	6 (50.0)	3 (42.9)		
Age (years)		39.3 ± 11.0	40.7 ± 11.0	36.9 ± 10.5	3.96	0.86

The PBMCs were infected with ZIKV and lysed at 16hpi. RNA was extracted from the cell lysate and used to assess ZIKV RNA quantities using qPCR. Interestingly, when cells were infected with ZIKV at an MOI of 0.1, the psoriasis patient PBMCs had significantly less virus RNA present by 16hpi than those taken from healthy donors (Figure 7.3A). To check that this effect was not dependent on virus dose, we also infected cells with a lower MOI of ZIKV, 0.01. However, the same reduction in virus RNA in psoriasis patient PBMCs compared to healthy controls was observed when a lower dose was used (Figure 7.3B). This demonstrates that psoriasis patient PBMCs are more resistant to ZIKV infection than those from healthy individuals *in vitro*.

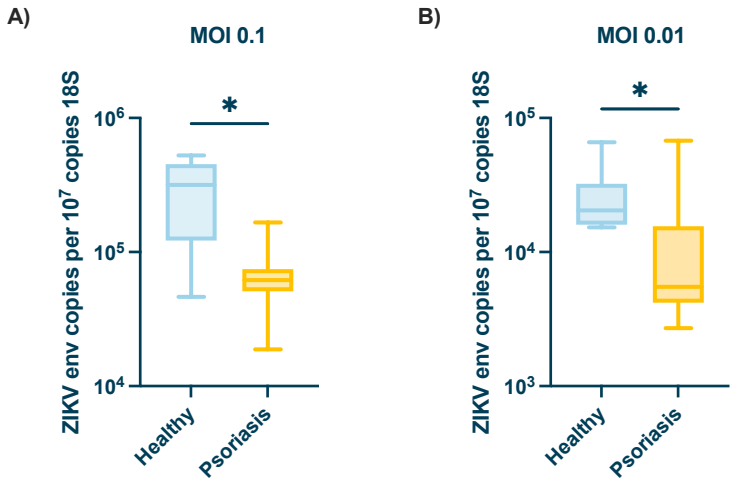

Figure 7.3 | PBMCs from psoriasis patients are less susceptible to arbovirus infection

(A, B) Quantities of viral RNA present at 16hpi in PBMCs infected with ZIKV at an MOI of 0.1 **(A)** or 0.01 **(B)**. PBMCs isolated from psoriasis patient *(n=12)* or healthy control donor *(n=7)* blood samples.

ZIKV RNA (*env* gene) copy number was determined by qPCR. Plots show the median value ± interquartile range. Data were analysed using Mann-Whitney test (*$P < 0.05$).

A key hallmark of psoriasis development is dysregulation of the type I IFN system[267]. Although this hypothesised to contribute towards disease in patients, this dysregulation could contribute to enhanced protection against infection, as observed in the previous figure. Therefore, we set out to characterise expression of the type I IFNs and associated ISGs in PBMCs during ZIKV infection using qPCR. IFN-α quantities were significantly higher in PBMCs from psoriasis patients by 16hpi compared to those from healthy donors (Figure 7.4A). There was no significant difference in expression of the other key type I IFN, IFN-β, between the two groups, although there was a trending increase in expression of this gene in psoriasis patient PBMCs, although there was great variation within the group. The type I IFNs stimulate antiviral responses in cells through induction of ISGs. Interestingly though, when IFN-α and IFN-β expression was examined at rest, there was no difference in quantities of either between PBMCs from psoriasis patients and healthy donors (Figure 7.4B). This suggests that psoriasis patient PBMCs are better able to induce type I IFN when stimulated with virus during infection.

Therefore, as we had found an increase in IFN-α in psoriasis patient PBMCs during infection, we also quantified ISG expression to see if there was a corresponding increase in these antiviral genes. Despite not being statistically significantly different, there was a 100-fold difference in the median expression quantity of the ISGs RSAD2 and CXCL10 in psoriasis patient PBMCs by 16hpi, compared to those from healthy donors (Figure 7.4C). We also investigated whether key antiviral pattern recognition receptors, RIG-I and MDA5, are upregulated in psoriasis patient PBMCs during infection, as an increase in expression of those could lead to an increase in virus detection, which could partially explain the more efficient clearance of virus observed in these cells. Additionally, RIG-I is induced by type I IFN and so can provide further insights in to the role of this system in the phenotype observed. There was a significant increase in expression of RIG-I in PBMCs from psoriasis patients during infection compared to healthy controls, but no significant difference in quantities of MDA5. Together, this shows that PBMCs from psoriasis patients had more profound induction of IFN-α during infection and this resulted in higher expression of the IFN-inducible PRR RIG-I which can recognise ZIKV and kickstart downstream responses against the virus.

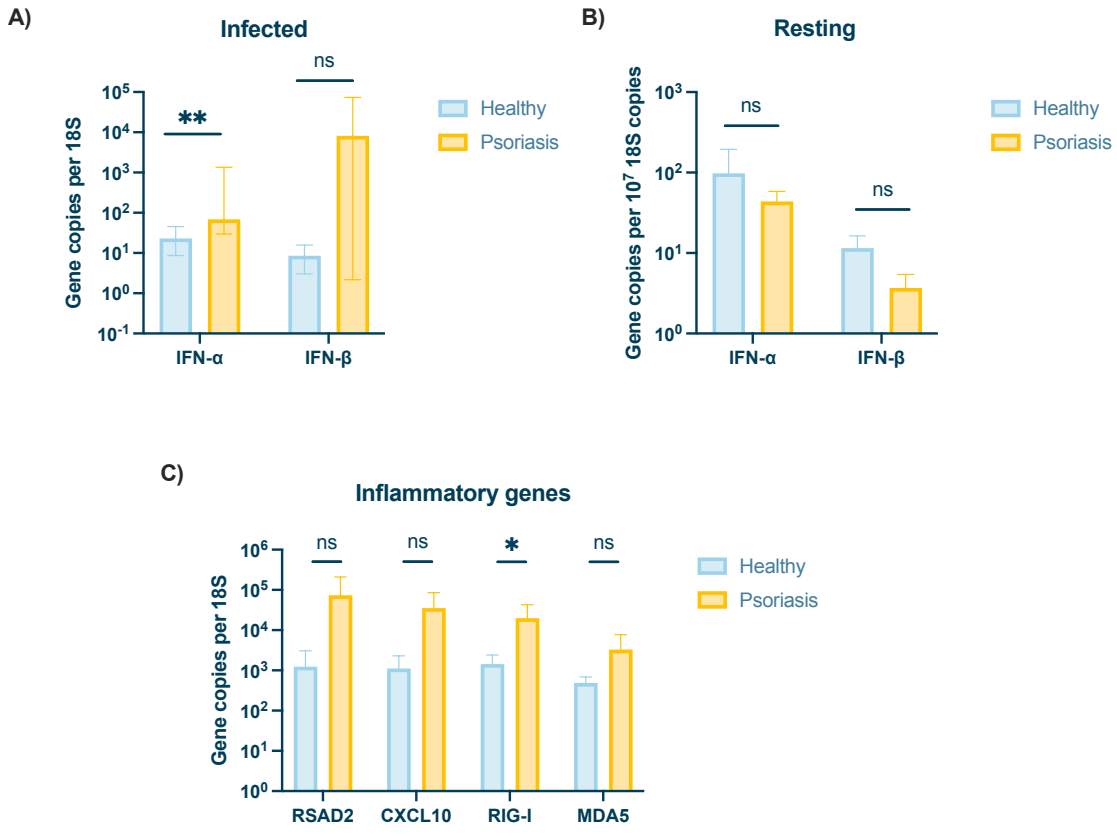

Figure 7.4 | Psoriasis patient PBMCs have a more robust induction of key antiviral genes post-infection

(A-C) IFN-α and IFN-β **(A, B)** or inflammatory **(C)** gene expression at rest **(B)** or at 16hpi **(A, C)** in PBMCs infected with ZIKV at an MOI of 0.01. PBMCs isolated from psoriasis patient *(n=12)* or healthy control donor *(n=7)* blood samples.
Gene expression was determined by qPCR. Plots show the median value ± interquartile range. Data were analysed using Mann-Whitney test (**P < 0.05, **P < 0.01*).

Psoriasis can vary greatly between individuals in terms of its severity. This is measured by clinicians using the Psoriasis Area and Severity Index (PASI), which takes in to account the surface area of the body which is covered with lesions and also how severe the lesions are[257]. More severe disease presentations result in higher PASI scores. Our data thus far suggests that the inflammatory environment state in individuals with psoriasis, although detrimental in terms of disease, seems to prime cells to better respond to virus infection. Therefore, we hypothesised that PBMCs from patients with more severe forms of disease may show increased protection against virus. Using each patient's PASI score as an indicator of disease severity, we investigated whether there was such a link between the two. Overall, our patient cohort had particularly severe symptoms, with an average PASI score of 12.7, where a score greater than 10 is an indicator of severe disease. However, there was no correlation (R^2 = 0.01686) between PASI score and quantities of virus RNA in PBMCs by 16hpi (Figure 7.5A). Most of the samples were clustered together in terms of virus load. In fact, PBMCs from one patient with completely resolved symptoms had similar quantities of virus RNA to the rest of the cohort. This suggests that there is no link between protection from virus and the clinical parameters used to define PASI score/disease severity.

Due to the highly immunologic nature of the disease, the main treatment options for psoriasis are immune-modulators, whether it be anti-inflammatory steroids or biologics against key cytokines such as TNF-α, IL-17 and IL-23. Analysing whether cells from patients receiving these interventions exhibit difference in ZIKV susceptibility, provides a powerful way to investigate the role of these immune pathways in the protection from ZIKV infection. Here, we isolated

PBMCs from untreated patients or treated patients, infected cells with ZIKV as before, and assessed virus RNA in cells at 16hpi. Surprisingly, there was no difference in quantities of virus between treated and untreated patient PBMCs following infection with ZIKV at a high (MOI 0.1) or low (MOI 0.01) dose (Figure 7.5A-B). Therefore, blunting of the immune system via psoriasis treatment did not affect the protection against ZIKV infection observed in psoriasis patient PBMCs.

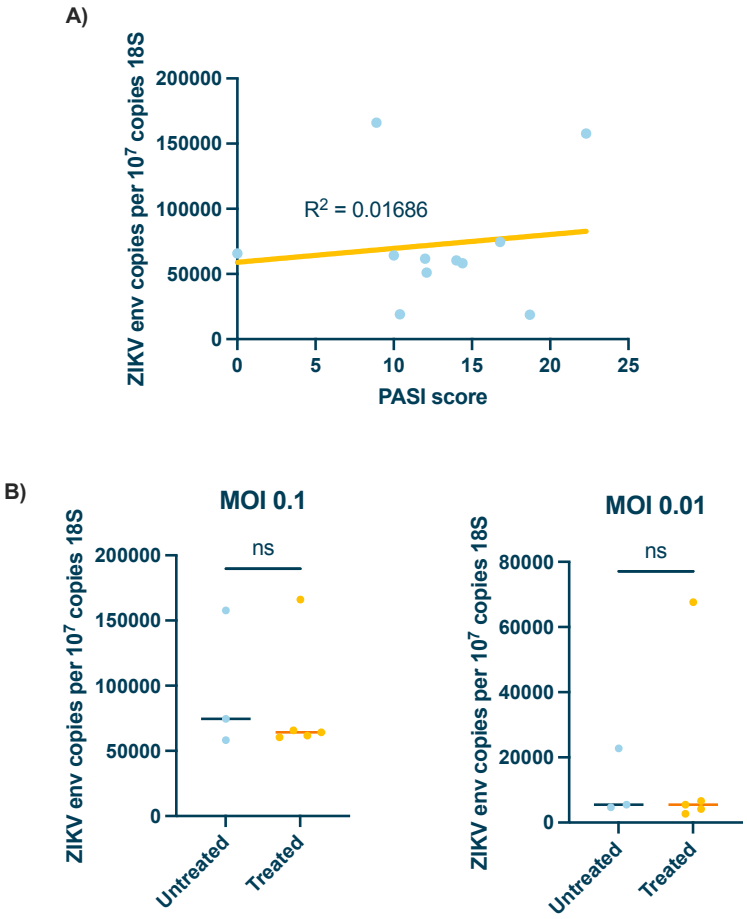

Figure 7.5 | Clinical indicators are not associated with protection from infection

(A, B) PBMCs from psoriasis patients were infected with ZIKV at an MOI of 0.1 **(A, B)** or 0.01 **(B)**. Quantities of ZIKV RNA present in cells at 16hpi was measured and compared against the patients PASI score **(A)** or between patients on immunosuppressant drugs (Treated) and those not on immunosuppressant drugs (Untreated) **(B)**. ZIKV RNA (*env* gene) copy number was determined by qPCR. Plots show the median value ± interquartile range. Data were analysed using Mann-Whitney test (*ns* = *not significant*).

7.4 PBMCs from patients with systemic sclerosis, a systemic inflammatory disease, are also partially protected from ZIKV infection

After confirming that PBMCs from patients with psoriasis, an inflammatory skin condition, are protected from ZIKV infection, we considered whether this effect is specific to psoriasis or whether it may extend to other inflammatory diseases. Systemic sclerosis is an inflammatory systemic disease which causes extensive fibrosis across the body[270]. While the skin and joints are the main affected organs, this can impact the blood and internal organs as well. Like psoriasis, type I IFN is also implicated in the pathogenesis of systemic sclerosis[427]. An IFN score can be used to stratify patients to help indicate whether a patient is at risk of developing more severe disease[284]. This clear association between type I IFN and systemic sclerosis outcomes, led us to consider whether PBMCs from patients with systemic sclerosis may also have altered susceptibility to arbovirus infection.

To investigate this, we isolated PBMCs from blood samples from systemic sclerosis patients and from healthy donors and infected these with ZIKV for 16h, before RNA was extracted from cells. Initially, when PBMCs were infected at the higher MOI of 0.1, there was a trend for less virus RNA in the systemic sclerosis patient PBMCs, although not reaching statistical significance, by 16hpi, compared to those from healthy donors (Figure 7.6A). Following infection with a lower dose of ZIKV (MOI 0.01), a statistical difference between the two groups was clear. Here, there were significantly lower quantities of virus RNA present in the PBMCs from systemic sclerosis patients compared to healthy donor cells (Figure 7.6B). Therefore, systemic sclerosis patient PBMCs also show protection from ZIKV infection. However, protection was restricted to specific virus doses and the effect was less substantial than that observed in PBMCs from psoriasis patients.

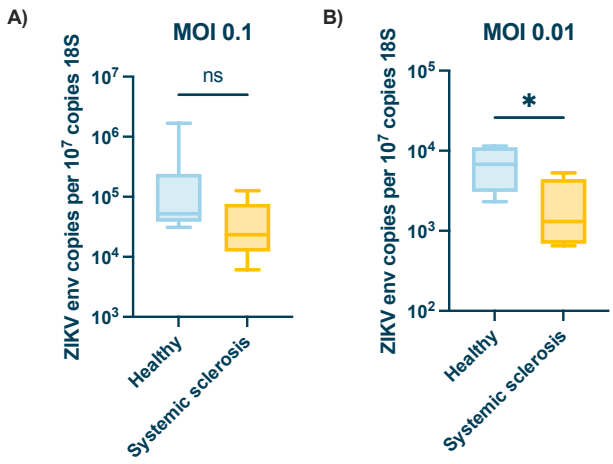

Figure 7.6 | Systemic sclerosis patient PBMCs are partially protected from ZIKV infection

(A, B) Quantities of viral RNA present at 16hpi in PBMCs infected with ZIKV at an MOI of 0.1 **(A)** or 0.01 **(B)**. PBMCs isolated from systemic sclerosis patient *(n=10)* or healthy control donor *(n=7)* blood samples.

ZIKV RNA (*env* gene) copy number was determined by qPCR. Patient samples were collected by Prof Francesco Del Galdo and Dr Stefano Di Donato. Plots show the median value ± interquartile range. Data were analysed using Mann-Whitney test (*ns = not significant, *P < 0.05*).

We had shown in Figure 7.4 that type I IFNs were more robustly induced in psoriasis patient PBMCs during ZIKV infection and that this likely contributes to the protection against infection observed in these cells. Since type I IFN is an inherent part of the driving mechanisms behind both psoriasis and systemic sclerosis, we also interrogated expression of IFN-β in PBMCs from systemic sclerosis patients to determine whether this could explain the partial protection against infection observed in these cells. When we examined expression of this type I IFN in cells 16h after infection with ZIKV, we found that PBMCs from systemic sclerosis patients had significantly higher quantities of IFN-β expression than cells from healthy donors (Figure 7.7A). In addition, when quantities of expression of this gene before virus infection were interrogated in the two populations, we found that systemic sclerosis patient PBMCs also had significantly higher quantities of IFN-β at rest, compared to cells from healthy controls (7.7B). When we investigated whether this heightened IFN-β expression drove higher expression of the prototypic ISG, RSAD2, we found that there was no difference in quantities of this gene by 16hpi between PBMCs from systemic sclerosis patients and those from healthy donors (Figure 7.7C).

Therefore, the difference in IFN-β expression between the two populations was not likely induced by virus, as baseline quantities of this gene were already higher in PBMCs from systemic sclerosis patients and this did not result in an increase in expression of key antiviral ISG, RSAD2.

To further investigate the potential impact of disease-associated IFN production and protection against ZIKV infection, we compared quantities of virus RNA present in systemic sclerosis patient PBMCs by 16hpi to each patient's clinical IFN score to determine whether higher IFN scores, obtained from our clinical collaborator Dr. Di Donato, were linked to lower quantities of virus replication during infection. However, there was no correlation (R^2 = 0.0056) between IFN score and quantities of RNA in PBMCs by 16hpi (Figure 7.7D). This demonstrates that there is no link between high IFN production in patients and greater protection against ZIKV infection. Nevertheless, together, the data in Figures 7.6 and 7.7 shows that protection against ZIKV is not limited to PBMCs from psoriasis patients as this effect was also observed in PBMCs from systemic sclerosis patients, albeit to a lesser extent.

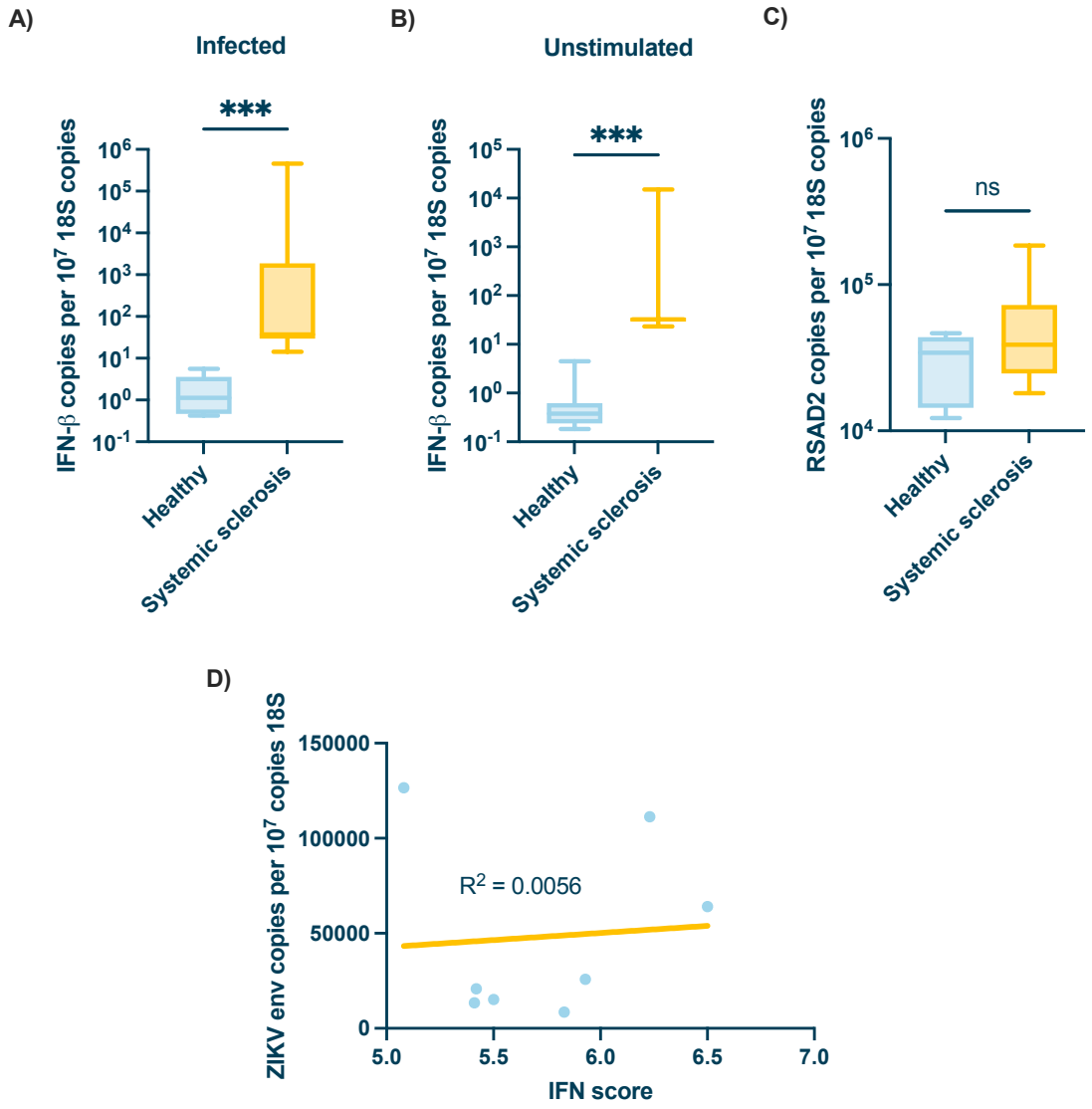

Figure 7.7 | PBMCs from SSc patients have increased type I IFN expression at rest but this is not linked to virus quantities during infection

(A-D) Quantities of expression of IFN-β **(A, B)** or RSAD2 **(C)** at 16hpi in PBMCs infected with ZIKV at an MOI of 0.01 **(A, C)** or at rest **(B)**. Quantities of ZIKV RNA present in cells at 16hpi was measured and compared against the patients IFN score **(D)**. PBMCs isolated from systemic sclerosis patient *(n=10)* or healthy control donor *(n=7)* blood samples.

Gene expression was determined by qPCR. Patient samples were collected by Prof Francesco Del Galdo and Dr Stefano Di Donato. Plots show the median value ± interquartile range. Data were analysed using Mann-Whitney test (****P < 0.001*).

7.5 Less virus permissive monocytes present in psoriasis patient PBMCs prior to infection

To further elucidate what could account for the reduced quantity of ZIKV RNA in PBMCs following infection of psoriasis patient-derived cells, we considered whether psoriasis patients may have lower numbers of virus-permissive cell types, belonging to the PBMC compartment. Within PBMCs, ZIKV primarily infects monocytes, but also replicates in DCs[142]. Furthermore, pDCs are potent producers of type I IFN and are implicated in psoriasis pathogenesis[267,428]. Therefore, altered numbers of these within psoriasis patient PBMCs could also contribute to the protection from infection observed in these cells e.g. via heightened IFN production. Therefore, we sought to characterise the proportions of different cell populations within the PBMC sample from psoriasis patients and healthy donors, both before and after infection.

To investigate this, PBMCs were isolated from blood from psoriasis patients with severe disease and from healthy donors. These cells were infected with ZIKV, either at an MOI of 0.1 or 0.01, and cells were collected at 16hpi for staining for cell phenotyping using flow cytometry. A fluorescent antibody panel was designed to stain against extracellular markers to identify and quantify T cells, B cells, natural killer (NK) cells, classical monocytes ($CD14^{++}CD16^{-}$), intermediate monocytes ($CD14^{++}CD16^{+}$), non-classical monocytes ($CD14^{+}CD16^{++}$), pDCs and myeloid DCs (mDCs). As CD16+ monocytes, both the intermediate and non-classical subsets, are the main target for ZIKV infection in PBMCs and so these cells were of particular interest here[424]. Importantly, we found that PBMCs from psoriasis patients contain significantly less non-classical monocytes than healthy donor PBMCs prior to infection (Figure 7.8F). Perhaps related to this, there was a reciprocal trend for increased numbers of intermediate monocytes. Indeed, there were notable trends in the numbers of other cell types too, although none that were statistically significant. In summary, there appeared to be more NK cells, intermediate monocytes and pDCs within psoriasis patient PBMCs, compared to healthy donors (Figure 7.8C, E, G). T cells, B cells and mDCs did not appear to change considerably in number (Figure 7.8A, B, H). The classical monocyte population appeared to expand during infection of both healthy donor cells and those from psoriasis patients (Figure 7.8D). The reduction in non-classical monocytes within psoriasis patient PBMCs prior to infection has the potential to contribute to the lower quantities of ZIKV replication observed earlier, as these cells are permissive to virus infection.

Furthermore, the increasing trend observed in the number of other cell types, particularly the type I IFN-producing pDCs, could have implications for the mechanism driving the protective phenotype.

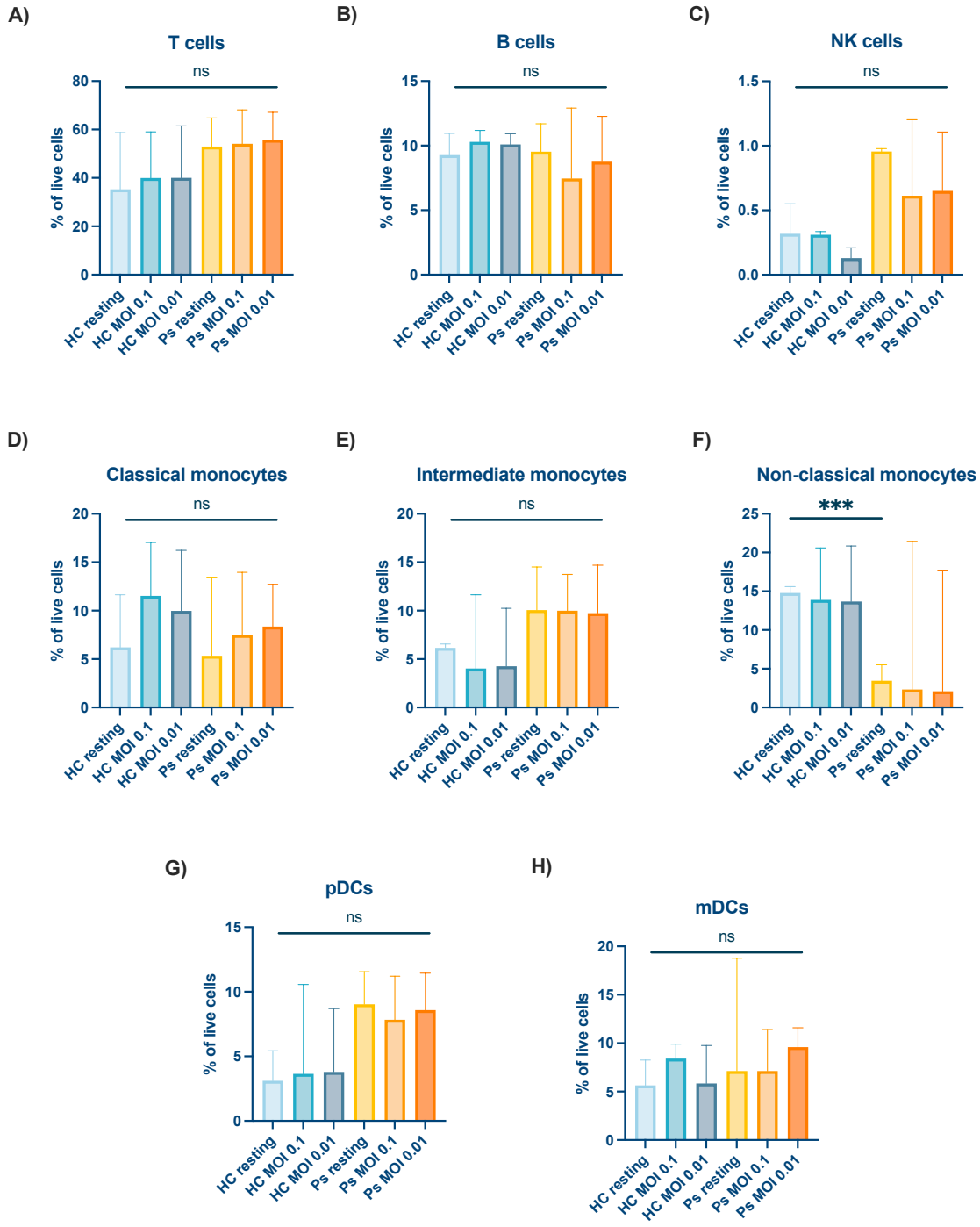

Figure 7.8 | Reduction in numbers of non-classical monocytes in psoriasis patient PBMCs at rest compared to healthy controls

(A-H) PBMCs isolated from psoriasis patient *(n=5)* or healthy control donor *(n=5)* blood samples and infected at MOI 0.1 of ZIKV *in vitro* or left resting. Cells were stained with fluorescent antibodies against extracellular markers at 16hpi. Cell numbers were

counted based on gating strategy shown in Figure 2.6 using flow cytometry. Plots show percent of each cell type out of all live cells.

Plots show the median value ± interquartile range. HC = healthy control, Ps = psoriasis. Data were analysed using Kruskal-Wallis test with Dunn's multiple comparison test (*ns = not significant, ***P < 0.001*).

7.6 Transcriptome analysis reveals several DEGs during infection of psoriatic PBMCs compared to healthy cells

To gain further insight in to what may be driving the protection against virus infection in psoriasis patient PBMCs, we used RNAseq analysis on these samples before and after infection. Whole transcriptome sequencing is used to assess differential gene expression in samples. This allowed us to investigate the extent to which gene expression differs in PBMCs from psoriasis patients compared to those from healthy donors at rest and also how expression changes during ZIKV infection of these cells. As before, isolated PBMCs from either psoriasis patients or healthy donors were infected with ZIKV at an MOI of 0.01. RNA was extracted from cells at 16hpi and sent for RNA sequencing, which was carried out by the Next Generation Sequencing (NGS) Facility in the University of Leeds. The comparisons made during RNAseq analysis are detailed in Figure 7.9.

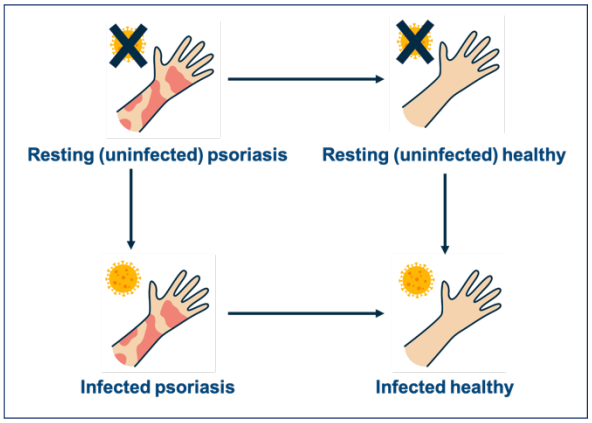

Figure 7.9 | Experimental design for RNAseq analysis

Diagram showing experimental groups sent for sequencing. Arrows indicate comparisons to be made between groups during analysis stage. Prior to sequencing, PBMCs isolated from psoriasis patient *(n=4)* or healthy control donor *(n=4)* blood samples and infected at MOI 0.1 of ZIKV *in vitro* or left resting. Cells were lysed 16hpi and RNA was extracted for sequencing.

Initial analysis of the RNAseq dataset was carried out by Dr Ian Carr, the principal bioinformatician at the University of Leed's NGS Facility, with further analysis carried out by this author. Initially, principal component analysis (PCA) was applied to the dataset to identify any relationships amongst variables within the dataset. This analysis showed that the groups, PBMCs from psoriasis patients (Ps) and those from healthy controls (HC) were not distinct, as clusters contained samples from both experimental groups (Figure 7.10). Further analysis identified the presence of a confounding variable within the data which was driving this: sex of the sample donor, meaning samples which came from females were clustered together and so were those which came from males. Following identification of this, Dr Ian Carr adjusted all subsequent analysis to take the impact of this factor in to account to ensure any differences in gene expression were due to the experimental conditions, rather than the sex of the donor.

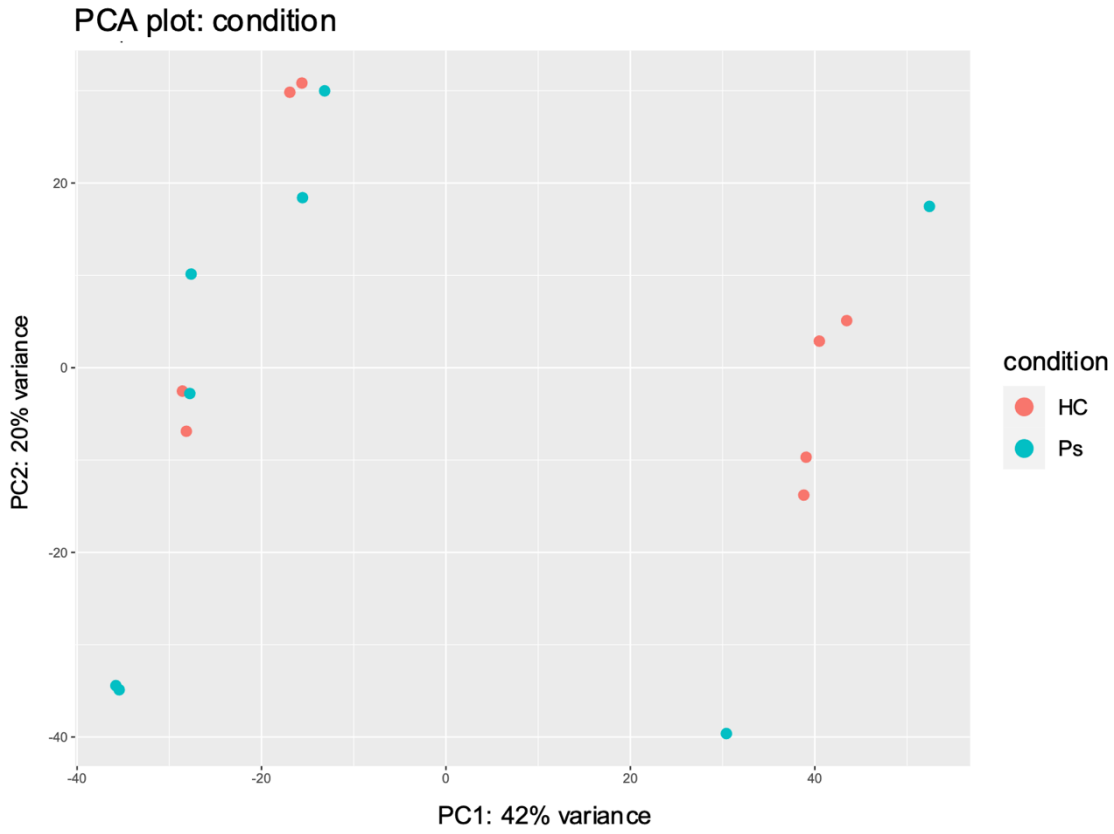

Figure 7.10 | Principal component analysis (PCA)

PCA of samples sent for RNAseq. HC = healthy control, Ps = psoriasis

A heatmap of genes which are differentially expressed between experimental groups and individual samples was created. Each donor had one sample which had been isolated and rest and another which had been infected with ZIKV, meaning we could examine the impact of infection on PBMCs within individuals. Examination of the hierarchical clustering of samples shows that the most closely linked samples within the dataset, in terms of differential gene expression, are those from the same donor (Figure 7.11). Furthermore, the samples which came from psoriasis patients were most different from samples from healthy donors, regardless of whether or not the sample had been infected. Therefore, the biggest variable driving differences in gene expression is disease state i.e. whether the sample came from a healthy donor or a psoriasis patient, regardless of whether or not that sample had been infected.

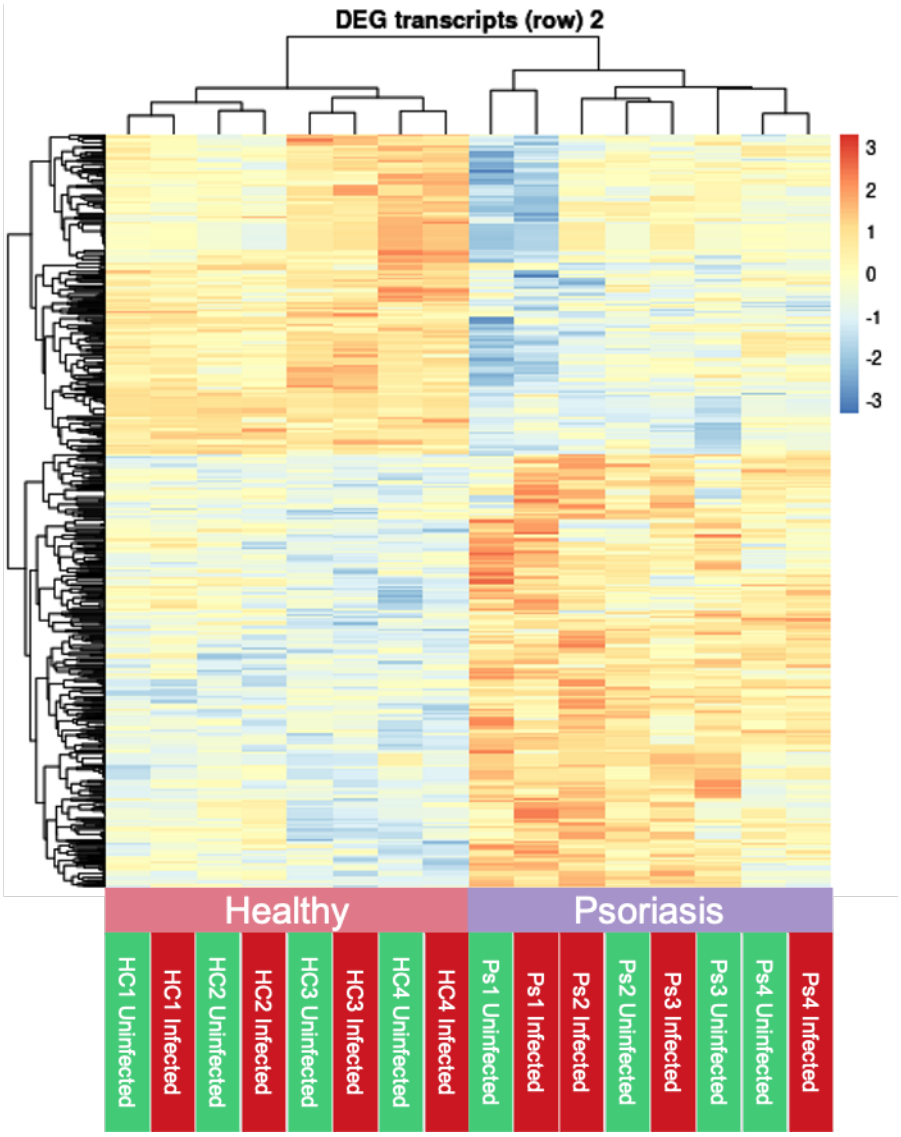

Figure 7.11 | Biggest factor driving variation in gene expression between individuals is disease state, rather than virus infection

Heatmap showing hierarchical clustering of RNAseq samples. This shows the overall results of cluster analysis, clustered using the log2 value. Genes with high expression levels are shown in red and genes with low expression levels are shown in blue. DEGs with a Log2Fold change of >2 or <-2 and padj of <0.05 were included for analysis. HC = healthy control, Ps = psoriasis. Numbers refer to donor number e.g. the samples 'HC1 Uninfected' and 'HC1 Infected' both game from the same donor (1).

Volcano plots can be used to identify differentially expressed genes (DEGs) between two groups, based on pre-determined statistical cut-offs. In these plots, red dots represent genes which surpassed the cut-off (Log2Fold change of >2 or <2 and padj of <0.05) for classification as being differentially expressed. Interestingly, few genes were differentially expressed following infection of psoriasis patient PBMCs (Figure 7.12A) or following infection of healthy donor PBMCs (Figure 7.12B) compared to resting cells from each cohort. When PBMCs from healthy controls under resting conditions were compared to those at rest from psoriasis patients (Figure 7.12C), there were 51 DEGs, suggesting some differences in gene expression between these groups. However, the highest number of DEGs, 278, was observed in the infected samples from psoriasis patients compared to those from healthy donors (Figure 7.12D). This data shows that there was limited difference in gene expression within cohorts, e.g. psoriasis patients or healthy donors, following infection. Importantly though, ZIKV infection of PBMCs drove the biggest difference in gene expression between PBMCs from psoriasis patients and those from healthy donors, which suggests some of these genes could be involved in the protection against virus infection observed in cells from psoriasis patients.

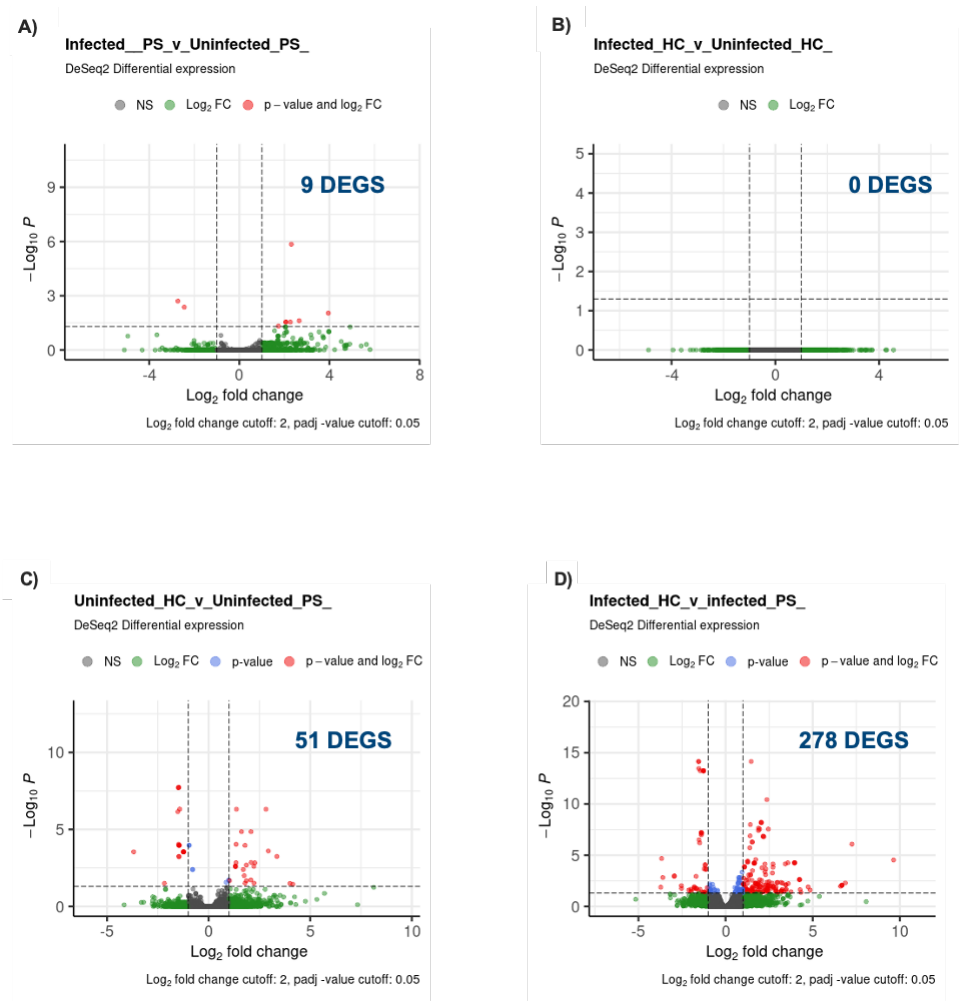

Figure 7.12 | Volcano plots of RNAseq data

(A-D) Volcano plots of DEGs identified by RNAseq. Each plot shows a different comparison between groups, as indicated by the title above each plot. Number of DEGs in each comparison labelled in blue on each plot. DEGs with a Log2Fold change of >2 or <2 and padj of <0.05 were included for analysis. HC = healthy control, Ps = psoriasis

Based on the results shown in the previous figure which demonstrated that there were a high number of DEGs in PBMCs from healthy controls compared to those from psoriasis patients following ZIKV infection, we sought to interrogate some of these DEGs to determine whether they could provide insight in to a possible mechanism driving protection from infection, as observed in psoriasis PBMCs. Based on the fold difference, we identified the top 50 over-expressed and top 50 under-expressed genes between the two groups. We then identified any genes within these lists which had a function related to immunity. We identified 8 genes of interest within the ‘over-expressed’ list (Table 7.2) and 5 within the ‘under-expressed’ list (Table 7.3). Differences in transcript

expression of each of the over-expressed genes is shown in Figure 7.13 and for the under-expressed genes in Figure 7.14. The function of these range from chemotactic activity to immunosuppression and so have the potential to interfere with virus infection in a number of ways, thus potentially contributing to the protection of psoriasis patient PBMCs. The identification of these DEGs with broadly immune-related functions provide us with potential targets for future investigation in to the mechanism driving protection against infection in psoriasis patient PBMCs.

Table 7.2 | Immune-related genes amongst the top 50 over-expressed genes during infection of psoriasis patient PBMCs

Selected genes with immune-related functions out of the list of the top 50 over-expressed genes, based on fold difference, in infected, psoriasis patient PBMCs compared to infected, healthy donor PBMCs. DEGs were determined as those with a Log2Fold change of >2 or <-2 and padj of <0.05. 'Position' refers to the position the gene holds in the list of the top 50 over-expressed genes. 'RefSeq' is the reference given to the transcript in the NCBI Gene database. 'Symbol' is the gene name.

Position	RefSeq	Symbol	Fold difference	padj
1	NM_002638	PI3	800.991201	2.94E-05
3	NR_049769	C1QTNF1	116.95184	0.00516928
10	NM_006419	CXCL13	20.0735637	0.04305974
29	NM_194294	IDO2	9.45407488	0.02247526
33	NM_001256579	SAMSN1	9.12918005	0.03464424
37	NM_001244910	FCGR1B	7.74398073	0.00471363
46	NM_170776	ADGRG3	6.5892994	0.00014924
49	NM_198461	LONRF2	6.30781862	0.00537256

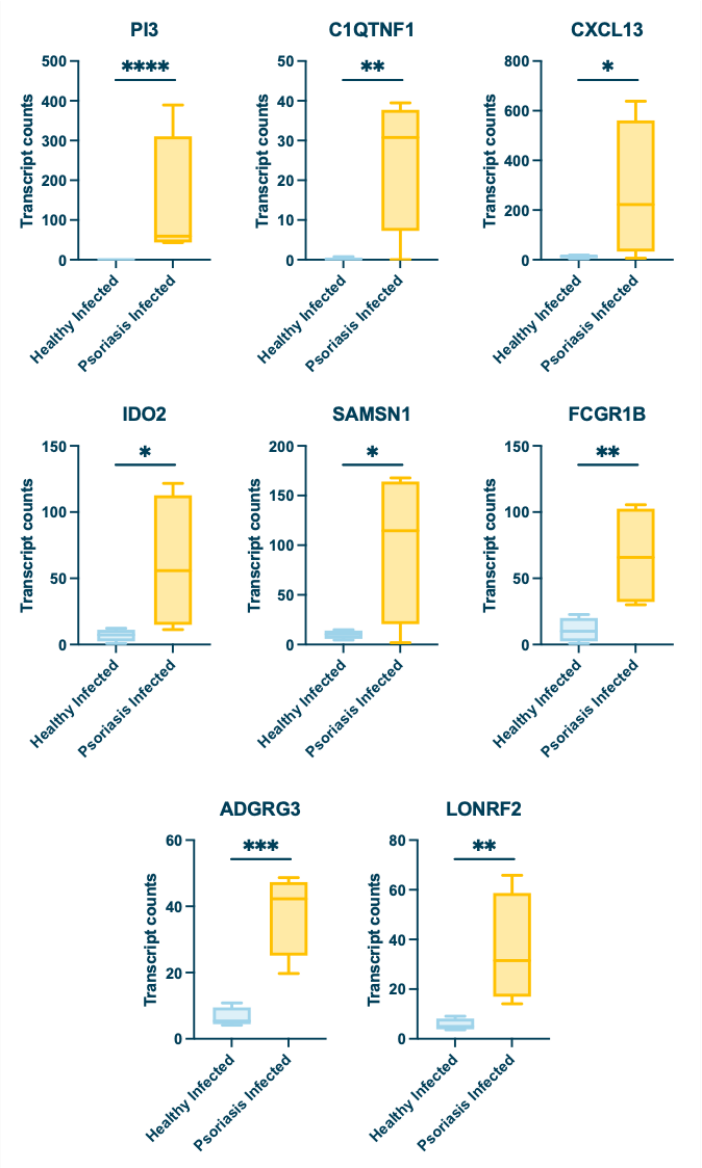

Figure 7.13 | Transcript counts of immune-related genes with highest level of over-expression in infected, psoriasis patient PBMCs compared to infected, healthy donor PBMCs

Transcript counts for PI3, C1QTNF1, CXCL13, IDO2, SAMSN1, FCGR1B, ADGRG3 and LONRF2.

PBMCs were either isolated from blood from psoriasis patients or healthy donors. Cells were then infected with ZIKV at an MOI 0.1. Cells were lysed 16hpi and RNA was extracted for sequencing.

Table 7.3 | Immune-related genes amongst the top 50 under-expressed genes during infection of psoriasis patient PBMCs

Selected genes with immune-related functions out of the list of the top 50 under-expressed genes, based on fold difference, in infected, psoriasis patient PBMCs compared to infected, healthy donor PBMCs. DEGs were determined as those with a

Log2Fold change of >2 or <-2 and padj of <0.05. ‘Position’ refers to the position the gene holds in the list of the top 50 under-expressed genes. ‘RefSeq’ is the reference given to the transcript in the NCBI Gene database. ‘Symbol’ is the gene name.

Position	RefSeq	Symbol	Fold difference	padj
2	NM_006498	LGALS2	0.52320262	0.0266783
6	NM_001099221	TIFAB	0.47654231	0.04268498
39	NM_001145808	ITGAM	0.28758324	0.0118557
45	NM_005699	IL18BP	0.17194414	0.00954233
47	NM_002704	PPBP	0.12969768	0.00114046

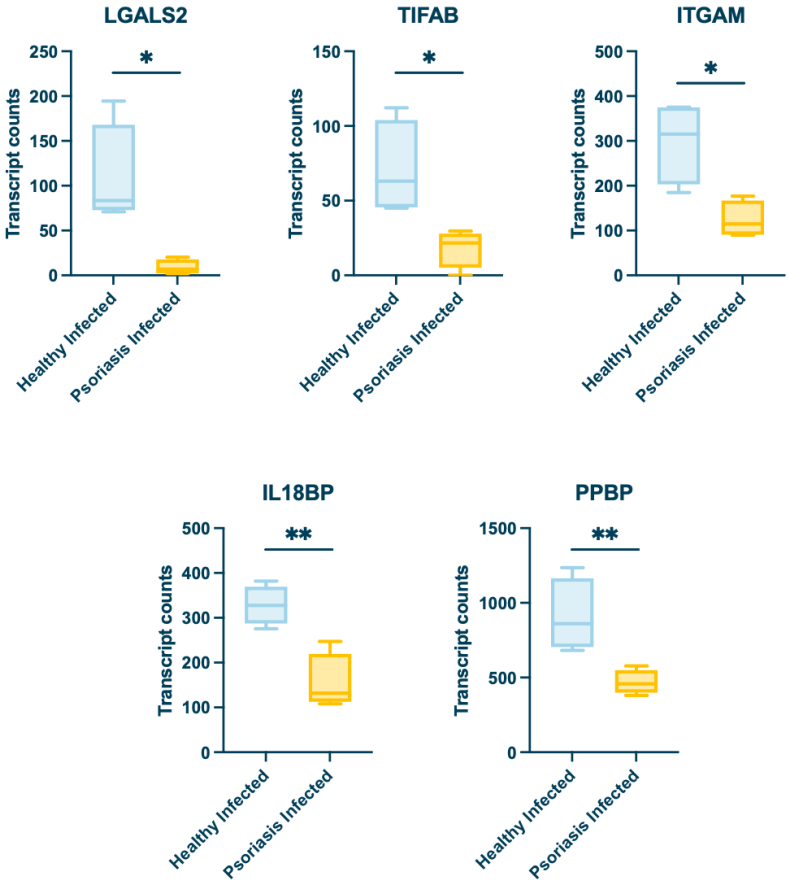

Figure 7.14 | Transcript counts of immune-related genes with highest level of under-expression in infected, psoriasis patient PBMCs compared to infected, healthy donor PBMCs

Transcript counts for LGALS2, TIFAB, ITGAM, IL18BP and PPBP.

PBMCs were either isolated from blood from psoriasis patients or healthy donors. Cells were then infected with ZIKV at an MOI 0.1. Cells were lysed 16hpi and RNA was extracted for sequencing.

7.7 Summary and conclusion

Following on from our investigation in to the effects of UV exposure of the skin on susceptibility to arbovirus infection, we sought to understand the impact of another driver of skin inflammation on outcomes to arbovirus infection: the disease state in the inflammatory skin disease, psoriasis. Our group had previously shown that lesional skin explants from psoriasis patients are less susceptible to ZIKV infection than non-lesional skin from the same patient (unpublished data). As much of the immune dysregulation is also observed in the blood of psoriatic patients, we hypothesised that psoriatic PBMCs may show similar resistance to infection. This is key as, these same cells are also the principle target for ZIKV in humans.

Before working with psoriatic PBMCs, optimal conditions for *in vitro* infection of ZIKV infection of healthy human PBMCs were established (Figure 7.1). Subsequently, pre-treatment with innate immune agonists was used to induce a primed, inflammatory state in healthy PBMCs, modelling that observed in psoriasis, and the outcome of ZIKV infection in these pre-primed cells was examined, as a proof of principle for our main hypothesis. While pre-priming with the TLR7 agonist imiquimod did not impact ZIKV infection, pre-treating cells with poly(dA:dT), a DNA analogue which stimulates a wide range of PRRs and models a systemic inflammatory environment, significantly reduced quantities of ZIKV present in cells (Figure 7.2). This suggested that pre-priming of the innate immune system in this way appeared to allow cells to better resist subsequent ZIKV infection. This proof of principal experiment provided an indication that the systemic inflammation observed in psoriasis might lead to psoriatic PBMCs being protected against ZIKV infection.

Subsequent investigations in to the susceptibility of psoriatic PBMCs to ZIKV infection *in vitro* compared to healthy PBMCs found that cells from psoriasis patients were protected from virus infection, at two different virus doses, evidenced by 10-fold lower quantities of virus RNA in the cells (Figure 7.3). Importantly, this is the first time that psoriatic cells have been shown to be more protected against virus infection[415–417]. This novel finding suggests that the inflammatory profile of psoriasis patient PBMCs provides resistance to arbovirus infection *in vitro*. Enhanced arbovirus replication in the blood can facilitate viral spread around the body, resulting in more severe disease[118,119]. Therefore, this resistance to infection in psoriatic PBMCs suggests these patients may be less susceptible to severe arbovirus disease outcomes. As our group had previously shown that lesional skin is also less susceptible to ZIKV infection than non-lesional skin from the same patient, this may mean that the virus would be less likely to dissemination from the skin in a psoriasis patient in the first place.

Interestingly, resistance to ZIKV infection was consistent across the psoriasis patient cohort and was not dependent on PASI-defined disease severity, or the use of treatments which interfere with the immune system (Figure 7.5). This suggests that the mechanism driving this protective phenotype is likely a core component of psoriasis pathogenesis that underlies patient susceptibility to develop lesions. Critically, psoriasis patient PBMCs demonstrated more robust upregulation of the type I IFN, IFN-α, in response to virus (Figure 7.4). These cells also expressed more of the gene encoding the IFN-stimulated PRR RIG-I, capable of recognising virus and amplifying the antiviral response. Increased expression of ISGs can be linked with higher quantities of virus during infection[117]. However, these cells had relatively low quantities of ZIKV RNA compared to infected healthy cells, and so enhanced IFN expression is unlikely to be directly driven by virus quantity. Our group had previously found that therapeutic induction of type I IFN post-arbovirus infection results in better clearance of the virus[119]. Therefore, it appears that because psoriatic PBMCs are better able to induce this protective system when stimulated by virus, this leads to an immune environment in cells which is more beneficial to the host in terms of protection from virus. To determine whether type I IFNs are critical for this phenotype, it would be useful to block downstream JAK-STAT signalling in these cells during infection, using the anti-JAK inhibitor ruxolinitib.

We broadened the scope of our investigation to include PBMCs from another inflammatory disease, systemic sclerosis, to determine whether increased resistance to ZIKV infection was specific to psoriatic PBMCs. Notably, systemic sclerosis is linked with high type I IFN expression, although it is unclear whether this is a driver of disease or triggered by the disease state[427]. This characteristic, together with our previous finding that psoriatic PBMCs expressed IFN-α more highly during ZIKV infection, led us to consider whether PBMCs from systemic sclerosis patients may also be primed to better respond to infection. We found that these cells were also protected from ZIKV infection but only following infection with a low virus dose (Figure 7.6). The magnitude of protection was also smaller than that observed in psoriatic PBMCs. Upon interrogation of type I IFN expression, we found that although IFN-α expression was higher in PBMCs from systemic sclerosis patients compared to healthy PBMCs during ZIKV infection, quantities of this were already raised at rest in the patient PBMCs (Figure 7.7). This suggests that expression is permanently high in these cells and is not brought about in response to e.g. virus stimulus. Furthermore, there was no increase in expression of a prototypic ISG RSAD2 following infection. Therefore, the type I IFN system does not seem to be induced in response to virus to the same extent as that observed in psoriatic PBMCs, which could explain the less substantial reduction in susceptibility to ZIKV. Furthermore, PBMCs from patients with a high IFN score, indicating high IFN levels in serum, did not correlate with protection from virus.

Assuming that type I IFN function underlies the increased resistance to ZIKV in both psoriasis and systemic sclerosis, these data suggest that more potent resistance to ZIKV is afforded when host PBMCs induce IFN-α more highly following infection, as is the case in psoriatic PBMCs, rather than exhibit higher baseline levels prior to infection, as observed in PBMCs from systemic sclerosis patients. This is supported by our previous work showing that using an agonist to induce type I IFN responses early following arbovirus infection in the skin helps the host to better control the virus[119]. Nevertheless, this provides evidence of resistance to ZIKV infection in PBMCs from not just psoriasis patients, but also another inflammatory disease too. This suggests that cells from patients with other conditions in this category may also be pre-primed to better respond

to ZIKV infection. Type I IFN dysregulation is involved in the pathogenesis of both psoriasis and systemic sclerosis. It remains to be observed whether resistance to infection would also apply to other inflammatory conditions with no type I IFN involvement, such as the TNF-α driven disease hidradenitis suppurativa. In the future, expanding the investigation to explore PBMCs from such conditions is critical, both to test the limits of this phenotype and further unpick the involvement of type I IFN. However, it is highly likely that other mechanisms underlie this resistance to ZIKV infection and that this is not solely attributable to type I IFN.

We also quantified the cell types present in the PBMC compartment in samples from psoriasis patients and healthy donors, before and after ZIKV infection, to determine whether the proportion of any of these was different. Interestingly, there were less virus-permissive non-classical monocytes within psoriatic PBMCs prior to infection compared to healthy PBMCs (Figure 7.8). These cells are one of the main targets of ZIKV infection in human PBMCs and so a reduction in the numbers of these within the PBMC compartment in psoriasis patients at the outset could partially explain the resistance to infection, as the virus would have less target cells to replicate within[142]. There was also an increasing trend in the numbers of NK cells, intermediated monocytes and pDCs in psoriatic PBMCs. The sample number of this experiment was relatively small considering the heterogeneity of human populations and so expanding the number of participants in the future could help elucidate whether there definitely are more of these cell types within the PBMC compartment in psoriasis patients. If there are, this could also further indicate the mechanism driving resistance to ZIKV infection. Of particular note is the potential role of pDCs. These cells are potent producers of type I IFN and as such are critical in this capacity during arbovirus infection *in vivo*[151]. They have also previously been implicated in the onset of psoriasis, meaning it is likely that their number is increased within psoriatic PBMCs[267,428]. Together, this could mean that these cells contribute to the higher levels of IFN-α expression following infection shown in Figure 7.4 and thus to the lower susceptibility to ZIKV infection. Although it is worth noting that we showed in Figure 7.2 that pre-treatment of PBMCs with imiquimod, a TLR7 agonist did not protect from subsequent arbovirus infection and pDCs are the primary cell type which express TLR7 constitutively, suggesting that therapeutic

induction of type I IFN responses in these cells is not critical for protection from virus[429]. However, this may also have been limited by attempts to induce IFN production pre-infection, rather than post-infection, as we now think is vital for better control of virus, based on our work with systemic sclerosis patient samples. Their role in this phenotype could be further elucidated by blocking secretion of type I IFN by pDCs specifically, using an antibody (CBS004) developed by a member of our collaborator Francesco Del Galdo's lab group[430].

Outside of a change in the number of specific cell types within the psoriatic PBMC compartment, there are other changes which could be contributing to the resistance to ZIKV infection. Individual cell types, such as monocytes, may be less inherently susceptible to infection in psoriasis patients due to exposure to modulating factors present due to the disease state. Cells which are normally permissive to infection may be pre-primed, making them more efficient at clearing virus before productive infection takes place. To investigate this, we could make use of a fluorescent strain of ZIKV to allow for quantification of infected cell types using flow cytometry. This is an approach that we briefly trialled, however, after several attempts, we were unable to optimise this to get reliable staining for ZIKV-infected cells. Therefore, we did not move forward with this work. Alternatively, individual cell types could be isolated and then infected with ZIKV to determine whether certain cell types are less susceptible to infection when derived from psoriatic PBMCs. Although, in the case of monocytes, this also presents challenges as many isolation kits available from suppliers isolate CD14+ monocytes by removing CD16+ monocytes. However, we believe non-classical monocytes, which are double positive for CD14 and CD16, are involved in this and so it is critical to include these cells in any studies. We are further constrained by the small volumes of blood samples we receive from patients involved in this study, as many kits which include CD16+ cells in the isolated sample require large volumes of blood. Therefore, we would need to further consider how best to move forward with this work.

Transcriptome analysis of PBMCs from psoriasis patients and healthy donors, both resting or ZIKV infected allowed for assessment of DEGs which may be driving resistance to infection in psoriatic PBMCs (Figure 7.9). Following quality control of the dataset (Figure 7.10), we assessed overall differential gene

expression between individuals and identified that the biggest variable driving this was disease state e.g. whether or not the donor had psoriasis, rather than whether the sample had been infected or not (Figure 7.11). This finding is expected as there is a genetic component driving psoriasis pathogenesis[431].

Upon further investigation of DEGs between experimental groups, rather than individual samples, it was clear that ZIKV infection did not drive significant changes to gene expression, either in healthy PBMCs or psoriatic PBMCs, compared to disease state (Figure 7.12). While this did support our finding from Figure 7.11, this was surprising as the anti-flavivirus response does require significant upregulation of genes[432–434]. This may be because ZIKV infects a relatively low frequency of cells of in the total PBMC compartment, while psoriasis affects a larger subset of cells including the more numerous T cell subsets in PBMCs. There was also some altered gene expression between resting psoriatic cells and healthy PBMCs, with these likely contributing to the disease state. Importantly, the biggest change in gene expression was between the infected psoriatic PBMCs and the infected healthy cells. Therefore, it appears that expression starts to diverge more dramatically between the healthy cells and those from psoriasis patients during ZIKV infection. This provides further evidence reinforcing our earlier conclusion that psoriatic PBMCs are likely protected from ZIKV infection by their ability to better induce expression of antiviral genes, such as type I IFN.

Finally, a list of genes with functions relating to immunity that were also in the top 50 most over- or most under-expressed genes between infected PBMCs from psoriasis patients compared to healthy donors was compiled (Tables 7.1-2, Figures 7.13-14). This list identifies a number of genes which may contribute to the reduced susceptibility of psoriatic PBMCs to ZIKV infection and, therefore, provides several targets for future work to further elucidate any potential involvement. One promising candidate is interleukin-18 binding protein (IL-18BP), which was significantly under-expressed during infection of psoriatic PBMCs compared to healthy cells. IL-18BP scavenges the pro-inflammatory cytokine IL-18. Therefore, downregulation of IL-18BP may mean that there is more available IL-18 during infection of psoriatic PBMCs. If this is the case, this would not appear in RNAseq analysis, as gene expression of IL-18 would not

change, however, availability of protein may and this could be measured using an ELISA. IL-18 can stimulate several PBMC sub-types including T cells, macrophages and DCs, via the IL-18 receptor. Specifically, this has been shown to be involved during arbovirus infection, including through regulation of IFN-γ expression during DENV infection *in vitro*[435,436]. Therefore, it would be informative to investigate the outcome of adding recombinant IL-18BP during ZIKV infection of psoriatic PBMCs.

Overall, this chapter has clearly demonstrated that psoriatic PBMCs, and to some extent PBMCs from systemic sclerosis patients, are less susceptible to infection with a medically relevant arbovirus, ZIKV. Although not upregulated at rest, the type I IFN system was more readily induced during ZIKV infection and this may contribute to resistance to infection. Importantly, there are also less virus-permissive monocytes present within the psoriatic PBMC compartment. Finally, several candidate DEGs were identified, for use in future investigations, which may contribute to this phenotype in psoriatic PBMCs.

Unfortunately, clinical sample availability for this project was limited, largely due to the COVID-19 pandemic and healthcare service recovery afterwards. Therefore, this was a limiting factor in further progression of this work. However, these preliminary results show great promise and there is much that could be done in the future to advance this project further.

Chapter 8: General discussion

8.1 Project rationale: Identifying factors which modulate host susceptibility to arbovirus infection

Over half of people worldwide are at risk of contracting a mosquito-borne virus infection[6]. The global burden of arbovirus infection is expected to rise dramatically over the coming decades, with climate change being a particularly important driver of this[7,40,41]. This heterogeneous group of viruses can have debilitating or potentially lethal consequences for those infected. There are no antivirals available to treat arbovirus infection and no vaccines available for many serious arboviral threats, including ZIKV. The situation is further complicated by the fact that the symptoms which manifest during mild disease are shared by many of these viruses[437]. This makes definitive diagnosis extremely challenging without the use of laboratory tests, which can be prohibitively expensive in regions of endemicity[438]. It is critical that we develop a better understanding of factors which alter the course of infection and make individuals more susceptible to severe disease.

Our lab group and others have previously shown that the virus-transmitting mosquito bite enhances arbovirus infection by promoting an inflammatory environment at the skin, which is beneficial to the virus[120,134]. This led us to begin work to identify other factors which modulate inflammation at the skin and so may play a role in altering host susceptibility to arbovirus infection in a similar manner. One such factor that is of great relevance to arbovirus transmission is exposure to UVR from the Sun. Levels of solar radiation are highest in regions of the world where arboviruses are also endemic[35,221]. UV exposure can also interfere with inflammatory responses in the skin, including to some viruses, such as HSV[240,249]. Yet, prior to the work in this thesis, it was unknown whether UV exposure of the skin modulates susceptibility to arbovirus infection.

Another factor which has the potential to modulate susceptibility to arbovirus infection is the presence of a pre-existing inflammatory state in the host due to an inflammatory condition. There are a wide spectrum of conditions, driven by a range of distinct molecular events, which fall into this category. Type I IFN dysregulation is involved in the pathogenesis of two such conditions: psoriasis and systemic sclerosis[267,278–280]. Furthermore, both of these conditions

predominantly affect the skin but also drive systemic inflammation[284,286–288]. As such, we considered whether PBMCs from the blood of these patients may be pre-primed to better respond to virus infection, due to this systemic inflammatory state induced by each disease.

This thesis sought to investigate whether pre-existing skin inflammation, either as a result of UV exposure or due to inflammatory disease, modulates host susceptibility to arbovirus infection.

8.2 Summary of key findings

This thesis identified two key inflammatory factors which influence host susceptibility to arbovirus infection: an environmental factor, UV exposure, and a host factor, pre-existing inflammatory conditions. Erythemal UV exposure of the skin of mice, modelling sunburn, prior to infection increases host susceptibility to infection with the arbovirus SFV. The resultant increase in virus RNA in the skin and blood peaks at 24h and 1-week post-UV exposure. However, the mechanisms driving this enhancement of infection at each timepoint are unique to each. At 24h post-UV, the skin environment is highly inflammatory and recruited monocytes and macrophages are infected by virus. By 1-week post-UV, the skin has begun to heal the UV-exposed skin which inadvertently can make host skin more susceptible to virus. Cells proliferate to rebuild the tissue, but SFV, which has oncolytic properties, infects these proliferating cells. The virus also replicates within fibroblasts, the cellular building blocks used to facilitate cutaneous repair. Treatment of the UV burn with topical corticosteroid partially protected against certain aspects of UV-mediated enhancement of infection, including early viremia and inflammatory infiltrate to the brain during dissemination of the virus at later timepoints p.i.. Surprisingly, enhancement of SFV infection also occurs in skin exposed to one or several low dosages of UV, mimicking daily tanning exposure, in combination with a mosquito bite. Mice are unable to effectively induce key antiviral immune genes, ISGs, in a timely-manner during infection in this model. Interestingly, mosquito behaviour towards UV-exposed skin is also altered. Mosquitos are more likely to feed on a UV-exposed mouse and the insects spend longer probing UV-exposed skin during feeding. Finally, susceptibility to ZIKV infection in PBMCs from patients with one of two inflammatory conditions, which cause

systemic inflammatory effects, were also investigated: psoriasis and systemic sclerosis. PBMCs from both patient groups exhibit enhanced protected against infection with ZIKV. Together, the data from this thesis shows that pre-existing inflammation within the host, caused either by an environmental or host disease factor, can greatly influence susceptibility to arbovirus infection.

8.3 Arbovirus infection is enhanced *in vivo* following an erythemal UV burn

UV exposure of the skin prior to infection enhances subsequent infection with SFV *in vivo*. UV-exposed mice had higher quantities of virus RNA in the skin and increased viremia by 24hpi. This was shown to be true following a single, erythemal dose of UV, modelling sunburn, as early as 24h post-exposure, up to 2-weeks after the burn had taken place. The most severe increase in susceptibility to arbovirus infection was observed in mice exposed to an erythemal dose of UV 1-week prior to infection. These mice had the highest quantities of virus present by 24hpi, but also had significantly more virus spreading to the brain, where SFV replicates efficiently and can cause clinically apparent pathology, by 4 days p.i.. ZIKV infection was also shown to be more clinically severe in those mice pre-exposed to UV.

This is the first time that UV exposure of the skin has been shown to increase susceptibility of a host to virus infection. Previously, it has been reported that latent HSV and VZV, infections can be reactivated by UV[249,250]. However, there is no evidence that UV exposure can affect the initial establishment of the virus, making the findings in this thesis a unique contribution to the field.

The *in vivo* model used to investigate this was designed to model natural transmission as closely as possible. It pairs an established mouse model of erythemal UV exposure, mimicking sunburn, with a model of natural arbovirus transmission[120,240]. This combines the mosquito bite with virus inoculation via a microneedle, thus taking in to account any effect the mosquito bite, a known enhancer of infection, may have. Furthermore, the inoculation of sub-microlitre volumes of virus via a microneedle mimics the transmission of virus through the mosquito's mouth parts. Injecting virus using a needle, rather than an infected mosquito, allows for the control of virus titre injected to minimise any variance in

infectious dose between mice. All of these aspects of the experimental design align the mouse model closely with natural arbovirus transmission in an individual exposed to a UV burn. However, it is worth noting that the UV lamp used for exposures emits mostly UVB light, whereas the Sun emits mostly UVA. However, UVB is the most harmful type used and also the type which causes sunburn and so is widely used as a model to study this. Nevertheless, the effect of natural sunlight on human skin may differ.

In the future, collection of healthy human skin explants and those from individuals with sunburn and *in vitro* infection of these with an arbovirus could help determine whether this does apply to humans. Although we do have a clinical dermatologist collaborator who could collect these for us, the number of patients presenting to a clinician with sunburn is low and so access to samples may be limited. Furthermore, skin explants do not always reproduce results observed *in vivo* due to their removal from the whole, physiological system. For example, mosquito-bite enhancement only occurs *in vivo* in mice, not in murine skin explants[126]. This suggests that *in vivo*-processes are essential for this effect and the same may be true for UV-mediated enhancement of infection. This is supported by the findings of this thesis that showed that cells isolated from the skin of UV-exposed mice did not exhibit a cell autonomous difference in susceptibility to virus *in vitro*. Nevertheless, this approach would still be worth exploring.

If this finding translates to humans, this will present a novel health risk associated with environmental UV exposure. This is of great relevance to arbovirus transmission in areas of endemicity where individuals are exposed both to high levels of UV light from the sun but also to co-circulating arboviruses[35,221]. This has the potential to impact individuals who live in these regions but also tourists who are visiting, and who are less likely to have pre-existing immunity to these viruses[439]. Furthermore, the increase in global warming which is driving the expansion of the arbovirus vector in to new regions means that even more people will be exposed both to arboviruses and to high levels of UV light in the future[7,41,293].

This thesis has not considered the variation amongst populations and how this may affect responses to UV and resultant enhancement of arbovirus infection. There are several factors which could be of relevance in this way: from sex to an individual's skin tone. Mice are genetically homogeneous compared to humans, but even they have been shown to respond at different magnitudes to UV exposure based on their sex. Male mice exhibit a more exaggerated response to UV exposure than female mice[325,440]. Although it has not been definitively determined whether human male and females respond differently to UV, rates of skin cancer, of which UV exposure is the main causative agent, are higher in males than females[441]. However, it remains to be seen whether this is due to behavioural factors, such as being outdoors more due to work, rather than differing responses to UV between the sexes.

With relation to skin tones, as arboviruses are so widespread around the world, the populations which are affected are hugely diverse. Higher levels of melanin in the skin result in darker skin tones. Melanin protects against some of the damaging consequences of UV exposure, including erythema and DNA damage[243,442,443]. As a result, individuals with dark skin burn less following an equivalent UV exposure, than those with paler skin[444]. Therefore, whether skin tone would affect UV-mediated enhancement of infection remains to be seen. The *Mc1r*$^{e/e}$ mouse model replicates very pale, light-haired individuals who are unable to tan due to deficient melanin pigmentation[383]. This mouse model can be induced to tan, e.g. produce melanin, through the topical application of a molecule, forskalin, without the need for UV exposure. Investigating arbovirus infection in this model would shed some light on the importance of melanin in the mechanism. Alternatively, as mentioned earlier, human skin explants could be used to ascertain whether UV-mediated enhancement of infection occurs in human tissue also. This study could be expanded to include samples from individuals with different skin types, to determine whether skin tone impacts this effect. However, it is worth noting that we used two different doses of UV exposure in this thesis, the erythemal dose equivalent to 2 MED and the sub-erythemal dose equivalent to 0.1 MED. The MED, the minimal dose of UV required to cause erythema, is much lower in individuals with paler skin compared to those with darker skin[444]. Therefore, the different MEDs used in this thesis partially represents the response in different skin tones and suggests

that infection is enhanced at a range of MEDs. Although, the impact of different levels of melanin is still not taken in to account in our study.

8.4 Increase in susceptibility to arbovirus infection at 24h post-UV driven by similar mechanism as mosquito bite-mediated enhancement of infection

Despite displaying a similar phenotype at 24h and 1-week post-UV, the mechanisms driving this increase in susceptibility to arbovirus infection at each timepoint appear to be distinct. They share some commonalities, in that the enhancement does not appear to be driven by immunosuppression of the antiviral response at either timepoint. Mice still induce a robust type I IFN response during infection and enhancement was still observed at 24h post-UV in *ifnar-/-* mice. However, from here the stories diverge at these two timepoints post-UV.

In mice exposed to UV 24h prior to infection, the skin environment is highly inflammatory, characterised by recruitment of myeloid cells, likely facilitated by an increase in vascular permeability in response to UV exposure. Some members of this inflammatory infiltrate, primarily monocytes and macrophages, are permissive to virus infection. It appears that SFV utilises these cells for replication. This is reminiscent of the mechanism underlying enhancement of arbovirus infection following a mosquito bite[120,126]. Interestingly, mosquito-bite mediated enhancement of infection can be alleviated in mice by stimulating the innate immune system early following infection, through the use of a TLR7 agonist imiquimod[119]. This may also be of use during infection following UV exposure of skin.

To definitively confirm our proposed mechanism for UV-mediated enhancement of infection at 24h post-UV, *Ccr2-/-* mice, which have an absence of bone marrow derived monocyte recruitment, could be used. Here we would hypothesis that an increase in susceptibility should be alleviated in these mice if recruitment of these cells is essential for the phenotype. If this does apply, then this opens up the possibility that other as-yet unidentified factors which drive a

highly inflammatory environment at the skin, characterised by neutrophil and monocyte recruitment, could increase host susceptibility to infection.

8.5 Wound healing provides a microenvironmental niche that enhances skin infection with SFV at 1-week post-UV

Contrastingly, the mechanisms driving enhanced SFV infection in mice exposed to erythemal UV 1 week before appears to be linked with aspects of the wound healing process. The skin at this timepoint is characterised by epidermal hyperplasia, expansion of the macrophage population, and an increase in expression of the prototypic wound healing molecule ARG1. These are all indicative of cutaneous wound healing, suggesting that the burn is undergoing this process at this timepoint. This environment allows for more efficient virus replication. UV exposure drives proliferation of cells in the skin at this timepoint, likely as part of the wound healing process, and SFV preferentially infects these. While we did not identify the phenotype of the proliferating cells, there were more infected fibroblasts in the skin of UV-exposed mice and it is known that fibroblasts proliferate during wound-healing in order to provide the supporting structure on which the damaged tissue can be repaired.

Interestingly, though this increase in infected fibroblasts cannot simply be explained by an increase in the numbers of fibroblasts in wounded tissue, as their number remained the same as at rest. Therefore, it seems that fibroblasts are simply more susceptible to arbovirus infection in UV-exposed tissue during this wound-healing phase. One explanation for this could be that fibroblasts adopt a ‘macrophage-like’ phenotype during wound healing[206]. This is characterised by upregulation of ARG-1, of which we saw an increase in the CD45- cell population by this timepoint[353]. To further investigate this, we could isolate fibroblasts from UV-exposed skin and infect them *in vitro* to determine whether they are more inherently susceptible following a UV exposure. Additionally, analysis of fibroblast receptor expression would allow us to definitively determine whether these cells have adopted the ‘macrophage-like’ phenotype. This could also be used to assess whether fibroblasts have altered expression of the SFV entry receptor, very-low-density lipoprotein receptor, or VLDLR, by 1-week post-UV, which could facilitate the increase in permissiveness of these cells to virus infection[445,446].

Not only has this study highlighted the increase in host susceptibility to arbovirus infection at 1-week post-UV, it has also shed light on some of the cutaneous events that take place at this timepoint during the wound healing process. Knowledge on what occurs at the skin at this timepoint post-UV was extremely limited prior to this work. Further investigation is needed to investigate whether this effect is specific to a UV burn or whether other cutaneous wounds, for example a thermal burn, are also more susceptible to arbovirus infection. Thermal burns are highly susceptible to bacterial infections but this is thought to be due to breakage of the skin barrier and exposure of the tissue to the environment, rather than the internal mechanisms within the skin making the host more susceptible[447].

8.6 Low dose exposures to UV, modelling suntan, are sufficient for enhancing arbovirus infection

Unexpectedly, repeated, sub-erythemal exposures of the skin to UV, mimicking daily, tanning doses in humans, was also sufficient to enhance arbovirus infection. However, this enhancement was dependent on the virus being transmitted into mosquito bitten skin. This suggests that the mechanism driving UV-mediated enhancement of infection at this lower UV dose is interlinked with the molecular events which occur in response to a bite. There were more monocytes recruited during infection of mice exposed to repeated, low UV doses prior to infection and these may potentially provide the virus with new cellular targets, although we did not confirm this. A unique aspect of this UV exposure regimen was that UV-exposed mice appeared to exhibit a blunted induction of ISG expression, relative to virus quantity. Here, while expression of the type I IFN IFN-β was increased in UV-exposed mice during infection, upregulation of the downstream ISGs, the antiviral effector molecules of the system, was less pronounced in these mice, considering that the virus quantities were much higher. This assumes that ISG expression corelates with virus quantities, as sometimes is evident in e.g. neural tissue[448]. Together, this might suggests that lower, repeated exposures to UV drives a more immunosuppressive state in the skin, which is less able to respond to virus infection by upregulating ISG expression.

This finding is perhaps of even greater relevance to individuals who live in global regions where arboviruses are endemic, than our earlier findings relating to the impact of an erythemal UV exposure. People who live in warmer regions with high levels of solar radiation may have to carry out daily tasks that involve going outdoors e.g. shopping, commuting etc[224]. Therefore, these individuals are exposed to regular, sub-erythemal quantities of UV, such as the exposure modelled in this thesis[247]. If the findings of this thesis, that enhancement of infection even occurs following these types of exposures, then this has implications for individuals living in arbovirus transmission zones, and could e.g. inform public health policies regarding sun exposure. Further work is needed to fully understand the extent of this enhancement, especially with relation to whether this drives progression to severe disease.

Furthermore, individuals in Western nations often expose themselves to UVR on purpose with the aim of getting a suntan[380,388,389]. Arboviruses are spreading to these nations and infecting individuals in populations with no pre-existing immunity[41]. The implications of the combination of tanning doses of UV on infection outcomes and this immunological naivety to arboviruses remain to be seen.

Upon investigation of the limits of UV-mediated enhancement of arbovirus infection, it was shown that even a single low dose of UV exposure prior to infection was able to increase host susceptibility to arbovirus infection, provided the infection took place within 24h of the exposure. However, this modulation of host susceptibility to arbovirus infection was limited to the UV-exposed site. If this finding translates to humans, this gives hope that UV-mediated enhancement of infection could be prevented by protecting skin from UV exposure through traditional methods, e.g. covering exposed skin with clothing or applying sunscreen, as is recommended for protection against melanoma[449]. However, not all cross-sections of the population engage with sun safety guidance to the same extent. In a study carried out in Australia, teenage males were the least likely to partake in these behaviours[450]. So, there is a danger that UV-mediated enhancement of infection could affect certain groups more than others. This could be mitigated by targeted public health guidance or campaigns. Raising awareness of the dangers of UV exposure has previously

been shown to be of great success in terms of reducing skin cancer and so could be of great benefit here also[451].

8.7 Steroid treatment of UV burn partially alleviates enhancement of infection

Two treatments were tested as a means of protecting against the increase in host susceptibility following an erythemal UV exposure: regular topical corticosteroid treatment of the burn and a single injection of vitamin D at the burn site. While vitamin D had no effect against UV-mediated enhancement of infection, treatment of the UV burn with steroids initially showed promise in this regard. The treatment reduced viremia during the early stages of SFV infection. However, at later timepoints p.i., the protection offered by steroids was very varied, depending on the assessment. This treatment did not limit virus dissemination to the brain by 4 days p.i. or restore the generation of serum neutralising antibodies, which was dented in UV-exposed mice, likely explaining the increase in virus reaching the brain in these mice. Although, steroid treated mice did have significantly lower numbers of cells infiltrating the brain by 4 days p.i., indicating that steroids may modulate extent of immunopathology elicited by virus. Together, this suggests that steroid treatment of a UV burn partially protects against UV-mediated enhancement. However, further work is needed to determine whether this would protect from clinical disease. This particular study was stopped before clinical signs became apparent in mice, but it would be useful to monitor them for development of clinical disease after 4 days p.i., both to assess whether erythemal UV exposure worsens progression to severe disease, which we expect it would do based on our findings, and to determine whether steroids offer protection in this regard. Nevertheless, if erythemal UV exposure can be definitively identified as a risk factor for severe disease, this could e.g. help clinicians to stratify at-risk infected patients, which in case of severe DENV could inform the provision of intravenous fluids, which can significantly reduce mortality rates[73].

Interestingly, due to their immunosuppressive effects, steroids have been shown to increase infection risk in e.g., patients who take steroids to treat inflammatory

conditions[452–454]. However, it has also been proposed that they can be used to manage sepsis, a condition characterised by an overactive, damaging immune response to infection[455]. Furthermore, the use of corticosteroids reduced mortality in critically ill COVID-19 patients with severe respiratory issues[456]. In our study, this dampening of the immune system by steroids appears to offer some protection against arbovirus infection in UV-exposed skin. This suggests that some aspects of the immune system are harmful to the host when the infection takes place in UV-exposed skin.

8.8 *Aedes aegypti* behave differently towards UV-exposed skin

As well as impacting the host response to infection, erythemal UV exposure of host skin also impacts mosquito behaviour during feeding. While mosquitos did not reach UV-exposed skin any quicker, more mosquitos landed on the skin and each insect spent a longer average time probing UV-exposed skin. This will not only result in more virus-enhancing salivary proteins being imbued in the skin but also likely a higher virus dose, as increased feeding by the vector has been shown to result in a higher virus dose being transmitted[457]. The use of infected mosquitos in our protocol in the future could confirm whether more virus is deposited in UV-exposed skin.

UV exposed mouse skin is significantly warmer than unexposed skin, and so this likely occurs due to the heat and humidity sensors present in *Aedes spp.* antennae, which they use to identify hosts[316,317]. However, we have not ruled out the contribution of other factors in this regard. For example, a recent study found that UV exposure changes the production of metabolites by the host skin microbiome in mice[458]. Furthermore, differences in the composition of the skin microbiota between hosts has also been shown to alter the likelihood of a mosquito feeding on a host[337]. Thus, if UV exposure also alters the microbiota of an individual, this could also contribute to the alterations in mosquito behaviour towards UV-exposed skin, shown here. 16S ribosomal RNA (rRNA) gene amplicon sequencing to characterise the microbiome composition in UV-exposed skin could be used in the future to determine whether the microbiota is more attractive to mosquitos[459].

If mosquito behaviour towards UV-exposed human skin is also altered, this could have implications for virus transmission in areas of endemicity. This, paired with the finding that the host is more susceptible to infection once virus has been transmitted, presents a worrying health risk of great relevance in regions where individuals are exposed to both arbovirus infection and high levels of UV light from the sun. If this translates to pathogenesis of arboviruses in humans, this could necessitate public health advice highlighting the importance of sun safety practices in transmission zones.

8.9 Psoriatic PBMCs are resistant to ZIKV infection

Outside of UV exposure of the skin, this thesis identified another factor which modulates host susceptibility to arbovirus infection: the presence of a pre-existing systemic inflammatory disease state in patients with either psoriasis or systemic sclerosis. PBMCs collected from psoriasis patients or systemic sclerosis patients exhibited increase resistance to ZIKV infection compared to cells from healthy control donors. This effect was most extreme in psoriatic PBMCs, which showed a greater degree of resistance when infected at varying virus MOIs. Critically, psoriatic PBMCs, but not those from systemic sclerosis patients, induced IFN-α to a much higher level than HCs following infection and levels were not higher at rest, meaning that this was more potently expressed following stimulation with virus. This subsequently led to increased expression of the IFN-induced PRR RIG-I. This receptor is used by cells to recognise virus infection and trigger further downstream Type I IFN antiviral responses via the transcription factors IRF3 and NF-κB[460]. Therefore, this may be one way by which these cells are more resistant to ZIKV infection.

Levels of resistance against ZIKV infection was not linked to the severity of disease in the patient who donated their PBMCs, in either psoriasis or systemic sclerosis patients. This is of particular importance with relation to systemic sclerosis. We had hypothesised that dysregulation of type I IFN responses in patients, a critical part of the pathogenesis of this disease, may provide resistance against arbovirus infection. However, a patients IFN score is used to measure disease severity, with a high score relating to high levels of serum ISGs[461]. Therefore, there does not appear to be a link between reduced

susceptibility to arbovirus infection and IFN dysregulation in the case of systemic sclerosis.

Interestingly, when the cellular profile of the PBMC compartment from psoriasis patient samples was compared to those donated by healthy donors at rest, it was noted that there were significantly less non-classical monocytes in psoriatic PBMCs. As these cells are known to be one of the primary targets of ZIKV infection in PBMCs[424], this smaller population size prior to infection may contribute to the resistance against ZIKV infection observed in patient cells.

Prior to this study, there was epidemiological evidence that there is lower incidence of infectious diseases amongst psoriasis patients compared to patients with another inflammatory skin disease eczema[415,416]. However, our study is the first to provide evidence that psoriasis patients may be less susceptible to a specific infectious agent. This adds to previous unpublished work by our group which found that psoriatic lesional skin is less susceptible to ZIKV infection than non-lesional skin from the same donor. Together, this shows that resistance occurs both at the skin and systemically. This has implications both for understanding arbovirus pathogenesis and aspects of a successful immune response against arboviruses but also for the molecular mechanisms underlying psoriasis.

However, a better understanding of the mechanism driving the resistance to ZIKV infection observed in psoriatic PBMCs is needed to shed light on these aspects. This thesis has identified several DEGs, through RNAseq analysis, which are either up- or down-regulated during infection, compared to healthy donor cells. These candidates, particularly IL-18BP, should be investigated in more depth as they have the potential to explain some of the underlying mechanisms of this phenotype.

The phenotype observed in psoriatic PBMCs is also the opposite of what was observed in UV-exposed skin, suggesting that the mechanisms behind each are very different. Interestingly, UV light therapy is sometimes used to treat psoriasis, which some hypothesise is due to its immunosuppressive properties[207]. It is worth considering whether this therapy dampens the aspects

of psoriatic skin that are also result in enhanced resistance to arbovirus infection. Therefore, identifying which aspects of UV exposure are damaging in terms of host response to infection and what makes psoriatic PBMCs better at fighting infection could help guide arbovirus treatment or vaccine design.

8.10 Overall conclusions

This thesis explored the possibility that host susceptibility to arbovirus infection could be altered by a pre-existing immunomodulated environment, as a result of UV exposure or inflammatory skin disease. UV exposure of the skin prior to infection *in vivo* makes the host more susceptible to virus infection. Contrastingly, psoriatic PBMCs are more resistant to virus infection. Together, this highlights the influence pre-existing inflammation, either at the skin or systemically, can have on virus infection outcomes. Furthermore, this shows how varied inflammatory tissue microenvironments can have profoundly different impacts on host susceptibility to virus. The effects of UV exposure on arbovirus infection, from impacting host response to infection to mosquito behaviour towards the UV-exposed host, has important implications for disease transmission and infection outcomes, especially for those regions with high environmental UV levels. While our finding in relation to psoriasis PBMCs can be built upon to better understand infection risk in these patients and also the underlying disease pathogenesis.

References

1. Conway, M. J., Colpitts, T. M. & Fikrig, E. Role of the vector in arbovirus transmission. *Annu Rev Virol* **1**, 71–88 (2014).
2. Weaver, S. C. & Reisen, W. K. *Present and Future Arboviral Threats*. *Antiviral Research* vol. 85 (2010).
3. Centers for Disease Prevention and Control. Arbovirus Catalog. https://wwwn.cdc.gov/arbocat/VirusBrowser.aspx (1958).
4. Huang, Y. J. S., Higgs, S. & Vanlandingham, D. L. Arbovirus-mosquito vector-host interactions and the impact on transmission and disease pathogenesis of arboviruses. *Front Microbiol* **10**, 1–14 (2019).
5. Wilder-Smith, A. *et al.* Epidemic arboviral diseases: priorities for research and public health. *Lancet Infect Dis* **17**, e101–e106 (2017).
6. Bhatt, S. *et al.* The global distribution and burden of dengue. *Nature* **496**, 504–507 (2013).
7. Messina, J. P. *et al.* The current and future global distribution and population at risk of dengue. *Nat Microbiol* **4**, 1508–1515 (2019).
8. Wilder-Smith, A. *et al.* Epidemic arboviral diseases: priorities for research and public health. *Lancet Infect Dis* **17**, e101–e106 (2017).
9. Paixão, E. S., Teixeira, M. G. & Rodrigues, L. C. Zika, chikungunya and dengue: The causes and threats of new and reemerging arboviral diseases. *BMJ Glob Health* **3**, (2018).
10. World Health Organization. Dengue – the Region of the Americas (Disease Outbreak News). https://www.who.int/emergencies/disease-outbreak-news/item/2023-DON475#:~:text=Some of the severe cases,5.2 million in 2019 globally. (2023).
11. European Centre for Disease Prevention and Control. Dengue cases January-December 2023. https://www.ecdc.europa.eu/en/publications-data/dengue-cases-january-december-2023#:~:text=In 2023%2C over six million,reported from 92 countries%2Fterritories (2024).
12. Kakkar, M. Dengue fever is massively under-reported in India, hampering our response. *BMJ* **345**, 1–2 (2012).
13. Suhrbier, A. Rheumatic manifestations of chikungunya: emerging concepts and interventions. *Nat Rev Rheumatol* **15**, 597–611 (2019).
14. de Souza, W. M. *et al.* Spatiotemporal dynamics and recurrence of chikungunya virus in Brazil: an epidemiological study. *Lancet Microbe* **4**, e319–e329 (2023).
15. de Souza, W. M. *et al.* Chikungunya: a decade of burden in the Americas. *Lancet Regional Health - Americas* **30**, 100673 (2024).
16. Ferreira de Almeida, I. *et al.* The expansion of chikungunya in Brazil. *Lancet Regional Health - Americas* **25**, 100571 (2023).
17. Pan American Health Organization/World Health Organization. PAHO/WHO data - weekly report. (2023).
18. Dick, G. W. A., Kitchen, S. F. & Haddow, A. J. Zika isolation and serological specificity. *Trans Royal Soc Trop Med Hyg* **46**, 509–520 (1952).
19. MacNamara, F. N. Zika virus: A report on three cases of human infection during an epidemic of jaundice in Nigeria. *Trans R Soc Trop Med Hyg* **48**, 139–145 (1954).
20. Chan, J. F. W., Choi, G. K. Y., Yip, C. C. Y., Cheng, V. C. C. & Yuen, K. Y. Zika fever and congenital Zika syndrome: An unexpected emerging arboviral disease. *Journal of Infection* **72**, 507–524 (2016).

21. Musso, D. & Gubler, D. J. Zika virus. *Clin. Microbiol. Rev* **29**, 487–524 (2016).
22. Campos, G. S., Bandeira, A. C. & Sardi, S. I. Zika virus outbreak, Bahia, Brazil. *Emerg Infect Dis* **21**, 1885–1886 (2015).
23. Hennessey, M., Fischer, M. & Staples, J. E. Zika Virus Spreads to New Areas — Region of the Americas, May 2015–January 2016. *MMWR Morb Mortal Wkly Rep* **65**, 55–58 (2016).
24. Gulland, A. Zika virus is a global public health emergency, declares WHO. *BMJ* **352**, i657 (2016).
25. World Health Organization. Countries and territories with current or previous Zika virus transmission. https://cdn.who.int/media/docs/default-source/documents/emergencies/zika/countries-with-zika-and-vectors-table_february-2022.pdf?sfvrsn=4dc1f8ab_5 (2022).
26. Powell, J. R. Mosquito-borne human viral diseases: Why aedes aegypti? *American Journal of Tropical Medicine and Hygiene* **98**, 1563–1565 (2018).
27. Rezza, G. Aedes albopictus and the reemergence of Dengue. *BMC Public Health* **12**, 72 (2012).
28. Weaver, S. C. & Barrett, A. D. T. Transmission cycles, host range, evolution and emergence of arboviral disease. *Nat Rev Microbiol* **2**, 789–801 (2004).
29. Wu, P., Yu, X., Wang, P. & Cheng, G. Arbovirus lifecycle in mosquito: Acquisition, propagation and transmission. *Expert Rev Mol Med* **21**, (2019).
30. Chang, Y. Y. H. & Judson, C. L. The role of isoleucine in differential egg production by the mosquito Aedes aegypti linnaeus (Diptera: Culicidae) following feeding on human or guinea pig blood. *Comp Biochem Physiol A Physiol* **57**, 23–28 (1977).
31. Harrington, L. C., Edman, J. D. & Scott, T. W. Why do female Aedes aegypti (Diptera: Culicidae) feed preferentially and frequently on human blood? *J Med Entomol* **38**, 411–422 (2001).
32. Achee, N. L. *et al.* A Critical Assessment of Vector Control for Dengue Prevention. *PLoS Negl Trop Dis* **9**, 1–19 (2015).
33. Achee, N. L. *et al.* Alternative strategies for mosquito-borne arbovirus control. *PLoS Negl Trop Dis* **13**, 1–22 (2019).
34. Sandy Ong. Wolbachia goes to work in the war on mosquitoes. *Nature* **598**, (2021).
35. Leta, S. *et al.* Global risk mapping for major diseases transmitted by Aedes aegypti and Aedes albopictus. *International Journal of Infectious Diseases* **67**, 25–35 (2018).
36. Brady, O. J. *et al.* Modelling adult Aedes aegypti and Aedes albBrady, O. J., Johansson, M. a, Guerra, C. a, Bhatt, S., Golding, N., Pigott, D. M., … Hay, S. I. (2013). Modelling adult Aedes aegypti and Aedes albopictus survival at different temperatures in laboratory and fie. *Parasit Vectors* **6**, 351 (2013).
37. Laursen, W. J. *et al.* Humidity sensors that alert mosquitoes to nearby hosts and egg-laying sites. *Neuron* **111**, 874-887.e8 (2023).
38. Vogels, C. B. F. *et al.* Arbovirus coinfection and co-transmission: A neglected public health concern? *PLoS Biol* **17**, 1–16 (2019).
39. Kraemer, M. U. G. *et al.* The global distribution of the arbovirus vectors Aedes aegypti and Ae. Albopictus. *Elife* **4**, 1–18 (2015).
40. Whitehorn, J. & Yacoub, S. Global warming and arboviral infections. *Clinical Medicine* **19**, 149–152 (2019).
41. Kraemer, M. U. G. *et al.* Past and future spread of the arbovirus vectors Aedes aegypti and Aedes albopictus. *Nat Microbiol* **4**, 854–863 (2019).

42. European Centre for Disease Prevention and Control. Autochthonous vectorial transmission of dengue virus in mainland EU/EEA, 2010-present. (2024).
43. Brady, O. J. & Hay, S. I. The first local cases of Zika virus in Europe. *The Lancet* **394**, 1991–1992 (2019).
44. Giron, S. *et al.* Vector-borne transmission of Zika virus in Europe, southern France, August 2019. *Euro Surveill* **24**, 1–4 (2019).
45. Wilkerson, R. C., Linton, Y. M. & Strickman, D. *Mosquitoes of the World*. (Johns Hopkins University Press, Baltimore, Maryland, USA, 2020).
46. European Centre for Disease Prevention and Control. Aedes invasive mosquitoes - current known distribution: October 2023. https://www.ecdc.europa.eu/en/publications-data/aedes-invasive-mosquitoes-current-known-distribution-october-2023 (2023).
47. Weaver, S. C. & Reisen, W. K. Present and future arboviral threats. *Antiviral Res* **85**, 328–345 (2010).
48. Mordecai, E. A., Ryan, S. J., Caldwell, J. M., Shah, M. M. & LaBeaud, A. D. Climate change could shift disease burden from malaria to arboviruses in Africa. *Lancet Planet Health* **4**, e416–e423 (2020).
49. McKenzie, B. A., Wilson, A. E. & Zohdy, S. Aedes albopictus is a competent vector of Zika virus: A meta-analysis. *PLoS One* **14**, 1–16 (2019).
50. Vega-Rúa, A. *et al.* Vector competence of Aedes albopictus populations for chikungunya virus is shaped by their demographic history. *Commun Biol* **3**, 25–28 (2020).
51. Peng, H. J. *et al.* A local outbreak of dengue caused by an imported case in Dongguan China. *BMC Public Health* **12**, (2012).
52. Liu-Helmersson, J., Stenlund, H., Wilder-Smith, A. & Rocklöv, J. Vectorial capacity of Aedes aegypti: Effects of temperature and implications for global dengue epidemic potential. *PLoS One* **9**, (2014).
53. Colón-González, F. J. *et al.* Projecting the future incidence and burden of dengue in Southeast Asia. *Nat Commun* **14**, (2023).
54. Simmons, C. P., Farrar, J. J., Chau, N. V. V. & Wills, B. Dengue. *New England Journal of Medicine* **366**, 1423–32 (2012).
55. Mallhi, T. H., Khan, A. H., Sarriff, A., Adnan, A. S. & Khan, Y. H. Determinants of mortality and prolonged hospital stay among dengue patients attending tertiary care hospital: A cross-sectional retrospective analysis. *BMJ Open* **7**, 1–12 (2017).
56. Libraty, D. H. *et al.* High circulating levels of the dengue virus nonstructural protein NS1 early in dengue illness correlate with the development of dengue hemorrhagic fever. *Journal of Infectious Diseases* **186**, 1165–1168 (2002).
57. Ioos, S. *et al.* Current Zika virus epidemiology and recent epidemics. *Med Mal Infect* **44**, 302–307 (2014).
58. Duffy, M. R. *et al.* Zika Virus Outbreak on Yap Island, Federated States of Micronesia. *New England Journal of Medicine* **360**, 2536–2543 (2009).
59. Rasmussen, S. A., Jamieson, D. J., Honein, M. A. & Petersen, L. R. Zika Virus and Birth Defects — Reviewing the Evidence for Causality. *New England Journal of Medicine* **374**, 1981–1987 (2016).
60. Wang, A., Thurmond, S., Islas, L., Hui, K. & Hai, R. Zika virus genome biology and molecular pathogenesis. *Emerg Microbes Infect* **6**, 1–6 (2017).
61. James, S. H., Sheffield, J. S. & Kimberlin, D. W. Mother-to-child transmission of herpes simplex virus. *J Pediatric Infect Dis Soc* **3**, 19–23 (2014).

62. Lilleri, D. *et al.* Fetal Human Cytomegalovirus Transmission Correlates with Delayed Maternal Antibodies to gH/gL/pUL128-130-131 Complex during Primary Infection. *PLoS One* **8**, 1–13 (2013).
63. Schuler-Faccini, L. *et al.* Possible Association Between Zika Virus Infection and Microcephaly — Brazil, 2015. *MMWR Morb Mortal Wkly Rep* **65**, 59–62 (2016).
64. Oehler, E. *et al.* Zika virus infection complicated by Guillain-Barré syndrome - case report, French Polynesia, December 2013. *Eurosurveillance* **19**, 7–9 (2014).
65. Cao-Lormeau, V. M. *et al.* Guillain-Barré Syndrome outbreak associated with Zika virus infection in French Polynesia: A case-control study. *The Lancet* **387**, 1531–1539 (2016).
66. Mécharles, S. *et al.* Acute myelitis due to Zika virus infection. *The Lancet* **387**, 1481 (2016).
67. Kim, D. Y., Firth, A. E., Atasheva, S., Frolova, E. I. & Frolov, I. Conservation of a Packaging Signal and the Viral Genome RNA Packaging Mechanism in Alphavirus Evolution. *J Virol* **85**, 8022–8036 (2011).
68. Carteaux, G. *et al.* Zika Virus Associated with Meningoencephalitis. *New England Journal of Medicine* **374**, 1595–6 (2016).
69. Nakkhara, P., Chongsuvivatwong, V. & Thammapalo, S. Risk factors for symptomatic and asymptomatic chikungunya infection. *Trans R Soc Trop Med Hyg* **107**, 789–796 (2013).
70. Paixão, E. S. *et al.* Chikungunya chronic disease: A systematic review and meta-analysis. *Trans R Soc Trop Med Hyg* **112**, 301–316 (2018).
71. Puntasecca, C. J., King, C. H. & Labeaud, A. D. Measuring the global burden of Chikungunya and Zika viruses: A systematic review. *PLoS Negl Trop Dis* **15**, 1–18 (2021).
72. Pan American Health Organization. *Tool for the Diagnosis and Care of Patients with Suspected Arboviral Diseases*. (2017).
73. Dung, N. M. *et al.* Fluid Replacement in Dengue Shock Syndrome: A Randomized, Double-Blind Comparison of Four Intravenous-Fluid Regimens. *Clinical Infectious Diseases* **29**, 787–794 (1999).
74. Kling, K. *et al.* Duration of Protection after Vaccination Against Yellow Fever: A Systematic Review and Meta-Analysis. *Clinical Infectious Diseases* **75**, 2266–2274 (2022).
75. Sunwoo, J. S., Jung, K. H., Lee, S. T., Lee, S. K. & Chu, K. Reemergence of Japanese encephalitis in South Korea, 2010–2015. *Emerg Infect Dis* **22**, 1841–1843 (2016).
76. Ferguson, N. M. *et al.* Benefits and risks of the sanofi-pasteur dengue vaccine: Modeling optimal deployment. *Science (1979)* **353**, 1033–1036 (2016).
77. Hadinegoro, S. R. *et al.* Efficacy and Long-Term Safety of a Dengue Vaccine in Regions of Endemic Disease. *New England Journal of Medicine* **373**, 1195–1206 (2015).
78. Wilder-Smith, A. *et al.* Deliberations of the Strategic Advisory Group of Experts on Immunization on the use of CYD-TDV dengue vaccine. *Lancet Infectious Diseases* **19**, e31–e38 (2019).
79. U.S. Food and Drug Administration. FDA Approves First Vaccine to Prevent Disease Caused by Chikungunya Virus. (2023).
80. Mullard, A. FDA approves first chikungunya vaccine. *Nat Rev Drug Discov* **23**, 8–9 (2024).

81. Santos-Peral, A. *et al.* Prior flavivirus immunity skews the yellow fever vaccine response to cross-reactive antibodies with potential to enhance dengue virus infection. *Nat Commun* **15**, 1–17 (2024).
82. Katzelnick, L. C. *et al.* Zika virus infection enhances future risk of severe dengue disease. *Science (1979)* **369**, 1123–1128 (2020).
83. Katzelnick, L. C. *et al.* Antibody-dependent enhancement of severe dengue disease in humans. *Science (1979)* **358**, 929–932 (2017).
84. Hamel, R. *et al.* Biology of Zika Virus Infection in Human Skin Cells. *J Virol* **89**, 8880–8896 (2015).
85. Sirohi, D. *et al.* The 3.8A cryo-EM structure of Zika Virus. *Science (1979)* **1848**, 3047–3054 (2016).
86. Kuno, G. & Chang, G. J. J. Full-length sequencing and genomic characterization of Bagaza, Kedougou, and Zika viruses. *Arch Virol* **152**, 687–696 (2007).
87. Baronti, C. *et al.* Complete coding sequence of Zika virus from a French Polynesia outbreak in 2013. *Genome Announc* **2**, 2013–2014 (2014).
88. Yun, S. I. & Lee, Y. M. Zika virus: An emerging flavivirus. *Journal of Microbiology* **55**, 204–219 (2017).
89. Richard, A. S. *et al.* AXL-dependent infection of human fetal endothelial cells distinguishes Zika virus from other pathogenic flaviviruses. *Proc Natl Acad Sci U S A* **114**, 2024–2029 (2017).
90. Hasan, S. S., Sevvana, M., Kuhn, R. J. & Rossmann, M. G. Structural biology of Zika virus and other flaviviruses. *Nat Struct Mol Biol* **25**, 13–20 (2018).
91. Dai, L. *et al.* Structures of the Zika Virus Envelope Protein and Its Complex with a Flavivirus Broadly Protective Antibody. *Cell Host Microbe* **19**, 696–704 (2016).
92. Fritz, R., Stiasny, K. & Heinz, F. X. Identification of specific histidines as pH sensors in flavivirus membrane fusion. *Journal of Cell Biology* **183**, 353–361 (2008).
93. Welsch, S. *et al.* Composition and Three-Dimensional Architecture of the Dengue Virus Replication and Assembly Sites. *Cell Host Microbe* **5**, 365–375 (2009).
94. Iglesias, N. G. & Gamarnik, A. V. Dynamic RNA structures in the dengue virus genome. *RNA Biol* **8**, 249–257 (2011).
95. Cox, B. D., Stanton, R. A. & Schinazi, R. F. Predicting Zika virus structural biology: Challenges and opportunities for intervention. *Antivir Chem Chemother* **24**, 118–126 (2015).
96. Jain, R., Coloma, J., García-Sastre, A. & Aggarwal, A. K. Structure of the NS3 helicase from Zika virus. *Nat Struct Mol Biol* **23**, 752–754 (2016).
97. Pierson, T. C. & Diamond, M. S. Degrees of maturity: The complex structure and biology of flaviviruses. *Curr Opin Virol* **2**, 168–175 (2012).
98. Zaid, A. *et al.* Arthritogenic alphaviruses: epidemiological and clinical perspective on emerging arboviruses. *Lancet Infect Dis* **3099**, (2020).
99. Caluwé, L. De, Ariën, K. K. & Bartholomeeusen, K. Host Factors and Pathways Involved in the Entry of Mosquito-Borne Alphaviruses. *Trends Microbiol* 1–14 (2020) doi:10.1016/j.tim.2020.10.011.
100. Forrester, N. L. *et al.* Genome-Scale Phylogeny of the Alphavirus Genus Suggests a Marine Origin. *J Virol* **86**, 2729–2738 (2012).
101. Fazakerley, J. K. Pathogenesis of Semliki Forest virus encephalitis. *J Neurovirol* **8**, 66–74 (2002).
102. Solignat, M., Gay, B., Higgs, S., Briant, L. & Devaux, C. Replication cycle of chikungunya: A re-emerging arbovirus. *Virology* **393**, 183–197 (2009).

103. Burt, F. J. *et al.* Chikungunya virus: an update on the biology and pathogenesis of this emerging pathogen. *Lancet Infect Dis* **17**, e107–e117 (2017).
104. Rupp, J. C., Sokoloski, K. J., Gebhart, N. N. & Hardy, R. W. Alphavirus RNA synthesis and non-structural protein functions. *Journal of General Virology* **96**, 2483–2500 (2015).
105. Zhang, R. *et al.* Mxra8 is a receptor for multiple arthritogenic alphaviruses. *Nature* **557**, 570–574 (2018).
106. McAllister, N. *et al.* Chikungunya virus strains from each genetic clade bind sulfated glycosaminoglycans as attachment factors. *J Virol* **94**, 1–19 (2020).
107. Pastorino, B. A. M. *et al.* Expression and biochemical characterization of nsP2 cysteine protease of Chikungunya virus. *Virus Res* **131**, 293–298 (2008).
108. Kallio, K., Hellström, K., Jokitalo, E. & Ahola, T. RNA Replication and Membrane Modification Require the Same Functions of Alphavirus Nonstructural Proteins. *J Virol* **90**, 1687–1692 (2016).
109. Ou, J. H., Rice, C. M., Dalgarno, L., Strauss, E. G. & Strauss, J. H. Sequence studies of several alphavirus genomic RNAs in the region containing the start of the subgenomic RNA. *Proc Natl Acad Sci U S A* **79**, 5235–5239 (1982).
110. Thomas, S. *et al.* Chikungunya virus capsid protein contains nuclear import and export signals. *Virol J* **10**, 1–13 (2013).
111. Jones, P. H. *et al.* BST-2/tetherin-mediated restriction of chikungunya (CHIKV) VLP budding is counteracted by CHIKV non-structural protein 1 (nsP1). *Virology* **438**, 37–49 (2013).
112. Lim, P. J. & Chu, J. J. H. A Polarized Cell Model for Chikungunya Virus Infection: Entry and Egress of Virus Occurs at the Apical Domain of Polarized Cells. *PLoS Negl Trop Dis* **8**, (2014).
113. Smithburn, K. & Haddow, A. Semliki Forest virus. 1. Isolation and pathogenic properties. *Journal of Immunology* **49**, 141–57 (1944).
114. Braack, L., Gouveia De Almeida, A. P., Cornel, A. J., Swanepoel, R. & De Jager, C. Mosquito-borne arboviruses of African origin: Review of key viruses and vectors. *Parasit Vectors* **11**, (2018).
115. Mathiot, C. *et al.* An Outbreak of Human Semliki Forest Virus Infections in Central African Republic. *American Journal of Tropical Medicine and Hygiene* **42**, 386–393 (1990).
116. Willems, W. R. *et al.* Semliki forest virus: Cause of a fatal case of human encephalitis. *Science (1979)* **203**, 1127–1129 (1979).
117. Fragkoudis, R. *et al.* The type I interferon system protects mice from Semliki Forest virus by preventing widespread virus dissemination in extraneural tissues, but does not mediate the restricted replication of avirulent virus in central nervous system neurons. *Journal of General Virology* **88**, 3373–3384 (2007).
118. Ferguson, M. C. *et al.* Ability of the Encephalitic Arbovirus Semliki Forest Virus To Cross the Blood-Brain Barrier Is Determined by the Charge of the E2 Glycoprotein. *J Virol* **89**, 7536–7549 (2015).
119. Bryden, S. R. *et al.* Pan-viral protection against arboviruses by activating skin macrophages at the inoculation site. *Sci Transl Med* **12**, (2020).
120. Pingen, M. *et al.* Host Inflammatory Response to Mosquito Bites Enhances the Severity of Arbovirus Infection. *Immunity* **44**, 1455–1469 (2016).
121. Pennemann, F. L. *et al.* Cross-species analysis of viral nucleic acid interacting proteins identifies TAOKs as innate immune regulators. *Nat Commun* **12**, 1–22 (2021).

122. Bradish, C. J., Allner, K. & Maber, H. B. The virulence of original and derived strains of Semliki forest virus for mice, guinea-pigs and rabbits. *J Gen Virol* **12**, 141–160 (1971).
123. Wauquier, N. *et al.* The acute phase of Chikungunya virus infection in humans is associated with strong innate immunity and T CD8 cell activation. *Journal of Infectious Diseases* **204**, 115–123 (2011).
124. Ngono, A. E. & Shresta, S. Immune Response to Dengue and Zika. *Annu Rev Immunol* **36**, 279–308 (2018).
125. Pingen, M., Schmid, M. A., Harris, E. & McKimmie, C. S. Mosquito Biting Modulates Skin Response to Virus Infection. *Trends Parasitol* **33**, 645–657 (2017).
126. Lefteri, D. A. *et al.* Mosquito saliva enhances virus infection through sialokinin-dependent vascular leakage. *Proc Natl Acad Sci U S A* **119**, (2022).
127. Rita E. Chen, M. S. & Diamond. Dengue mouse models for evaluating pathogenesis and countermeasures. *Physiol Behav* **176**, 139–148 (2021).
128. Lazear, H. M. *et al.* A Mouse Model of Zika Virus Pathogenesis. *Cell Host Microbe* **19**, 720–730 (2016).
129. Thompson, M. R., Kaminski, J. J., Kurt-Jones, E. A. & Fitzgerald, K. A. Pattern recognition receptors and the innate immune response to viral infection. *Viruses* **3**, 920–940 (2011).
130. Nasirudeen, A. M. A. *et al.* RIG-i, MDA5 and TLR3 synergistically play an important role in restriction of dengue virus infection. *PLoS Negl Trop Dis* **5**, (2011).
131. Her, Z. *et al.* Loss of TLR3 aggravates CHIKV replication and pathology due to an altered virus-specific neutralizing antibody response. *EMBO Mol Med* **7**, 24–41 (2015).
132. Sun, B. *et al.* Dengue virus activates cGAS through the release of mitochondrial DNA. *Sci Rep* **7**, 1–8 (2017).
133. Baum, A. & García-Sastre, A. Induction of type i interferon by RNA viruses: Cellular receptors and their substrates. *Amino Acids* **38**, 1283–1299 (2010).
134. Schmid, M. A. *et al.* Mosquito Saliva Increases Endothelial Permeability in the Skin, Immune Cell Migration, and Dengue Pathogenesis during Antibody-Dependent Enhancement. *PLoS Pathog* **12**, 1–25 (2016).
135. Depinay, N., Hacini, F., Beghdadi, W., Peronet, R. & Mécheri, S. Mast Cell-Dependent Down-Regulation of Antigen-Specific Immune Responses by Mosquito Bites. *The Journal of Immunology* **176**, 4141–4146 (2006).
136. Rosales, C. Neutrophil: A cell with many roles in inflammation or several cell types? *Front Physiol* **9**, 1–17 (2018).
137. Hiroki, C. H. *et al.* Neutrophil Extracellular Traps Effectively Control Acute Chikungunya Virus Infection. *Front Immunol* **10**, 1–11 (2020).
138. Sung, P. S., Huang, T. F. & Hsieh, S. L. Extracellular vesicles from CLEC2-activated platelets enhance dengue virus-induced lethality via CLEC5A/TLR2. *Nat Commun* **10**, 1–13 (2019).
139. Uraki, R. *et al.* Aedes aegypti AgBR1 antibodies modulate early Zika virus infection of mice. *Nat Microbiol* **4**, 948–955 (2019).
140. Hastings, A. K. *et al.* Aedes aegypti NeSt1 Protein Enhances Zika Virus Pathogenesis by Activating Neutrophils . *J Virol* **93**, 1–16 (2019).
141. Lin, T. *et al.* CXCL10 Signaling Contributes to the Pathogenesis of Arthritogenic Alphaviruses. *Viruses* **12**, 1–13 (2020).

142. Michlmayr, D., Andrade, P., Gonzalez, K., Balmaseda, A. & Harris, E. CD14+CD16+ monocytes are the main target of Zika virus infection in peripheral blood mononuclear cells in a paediatric study in Nicaragua. *Nat Microbiol* **2**, 1462–1470 (2017).
143. Kelvin, A. A. *et al.* Inflammatory cytokine expression is associated with Chikungunya virus resolution and symptom severity. *PLoS Negl Trop Dis* **5**, (2011).
144. Poo, Y. S. *et al.* CCR2 Deficiency Promotes Exacerbated Chronic Erosive Neutrophil-Dominated Chikungunya Virus Arthritis. *J Virol* **88**, 6862–6872 (2014).
145. Schilte, C. *et al.* Type I IFN controls chikungunya virus via its action on nonhematopoietic cells. *Journal of Experimental Medicine* **207**, 429–442 (2010).
146. Hwang, S. Y. *et al.* A null mutation in the gene encoding a type I interferon receptor component eliminates antiproliferative and antiviral responses to interferons α and β and alters macrophage responses. *Proc Natl Acad Sci U S A* **92**, 11284–11288 (1995).
147. Johnson, A. J. & Roehrig, J. T. New Mouse Model for Dengue Virus Vaccine Testing. *J Virol* **73**, 783–786 (1999).
148. Marín-Lopez, A. *et al.* Modeling arboviral infection in mice lacking the interferon alpha/beta receptor. *Viruses* **11**, 1–25 (2019).
149. Grant, A. *et al.* Zika virus targets human STAT2 to inhibit type I interferon signaling. *Cell Host Microbe* **19**, 882–890 (2016).
150. Webb, L. G. *et al.* Chikungunya virus antagonizes cGAS-STING mediated type-I interferon responses by degrading cGAS. *PLoS Pathog* **16**, 1–28 (2020).
151. Webster, B. *et al.* Plasmacytoid dendritic cells control dengue and chikungunya virus infections via IRF7-regulated interferon responses. *Elife* **7**, 1–23 (2018).
152. Pichyangkul, S. *et al.* A Blunted Blood Plasmacytoid Dendritic Cell Response to an Acute Systemic Viral Infection Is Associated with Increased Disease Severity. *The Journal of Immunology* **171**, 5571–5578 (2003).
153. Décembre, E. *et al.* Sensing of Immature Particles Produced by Dengue Virus Infected Cells Induces an Antiviral Response by Plasmacytoid Dendritic Cells. *PLoS Pathog* **10**, (2014).
154. Schmid, M. A. & Harris, E. Monocyte Recruitment to the Dermis and Differentiation to Dendritic Cells Increases the Targets for Dengue Virus Replication. *PLoS Pathog* **10**, (2014).
155. Cerny, D. *et al.* Selective Susceptibility of Human Skin Antigen Presenting Cells to Productive Dengue Virus Infection. *PLoS Pathog* **10**, (2014).
156. Libraty, D. H., Pichyangkul, S., Ajariyakhajorn, C., Endy, T. P. & Ennis, F. A. Human Dendritic Cells Are Activated by Dengue Virus Infection: Enhancement by Gamma Interferon and Implications for Disease Pathogenesis. *J Virol* **75**, 3501–3508 (2001).
157. Ngono, A. E. & Shresta, S. Immune Response to Dengue and Zika. *Annu Rev Immunol* **36**, 279–308 (2018).
158. Wauquier, N. *et al.* The acute phase of Chikungunya virus infection in humans is associated with strong innate immunity and T CD8 cell activation. *Journal of Infectious Diseases* **204**, 115–123 (2011).
159. Schneider, B. S., Soong, L., Zeidner, N. S. & Higgs, S. Aedes aegypti Salivary Gland Extracts Modulate Anti-Viral and TH1/TH2 Cytokine Responses to Sindbis Virus Infection. *Viral Immunol* **17**, 565–573 (2004).

160. Yauch, L. E. *et al.* A Protective Role for Dengue Virus-Specific CD8 + T Cells . *The Journal of Immunology* **182**, 4865–4873 (2009).
161. Elong Ngono, A. *et al.* Mapping and Role of the CD8+ T Cell Response During Primary Zika Virus Infection in Mice. *Cell Host Microbe* **21**, 35–46 (2017).
162. Hatch, S. *et al.* Intracellular cytokine production by dengue virus-specific T cells correlates with subclinical secondary infection. *Journal of Infectious Diseases* **203**, 1282–1291 (2011).
163. Teo, T.-H. *et al.* A Pathogenic Role for CD4 + T Cells during Chikungunya Virus Infection in Mice . *The Journal of Immunology* **190**, 259–269 (2013).
164. Yauch, L. E. *et al.* CD4 + T Cells Are Not Required for the Induction of Dengue Virus-Specific CD8 + T Cell or Antibody Responses but Contribute to Protection after Vaccination . *The Journal of Immunology* **185**, 5405–5416 (2010).
165. Fazakerley, J. K. Semliki forest virus infection of laboratory mice: a model to study the pathogenesis of viral encephalitis. *Arch Virol* 179–190 (2004) doi:10.1007/978-3-7091-0572-6_16.
166. Miner, J. J. *et al.* Brief report: Chikungunya viral arthritis in the United States: A mimic of seronegative rheumatoid arthritis. *Arthritis and Rheumatology* **67**, 1214–1220 (2015).
167. Miner, J. J. *et al.* Therapy with CTLA4-Ig and an antiviral monoclonal antibody controls chikungunya virus arthritis. *Sci Transl Med* **9**, 1–22 (2017).
168. Jurado, K. A. *et al.* Antiviral CD8 T cells induce Zika-virus-associated paralysis in mice. *Nat Microbiol* **3**, 141–147 (2018).
169. Duangchinda, T. *et al.* Immunodominant T-cell responses to dengue virus NS3 are associated with DHF. *Proc Natl Acad Sci U S A* **107**, 16922–16927 (2010).
170. Chua, C. L., Sam, I. C., Chiam, C. W. & Chan, Y. F. The neutralizing role of IgM during early Chikungunya virus infection. *PLoS One* **12**, 1–16 (2017).
171. Rey, F. A., Stiasny, K., Vaney, M., Dellarole, M. & Heinz, F. X. The bright and the dark side of human antibody responses to flaviviruses: lessons for vaccine design. *EMBO Rep* **19**, 206–224 (2018).
172. Jin, J. *et al.* Neutralizing Antibodies Inhibit Chikungunya Virus Budding at the Plasma Membrane. *Cell Host Microbe* **24**, 417-428.e5 (2018).
173. Upasani, V. *et al.* Impaired antibody-independent immune response of b cells in patients with acute dengue infection. *Front Immunol* **10**, 1–13 (2019).
174. Jain, J. *et al.* Evaluation of an immunochromatography rapid diagnosis kit for detection of chikungunya virus antigen in India, a dengue-endemic country. *Virol J* **15**, 1–6 (2018).
175. Chua, C. L., Sam, I. C., Chiam, C. W. & Chan, Y. F. The neutralizing role of IgM during early Chikungunya virus infection. *PLoS One* **12**, 1–16 (2017).
176. Wahala, W. M. P. B. & de Silva, A. M. The human antibody response to dengue virus infection. *Viruses* **3**, 2374–2395 (2011).
177. Prince, H. E., Seaton, B. L., Matud, J. L. & Batterman, H. J. Chikungunya virus RNA and antibody testing at a national reference laboratory since the emergence of chikungunya virus in the Americas. *Clinical and Vaccine Immunology* **22**, 291–297 (2015).
178. Kam, Y. W. *et al.* Early appearance of neutralizing immunoglobulin G3 antibodies is associated with chikungunya virus clearance and long-term clinical protection. *Journal of Infectious Diseases* **205**, 1147–1154 (2012).

179. Halstead, S. B., Shotwell, H. & Casals, J. Studies on the pathogenesis of dengue infection in monkeys. II. Clinical laboratory responses to heterologous infection. *J Infect Dis* **128**, 6 (1973).
180. Lum, F. M. *et al.* Antibody-mediated enhancement aggravates chikungunya virus infection and disease severity. *Sci Rep* **8**, 1–14 (2018).
181. Arcà, B. & Ribeiro, J. M. Saliva of hematophagous insects: a multifaceted toolkit. *Curr Opin Insect Sci* **29**, 102–109 (2018).
182. Martin-Martin, I. *et al.* Aedes aegypti sialokinin facilitates mosquito blood feeding and modulates host immunity and vascular biology. *Cell Rep* **39**, 110648 (2022).
183. Calvo, E., Mans, B. J., Andersen, J. F. & Ribeiro, J. M. C. Function and evolution of a mosquito salivary protein family. *Journal of Biological Chemistry* **281**, 1935–1942 (2006).
184. Manning, J. E., Morens, D. M., Kamhawi, S., Valenzuela, J. G. & Memoli, M. Mosquito Saliva: The Hope for a Universal Arbovirus Vaccine? *Journal of Infectious Diseases* **218**, 7–15 (2018).
185. Nestle, F. O., Di Meglio, P., Qin, J. Z. & Nickoloff, B. J. Skin immune sentinels in health and disease. *Nat Rev Immunol* **9**, 679–691 (2009).
186. Wong, R., Geyer, S., Weninger, W., Guimberteau, J. C. & Wong, J. K. The dynamic anatomy and patterning of skin. *Exp Dermatol* **25**, 92–98 (2016).
187. Proksch, E., Brandner, J. M. & Jensen, J. M. The skin: An indispensable barrier. *Exp Dermatol* **17**, 1063–1072 (2008).
188. Pfisterer, K., Shaw, L. E., Symmank, D. & Weninger, W. The Extracellular Matrix in Skin Inflammation and Infection. *Front Cell Dev Biol* **9**, 1–19 (2021).
189. Briant, L., Desprès, P., Choumet, V. & Missé, D. Role of skin immune cells on the host susceptibility to mosquito-borne viruses. *Virology* **464–465**, 26–32 (2014).
190. Couderc, T. *et al.* A mouse model for Chikungunya: Young age and inefficient type-I interferon signaling are risk factors for severe disease. *PLoS Pathog* **4**, (2008).
191. Bustos-Arriaga, J. *et al.* Activation of the innate immune response against denv in normal non-transformed human fibroblasts. *PLoS Negl Trop Dis* **5**, (2011).
192. Lim, P.-Y., Behr, M. J., Chadwick, C. M., Shi, P.-Y. & Bernard, K. A. Keratinocytes Are Cell Targets of West Nile Virus In Vivo . *J Virol* **85**, 5197–5201 (2011).
193. Surasombatpattana, P. *et al.* Dengue virus replication in infected human keratinocytes leads to activation of antiviral innate immune responses. *Infection, Genetics and Evolution* **11**, 1664–1673 (2011).
194. Wu, S. J. L. *et al.* Human skin Langerhans cells are targets of dengue virus infection. *Nat Med* **6**, 816–820 (2000).
195. Agarwal, Y. *et al.* Development of humanized mouse and rat models with full-thickness human skin and autologous immune cells. *Sci Rep* **10**, 1–11 (2020).
196. Salgado, G., Ng, Y. Z., Koh, L. F., Goh, C. S. M. & Common, J. E. Human reconstructed skin xenografts on mice to model skin physiology. *Differentiation* **98**, 14–24 (2017).
197. Nguyen, A. V. & Soulika, A. M. The dynamics of the skin's immune system. *Int J Mol Sci* **20**, 1–53 (2019).
198. Eyerich, K., Eyerich, S. & Biedermann, T. The Multi-Modal Immune Pathogenesis of Atopic Eczema. *Trends Immunol* **36**, 788–801 (2015).
199. Zhou, X., Chen, Y., Cui, L., Shi, Y. & Guo, C. Advances in the pathogenesis of psoriasis: from keratinocyte perspective. *Cell Death Dis* **13**, (2022).

200. Ono, S., Egawa, G. & Kabashima, K. Regulation of blood vascular permeability in the skin. *Inflamm Regen* **37**, 1–8 (2017).
201. Nourshargh, S. & Alon, R. Leukocyte Migration into Inflamed Tissues. *Immunity* **41**, 694–707 (2014).
202. Brinkmann, V. *et al.* Neutrophil Extracellular Traps Kill Bacteria. *Science (1979)* **303**, 1532–1535 (2004).
203. Borregaard, N. Neutrophils, from Marrow to Microbes. *Immunity* **33**, 657–670 (2010).
204. Duque, G. A. & Descoteaux, A. Macrophage cytokines: Involvement in immunity and infectious diseases. *Front Immunol* **5**, 1–12 (2014).
205. Delavary, B. M., van der Veer, W. M., van Egmond, M., Niessen, F. B. & Beelen, R. H. J. Macrophages in skin injury and repair. *Immunobiology* **216**, 753–762 (2011).
206. Szondi, D. C., Wong, J. K., Vardy, L. A. & Cruickshank, S. M. Arginase Signalling as a Key Player in Chronic Wound Pathophysiology and Healing. *Front Mol Biosci* **8**, 1–17 (2021).
207. Armstrong, A. W. & Read, C. Pathophysiology, Clinical Presentation, and Treatment of Psoriasis: A Review. *JAMA - Journal of the American Medical Association* **323**, 1945–1960 (2020).
208. Eming, S. A., Krieg, T. & Davidson, J. M. Inflammation in wound repair: Molecular and cellular mechanisms. *Journal of Investigative Dermatology* **127**, 514–525 (2007).
209. Leoni, G., Neumann, P. A., Sumagin, R., Denning, T. L. & Nusrat, A. Wound repair: Role of immune-epithelial interactions. *Mucosal Immunol* **8**, 959–968 (2015).
210. Werner, S., Krieg, T. & Smola, H. Keratinocyte-fibroblast interactions in wound healing. *Journal of Investigative Dermatology* **127**, 998–1008 (2007).
211. Landén, N. X., Li, D. & Ståhle, M. Transition from inflammation to proliferation: a critical step during wound healing. *Cellular and Molecular Life Sciences* **73**, 3861–3885 (2016).
212. Schultz, G. S. & Wysocki, A. Interactions between extracellular matrix and growth factors in wound healing. *Wound Repair and Regeneration* **17**, 153–162 (2009).
213. Hinz, B. *et al.* The myofibroblast: One function, multiple origins. *American Journal of Pathology* **170**, 1807–1816 (2007).
214. Jacinto, A., Martinez-Arias, A. & Martin, P. Mechanisms of epithelial fusion and repair. *Nat Cell Biol* **3**, 117–123 (2001).
215. Witte, M. B. & Barbul, A. Role of nitric oxide in wound repair. *Am J Surg* **183**, 406–412 (2002).
216. Li, J., Zhang, Y. P. & Kirsner, R. S. Angiogenesis in wound repair: Angiogenic growth factors and the extracellular matrix. *Microsc Res Tech* **60**, 107–114 (2003).
217. Sim, S. L., Kumari, S., Kaur, S. & Khosrotehrani, K. Macrophages in Skin Wounds: Functions and Therapeutic Potential. *Biomolecules* **12**, 1659 (2022).
218. Hesketh, M., Sahin, K. B., West, Z. E. & Murray, R. Z. Macrophage phenotypes regulate scar formation and chronic wound healing. *Int J Mol Sci* **18**, 1–10 (2017).
219. Lucas, T. *et al.* Differential Roles of Macrophages in Diverse Phases of Skin Repair. *The Journal of Immunology* **184**, 3964–3977 (2010).
220. D'Orazio, J., Jarrett, S., Amaro-Ortiz, A. & Scott, T. UV radiation and the skin. *Int J Mol Sci* **14**, 12222–12248 (2013).

221. NASA Earth Observations. UV Index. https://neo.gsfc.nasa.gov/view.php?datasetId=AURA_UVI_CLIM_M (2011).
222. Matsumura, Y. & Ananthaswamy, H. N. Toxic effects of ultraviolet radiation on the skin. *Toxicol Appl Pharmacol* **195**, 298–308 (2004).
223. Bernard, J. J., Gallo, R. L. & Krutmann, J. Photoimmunology: how ultraviolet radiation affects the immune system. *Nat Rev Immunol* **19**, 688–701 (2019).
224. Godar, D. E. UV Doses Worldwide. *Photochem Photobiol.* **81**, 736–749 (2005).
225. International Agency for Resarch on Cancer. *Radiation - A Review of Human Carcinogens*. vol. 100D (International Agency for Research on Cancer, Lyon, France, 2012).
226. Han, A. & Maibach, H. I. Management of acute sunburn. *Am J Clin Dermatol* **5**, 39–47 (2004).
227. Kciuk, M., Marciniak, B., Mojzych, M. & Kontek, R. Focus on uv-induced dna damage and repair—disease relevance and protective strategies. *Int J Mol Sci* **21**, 1–33 (2020).
228. Sivamani, R. K., Crane, L. A. & Dellavalle, R. P. The benefits and risks of ultraviolet (UV) tanning and its alternatives: the role of prudent sun exposure. *Dermatol Clin.* **27**, (2009).
229. Holick, M. F. Biological effects of sunlight, ultraviolet radiation, visible light, infrared radiation and Vitamin D for health. *Anticancer Res* **36**, 1345–1356 (2016).
230. Webb, A. R. *et al.* Meeting vitamin D requirements in white caucasians at UK latitudes: Providing a choice. *Nutrients* **10**, 1–13 (2018).
231. Lee, J. W., Ratnakumar, K., Hung, K.-F., Rokunohe, D. & Kawasumi, M. Deciphering UV-induced DNA Damage Responses to Prevent and Treat Skin Cancer. *Photochemical and Photobiological Sciences* **96**, 478–499 (2020).
232. Ouhtit, A. *et al.* Temporal events in skin injury and the early adaptive responses in ultraviolet-irradiated mouse skin. *American Journal of Pathology* **156**, 201–207 (2000).
233. Bernard, J. J. *et al.* Ultraviolet radiation damages self noncoding RNA and is detected by TLR3. *Nat Med* **18**, 1286–1290 (2012).
234. Gallo, R. L. & Bernard, J. J. Innate immune sensors stimulate inflammatory and immunosuppressive responses to UVB radiation. *Journal of Investigative Dermatology* **134**, 1508–1511 (2014).
235. Lewis, W. *et al.* Regulation of ultraviolet radiation induced cutaneous photoimmunosuppression by Toll-like receptor-4. *Arch Biochem Biophys* **508**, 171–177 (2011).
236. Walterscheid, J. P., Ullrich, S. E. & Nghiem, D. X. Platelet-activating factor, a molecular sensor for cellular damage, activates systemic immune suppression. *Journal of Experimental Medicine* **195**, 171–179 (2002).
237. Liu, D. *et al.* UVA irradiation of human skin vasodilates arterial vasculature and lowers blood pressure independently of nitric oxide synthase. *Journal of Investigative Dermatology* **134**, 1839–1846 (2014).
238. Teunissen, M. B. M. *et al.* Ultraviolet B Radiation Induces a Transient Appearance of IL-4+ Neutrophils, Which Support the Development of Th2 Responses. *The Journal of Immunology* **168**, 3732–3739 (2002).
239. Klein, A. M., Brash, D. E., Jones, P. H. & Simons, B. D. Stochastic fate of p53-mutant epidermal progenitor cells is tilted toward proliferation by UV B during preneoplasia. *Proc Natl Acad Sci U S A* **107**, 270–275 (2010).

240. Cela, E. M. *et al.* Time-course study of different innate immune mediators produced by UV-irradiated skin: Comparative effects of short and daily versus a single harmful UV exposure. *Immunology* **145**, 82–93 (2015).
241. El-Abaseri, T. B., Putta, S. & Hansen, L. A. Ultraviolet irradiation induces keratinocyte proliferation and epidermal hyperplasia through the activation of the epidermal growth factor receptor. *Carcinogenesis* **27**, 225–231 (2006).
242. D'Mello, S. A. N., Finlay, G. J., Baguley, B. C. & Askarian-Amiri, M. E. Signaling pathways in melanogenesis. *Int J Mol Sci* **17**, 1–18 (2016).
243. Brenner, M. & Hearing, J. V. The protective role of melanin against UV. *Photochem Photobiology* **84**, 539–549 (2008).
244. Halliday, G. M. Inflammation, gene mutation and photoimmunosuppression in response to UVR-induced oxidative damage contributes to photocarcinogenesis. *Mutation Research - Fundamental and Molecular Mechanisms of Mutagenesis* **571**, 107–120 (2005).
245. Garmyn, M., Young, A. R. & Miller, S. A. Mechanisms of and variables affecting UVR photoadaptation in human skin. *Photochemical and Photobiological Sciences* **17**, 1932–1940 (2018).
246. Fitzpatrick, T. B. The Validity and Practicality of Sun-Reactive Skin Types I Through VI. *Arch Dermatol* **124**, 869–871 (1988).
247. Herlihy, E., Gies, P. H., Roy, C. R. & Jones, M. Personal dosimetry of solar UV radiation for different outdoor activities. *Photochem Photobiol.* **60**, 288–294 (1994).
248. Barbhaiya, M. & Costenbader, K. H. Ultraviolet radiation and systemic lupus erythematosus. *Lupus* **23**, 588–595 (2014).
249. Rooney, J. F. *et al.* UV light-induced reactivation of herpes simplex virus type 2 and prevention by acyclovir. *Journal of Infectious Diseases* **166**, 500–506 (1992).
250. Zak-Prelich, M., Borkowski, J. L., Alexander, F. & Norval, M. The role of solar ultraviolet irradiation in zoster. *Epidemiol Infect* **129**, 593–597 (2002).
251. Brown, E. L., Ullrich, S. E., Pride, M. & Kripke, M. L. The Effect of UV Irradiation on Infection of Mice with Borrelia burgdorferi¶. *Photochem Photobiol* **73**, 537 (2001).
252. Chen, Q. *et al.* Prevention of ultraviolet radiation-induced immunosuppression by sunscreen in Candida albicans-induced delayed-type hypersensitivity. *Mol Med Rep* **14**, 202–208 (2016).
253. Cannell, J. J. *et al.* Epidemic influenza and vitamin D. *Epidemiol Infect* **134**, 1129–1140 (2006).
254. Boere, T. M., Visser, D. H., Van Furth, A. M., Lips, P. & Cobelens, F. G. J. Solar ultraviolet B exposure and global variation in tuberculosis incidence: An ecological analysis. *European Respiratory Journal* **49**, (2017).
255. World Health Organization. *Global Report on Psoriasis*. *World Health Organization* (2016).
256. Deng, Y., Chang, C. & Lu, Q. The Inflammatory Response in Psoriasis: a Comprehensive Review. *Clin Rev Allergy Immunol* **50**, 377–389 (2016).
257. Rendon, A. & Schäkel, K. Psoriasis pathogenesis and treatment. *Int J Mol Sci* **20**, 1–28 (2019).
258. Greb, J. E. *et al.* Psoriasis. *Nat Rev Dis Primers* **2**, (2016).
259. Di Cesare, A., Di Meglio, P. & Nestle, F. O. The IL-23Th17 axis in the immunopathogenesis of psoriasis. *Journal of Investigative Dermatology* **129**, 1339–1350 (2009).

260. Wang, C. Q. F. *et al.* IL-17 induces inflammation-Associated gene products in blood monocytes, and treatment with ixekizumab reduces their expression in psoriasis patient blood. *Journal of Investigative Dermatology* **134**, 2990–2993 (2014).
261. Rønholt, K. & Iversen, L. Old and new biological therapies for psoriasis. *Int J Mol Sci* **18**, (2017).
262. Brandrup, F., Hauge, M., Henningsen, K. & Eriksen, B. Psoriasis in an Unselected Series of Twins. *Arch Dermatol* **114**, 874–878 (1978).
263. Farber, E. M., Nall, M. L. & Watson, W. Natural History of Psoriasis in 61 Twin Pairs. *Arch Dermatol* **109**, 207–211 (1974).
264. Teng, Y. *et al.* Infection-provoked psoriasis: Induced or aggravated (Review). *Exp Ther Med* **21**, 1–9 (2021).
265. Kim, G. K. & del Rosso, J. Q. Drug-provoked psoriasis: Is it drug induced or drug aggravated? understanding pathophysiology and clinical relevance. *Journal of Clinical and Aesthetic Dermatology* **3**, 32–38 (2010).
266. Paniz Mondolfi, A. E. *et al.* Generalized pustular psoriasis triggered by Zika virus infection. *Clin Exp Dermatol* **43**, 171–174 (2018).
267. Nestle, F. O. *et al.* Plasmacytoid predendritic cells initiate psoriasis through interferon-α production. *Journal of Experimental Medicine* **202**, 135–143 (2005).
268. Kim, T. G. *et al.* Dermal clusters of mature dendritic cells and T cells are associated with the CCL20/CCR6 chemokine system in chronic psoriasis. *Journal of Investigative Dermatology* **134**, 1462–1465 (2014).
269. Chan, J. R. *et al.* IL-23 stimulates epidermal hyperplasia via TNF and IL-20R2-dependent mechanisms with implications for psoriasis pathogenesis. *Journal of Experimental Medicine* **203**, 2577–2587 (2006).
270. Denton, C. P. & Khanna, D. Systemic sclerosis. *The Lancet* **390**, 1685–1699 (2017).
271. Rongioletti, F. *et al.* Scleredema. A multicentre study of characteristics, comorbidities, course and therapy in 44 patients. *Journal of the European Academy of Dermatology and Venereology* **29**, 2399–2404 (2015).
272. Elhai, M., Meune, C., Avouac, J., Kahan, A. & Allanore, Y. Trends in mortality in patients with systemic sclerosis over 40 years: A systematic review and meta-analysis of cohort studies. *Rheumatology (United Kingdom)* **51**, 1017–1026 (2012).
273. van den Hombergh, W. M. T. *et al.* An easy prediction rule for diffuse cutaneous systemic sclerosis using only the timing and type of first symptoms and auto-antibodies: Derivation and validation. *Rheumatology (United Kingdom)* **55**, 2023–2032 (2016).
274. Steen, V. D. Autoantibodies in systemic sclerosis. *Semin Arthritis Rheum* **35**, 35–42 (2005).
275. Asano, Y. & Sato, S. Vasculopathy in scleroderma. *Semin Immunopathol* **37**, 489–500 (2015).
276. Trojanowska, M. Cellular and molecular aspects of vascular dysfunction in systemic sclerosis. *Nat Rev Rheumatol* **6**, 453–460 (2010).
277. Allanore, Y. *et al.* Systemic sclerosis. *Nat Rev Dis Primers* **1**, (2015).
278. Skaug, B. & Assassi, S. Type I interferon dysregulation in Systemic Sclerosis. *Cytokine* **132**, 154635 (2020).

279. Kim, D. *et al.* Induction of interferon-α by scleroderma sera containing autoantibodies to topoisomerase I: Association of higher interferon-α activity with lung fibrosis. *Arthritis Rheum* **58**, 2163–2173 (2008).
280. York, M. R. *et al.* A macrophage marker, siglec-1, is increased on circulating monocytes in patients with systemic sclerosis and induced by type I interferons and toll-like receptor agonists. *Arthritis Rheum* **56**, 1010–1020 (2007).
281. Bhattacharyya, S. *et al.* FibronectinEDA promotes chronic cutaneous fibrosis through toll-like receptor signaling. *Sci Transl Med* **6**, 1–31 (2014).
282. Ho, Y. Y., Lagares, D., Tager, A. M. & Kapoor, M. Fibrosis - A lethal component of systemic sclerosis. *Nat Rev Rheumatol* **10**, 390–402 (2014).
283. Ross, R. L. *et al.* Targeting human plasmacytoid dendritic cells through BDCA2 prevents skin inflammation and fibrosis in a novel xenotransplant mouse model of scleroderma. *Ann Rheum Dis* **80**, 920–929 (2021).
284. Carriero, A. *et al.* Serum interferon score predicts clinical outcome at 12 months in diffuse cutaneous systemic sclerosis as measured by Global Ranked Composite Score (GRCS) and Composite Response Index in SSc (CRISS). *Rheumatology* **58**, (2019).
285. Furman, D. *et al.* Chronic inflammation in the etiology of disease across the life span. *Nat Med* **25**, 1822–1832 (2019).
286. Kagami, S., Rizzo, H. L., Lee, J. J., Koguchi, Y. & Blauvelt, A. Circulating Th17, Th22, and Th1 cells are increased in psoriasis. *Journal of Investigative Dermatology* **130**, 1373–1383 (2010).
287. Catapano, M. *et al.* IL-36 Promotes Systemic IFN-I Responses in Severe Forms of Psoriasis. *Journal of Investigative Dermatology* **140**, 816-826.e3 (2020).
288. Rawat, A. *et al.* A Neutrophil-Driven Inflammatory Signature Characterizes the Blood Transcriptome Fingerprint of Psoriasis. *Front Immunol* **11**, 1–14 (2020).
289. Pingen, M. *et al.* Host Inflammatory Response to Mosquito Bites Enhances the Severity of Arbovirus Infection. *Immunity* **44**, 1455–1469 (2016).
290. Bankhead, P. *et al.* QuPath: Open source software for digital pathology image analysis. *Sci Rep* **7**, 1–7 (2017).
291. Weaver, S. C., Charlier, C., Nikos, V. & Lecuit, M. Zika, Chikungunya, and Other Emerging Vector-Borne Viral Diseases. *Annu Rev Med.* **69**, 395–408 (2018).
292. Lam, P. K. *et al.* Clinical characteristics of dengue shock syndrome in vietnamese children: A 10-year prospective study in a single hospital. *Clinical Infectious Diseases* **57**, 1577–1586 (2013).
293. Lamy, K. *et al.* Clear-sky ultraviolet radiation modelling using output from the Chemistry Climate Model Initiative. *Atmos Chem Phys* **19**, 10087–10110 (2019).
294. Bernard, J. J. *et al.* Ultraviolet radiation damages self noncoding RNA and is detected by TLR3. *Nat Med* **18**, 1286–1290 (2012).
295. Cela, E. M. *et al.* Time-course study of different innate immune mediators produced by UV-irradiated skin: Comparative effects of short and daily versus a single harmful UV exposure. *Immunology* **145**, 82–93 (2015).
296. Skopelja-Gardner, S. *et al.* Acute skin exposure to ultraviolet light triggers neutrophil-mediated kidney inflammation. *Proc Natl Acad Sci U S A* **118**, 1–12 (2021).
297. Skopelja-Gardner, S. *et al.* Acute skin exposure to ultraviolet light triggers neutrophil-mediated kidney inflammation. *Proc Natl Acad Sci U S A* **118**, 1–12 (2021).

298. Skopelja-Gardner, S. *et al.* The early local and systemic Type I interferon responses to ultraviolet B light exposure are cGAS dependent. *Sci Rep* **10**, 1–14 (2020).
299. Rooney, J. F. *et al.* UV light-induced reactivation of herpes simplex virus type 2 and prevention by acyclovir. *Journal of Infectious Diseases* **166**, 500–506 (1992).
300. Zak-Prelich, M., Borkowski, J. L., Alexander, F. & Norval, M. The role of solar ultraviolet irradiation in zoster. *Epidemiol Infect* **129**, 593–597 (2002).
301. Brown, E. L., Ullrich, S. E., Pride, M. & Kripke, M. L. The Effect of UV Irradiation on Infection of Mice with Borrelia burgdorferi¶. *Photochem Photobiol* **73**, 537 (2001).
302. Chen, Q. *et al.* Prevention of ultraviolet radiation-induced immunosuppression by sunscreen in Candida albicans-induced delayed-type hypersensitivity. *Mol Med Rep* **14**, 202–208 (2016).
303. Boere, T. M., Visser, D. H., Van Furth, A. M., Lips, P. & Cobelens, F. G. J. Solar ultraviolet B exposure and global variation in tuberculosis incidence: An ecological analysis. *European Respiratory Journal* **49**, (2017).
304. Han, A. & Maibach, H. I. Management of acute sunburn. *Am J Clin Dermatol* **5**, 39–47 (2004).
305. Ross, R. L. *et al.* Targeting human plasmacytoid dendritic cells through BDCA2 prevents skin inflammation and fibrosis in a novel xenotransplant mouse model of scleroderma. *Ann Rheum Dis* **80**, 920–929 (2021).
306. Onuora, S. Adipocyte-myofibroblast transition: Linking intradermal fat loss to skin fibrosis in SSc. *Nat Rev Rheumatol* **11**, 63 (2015).
307. Nidavani, R. B., Mahalakshmi, A. M. & Shalawadi, M. Vascular permeability and evans blue dye: A physiological and pharmacological approach. *J Appl Pharm Sci* **4**, 106–113 (2014).
308. Bryden, S. R. *et al.* Pan-viral protection against arboviruses by activating skin macrophages at the inoculation site. *Sci Transl Med* **12**, (2020).
309. Martikainen, M. *et al.* Oncolytic alphavirus SFV-VA7 efficiently eradicates subcutaneous and orthotopic human prostate tumours in mice. *Br J Cancer* **117**, 51–55 (2017).
310. Vähä-Koskela, M. J. V. *et al.* Oncolytic capacity of attenuated replicative Semliki Forest virus in human melanoma xenografts in severe combined immunodeficient mice. *Cancer Res* **66**, 7185–7194 (2006).
311. Määttä, A. M. *et al.* Evaluation of cancer virotherapy with attenuated replicative Semliki Forest virus in different rodent tumor models. *Int J Cancer* **121**, 863–870 (2007).
312. Flomerfelt, F. & Gress, R. Analysis of Cell Proliferation and Homeostasis Using EdU Labeling. *Methods Mol Biol.* **1323**, 211–220 (2016).
313. Lefteri, D. A. *et al.* Mosquito saliva enhances virus infection through sialokinin-dependent vascular leakage. *Proc Natl Acad Sci U S A* **119**, (2022).
314. Reynoso, G. V. *et al.* Zika virus spreads through infection of lymph node-resident macrophages. *Cell Rep* **42**, 112126 (2023).
315. El-Abaseri, T. B., Putta, S. & Hansen, L. A. Ultraviolet irradiation induces keratinocyte proliferation and epidermal hyperplasia through the activation of the epidermal growth factor receptor. *Carcinogenesis* **27**, 225–231 (2006).
316. Laursen, W. J. *et al.* Humidity sensors that alert mosquitoes to nearby hosts and egg-laying sites. *Neuron* **111**, 874-887.e8 (2023).

317. Corfas, R. A. & Vosshall, L. B. The cation channel TRPA1 tunes mosquito thermotaxis to host temperatures. *Elife* **4**, 1–16 (2015).
318. Ziegler, R., Blanckenhorn, W. U., Mathis, A. & Verhulst, N. O. Video analysis of the locomotory behaviour of Aedes aegypti and Ae. japonicus mosquitoes under different temperature regimes in a laboratory setting. *J Therm Biol* **105**, 103205 (2022).
319. Vaughn, D. W. *et al.* Dengue Viremia Titer, Antibody Response Pattern, and Virus Serotype Correlate with Disease Severity. *Journal of Infectious Diseases* **181**, 2–9 (2000).
320. Lord, C. C., Rutledge, R. C. & Tabachnick, W. J. Relationships Between Host Viremia and Vector Susceptibility for Arboviruses. *J. Med. Entomol.* **43**, 623–630 (2006).
321. Wu, Y. *et al.* Zika virus evades interferon-mediated antiviral response through the co-operation of multiple nonstructural proteins in vitro. *Cell Discov* **3**, 1–14 (2017).
322. Breakwell, L. *et al.* Semliki Forest Virus Nonstructural Protein 2 Is Involved in Suppression of the Type I Interferon Response □. **81**, 8677–8684 (2007).
323. Blakqori, G. *et al.* La Crosse Bunyavirus Nonstructural Protein NSs Serves To Suppress the Type I Interferon System of Mammalian Hosts □. **81**, 4991–4999 (2007).
324. Lazear, H. M. *et al.* A Mouse Model of Zika Virus Pathogenesis HHS Public Access. *Cell Host Microbe* **19**, 720–730 (2016).
325. Skopelja-Gardner, S. *et al.* The early local and systemic Type I interferon responses to ultraviolet B light exposure are cGAS dependent. *Sci Rep* **10**, 1–14 (2020).
326. Sherwani, M. A. *et al.* Type I Interferons Enhance the Repair of Ultraviolet Radiation-Induced DNA Damage and Regulate Cutaneous Immune Suppression. *Int J Mol Sci* **23**, (2022).
327. de Pedro, I., Alonso-Lecue, P., Sanz-Gómez, N., Freije, A. & Gandarillas, A. Sublethal UV irradiation induces squamous differentiation via a p53-independent, DNA damage-mitosis checkpoint. *Cell Death Dis* **9**, (2018).
328. Fazakerley, J. K., Pathak, S., Scallan, M., Amor, S. & Dyson, H. Replication of the a7(74) strain of semliki forest virus is restricted in neurons. *Virology* vol. 195 627–637 Preprint at https://doi.org/10.1006/viro.1993.1414 (1993).
329. Inoue, H. & Tani, K. Multimodal immunogenic cancer cell death as a consequence of anticancer cytotoxic treatments. *Cell Death Differ* **21**, 39–49 (2014).
330. Lundstrom, K. Oncolytic alphaviruses in cancer immunotherapy. *Vaccines (Basel)* **5**, (2017).
331. Garcia-Tapia, D., Loiacono, C. M. & Kleiboeker, S. B. Replication of West Nile virus in equine peripheral blood mononuclear cells. *Vet Immunol Immunopathol* **110**, 229–244 (2006).
332. Ziegler, R., Blanckenhorn, W. U., Mathis, A. & Verhulst, N. O. Video analysis of the locomotory behaviour of Aedes aegypti and Ae. japonicus mosquitoes under different temperature regimes in a laboratory setting. *J Therm Biol* **105**, 103205 (2022).
333. Kelfkens, G. & Van der Leun, J. C. Skin temperature changes after irradiation with UVB or UVC: implications for the mechanism underlying ultraviolet erythema. *Phys Med Biol* **34**, 599–608 (1989).

334. Ninomiya, M., Katagiri, C., Hara, Y., Kubo, Y. & Yamashita, T. Tracking of cutaneous vascular structural changes post-UV irradiation using optical coherence tomography angiography. 226–232 (2020) doi:10.1111/phpp.12542.
335. Ribeiro, J. M. C., Rossignol, R. A. & Spielman, A. Aedes aegypti : Model for Blood Finding Strategy and Prediction of Parasite Manipulation. *Exp Parasitol* **60**, 118–132 (1985).
336. Xiang, B. W. W. *et al.* Dengue virus infection modifies mosquito blood-feeding behavior to increase transmission to the host. *Proc Natl Acad Sci U S A* **119**, (2022).
337. Verhulst, N. O. *et al.* Composition of human skin microbiota affects attractiveness to malaria mosquitoes. *PLoS One* **6**, (2011).
338. Benjamin, C. L. & Ananthaswamy, H. N. P53 and the Pathogenesis of Skin Cancer. *Toxicol Appl Pharmacol* **224**, 241–248 (2007).
339. Pandel, R. D., Poljšak, B., Godic, A. & Dahmane, R. Skin Photoaging and the Role of Antioxidants in Its Prevention. *ISRN Dermatol* (2013) doi:dx.doi.org/10.1155/2013/930164.
340. Narayanan, D. L., Saladi, R. N. & Fox, J. L. Ultraviolet radiation and skin cancer. *Int J Dermatol* **49**, 978–986 (2010).
341. Ouhtit, A. & Ananthaswamy, H. N. A model for UV-induction of skin cancer. *J Biomed Biotechnol* **2001**, 5–6 (2001).
342. Dennis, L. K. *et al.* Sunburns and Risk of Cutaneous Melanoma: Does Age Matter? A Comprehensive Meta-Analysis. *Ann Epidemiol* **18**, 614–627 (2008).
343. Scott, T. L. *et al.* Pigment-independent cAMP-mediated epidermal thickening protects against cutaneous UV injury by keratinocyte proliferation. *Exp Dermatol* **21**, 771–777 (2012).
344. Brenner, M. & Hearing, J. V. The protective role of melanin against UV. *Photochem Photobiology* **84**, 539–549 (2008).
345. Gamelli, R. L. & He, L.-K. *Wound Healing Methods and Protocols - Incisonal Wound Healing: Model and Analysis of Wound Breaking Strength*. *Methods in Molecular Medicine* vol. 78 (2003).
346. Yampolsky, M., Bachelet, I. & Fuchs, Y. Reproducible strategy for excisional skin-wound-healing studies in mice. *Nat Protoc* **19**, 1900–1916 (2023).
347. Leibovich, S. J. & Ross, R. The role of the macrophage in wound repair. A study with hydrocortisone and antimacrophage serum. *American Journal of Pathology* **78**, 71–99 (1975).
348. Ishida, Y., Gao, J. & Murphy, P. M. Chemokine Receptor CX3CR1 Mediates Skin Wound Healing by Promoting Macrophage and Fibroblast Accumulation and Function. *The Journal of Immunology* **180**, 569–579 (2008).
349. Delavary, B. M., van der Veer, W. M., van Egmond, M., Niessen, F. B. & Beelen, R. H. J. Macrophages in skin injury and repair. *Immunobiology* **216**, 753–762 (2011).
350. Shook, B., Xiao, E., Kumamoto, Y., Iwasaki, A. & Horsley, V. CD301b+ Macrophages Are Essential for Effective Skin Wound Healing. *Journal of Investigative Dermatology* **136**, 1885–1891 (2016).
351. Mirza, R., DiPietro, L. A. & Koh, T. J. Selective and specific macrophage ablation is detrimental to wound healing in mice. *American Journal of Pathology* **175**, 2454–2462 (2009).
352. Pauleau, A.-L. *et al.* Enhancer-Mediated Control of Macrophage-Specific Arginase I Expression. *The Journal of Immunology* **172**, 7565–7573 (2004).

353. Witte, M. B., Barbul, A., Schick, M. A., Vogt, N. & Becker, H. D. Upregulation of arginase expression in wound-derived fibroblasts. *Journal of Surgical Research* **105**, 35–42 (2002).
354. Kämpfer, H., Pfeilschifter, J. & Frank, S. Expression and Activity of Arginase Isoenzymes during Normal and Diabetes-Impaired Skin Repair. *Journal of Investigative Dermatology* **121**, 1544–1551 (2003).
355. Atkins, G. J., Sheahan, B. J. & Liljeström, P. The molecular pathogenesis of Semliki Forest virus: A model virus made useful? *Journal of General Virology* **80**, 2287–2297 (1999).
356. Scott, T. L. *et al.* Pigment-independent cAMP-mediated epidermal thickening protects against cutaneous UV injury by keratinocyte proliferation. *Exp Dermatol* **21**, 771–777 (2012).
357. Maschalidi, S. *et al.* Targeting SLC7A11 improves efferocytosis by dendritic cells and wound healing in diabetes. *Nature* **606**, 776–784 (2022).
358. Li, Z., Lamb, R., Coles, M. C., Bennett, C. L. & Ambler, C. A. Inducible ablation of CD11c+ cells to determine their role in skin wound repair. *Immunology* **163**, 105–111 (2021).
359. McGrath, J., Eady, R. & Pope, F. Anatomy and Organization of Human Skin. in *Rook's Textbook of Dermatology* 109–132 (2004). doi:https://doi.org/10.1002/9780470750520.ch3.
360. Clydesdale, G. J., Dandie, G. W. & Muller, H. K. Ultraviolet light induced injury: Immunological and inflammatory effects. *Immunol Cell Biol* **79**, 547–568 (2001).
361. Eming, S. A., Wynn, T. A. & Martin, P. Inflammation and metabolism in tissue repair and regeneration. *Science (1979)* **356**, 1026–1030 (2017).
362. Pearse, A. D., Gaskell, S. A. & Marks, R. Epidermal changes in human skin following irradiation with either UVB or UVA. *Journal of Investigative Dermatology* **88**, 83–7 (1987).
363. Rosario, R., Mark, G. J., Parrish, J. A. & Mihm, M. C. Histological changes produced in skin by equally erythemogenic doses of UV-A, UV-B, UV-C and UV-A with psoralens. *British Journal of Dermatology* **101**, 299–308 (1979).
364. Dvorak, H. F., Brown, L. F., Detmar, M. & Dvorak, A. M. Vascular permeability factor/vascular endothelial growth factor, microvascular hyperpermeability, and angiogenesis. *American Journal of Pathology* **146**, 1029–1039 (1995).
365. Wong, G. & Qiu, X. G. Type I interferon receptor knockout mice as models for infection of highly pathogenic viruses with outbreak potential. *Zool Res* **39**, 3–14 (2018).
366. Jenkins, S. J. *et al.* Local Macrophage Proliferation, Rather than Recruitment from the Blood, Is a Signature of TH2 Inflammation. *Science (1979)* **332**, 1284–1288 (2011).
367. Phillipson, M. & Kubes, P. The Healing Power of Neutrophils. *Trends Immunol* **40**, 635–647 (2019).
368. Devalaraja, R. M. *et al.* Delayed wound healing in CXCR 2 knockout mice. *Journal of Investigative Dermatology* **115**, 234–244 (2000).
369. Theilgaard-Mönch, K., Knudsen, S., Follin, P. & Borregaard, N. The Transcriptional Activation Program of Human Neutrophils in Skin Lesions Supports Their Important Role in Wound Healing. *The Journal of Immunology* **172**, 7684–7693 (2004).
370. Willenborg, S. *et al.* CCR2 recruits an inflammatory macrophage subpopulation critical for angiogenesis in tissue repair. *Blood* **120**, 613–625 (2012).

371. Haniffa, M., Gunawan, M. & Jardine, L. Human skin dendritic cells in health and disease. *J Dermatol Sci* **77**, 85–92 (2015).
372. Yi, C. *et al.* Targeted inhibition of endothelial calpain delays wound healing by reducing inflammation and angiogenesis. *Cell Death Dis* **11**, (2020).
373. Rakita, A., Nikolić, N., Mildner, M., Matiasek, J. & Elbe-Bürger, A. Re-epithelialization and immune cell behaviour in an ex vivo human skin model. *Sci Rep* **10**, 1–11 (2020).
374. Reichner, J. S. *et al.* Molecular and metabolic evidence for the restricted expression of inducible nitric oxide synthase in healing wounds. *American Journal of Pathology* **154**, 1097–1104 (1999).
375. Albina, J. E., Mills, C. D., Henry, W. L. & Caldwell, M. D. Temporal expression of different pathways of 1-arginine metabolism in healing wounds. *The Journal of Immunology* **144**, 3877–3880 (1990).
376. Avdic, S. *et al.* Human Cytomegalovirus Interleukin-10 Polarizes Monocytes toward a Deactivated M2c Phenotype To Repress Host Immune Responses. *J Virol* **87**, 10273–10282 (2013).
377. Boumaza, A. *et al.* Monocytes and macrophages, targets of severe acute respiratory syndrome coronavirus 2: The clue for coronavirus disease 2019 immunoparalysis. *Journal of Infectious Diseases* **224**, 395–406 (2021).
378. Ronaghan, N. J. *et al.* M1-like, but not M0- or M2-like, macrophages, reduce RSV infection of primary bronchial epithelial cells in a media-dependent fashion. *PLoS One* **17**, 1–21 (2022).
379. Stoermer, K. A. *et al.* Genetic Ablation of Arginase 1 in Macrophages and Neutrophils Enhances Clearance of an Arthritogenic Alphavirus. *The Journal of Immunology* **189**, 4047–4059 (2012).
380. Wehner, M. R. *et al.* International prevalence of indoor tanning a systematic review and meta-analysis. *JAMA Dermatol* **150**, 390–400 (2014).
381. Veierød, M. B., Couto, E., Lund, E., Adami, H. O. & Weiderpass, E. Host characteristics, sun exposure, indoor tanning and risk of squamous cell carcinoma of the skin. *Int J Cancer* **135**, 413–422 (2014).
382. Thieden, E., Philipsen, P. A., Sandby-Møller, J. & Wulf, H. C. Sunscreen use related to UV exposure, age, sex, and occupation based on personal dosimeter readings and sun-exposure behavior diaries. *Arch Dermatol* **141**, 967–973 (2005).
383. D'Orazio, J. A. *et al.* Topical drug rescue strategy and skin protection based on the role of Mc1r in UV-induced tanning. *Nature* **443**, 340–344 (2006).
384. Reyes-Cruz, E. Y. *et al.* Effect of immunosuppression by UV-B radiation on components of the innate immune response in skin lesions with Leishmania mexicana: Effect of UVB on the innate immune response in cutaneous infection by L. mexicana. *Acta Trop* **226**, (2022).
385. Ouhtit, A. *et al.* Temporal events in skin injury and the early adaptive responses in ultraviolet-irradiated mouse skin. *American Journal of Pathology* **156**, 201–207 (2000).
386. Jablonski, N. G. & Chaplin, G. Human skin pigmentation as an adaptation to UV radiation. *Proc Natl Acad Sci U S A* **107**, 8962–8968 (2010).
387. Ho, Y. Y., Lagares, D., Tager, A. M. & Kapoor, M. Fibrosis - A lethal component of systemic sclerosis. *Nat Rev Rheumatol* **10**, 390–402 (2014).
388. Buller, D. B. *et al.* Prevalence of sunburn, sun protection, and indoor tanning behaviors among Americans: Review from national surveys and case studies of 3 states. *J Am Acad Dermatol* **65**, S114.e1-S114.e11 (2011).

389. Stott, M. A. Tanning and sunburn: Knowledge, attitudes and behaviour of people in Great Britain. *J Public Health Med* **21**, 377–384 (1999).
390. Melia, J. & Bulman, A. Sunburn and tanning in a British population. *J Public Health (Bangkok)* **17**, 223–229 (1995).
391. NHS Inform. Sunburn. https://www.nhsinform.scot/illnesses-and-conditions/injuries/skin-injuries/sunburn/ (2023).
392. Faurschou, A. & Wulf, H. C. Topical Corticosteroids in the Treatment of Acute Sunburn. *Arch Dermatol Res* **144**, 620–624 (2008).
393. Greenwald, J. S., Parrish, J. A., Jaenicke, K. F. & Anderson, R. R. Failure of systemically administered corticosteroids to suppress UVB-induced delayed erythema. *J Am Acad Dermatol* **5**, 197–202 (1981).
394. Barnes, P. J. How corticosteroids control inflammation : Quintiles Prize Lecture 2005. *Br J Pharmacol* **148**, 245–254 (2006).
395. Berth-Jones, J. Topical Therapy. in *Rook's Textbook of Dermatology* (eds. Burns, T., Breathnach, S. M., Cox, N. & Griffiths, C.) (John Wiley & Sons, 2004).
396. Weidinger, S. & Novak, N. Atopic dermatitis. *The Lancet* **387**, 1109–1122 (2016).
397. Das, L. M., Binko, A. M., Traylor, Z. P., Peng, H. & Lu, K. Q. Vitamin D improves sunburns by increasing autophagy in M2 macrophages. *Autophagy* **15**, 813–826 (2019).
398. Jeffrey F. Scott, Lopa M. Das, Sayeeda Ahsanuddin, Yuqi Qiu, Amy M. Binko, Zachary P. Traylor, Sara M. Debanne, Kevin D. Cooper, Rebecca Boxer, and K. Q. L. Oral vitamin D rapidly attenuates inflammation from sunburn: an interventional study. *Journal of Investigative Dermatology* **72**, 2964–2979 (2017).
399. Holick, M. F. Vitamin D Status: Measurement , Interpretation and Clinical Application. *Ann Epidemiol* **19**, 73–78 (2009).
400. Nash, D. *et al.* The Outbreak of West Nile Virus Infection in the New York City Area in 1999. *New England Journal of Medicine* **344**, 1807–1814 (2001).
401. Murin, C. D., Wilson, I. A. & Ward, A. B. Antibody responses to viral infections: a structural perspective across three different enveloped viruses. *Nat Microbiol* **4**, 734–747 (2019).
402. Amor, S., Scallan, M. F., Morris, M. M., Dyson, H. & Fazakerley, J. K. Role of immune responses in protection and pathogenesis during Semliki Forest virus encephalitis. *Journal of General Virology* **77**, 281–291 (1996).
403. Fragkoudis, R., Ballany, C. M., Boyd, A. & Fazakerley, J. K. In Semliki Forest virus encephalitis, antibody rapidly clears infectious virus and is required to eliminate viral material from the brain, but is not required to generate lesions of demyelination. *Journal of General Virology* **89**, 2565–2568 (2008).
404. Fazakerley, J. K. Semliki forest virus infection of laboratory mice: a model to study the pathogenesis of viral encephalitis. *Arch Virol Suppl* 179–190 (2004) doi:10.1007/978-3-7091-0572-6_16.
405. Gauger, P. C. & Vincent, A. L. Serum Virus Neutralization Assay for Detection and Quantitation of Serum-Neutralizing Antibodies to Influenza A Virus in Swine. in *Animal Influenza Virus. Methods in Molecular Biology* (ed. Spackman, E.) (Humana Press, New York, NY., 2014). doi:doi.org/10.1007/978-1-4939-0758-8_26.
406. Clé, M. *et al.* Neurocognitive impacts of arbovirus infections. *J Neuroinflammation* **17**, 1–14 (2020).

407. Scott, J. F. *et al.* Oral Vitamin D Rapidly Attenuates Inflammation from Sunburn : An Interventional Study. *Journal of Investigative Dermatology* **137**, 2078–2086 (2017).
408. DiStasi, M. R. & Ley, K. Opening the flood-gates: how neutrophil-endothelial interactions regulate permeability. *Trends Immunol* **30**, 547–556 (2009).
409. Katzelnick, L. C. *et al.* Antibody-dependent enhancement of severe dengue disease in humans. *Science (1979)* **358**, 929–932 (2017).
410. Rey, F. A., Stiasny, K., Vaney, M., Dellarole, M. & Heinz, F. X. The bright and the dark side of human antibody responses to flaviviruses: lessons for vaccine design. *EMBO Rep* **19**, 206–224 (2018).
411. Zellweger, R. M., Prestwood, T. R. & Shresta, S. Antibodies enhance infection of LSECs in a model of ADE-induced severe dengue disease. *Cell Host Microbe* **7**, 128–139 (2010).
412. Michlmayr, D. *et al.* Defining the Chemokine Basis for Leukocyte Recruitment during Viral Encephalitis. *J Virol* **88**, 9553–9567 (2014).
413. Hajar, T. *et al.* A systematic review of topical corticosteroid withdrawal ('steroid addiction') in patients with atopic dermatitis and other dermatoses. *J Am Acad Dermatol* **72**, 541-549.e2 (2015).
414. Damour, A., Garcia, M., Seneschal, J., Lévêque, N. & Bodet, C. Eczema Herpeticum: Clinical and Pathophysiological Aspects. *Clin Rev Allergy Immunol* **59**, 1–18 (2020).
415. Henseler, T. & Christophers, E. Disease concomitance in psoriasis. *J Am Acad Dermatol* **32**, 982–986 (1995).
416. Christophers, E. & Henseler, T. Contrasting disease patterns in psoriasis and atopic dermatitis. *Arch Dermatol Res* **279**, 4–7 (1987).
417. Wolk, K. *et al.* IL-29 is produced by TH17 cells and mediates the cutaneous antiviral competence in psoriasis. *Sci Transl Med* **5**, (2013).
418. Greb, J. E. *et al.* Psoriasis. *Nat Rev Dis Primers* **2**, (2016).
419. Mease, P. J. *et al.* Prevalence of rheumatologist-diagnosed psoriatic arthritis in patients with psoriasis in European/North American dermatology clinics. *J Am Acad Dermatol* **69**, 729–735 (2013).
420. Yeung, H. *et al.* Psoriasis severity and the prevalence of major medical comorbidity: A population-based study. *JAMA Dermatol* **149**, 1173–1179 (2013).
421. Persson, P. G., Leijonmarck, C. E., Bernell, O., Hellers, G. & Ahlbom, A. Risk indicators for inflammatory bowel disease. *Int J Epidemiol* **22**, 268–272 (1993).
422. Kou, Z. *et al.* Monocytes, But Not T or B Cells, Are the Principal Target Cells for Dengue Virus (DV) Infection Among Human Peripheral Blood Mononuclear Cells. *J Med Virol* **80**, 134–146 (2008).
423. Wang, W. K. *et al.* Detection of dengue virus replication in peripheral blood mononuclear cells from dengue virus type 2-infected patients by a reverse transcription-real-time PCR assay. *J Clin Microbiol* **40**, 4472–4478 (2002).
424. Michlmayr, D., Andrade, P., Gonzalez, K., Balmaseda, A. & Harris, E. CD14+CD16+ monocytes are the main target of Zika virus infection in peripheral blood mononuclear cells in a paediatric study in Nicaragua. *Nat Microbiol* **2**, 1462–1470 (2017).
425. Aggio, J. B., Porto, B. N., Duarte dos Santos, C. N., Mosimann, A. L. P. & Wowk, P. F. Human Neutrophils Present Mild Activation by Zika Virus But Reduce the Infection of Susceptible Cells. *Front Immunol* **13**, 1–18 (2022).

426. Zhao, Y. *et al.* Single cell immune profiling of dengue virus patients reveals intact immune responses to zika virus with enrichment of innate immune signatures. *PLoS Negl Trop Dis* **14**, 1–25 (2020).
427. Kakkar, V. *et al.* Type 1 interferon activation in systemic sclerosis: a biomarker, a target or the culprit. *Curr Opin Rheumatol* **34**, 357–364 (2022).
428. Lande, R. *et al.* Plasmacytoid dendritic cells sense self-DNA coupled with antimicrobial peptide. *Nature* **449**, 564–569 (2007).
429. Hornung, V. *et al.* Quantitative Expression of Toll-Like Receptor 1–10 mRNA in Cellular Subsets of Human Peripheral Blood Mononuclear Cells and Sensitivity to CpG Oligodeoxynucleotides. *The Journal of Immunology* **168**, 4531–4537 (2002).
430. Ross, R. L. *et al.* Targeting human plasmacytoid dendritic cells through BDCA2 prevents skin inflammation and fibrosis in a novel xenotransplant mouse model of scleroderma. *Ann Rheum Dis* **80**, 920–929 (2021).
431. Tsoi, L. C. *et al.* Large scale meta-analysis characterizes genetic architecture for common psoriasis associated variants. *Nat Commun* **8**, 1–8 (2017).
432. Nascimento, E. J. M. *et al.* Gene expression profiling during early acute febrile stage of dengue infection can predict the disease outcome. *PLoS One* **4**, (2009).
433. Afroz, S., Giddaluru, J., Abbas, M. M. & Khan, N. Transcriptome meta-analysis reveals a dysregulation in extra cellular matrix and cell junction associated gene signatures during Dengue virus infection. *Sci Rep* **6**, 1–12 (2016).
434. Zanini, F., Pu, S. Y., Bekerman, E., Einav, S. & Quake, S. R. Single-cell transcriptional dynamics of flavivirus infection. *Elife* **7**, 1–21 (2018).
435. Tsai, C.-Y. *et al.* Type I IFNs and IL-18 Regulate the Antiviral Response of Primary Human γδ T Cells against Dendritic Cells Infected with Dengue Virus. *The Journal of Immunology* **194**, 3890–3900 (2015).
436. Chirathaworn, C., Rianthavorn, P., Wuttirattanakowit, N. & Poovorawan, Y. Serum IL-18 and IL-18BP Levels in Patients with Chikungunya Virus Infection. *Viral Immunol* **23**, (2010).
437. Pan American Health Organization. *Tool for the Diagnosis and Care of Patients with Suspected Arboviral Diseases*. http://iris.paho.org/xmlui/handle/123456789/33895 (2017).
438. Musso, D. & Gubler, D. J. Zika virus. *Clin. Microbiol. Rev* **29**, 487–524 (2016).
439. Aogo, R. A. *et al.* Effects of boosting and waning in highly exposed populations on dengue epidemic dynamics. *Sci Transl Med* **15**, 1–14 (2023).
440. Zhong, Q. Y. *et al.* Gender differences in UV-induced skin inflammation, skin carcinogenesis and systemic damage. *Environ Toxicol Pharmacol* **81**, 103512 (2021).
441. Bellenghi, M. *et al.* Sex and gender disparities in melanoma. *Cancers (Basel)* **12**, 1–23 (2020).
442. Shono, S., Imura, M., Ota, M. & Toda, K. The relationship of skin color, UVB-induced erythema, and melanogenesis. *Journal of Investigative Dermatology* **84**, 265–267 (1985).
443. Jablonski, N. G. & Chaplin, G. Human skin pigmentation as an adaptation to UV radiation. *Proc Natl Acad Sci U S A* **107**, 8962–8968 (2010).
444. Olson, R. L., Gaylor, J. & Everett, M. A. Skin Color, Melanin, and Erythema. *Arch Dermatol Res* **108**, 541–4 (1973).
445. Cao, D., Ma, B., Cao, Z., Zhang, X. & Xiang, Y. Structure of Semliki Forest virus in complex with its receptor VLDLR. *Cell* **186**, 2208-2218.e15 (2023).

446. Clark, L. E. *et al.* VLDLR and ApoER2 are receptors for multiple alphaviruses. *Nature* **602**, 475–480 (2022).
447. Jeschke, M. G. *et al.* Burn injury. *Nat Rev Dis Primers* **6**, (2020).
448. Fragkoudis, R. *et al.* The type I interferon system protects mice from Semliki Forest virus by preventing widespread virus dissemination in extraneural tissues, but does not mediate the restricted replication of avirulent virus in central nervous system neurons. *Journal of General Virology* **88**, 3373–3384 (2007).
449. Chang, C. *et al.* More skin, more sun, more tan, more melanoma. *Am J Public Health* **104**, e92–e99 (2014).
450. Pettigrew, S. *et al.* Predictors of sun protection behaviours and sunburn among Australian adolescents. *BMC Public Health* **16**, 1–8 (2016).
451. Shih, S. T. F., Carter, R., Heward, S. & Sinclair, C. Skin cancer has a large impact on our public hospitals but prevention programs continue to demonstrate strong economic credentials. *Aust N Z J Public Health* **41**, 371–376 (2017).
452. Wu, J., Keeley, A., Mallen, C., Morgan, A. W. & Pujades-Rodriguez, M. Incidence of infections associated with oral glucocorticoid dose in people diagnosed with polymyalgia rheumatica or giant cell arteritis: A cohort study in England. *Cmaj* **191**, E680–E688 (2019).
453. Dixon, W. G. *et al.* Immediate and delayed impact of oral glucocorticoid therapy on risk of serious infection in older patients with rheumatoid arthritis: A nested case-control analysis. *Ann Rheum Dis* **71**, 1128–1133 (2012).
454. Grijalva, C. G. *et al.* Initiation of tumor necrosis factor-αantagonists and the risk of hospitalization for infection in patients with autoimmune diseases. *JAMA* **306**, 2331–2339 (2011).
455. Lamontagne, F. *et al.* Corticosteroid therapy for sepsis: A clinical practice guideline. *BMJ (Online)* **362**, 1–8 (2018).
456. Sterne, J. A. C. *et al.* Association between Administration of Systemic Corticosteroids and Mortality among Critically Ill Patients with COVID-19: A Meta-analysis. *JAMA - Journal of the American Medical Association* **324**, 1330–1341 (2020).
457. Xiang, B. W. W. *et al.* Dengue virus infection modifies mosquito blood-feeding behavior to increase transmission to the host. *Proc Natl Acad Sci U S A* **119**, (2022).
458. Patra, V. *et al.* Ultraviolet exposure regulates skin metabolome based on the microbiome. *Sci Rep* **13**, 1–10 (2023).
459. Santiago-Rodriguez, T. M., Le François, B., Macklaim, J. M., Doukhanine, E. & Hollister, E. B. The Skin Microbiome: Current Techniques, Challenges, and Future Directions. *Microorganisms* **11**, 1–21 (2023).
460. Kell, A. M. & Gale, M. RIG-I in RNA virus recognition. *Virology* **479–480**, 110–121 (2015).
461. Carriero, A. *et al.* Serum interferon score predicts clinical outcome at 12 months in diffuse cutaneous systemic sclerosis as measured by Global Ranked Composite Score (GRCS) and Composite Response Index in SSc (CRISS). *Rheumatology* **58**, (2019).